PROGRESS REPORT

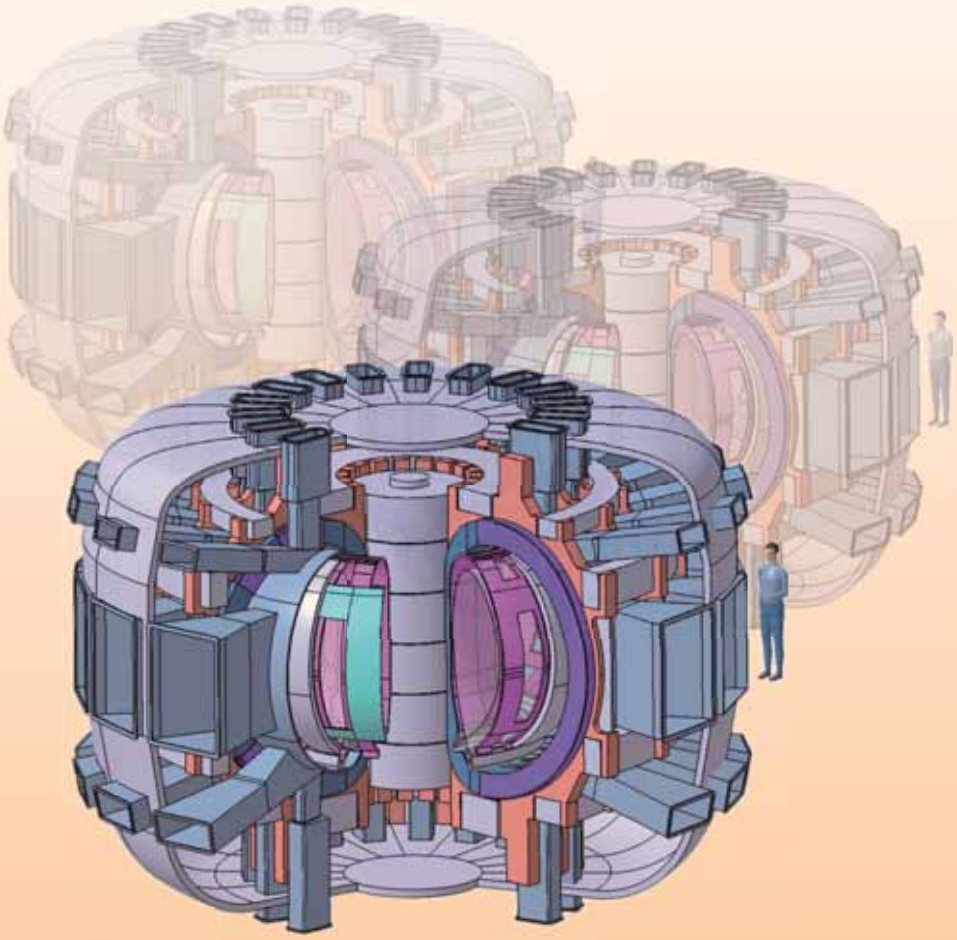

2008

EURATOM-ENEA ASSOCIATION *Fusion Activities - Progress Report*

ITALIAN NATIONAL AGENCY FOR NEW TECHNOLOGIES ENERGY AND THE ENVIRONMENT
Nuclear Fusion and Fission, and Related Technologies Department

This report was prepared by the Scientific Publications Office from contributions provided by the scientific and technical staff of ENEA's Nuclear Fusion and Fission, and Related Technologies Department.

Scientific editors: Paola Batistoni, Gregorio Vlad

Design and composition: Marisa Cecchini, Lucilla Crescentini, Lucilla Ghezzi

Artwork: Flavio Miglietta

Cover: Marisa Cecchini

English revision: Carolyn Kent

See http://**www.fusione.enea.it** for copy of this report

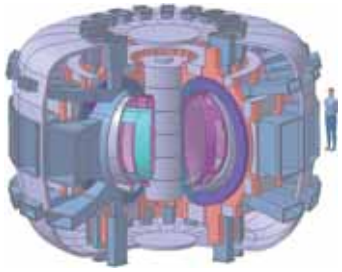

Cover picture:
FAST load assembly view

Published by:

ENEA - Nucleo di Agenzia
Edizioni Scientifiche,
Centro Ricerche Frascati,
C.P. 65
00044 Frascati Rome (Italy)

Tel.: +39(06)9400 5016
Fax: +39(06)9400 5015
e-mail: marisa.cecchini@frascati.enea.it

ENEA is increasing efforts in the development of fusion energy with regard to both physics and technology. In 2008, new scenarios were determined from the start of ITER construction and Fusion for Energy operation. The scientific and the emerging technology activities still belong to the Euratom programme, whereas the technology and engineering activities were devoted to Fusion for Energy and ITER International Office R&D grants and procurements. In order to maximize the synergy among all the laboratories involved in fusion, a number of consortia have been established to be prepared to answer the ITER and Fusion for Energy calls in the most appropriate and exhaustive way. Such is the case for the test blanket module design, characterisation and construction; the port plug where the radial neutron camera is allocated; neutron data; fuel cycle and electron cyclotron resonance heating power supply.

While the programme has been continued with FTU and the other scientific and technology facilities, ENEA was proactive in the analysis made by European Fusion Development Agreement for identifying the mission to be accomplished to properly exploit ITER and prepare for DEMO. In this framework, ENEA supported the need for a European satellite to complement JT–60SA and proposed FAST as a possible option for a new European experiment. FAST has been presented to the Fusion Facility Review Panel that analysed the needs of the European programme in the near–mid terms. ENEA also plays an important role in the Italian contribution to the Broader Approach as the agency in charge of the construction of part of the toroidal magnet and power supply of JT–60SA as well as the development of the International Fusion Materials Irradiation Facility target and advanced materials.

ENEA is also continuing physics and technology research on inertial fusion in the framework of the keep–in–touch activities within the Euratom programme and coordinates the Italian effort within the HiPER research infrastructure.

Finally ENEA is active in encouraging and supporting industries to participate in ITER through an information network dedicated to the procurement calls

(Euratom ENEA Association Head of Research Unit)

Aldo Pizzuto

Frascati, December 2008

1. Magnetic Confinement

The year 2008 was characterised by two major problems, which prevented the execution of a proper experimental campaign on FTU. After a few days of operation, the spring campaign was stopped by a major short circuit on the rotor of the flywheel generator supplying the poloidal coils. It was repaired in record time by Ansaldo, in Frascati, and was then ready for the autumn campaign. Unfortunately at the restart of operation an anomalous delay in the cooling time of the toroidal magnet suggested stopping operation in order to prevent major problems. Inspections inside the cryostat showed that the N_2 cooling system was obstructed by an accumulation of "perlite" in the ducts and filters, necessitating a complete check and refurbishment of the cooling system. To take advantage of this forced stoppage of the experimentation, a maintenance programme was implemented on the diagnostics. In particular, the Thomson scattering system, blow–off lasers and the ultraviolet SPRED system were refurbished. Visible Bremsstrahlung and H–alpha detection systems were upgraded to allow measurement of the large dynamics in the emission required by the new regime of operation at high density in the presence of lithizated walls.

A major effort was put into the soft–x–ray tomography systems. Both cameras were removed from the machine: i) a small vacuum leakage on the horizontal camera was fixed by modifying the output flange and connectors, and some Be windows were replaced; ii) the vertical camera was completely rewired thereby obtaining a significant improvement in the signal–to–noise ratio, which will allow full exploitation of the tomography system with the two arrays. In general the development of the soft–x–ray diagnostics, including tomography, for real–time application was the central topic of the collaboration with the French Commissariat à l'Energie Atomique (CEA).

Deeper data analysis was carried out on existing and recent FTU experiments. The results were summarised in an overview, to be published in a special issue of Nuclear Fusion, and five accompanying papers at the 22nd International Atomic Energy Agency (IAEA)–Fusion Energy Conference (FEC) in Geneva.

Understanding of dust dynamics in the plasma periphery progressed through further analysis of previous FTU experiments, which confirmed the evidence of hypervelocity particles (velocity >3–5 km/s). A new highly porous, very low density material, silica Aerogel, was characterised before insertion in FTU as a dust collector. The design of an electro-optical probe for hypervelocity dust detection has initiated.

A scan of lower hybrid power and plasma parameters was initiated on FTU to systematically test the electron fishbone theory developed in Frascati. A detailed analysis of hard x–rays emitted by the supra-thermal electrons generated by 0.5 MW of lower hybrid power has already shown evidence of the spatial redistribution of fast electrons, on the fishbone-mode time scale ~100 μs. The effective consequence on fast electron transport is visible from the emission profiles obtained by integrating on 3ms sliding windows during the mode activity.

Successful FTU results on using electron cyclotron resonance heating (ECRH) to avoid plasma disruptions were confirmed by experiments on ASDEX Upgrade conducted in a collaboration between ENEA–National Research Council (CNR–IFP) and the German Institute for Plasma Physics (IPP) Garching. The plasma disruptions, observed in Asdex Upgrade, induced by the density limit, have been avoided by ECRH power. Further experiments are also scheduled on TCV in a collaboration between ENEA–CNR(IFP) and the Swiss Research Centre on Plasma Physics (CRPP) Villigen.

The new high-density regime (highly peaked profiles and up to ~1.6 times the Greenwald limit) obtained in FTU with lithizated walls was carefully studied. Transport analysis of these discharges shows a 20% enhancement of the energy confinement time, with respect to the ITER97 L–mode scaling, correlated with a threshold in the peaking factor.

The formal theoretical analyses conducted by the Frascati group have led to deeper physical insights and, when applied to experimental observations, have motivated further and more focussed experiments on FTU. Major examples are represented by nonlinear Alfvén mode excitations by a large magnetic island (MiAE) and electron fishbones.

Participation in the JET experimental campaigns was increased to some extent. Six experimental campaigns (C20–C25) were executed in 2008 with ENEA's involvement mainly focussed on JET EP2 enhancement and in the realisation of advanced scenarii experiments.

Activities with regard to the Fusion Advanced Studies Torus (FAST) concentrated on optimisation of the conceptual design, taking into account suggestions that emerged in discussions with colleagues from the EU associations. The status of the project was also presented in an oral and four accompanying posters at the 22nd IAEA–FEC Conference in Geneva and submitted to Nuclear Fusion.

1.2 FTU Facility

Summary of machine operation

During 2008 several events prevented regular operation of FTU. At the beginning of the first experimental campaign, after problems with the cryogenic and vacuum systems in February, a major failure occurred in the motor flywheel generator (MFG3). A short circuit on the rotor electrical bars was detected by visual inspection and electrical measurements. ANSALDO had to carry out a very complex operation to extract the rotor from the stator. The damaged parts were then substituted and the rotor was reassembled in situ. At the same time, the device was completely overhauled to guarantee full efficiency. It should be noted that it was the efforts and support of ANSALDO that made it possible to have MFG3 on line at the beginning of September, i.e., five months after the major accident.

The second experimental campaign started in the middle of September, but was also characterised by several problems. The most important was the lengthening of the cooling time of the device. The cryostat was opened to inspect the ducts and filters of the cooling circuit and an obstruction caused by "perlite" deposition was removed from the cooling ducts.

The machine was the greatest source of downtime with a 44.5% share (fig. 1.1).

Table 1.I – Summary of FTU operations in 2008

	Jan.	Feb.	March	April	May	June	July	Aug.	Sept.	Oct.	Nov.	Dec.	Total
Total pulses (p)	0	48	35	0	0	0	0	0	114	142	172	11	522
Successful pulses (sp)	0	44	28	0	0	0	0	0	96	125	146	10	449
I(sp)		0.92	0.80						0.84	0.88	0.85	0.91	0.86
Potential operational days	0.0	2.5	6.0	0	0	0	0	0	9.0	14.5	12.0	4.0	48.0
Real operational days (d)	0.0	2.5	2.0	0	0	0	0	0	5.0	5.5	9.5	1.0	25.5
I(ed)		1.00	0.33						0.56	0.38	0.79	0.25	0.53
Experimental minutes	0	881	484	0	0	0	0	0	1743	2267	2923	187	8485
Delay minutes	0	740	1010	0	0	0	0	0	1349	1131	3134	431	7795
I(et)		0.54	0.32						0.56	0.67	0.48	0.30	0.52
A(sp/d)		17.60	14.00						19.20	22.73	15.37	10.00	17.61
A(p/d)		19.20	17.50						22.80	25.82	18.11	11.00	20.47

Delay per system (minutes)

	Jan.	Feb.	March	April	May	June	July	Aug.	Sept.	Oct.	Nov.	Dec.	Total	%
Machine	0	646	325	0	0	0	0	0	89	82	1910	419	3471	44.5
Power supplies	0	47	665	0	0	0	0	0	576	485	682	12	2467	31.6
Radiofrequency	0	0	0	0	0	0	0	0	0	0	0	0	0	0.0
Control system	0	0	0	0	0	0	0	0	173	52	0	0	225	2.9
DAS	0	0	20	0	0	0	0	0	218	60	190	0	488	6.3
Feedback	0	0	0	0	0	0	0	0	0	268	0	0	268	3.4
Network	0	0	0	0	0	0	0	0	0	0	0	0	0	0.0
Diagnostic systems	0	0	0	0	0	0	0	0	3	3	120	0	126	1.6
Analysis	0	0	0	0	0	0	0	0	191	152	91	0	437	5.6
Others	0	44	0	0	0	0	0	0	99	29	141	0	313	4.0
TOTAL	0	740	1010	0	0	0	0	0	1349	1131	3134	431	7795	100

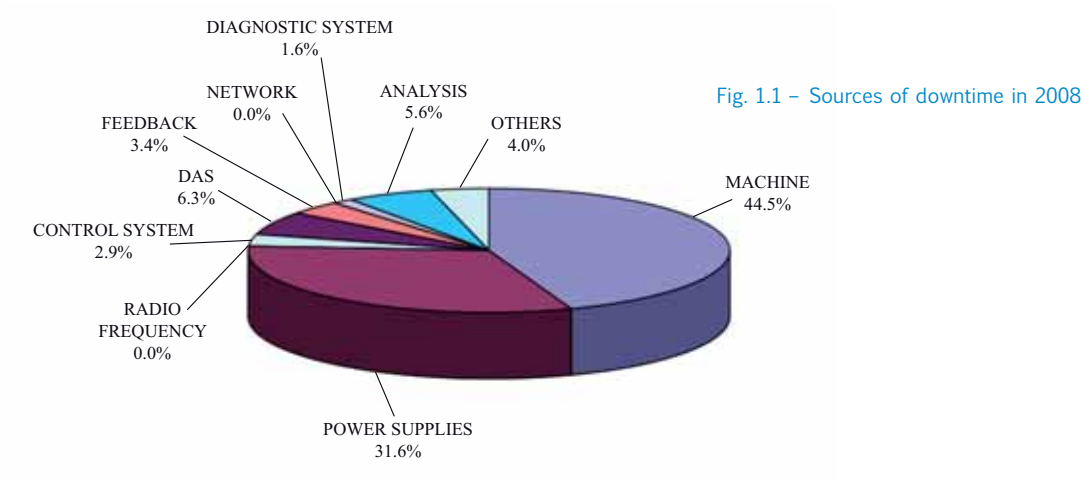

Fig. 1.1 – Sources of downtime in 2008

During 2008, 449 shots were successfully completed out of a total of 522 performed in 25.5 operational days. The average number of successful daily pulses was 17.61. Table 1.I gives a summary of the data.

Control and Data Acquisition System. The following activities were carried out:

- Development of the new architecture of the general data acquisition system continued: a compact PCI system was purchased and will be used as a prototype, using the LabView development software. The system is made up of 128 analog inputs, 12 timers/counters and an Intel Core Duo CPU.
- A new statistical and messaging system (hardware and software) provides information to the FTU control room during experiments and produces useful statistical data about machine availability.
- A new MATLAB tool displays slow analog signals (e.g., temperatures and vacuum measurements) from the FTU plants.
- The F coil anti–windup algorithm, designed to suppress current control instability in the low regime of operation, is still being debugged.
- To control plasma elongation by using the V coil, a new algorithm has been implemented and will be tested according to the experimental session requirements.
- ENEA participated in the ITER CODAC review process, contributing to the definition of the technical specifications of the system.

Web activity. The English version of the ENEA–Fusion website and revision has nearly been completed according to Italian law and international directives about site "accessibility". A full version of a Web file sharing facility with archive and database functions is under completion.

ITM task force Gateway

The European Fusion Development Agreement (EFDA) Integrated Tokamak Modelling (ITM) Gateway project started in October 2007 was commissioned at the end of January 2008. Access to the restricted Infrastructure and Software Integration Project (ISIP) Users Group was allowed in order to install and configure ITM software tools (scientific libraries, public domain software and message–passing middleware for parallel applications). This first phase continued until the end of February 2008.

The Gateway hardware resources consisting of a cluster of 16 HPC nodes in a multicore architecture with an Infiniband_based interconnection were delivered at commissioning date and achieved a peak performance of ≈1 TFlops, 3 front–end nodes and ≈100 TB of shared and fast storage data area, including server infrastructures. The ENEA Portici CRESCO Data Centre housing the Gateway has supplied all hosting services, such as 1Gbps WAN link, electrical and cooling systems and data backup service. The final costs of the Gateway hardware remained within the project budget (≈360 k€). The Gateway hardware/software resources were delivered to the ITM User Group at the beginning of March 2008 and standard operations started under the responsibility of the Gateway Operation Steering Group, which supports the Gateway User Board requests. The group provides full–scale support to ITM users to allow them to develop ITM software and data–access facilities. Users' accounts and software repository project management tools and a trouble ticket system to support the users' help desk were also delivered. About 100 users accessed the Gateway during 2008 and began compiling their own codes and testing (successfully) the ITM software tools.

1.3 FTU Experimental Results

X–tomography: status of soft–x–ray diagnostic

Soft–x–ray radiation emitted from the plasma in the energy range from 1 to 15 keV is detected with a set of silicon diodes and a large number of collimated lines of sight. The system includes a horizontal and a vertical camera with 68 horizontal and 44 vertical lines of sight which cover the whole vacuum vessel from the centre to the edge, in a single poloidal cross section. The energy range is determined by a set of 50–μm–thick beryllium windows located in front of all the collimators. The detected signals represent the soft–x emissivity of the plasma integrated on the energy range and on the line of sight. All these signals are acquired at high frequency (200 kHz) during the whole discharge (1.9 s) to obtain a time resolution of 5 μs. Data are analysed to calculate the profile of soft–x brilliance (W/m^2) as a function of minor radius, in both a horizontal and a vertical view, and the 2D local soft–x emissivity (W/m^3) inside the plasma via tomographic reconstruction.

The 2D tomographic reconstruction technique is based on the geometry of plasma surfaces, which are described by a generalisation of Lao–Hirschman geometry and fitted with the equilibrium reconstruction. This technique is quite different from other standard inversion techniques and presents various advantages due to the minimum physical constraints used in the calculation. In a first step, the emissivity on a point of the outer plasma surface is calculated using the flux of two (or four with two cameras) lines of sight tangent to the plasma surface. Then, the emissivity of the other surfaces is calculated by subtracting the contribution of the outer surfaces from the line integral of other lines of sight. Hence, at each plasma surface, two (or four with two cameras) “calculated local emissivities” allow one to get information on the angle dependence of the emissivity on surfaces.

This diagnostic system is extensively used to investigate magnetohydrodynamic (MHD) activity and impurity transport in plasma discharges. It is particularly used to investigate positions and amplitudes of MHD modes, their structure and dynamics, and to study fast events such as disruptions.

During 2008 the diagnostic was used in some studies on plasma physics presented at the 22nd IAEA Fusion Energy Conference 13–18 October 2008 Geneva, Switzerland [1.1,1.2].

The signals from the vertical camera were affected by strong noise for a long time and remained practically unused. A programme to upgrade the diagnostic system was started in order to obtain a full two-camera tomographic reconstruction and then a better space resolution. Noise on all vertical signals has been reduced to a negligible value by using a new type of cable connection and by taking special care in minimising loops in the circuit geometry. The main advantage of this upgrade is the possibility to obtain two independent profiles of soft–x brilliance and two independent one–camera tomographic reconstructions, one from the horizontal and one from the vertical camera. Moreover, the simultaneous use of signals from the two cameras allows a more accurate two-camera tomographic reconstruction based on the calculation of four plasma emissivities at each plasma surface. As a consequence, a relevant improvement in the investigation of MHD activity can be achieved; for example, a better determination of the mode structure, because four independent modes can be determined at each surface for each toroidal mode number n, or a better determination of the position, dimension and internal structure of magnetic islands, thanks to the better spatial resolution.

Real–time ECRH antenna

The new ECRH launcher. Development of the new electron cyclotron resonance heating (ECRH) fast–steerable launcher [1.3] continued. The prototype of the launching mirror mechanics which enable the required scanning speed (1 cm in 10 ms to track rational surfaces in the FTU) was designed and constructed. The position of the mirror was defined to provide a continuous scanning range in poloidal and toroidal directions during the plasma pulse. The wide range, available in the toroidal angle (up to ±40 degrees), is in fact required (fig. 1.2) for the experiment of over-dense heating (based on O–X–B conversion) to be realised in the high–density plasmas obtained in operations using the liquid lithium

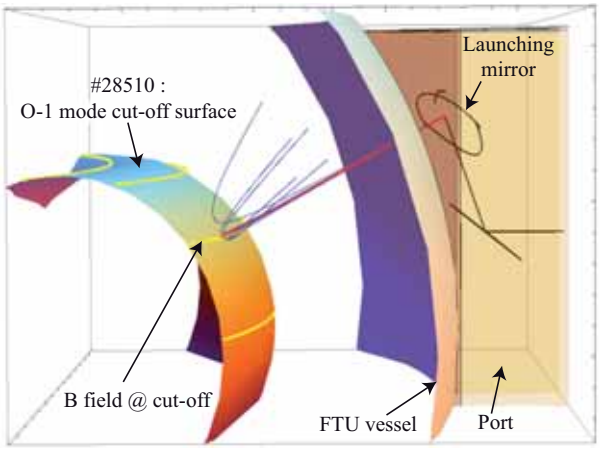

Fig. 1.2 – 3D view of a poloidal section of FTU in the proximity of the new launcher. The O–1 mode cut–off surface, magnetic field lines (yellow) and some rays paths, calculated using the ECWGB ray tracing code, are shown for discharge #28510. The red ray is the only one to be launched with the proper launching angles for optimal O–X conversion; all the other cases (blue) experience reflection at the cut-off surface

limiter [1.4]. The launcher (fig. 1.3) injects two independent beams from symmetrical positions with respect to the horizontal plane. A zooming system composed of two mirrors on sliding mountings allows control of the power deposition width. The launcher design has been optimised so that the antenna can also be used for diagnostic purposes: by switching to low–power lines, a collective Thomson scattering (CTS) experiment in ITER–relevant conditions can be housed in the central part of the launcher. The overall system has also been designed to accommodate double the power. In fact the development of a beam combiner (FADIS [1.5]) will make it possible to inject two gyrotron beams in one line and deliver to the plasma the full ECRH system power. Any increase in temperature of the movable mirrors will be limited by covering the rear side with a high emissivity coating to obtain efficient radiative cooling. Place will be reserved for future arrangements of additional components, such as remote steering waveguides.

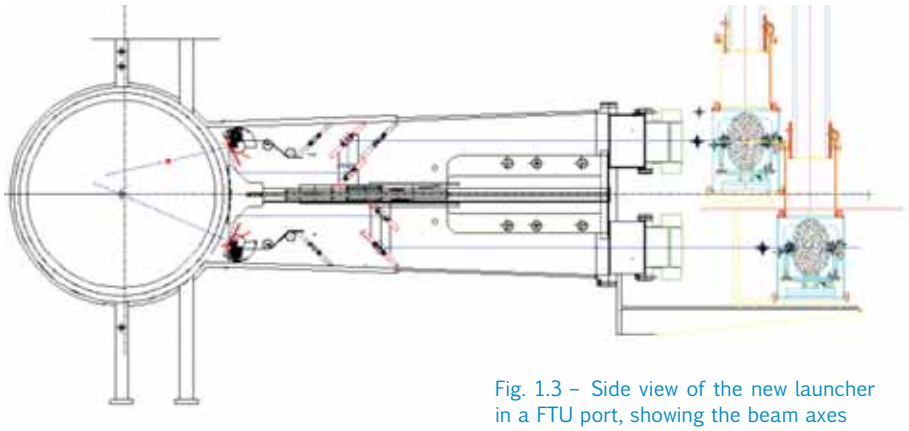

Fig. 1.3 – Side view of the new launcher in a FTU port, showing the beam axes

Soft–x–ray diagnostics

A collaboration was started in 2008 between ENEA Frascati and the Commissariat à l'Energie Atomique (CEA) Cadarache to improve the soft–x–ray diagnostics and the related analysis, with a view to real–time applications. A new technique has been especially developed for determining the detection efficiency of silicon surface barrier diodes (SBD) as a function of the energy of the x–ray photons, in the range 1–25 keV, used for tomography at Tore Supra. The response of these diodes was studied, with different polarizations in the interval 0–120 V, by means of a low–power portable x–ray tube, with the high voltage (HV) ranging between 10 and 25 KV. For each value of HV, several absorbing filters were used (from 0 to 12 aluminium foils, 15 μm thick) to probe the diode response, for the different spectral regions. Measuring the output spectra with a Peltier cooled Si–PIN diode and taking into account the effects of

[1.1] R. Cesario, et al., *Fishbone-like internal kink instability driven by suprathermal electrons on FTU generated by lower hybrid radiofrequency power,* Proceedings of the the 22nd IAEA Fusion Energy Conference (Geneva 2008), IAEA Vienna, on line at http://www.fec2008.ch/preprints/ex_p8-12.pdf

[1.2] A. Biancalani et al., *Shear Alfvén wave continuous spectrum in the presence of a magnetic island*, Proceedings of the 22nd IAEA Fusion Energy Conference (Geneva 2008), IAEA Vienna, on line at http://www.fec2008.ch/preprints/th_p3-5.pdf

[1.3] A. Bruschi et al., *A new launcher for real-time ECRH experiments on FTU*, to be published in Fusion Sci. Technol.

[1.4] A. A. Tuccillo et al., *Overview of FTU results*, Proceedings of the 22nd IAEA Fusion Energy Conference (Geneva 2008), IAEA Vienna, on line at http://www.fec2008.ch/preprints/ov_5-1.pdf and to be published in Nucl. Fusion

[1.5] O. D'Arcangelo et al., *Tests of a 105 GHz prototype diplexer combiner based on square corrugated waveguide*, to be published in Fusion Eng. Des.

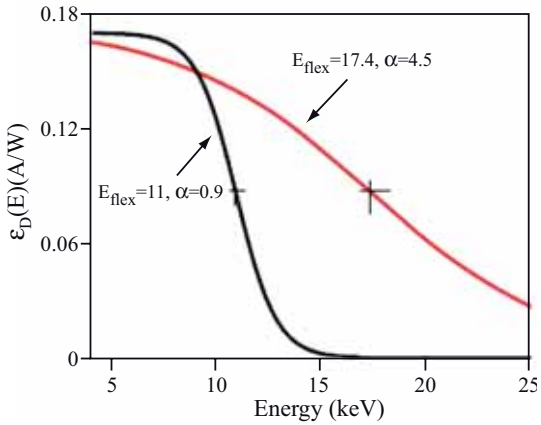

Fig. 1.4 – Best fit detection efficiency of SBD diode with (red line) and without biasing

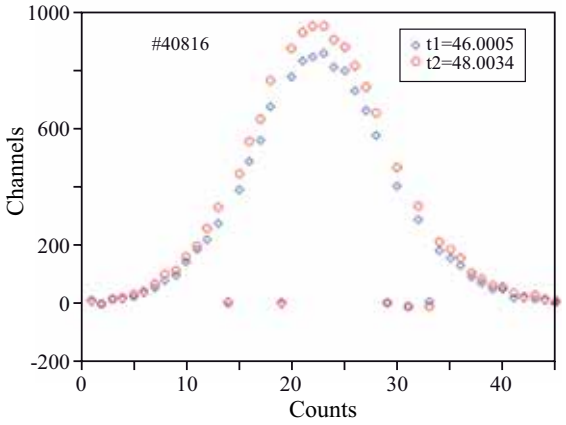

Fig. 1.5 – Spatial profiles of brightness with horizontal tomography SXR camera at Tore Supra at two different times

the different absorbers (air, Be, Al) in front of the detector, the absorption efficiency curve was derived by means of a best fit with a two-parameter function. The result is that this curve is a very sensitive function of the diode polarization. For example, the flex, originally at 11 keV without bias, moves to higher energy when polarization is increased, reaching 17 keV at 55 V (fig. 1.4). This value was found to be the best compromise between wide detection efficiency on the one hand and stability and reliability on the other. Knowledge of the energy dependence of the detection efficiency is crucial to simulate the soft–x–ray (SXR) measurements and derive information on impurities. By acting on the polarization it is possible to change the spectral range where the diode converts the x–ray photons and, by combining the range with suitable absorbing filters, one can tailor the spectral diode response in different energy bands. This could be extremely useful for advanced and more flexible SXR tomography.

The results were used to fully calibrate the tomography SXR cameras of Tore Supra. The diode response as a function of the photon flux was almost linear over nearly three orders of magnitude. Apart from a limited number of faulty detectors, promptly replaced with new ones, the spread of the diode responses (84 detectors) was about 20% of the average value, so it was possible to derive the calibration factor for each detector of the tomography system. A similar calibration was performed for the gains of the electronic chains and showed a lower spread compared to the diode responses. The effect of the room temperature, in the range 15°–40°, was also studied and revealed that up to 35° the linearity of the diode response and the calibration factors remain constant. The calibration greatly improved the data quality and now accurate tomography inversions are possible in a wide set of plasma configurations. This research activity demonstrates the possibility of discriminating slight and localised changes in the 2D spatial distribution of the SXR intensity (fig. 1.5).

Dusty plasmas

During 2008 research activity on dust in tokamaks was carried out in collaboration with the Universities of Naples and Molise, the Royal Institute of Technology (KTH) of Stockholm and the Institute of Plasma Physics (IFP) – National Research Council (CNR), Milan. Despite the lack of new experimental data from FTU, new results were achieved concerning the analysis of previous experiments, the development of the project for dust capture on aerogels and the design of an electro-optical probe for hypervelocity dust detection. A detailed paper on the evidence found in FTU discharges of hypervelocity (i.e., at relative velocity >3–5 km/s) dust impacts on electrostatic probes was published [1.6], improving the previous analysis [1.7]. In particular, it was shown that i) the number of large (>6 rms) amplitude spikes in the ion saturation current collected by an equatorial probe and which can be ascribed to impact ionization events, is roughly equal to the number of the craters (with diameters >10 mm) found by the optical microscope on the probe surface; ii) the largest craters, observed by scanning electron microscope

(SEM), exhibit typical features of impact craters, and no evidence of craters due to unipolar arcs can be detected. It was also pointed out that impact ionization phenomena in a plasma environment are different to those in pure vacuum conditions, and empirical data in vacuum can be used only to evaluate an upper limit of the size and/or of the velocity of the dust grains responsible for impact ionization events. Although no direct evidence of hypervelocity dust impacts was found, further research on this topic seems important for fusion reactor development: the erosion evaluated in the FTU discharges on molybdenum surfaces is of the order of 1 nm/s, which is harmful for reactors, as pointed out during the first meeting of the IAEA Coordinated Research Project (CRP) on Dust in Fusion Devices, held in Wien, 10–12 October 2008. Aerogel targets, widely used to collect hypervelocity cosmic dust, were proposed as a diagnostic for hypervelocity dust in tokamaks. The compatibility of this material with tokamak operations was assessed and it was planned to perform experiments on aerogel target exposure during FTU plasma discharges, using the sample introduction system. Aerogel targets in a magnetic mirror configuration were successfully exposed in the CUSP machine of IFP, as a first step in the development of a diagnostic for nanometer–sized dust particles. The nanometer scale of the highly porous structure of aerogels might indeed provide an ideal method to collect nanoparticles in tokamaks and evaluate their composition and size distribution. Progress was achieved in designing an electro–optical probe to discriminate impact ionization events by simultaneous observation of ion saturation current spikes and the light emission associated with such events. A conceptual scheme of the diagnostic was proposed in a contributed paper at the IAEA fusion conference [1.8]. A review paper on dust diagnostics in a fusion device was also published [1.9].

Fishbone–like internal kink instability driven by supra–thermal electrons generated by LH radiofrequency power

The fishbone–like internal kink instabilities driven by supra-thermal electrons generated by lower hybrid current drive (LHCD) and ECRH power should provide a strong contribution to burning plasma research. The interaction of trapped alpha particles with low-frequency MHD modes in burning plasmas is, indeed, characterised by small dimensionless orbits similar to those of electrons, so that the trapped particle averaged bounce depends on energy, not on mass. Fast electrons on low-frequency MHD modes can usefully give a way to model the charged fusion product effects [1.10].

The new electron fishbone studies in FTU, unlike those in [1.10], are done at lower LH power (≤0.5 MW instead of 1.7 MW) in order to investigate the simpler case of a single burst. The fast electron bremsstrahlung (FEB) camera available on FTU was utilised as the main tool for producing the present work. The original feature of a high time resolution available for data analysis, consisting of the minimum time discrimination of 4 μs (all inclusive), characterises the FEB camera [1.1]. A new tool for MHD data analysis based on SXR tomography [1.11] was also used, together with modelling of the q–profile evolution based on the kinetic and magnetic data of the experiment. In this way the experiment operations necessary for fishbone destabilisation were addressed in order to control, by means of a suitable LH power waveform, the q-profile evolution when approaching $q_{min} \approx 1$ and thereby produce with the necessary precision the conditions indicated by the theory in [1.10].

As the main result, a marked radial distribution of electrons occurs (across layers centred at r/a ≈0.20–0.33) during the dynamic evolution of a fishbone burst (one single mode, no transition [1.10]), as observed by the MHD diagnostic. This is in phase with fishbone oscillation, has the same time scale, and the same radial position of the emission peak seen by the x–ray tomography diagnostic.

[1.6] S. Ratynskaia et al., Nucl. Fusion **48**, 015006 (2008)

[1.7] C. Castaldo et al., Nucl. Fusion **47**, L5 (2007)

[1.8] C. Castaldo et al., *Detection of dust particles in FTU,* Proceedings of the 22nd IAEA Fusion Energy Conference (Geneva 2008), IAEA Vienna, on line at http://www.fec2008.ch/preprints/ex_p4-5.pdf

[1.9] S. Ratynskaia et al., Plasma Phys. Control. Fusion **50**, 124046 (2008)

[1.10] F. Zonca et al., Nucl. Fusion **47**, 1588-1597 (2007)

[1.11] P. Smeulders, *Tomography on Lao-Hirschman type of equilibria using mode rotation*, Proceedings of the 34th EPS Conference on Plasma Physics (Warsaw 2007), ECA Vol. **31F**, P-5.069 (2007) on line at: http://epsppd.epfl.ch/Warsaw/pdf/P5_069.pdf

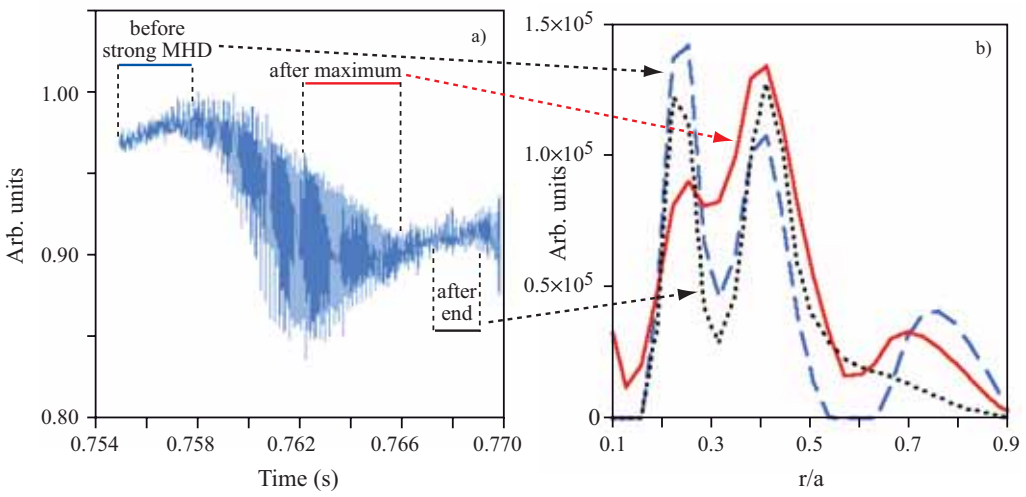

Fig. 1.6 – a) MHD fishbone bursts appearing during the LH power phase (0.5 MW). b) Time–integrated radial profiles of fast electron data by the FEB camera at different time windows: just before and after the maximum, and at the end of the strong MHD occurrence (as indicated in a). The profiles are plotted with the normalised minor radius in abscissa and refer to an energy range of 40 – 60 keV

Figure 1.6a shows MHD fishbone bursts appearing during the LH power phase (0.5 MW) during a shot in which the aforementioned condition of the q-profile evolution indicated by the theory has been experimentally set up. Figure 1.6b represents the time-integrated radial profiles of the fast electron data by the FEB camera. Hard–x analysis displays sliding time windows centred at the beginning (unperturbed distribution), after the burst peak (maximum redistribution) and at the burst minimum (evidence of partial reconstruction of electron distribution). Such evidence of mode nonlinear evolution and supra-thermal electron radial redistributions is consistent with mode nonlinear dynamics [1.10].

The available modelling tools and FTU facilities (lithizated vessel, LHCD system and the new high precision analysis tool for FEB data) were useful for performing an accurate search for the electron–fishbone–like instability, which is expected to occur for $q_{min} \approx 1$. Due to the relatively slow current diffusion intentionally obtained during the experiment by utilising the lithizated vessel, this search could be extended to the fishbone-like instability expected to occur also for $q_{min} \geq 2$. In the latter case, it would be sufficient to perform LH coupling by properly advancing the radiofrequency (rf) power waveform, as the modelling indicates ($t \geq 0.15$ s). Also higher LH power (up to 2 MW) than in the related experiments would be utilised. This study will be performed in the next experiments planned on FTU.

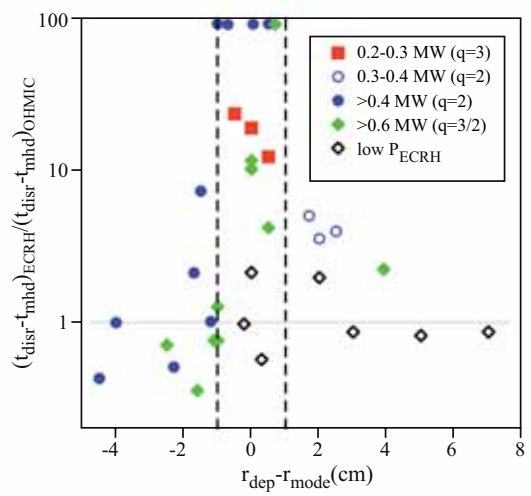

Fig. 1.7 – Results of r_{dep} scan in FTU for Mo–injection and density limit disruptions; t_{disr}=disruption time; t_{mhd}=MHD activity starting time (corresponding to the onset of the strong MHD activity preceding the disruption), r_{mode}=mode location; r_{dep}=ECRH deposition location

Disruption control on FTU and ASDEX Upgrade with ECRH

A possible method to control disruptions and thereby avoid them is given by the use of ECRH. Experiments have been carried out in FTU, based on the concept of triggering a disruption in stationary plasma and then injecting ECRH power by using a precursor signal (loop voltage) as a real-time automatic trigger. The localised injection of ECRH on a rational surface, leading to the stabilisation of MHD modes, has been found to delay or avoid the disruption (fig. 1.7). Experiments have been carried out in FTU on disruptions induced by impurity (Mo) injection and density limit by strong gas puffing [1.12]. The same experiments were proposed and carried out in June 2008 on ASDEX Upgrade as a

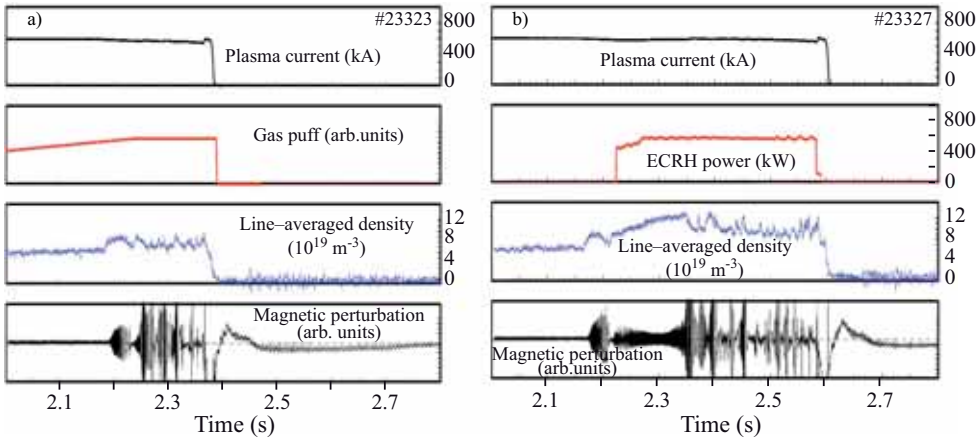

Fig. 1.8 – ASDEX Upgrade density limit experiments: a) reference disruption; b) with ECRH injection on the q=2 surface

collaboration between ENEA Frascati, IFP Milan and the Plasma Physics Institute (IPP) Garching. It was confirmed that when ECRH is absorbed on the q=2 rational surface the disruption in L–mode plasmas (I_p=0.6 MA, B_T=2.5 T, P_{ECRH}=0.6 MW~P_{OHM}) is delayed. The injection of ECRH close to q=2 significantly delays the 2/1 onset and prolongs the duration of the discharge (fig. 1.8). Mode control is then lost when the increase in density (which was not feedback-controlled during this phase) moves the power deposition progressively outside the q=2 surface.

Liquid lithium limiter experiment: transport analysis

A liquid lithium limiter (LLL) based on the capillary porous system (CPS) [1.13,1.14] has been installed on FTU since 2005. The LLL experiment is aimed at studying plasma performance in the presence of lithizated walls and at testing the CPS capability to confine liquid lithium in the presence of the heavy heat loads that FTU can produce. Since its installation operations have benefited from faster restarts after shutdowns, clean operations with $Z_{Eff} \sim 1$ in a wide range of densities and easy access to high density, up to 1.6 times the Greenwald limit. Interestingly, a strongly peaked density profile is obtained up to the highest density values, which for many aspects recalls that obtained in pellet–fuelled discharges [1.15]. In lithizated discharges intrinsic metallic impurities (Mo, Fe, Ni) are strongly reduced ($Z_{Eff} \sim 1$), while an increase in temperature in the scrape–off layer (SOL), with respect to that measured in ordinary non–lithizated ohmic discharges, is measured by the Langmuir probes, both at I_p= 0.5 MA and I_p = 0.75 MA [1.16].

A large database of ohmic discharges obtained with the LLL points out some peculiar aspects of enhanced confinement behaviour. A detailed transport analysis as well as a study of the confinement properties of the new scenario were performed, focussing in particular on comparison with the results of analogous studies on the bulk of ohmic "pre-lithium" FTU discharges [1.17]. The analysed database contains discharges with I_p=0.5 MA, B_T=6 T, $\bar{n}_e$=0.6–2.8×10^{20} m^{-3} and a few discharges at higher plasma current (0.7–0.75 MA).

Transport analysis was performed with the JETTO code [1.18], taking as input the Z_{Eff} evolution from visible bremsstrahlung signals and the electron temperature and density profiles from Thomson

[1.12] B. Esposito et al., Phys. Rev. Letts **100**, 045006 (2008)

[1.13] M.L. Apicella et al., J. Nucl. Mater. **363-365**, 1346 (2007)

[1.14] G. Mazzitelli et al., *Status and perspectives of the liquid material experiments in FTU and ISTTOK*, Proceedings of the 22nd Int. Conf. on Fusion Energy (Geneva 2008), IAEA Vienna, on line at http://www.fec2008.ch/preprints/ex_p4-6.pdf

[1.15] G. Mazzitelli et al., *Experiments on FTU with a liquid lithium limiter,* Proceeding of the 34th EPS Conference on Plasma Physics (Warsaw 2007), ECA Vol. **31F**, O2.001 (2007), on line at: http://epsppd.epfl.ch/Warsaw/pdf/O2_001.pdf

[1.16] V. Pericoli-Ridolfini et al., Plasma Phys. Control. Fusion **49**, S123 (2007)

[1.17] B. Esposito et al., Plasma Phys Control. Fusion. **46**, 1793 (2004)

[1.18] G. Cenacchi and A. Taroni, Proceedings of the 8th Computational Physics, Computing in Plasma Physics (Eibsee 1986), EPS Vol. **10D**, 57 (1986)

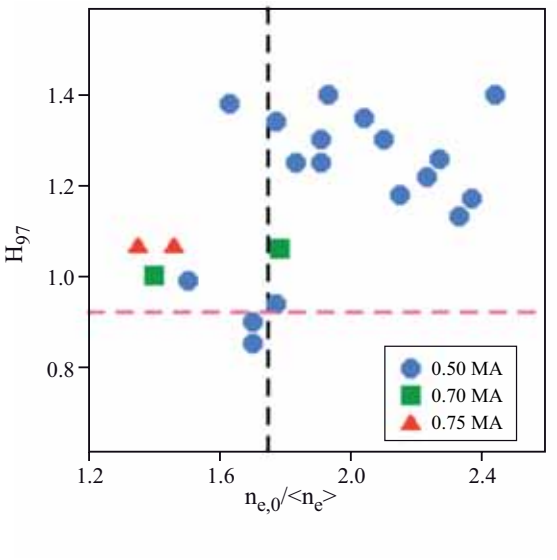

Fig. 1.9 – H_{97} vs volume peaking factor in lithizated discharges

scattering and CO_2 interferometer diagnostics, respectively. The ion temperature profile is derived by assuming a neoclassical transport model with an "anomalous" multiplicative coefficient calibrated on the constraint of matching the experimental neutron rate. The radiation power density profile was derived from bolometry, taking into account spectroscopy data on the impurity concentrations (mainly Li and a very small fraction of O).

In all the analysed discharges ion transport is neoclassical with an anomaly coefficient close to 1. In high (and peaked profile) density discharges a sharp transition from a low to a higher energy confinement regime occurs as soon as the density profile effectively begins to peak at typical threshold values of 1.75–1.8. The improved confinement results in an enhancement of the ITER97 L-mode scaling (H_{97}), which increases from $H_{97} \cong 0.92$ to $H_{97} \cong 1.25$.

The transport analysis shows that in the peaked high-density phase electron thermal conductivity (χ_e) is about a factor of two lower than in the non–peaked phase and has a value of ~0.2 m^2/s, which is typical of the saturated ohmic confinement (SOC) regime [1.17]. However, in the peaked phase heat transport continues to be dominated by electron conductivity, whilst ion conductivity remains very low and quite close to its neoclassical value. Analysis of the entire database of lithizated discharges (n_e ranging from 0.6 to 2.8×10^{20} m^{-3}) confirms the existence of a threshold in the peaking factor at which the improved confinement regime described above appears.

The results of the analysis are reported in figure 1.9, which shows the enhancement of the ITER97 L–mode scaling of energy confinement time, (H_{97}) vs the volume peaking factor ($n_{e0}/<n_e>$). The presence of a second regime of better confinement, up to a factor of 1.4 above $\tau_{ITER97-L}$, is obtained as the general behaviour of lithizated discharges, at least at I_p=500 kA. The few cases analysed at 700 and 750 kA are also reported in the figure, but more data should be considered in order to tell whether an analogous transition also occurs at higher currents. It is important to note that, regardless of the density value, almost all the lithizated–wall discharges tend to peak the density profile above the threshold value [1.19].

Fig 1.10 – Top view and cross section of the panel liquid limiter for FTU

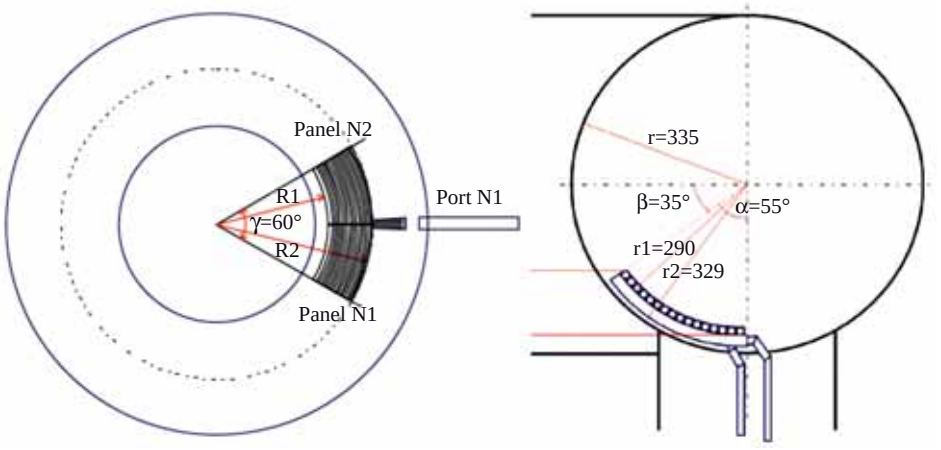

A statistical comparison between τ_E of the lithizated discharges with that of the pre–lithium FTU ohmic discharges, both gas-fuelled and pellet–fuelled in the SOC phase, shows that the presence of lithizated walls produces a rise in the saturated confinement threshold value, from about 45–50 ms to about 65–70 ms. As in

the case of pellet fuelled discharges, this behaviour is accompanied by a sharp increase in the peaking of the density profile and by full neoclassical ion transport.

The technological aspects of using a metallic liquid divertor on the Fusion Advanced Studies Torus (FAST) and/or the first wall of DEMO require new developments. It would be desirable to build a limiter able to act as the main limiter and to demonstrate its capability to be cooled and refuelled during the plasma discharge on FTU. The proposal is to insert a wide panel (~60° in the toroidal direction) in the bottom of FTU as illustrated in figure 1.10. Initially, a single base element of the panel will be inserted on FTU using the same mechanical structure as built for the actual LLL [1.14], but including the full cooling and lithium refilling system. If the single base element experiment is successful, the complete panel limiter will be mounted later on.

A programme on diagnostics for ITER

The programme on developing diagnostics for ITER started in 2006. Proposals were presented and discussed by the ENEA Frascati scientific community. The results were presented at the meeting of 12th International Tokamak Physical Activity (ITPA) Topical Group Diagnostics at Princeton (March 2007), where the programme was discussed and found coherent with the high priority R&D needs for ITER as identified by the ITPA.

A set of high priority systems was therefore chosen to be implemented during 2007-2008:

- Dust-detection techniques.
- Proposal for evolution of the FTU collective Thomson scattering in ITER–relevant direction.
- Refractometry to measure the density line-integral.
- First mirror test.

A new proposal concerning diagnostics for ITER was elaborated in 2008 in collaboration with Forschungzeuntrum Julich (FZJ) and TRINITI, Russian Federation and presented at the High–Temperature Plasma Diagnostic Conference (2008). The aim of the diagnostics is to detect the fast displacement (~5 ms) of alpha particles occurring inside the plasma because of interactions with Alfvén waves.

Dust dynamics (for safety, divertor and plasma–wall interaction)

Safety. The dynamics of dust during an accident is being studied in a model experiment named STARDUST, which is a small linear device developed in collaboration with the University of Rome Tor Vergata. A new device with toroidal symmetry has also been considered in recent studies. Simulation codes have been developed to predict the behaviour of the fluid during an accident. Diagnostics for measuring the flow of the dust, density, species and for imaging the flow dynamics are being considered.

Divertor and plasma–wall interaction. The dynamics of dust after a disruption is being studied with the Thomson scattering system on FTU and recently on JET.

Demonstration of collective Thomson scattering in ITER–relevant conditions. The collective Thomson scattering (CTS) diagnostic of ITER will be based on the injection of a millimeter–wave beam at a frequency below the first electron cyclotron (EC) resonance. The two CTS experiments presently running on ASDEX and TEXTOR make use of frequencies between the first and the second EC harmonics. These propagation conditions can be reproduced only in a high-field device such as FTU. In previous CTS experiments performed in FTU, where an in-vessel launcher inserted in one of the vertical ports was used, however, the spectra observed (fig. 1.11a) were affected by perturbation of the gyrotron output induced by spurious reflections in the launching antenna, while the bandwidth of the expected spectra was of the order 300 MHz. Dedicated measurements showed that similar spectra were present also in

[1.19] M. Romanelli et al., Nucl. Fusion **46,** 412 (2006)

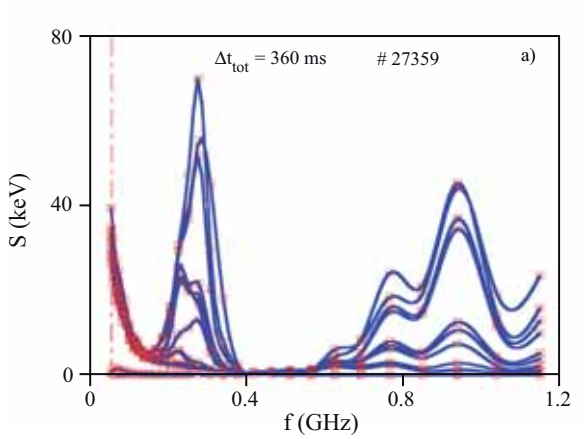

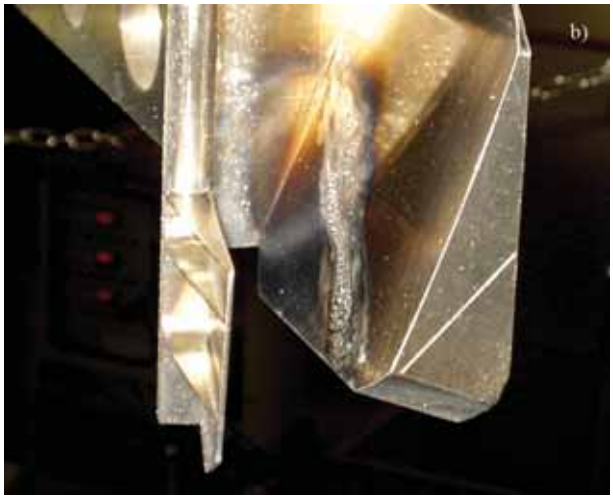

Fig. 1.11 – a) Example of strong anomalous spectra, including spectral lines, possibly ascribable to secondary gyrotron modes excited by back reflections. b) Well-localised damage on the mirrors of the former CTS launching antenna

the launched radiation. The reflections are ascribable to the crossing of the EC resonance (and of the X-mode cut-off very close to it) in the beam injection port. This was confirmed by inspection of the launching mirrors showing that damage had occurred in the last mirror near the resonance layer (fig. 1.11b). Due to the similar conditions, the problem of possible back-reflections also extends to ITER. It is therefore necessary to demonstrate the feasibility of CTS in the same conditions as envisaged for ITER, and this can be done only in FTU. In this perspective a new CTS experiment in the ITER-relevant configuration has been started in FTU, using two lines of the ECRH launcher as CTS antennas.

A time-of-flight refractometer proposed for ITER line-density monitor. Time-of-flight (TOF) refractometry is based on the measurement of the delay time of a small package of rf waves crossing the plasma and reflected back by the inner wall of the tokamak vacuum vessel (double-pass horizontal probing). As the distance travelled by the waves is constant, this is a direct measurement of the wave group velocity [1.20,1.21]. Using the cold plasma refractive index (for the X mode), the delay time can be related to the line-integrated density of the plasma (when $f_p << f_c, f$)

$$\tau_{gr,X} \approx k \cdot \frac{f^2 + f_c^2}{(f^2 - f_c^2)^2} \cdot \int_l N(z)dz \qquad (1)$$

where k is a numerical coefficient, f the probing wave frequency, f_c the EC frequency at the centre of the plasma column, f_p the plasma frequency and N is the plasma density [1.22].

Refractometry, using long wavelengths (frequency about 60–100 GHz on X-mode for ITER), does not employ a polished mirror for the reflection, but any metallic surface present in the inner wall of the vacuum vessel. The launcher and the receiver are metallic hornets without stringent constraints and can be located in any position. These characteristics make refractometry very attractive for ITER density measurements, as using a plasma-facing mirror is quite a problem. The working density and magnetic field in ITER are similar to those of FTU, and even though the sizes are much smaller, FTU is a very

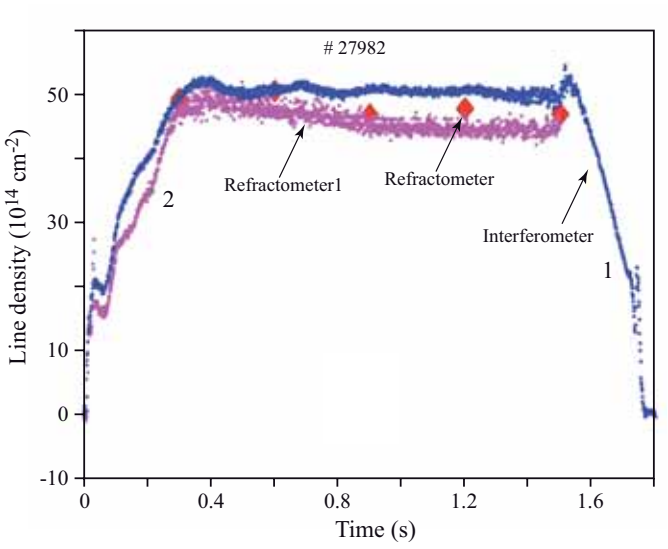

Fig. 1.12 – Density measured by the interferometer (blue dots) compared with density obtained by the refractometer (purple dots) using a fixed profile approximation and taking the experimental density profile into account (red diamonds)

Fig. 1.13 – Holder for mirror exposure in the FTU SOL

good test bench for this diagnostic. A TOF refractometer borrowed from the TRINITI laboratory was used on FTU for a first test (fig. 1.12).

First mirrors. The production and characterisation of rhodium–coated metallic mirrors continued in the framework of the work programme on ITER–Relevant First Mirrors of the ITPA Topical Group on Diagnostics. A collaboration was established with CNR Milan to compare different deposition technologies. Mirror holders suitable for testing mirror exposure in FTU were manufactured and inserted in the FTU scrape–off layer (SOL) with the use of the sample introduction system (fig. 1.13). An agreement was made with the National Institute of Nuclear Physics (INFN) to test the effect of ITER–relevant SXR fluence on protective dielectric coatings deposited on metallic mirrors. The test mirrors, provided by the Kharkov Institute of Physics and Technology (Ukraine) and the Ioffe Physical Technical Institute (Russian Federation), will be exposed to the x-ray source of the INFN DAFNE facility.

KU1 and KS–4V substrate SiO_2 overcoated Al mirrors. The commercially available high–quality mirrors (ultraviolet–visible–near–infrared range) being considered for diagnostic systems and remote handling applications in ITER consist of a thin evaporated aluminium reflective layer on a solid glass substrate, usually Pyrex (borosilicate) glass, which is protected (overcoated) with a suitable dielectric (SiO, SiO_2, MgF_2) layer. Previous work on overcoated dielectric mirrors identified several radiation problems, including degradation of ultraviolet–visible reflectivity due to coating thickness and/or refractive index modification, unreliability of manufacturers' specifications (e.g., HfO_2 coating instead of MgF_2 with a possible transmutation problem), and also conversion of SiO coatings to SiO_2 leading to coating swelling and cracking.

Irradiation work has so far been carried out using gamma sources; however, to examine the stability of reflectivity and coatings following neutron irradiation it is necessary to overcome the problem of activation of the Pyrex glass substrate due to the boron content. Boron has a large low energy neutron capture cross–section and causes severe limitations for post–irradiation examination (PIE). To surmount this difficulty prototype mirrors were prepared with the standard Pyrex substrate support being replaced by high purity silica provided by CIEMAT in the context of a collaboration with ENEA (KU1 and KS–4V from the Russian Federation). To avoid the SiO to SiO_2 conversion problem, in collaboration with ENEA the Al layer was overcoated with SiO_2. X ray photoelectron spectra analysis of the surface was performed and showed the overcoating to be ≈100% SiO_2. The reflectivity (fig. 1.14) of these prototype mirrors from the ultraviolet to infrared (200 to 2500 nm) was examined and showed high reflectivity (>80%), even down to 200 nm.

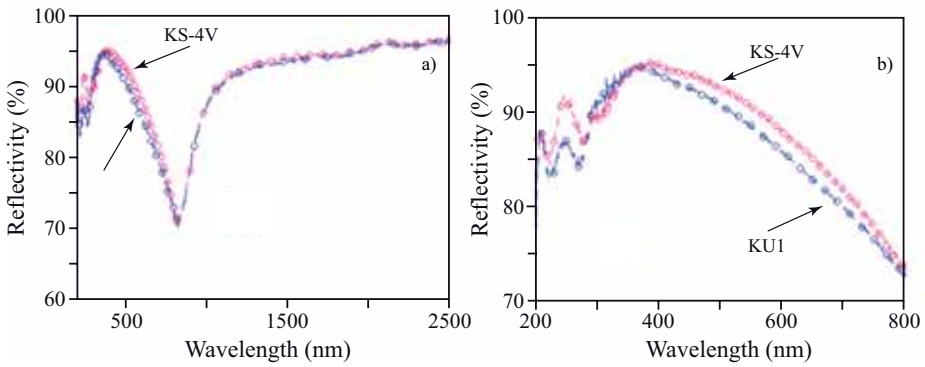

Fig. 1.14 – Reflectivity of SiO_2 coated Al on KU1 and KS–4V substrates. a) Full wavelength range; b) enlargement of low wavelength range

[1.20] V.G. Petrov, A.A. Petrov and A.N. Romannikov, *Time-of-fligth refractometry for robust line-averged density and plasma vertical position measurements on the T-11M tokamak*, Proceedings 29th EPS Conference on Plasma Physics and Controlled Fusion (Montreux 2002), ECA Vol. **26B** (2002), P–4.127

[1.21] A.A. Petrov et al., Plasma Phys. Reports **28**, 10, 806–813 (2002)

[1.22] A.A. Petrov, V.G., Rev. Sci. Instrum. **74**, 1465 – 1469 (2003)

New fast–ion diagnostic based on CXRS on heating beams. The problem of detecting the fast displacement of alpha particles as a consequence of interaction with Alfvén eigenmodes can be solved by using active spectroscopy on heating beams.

It has been demonstrated [1.23], using a model benchmarked on JET data, that it is possible to detect the fast displacement of alpha particles with a time resolution of 5 ms and a space resolution of 15 cm by using the visible light from active charge exchange recombination spectroscopy (CXRS) on heating beams. This light can be collected on equatorial port #3, using the periscope already used for the MSE system.

This proposal is being considered by the US team which is developing the ITER MSE system. Possibly, the concept of this new system could be tested on JET.

1.4 Plasma Theory

Theoretical research has mainly addressed the complex behaviour characteristic of burning plasmas. The research has been concentrated on issues ranging from fundamental dynamics to their application in experimental observations, connecting them by means of advanced numerical simulations that exploit the latest massively parallel architectures for high–performance computing. All these efforts have had a significant impact on the FAST conceptual design. (See the section on FAST for the activities specific to this project.)

Formal theoretical analyses have lead to deeper physical insights and – when applied to experimental observations – have often motivated further and more focussed experiments, as in the case of nonlinear Alfvén mode excitations by a large magnetic island in FTU.

Similar considerations apply to the observation of fishbones at unexpectedly high frequencies in JET, which is well interpreted as experimental evidence of high–frequency fishbones in the geodesic acoustic mode (GAM) and beta-induced Alfvén eigenmode (BAE) frequency range.

Since the relationship of MHD and low–frequency fluctuations of the shear Alfvén wave (SAW) spectrum with micro–turbulence has important implications for the long time scale dynamic behaviour in burning plasmas, the effects of trapped particle dynamics on the structures of low–frequency SAW continuous spectrum have been investigated.

Massively parallel numerical simulations have been performed with the hybrid MHD gyrokinetic code (HMGC). In particular, HMGC was used to investigate energetic ion transport and fully nonlinear Alfvénic fluctuations for a reversed shear, strongly beam heated, DIII–D discharge.

A completely new version of HMGC, solving the fully compressible gyrokinetic energetic ion dynamics in general geometry, has been implemented and is being tested.

Furthermore, in order to address a number of burning plasma physics issues, e.g., fast ion transport due to collective mode excitations and cross–scale couplings of micro–turbulence with meso–scale fluctuations due to energetic particles themselves, various research projects are being pursued in the framework of international collaborations.

Fundamental properties of rf wave interactions with burning plasmas have been investigated with the use of asymptotic analyses for the separation of scales in the integro–differential system describing LH wave propagation and with Hamiltonian perturbation theory methods.

Shear Alfvén wave continuous spectrum in the presence of a magnetic island

The well–established collaboration between ENEA Frascati, the University of Pisa and the University of California at Irvine (UCI) to study shear SAW nonlinear behaviour continued. The work entailed strong

connection and synergy between theory and experiments. The SAW continuous spectrum was calculated for finite–β tokamak equilibria in the presence of a finite–size magnetic island, adopting a slab model and constant–Ψ approximation near the corresponding rational surface. It was shown that the BAE continuum accumulation point (CAP) [1.24–1.26] had not changed in frequency but had merely shifted in space. The most remarkable feature was found to be the presence of new CAPs at the O–point of the island. This fact was shown to be important for its implication on the existence of new magnetic–island–induced Alfvén eigenmodes (MiAEs), excited via wave–particle resonances provided that the island size be sufficiently wide with respect to the mode radial localisation. The value of the MiAE–CAP frequency was calculated, neglecting the metric variations along the field lines, and compared with the preliminary experimental data of modes with frequency belonging to the same range [1.27].

Following the same guideline, the theoretical analysis of the SAW continuous spectrum has been improved to include higher order effects of magnetic island flux surfaces geometries in the SAW dynamics [1.2]. In particular, the high–eccentricity of the field lines, corresponding to perturbatively small magnetic islands, was studied, giving the MiAE–CAP frequency:

$$f_{MiAE-CAP} = f_{BAE-CAP}\sqrt{1+q_0|s|n_{isl}^2\frac{B_{isl}}{B_{pol}}\frac{f_A^2}{f_{BAE-CAP}^2}\left(l^2-1\right)} \quad , \qquad (2)$$

with $l=1,2,\ldots$. Here q_0, s, and B_{pol} are, respectively, the values of the safety factor, shear and poloidal magnetic field calculated at the rational surface of the island, while B_{isl} is the amplitude of the island radial magnetic field with n_{isl} the toroidal mode number and f_A the Alfvén frequency, $f_A=v_A/(2\pi qR)$, with $f_A=B/\sqrt{4\pi\rho}$ and ρ the mass density.

The theoretical MiAE–CAP frequency was compared with new FTU experimental data of low–frequency modes. Theoretical analyses showed that these modes could be interpreted as BAE modes [1.28], yet their measured frequency has been found to depend on the island amplitude as well. The magnetic island width was measured with a soft–x–ray diagnostic, and the magnetic island fluctuating field at the rational surface was reconstructed from the magnetic fluctuating field at the Mirnov coil position. As a result of this procedure, the observed mode frequency dependence on the magnetic island width was studied and found to be consistent with the MiAE CAP scaling [1.2].

High–frequency fishbones at JET: theoretical interpretation of experimental observations

The following activity is an ongoing collaboration with the UCI, US and the Institute for Fusion Theory and Simulation, Zhejiang University, Hangzhou, P.R.C. The existence of fishbone fluctuations at frequencies comparable with those of GAMs and BAEs was demonstrated theoretically in a recent work [1.10]. The 2008 activities showed that observation of fishbones at unexpectedly high frequencies in JET [1.29] is well interpreted as experimental evidence of high (GAM/BAE range) frequency fishbones. Research was also carried out to find out what could be obtained from experimental data to get a better comprehension of both supra-thermal particles as well as thermal plasma properties.

The relationship of MHD and low-frequency fluctuations of the SAW spectrum with micro–turbulence

[1.23] R. De Angelis et al., Rev. Sci. Instrum. **79**, 10E517 (2008)
[1.24] M.S. Chu et al., Phys. Fluids **B4**, 3713 (1992)
[1.25] A.D. Turnbull et al., Phys. Fluids **B5**, 2546 (1993)
[1.26] F. Zonca, L. Chen and R.A. Santoro, Plasma Phys. Control. Fusion **38**, 2011 (1996)
[1.27] A. Biancalani et al., *Continuous spectrum of shear Alfvén waves in the presence of a magnetic island*, Proceedings of the 35th EPS Conference on Plasma Physics (Hersonissos 2008) ECA Vol. **32D**, P1–051 (2008), on line at http://epsppd.epfl.ch/Hersonissos/pdf/P1_051.pdf
[1.28] S.V. Annibaldi, F. Zonca and P. Buratti, Plasma Phys. Control. Fusion **49**, 475 (2007)
[1.29] F. Nabais et al., Phys. Plasmas **12**, 102509 (2005)

has important implications for the long time scale dynamic behaviour in burning plasmas [1.30–1.34]. In the kinetic thermal ion (KTI) frequency gap of the SAW continuous spectrum [1.31], i.e., at frequencies of the order of the thermal ion transit frequency, all these phenomena occur on similar time scales, facilitating cross–scale couplings and enhancing their mutual interactions via a direct link between drift–wave turbulence (DWT), zonal flows (ZFs) [1.35] and GAMs [1.36] on the one hand and the SAW spectrum on the other, driven by both energetic as well as thermal particles. An example of such interactions is plasma nonlinear behaviour, which occurs due to mediation by zonal structures, i.e., the nonlinear equilibria [1.37] that are formed, e.g., by zonal flows [1.35], zonal fields [1.38–1.40] and radial corrugations of equilibrium profiles [1.30,1.41]. Other examples that have been recently explored [1.34] concern the close relationship between GAM and SAW spectra [1.42,1.43].

Particular evidence of the relationship of MHD and low frequency fluctuations of the SAW spectrum has been explored, i.e., the existence of fishbone fluctuations at frequencies comparable with those of GAM and BAE [1.44,1.45]. The possibility of exciting fishbone oscillations in the GAM/BAE frequency range was demonstrated analytically [1.10,1.46], but no clear experimental evidence confirming theoretical expectations has been reported so far. Experimental observation of this phenomenology would be important as it would provide an element of verification for the conceptual framework describing the MHD/SAW/DWT interplay mentioned above. The observation of fishbones at unexpectedly high frequencies in JET [1.29] has been demonstrated to be well interpreted as experimental evidence of fishbone oscillations in the GAM/BAE frequency range [1.10].

In the given theoretical framework [1.10], it has also been shown that, from the mere observation of the fluctuation frequency spectrum, quantitative information can be obtained concerning both supra–thermal particles as well as thermal plasma properties.

Effects of trapped particle dynamics on the structures of low-frequency shear Alfvén continuous spectrum

In collaboration with the Department of Physics, University of Tor Vergata, the structure of the low–frequency shear Alfvén wave (SAW) continuous spectrum due to resonant wave–particle interactions with magnetically trapped thermal ions in tokamaks has been analytically derived. The theoretical description asymptotically recovers known results in the relevant limits at both high and low frequencies; furthermore, it is relevant for assessing the accurate kinetic structures that are due to SAW and acoustic wave spectra in toroidal geometry.

As there is a continuous transition between various SAW and MHD fluctuation branches in many situations of experimental interest, the results obtained during 2008 are of practical relevance for their interpretation when used in the theoretical framework of the general “fishbone–like” dispersion relation [1.26,1.10,1.31,1.32,1.47–1.49].

The kinetic layer wave equation and the corresponding expression for the generalised “inertia”, entering the general “fishbone-like” dispersion relation, is derived by treating resonant wave–particle interactions and SAW coupling with acoustic waves on the same footing and extending the validity regime of prior analyses to the whole frequency range $0 << |\omega| << v_A/(qR)$, i.e., including wave–particle interactions for both circulating as well as trapped particles.

To make the problem analytically tractable, all trapped particles have been assumed as deeply trapped and all circulating particles as well circulating. Despite this assumption, the theoretical description presented here captures the essential qualitative features of the structures of the low–frequency SAW continuous spectrum due to resonant wave-particle interactions with magnetically trapped thermal ions. The functional forms of asymptotic limits are reproduced at both low and high frequencies, while relevant wave-particle interactions are maintained, allowing one to clarify the important physics effects of trapped particles on the low–frequency structures of SAW continuous spectrum in toroidal geometry. In particular, it has been shown that the trapped particle contribution is not only important but becomes dominant at frequencies of the order of the thermal ion bounce frequency. This result was expected on the basis of the low-frequency expression of the MHD inertia enhancement [1.50]; however, in the light

of the analysis, it is evident that kinetic treatment of the thermal plasma components is needed for a realistic description of thermonuclear plasmas, in which SAW, MHD and drift wave turbulence will characterise the complex behaviour mediated by their mutual interactions [1.30–1.34].

Fully nonlinear particle simulation of neutral–beam-heated DIII-D discharges

The collaboration begun in 2007 [1.51] with UCI and General Atomics, San Diego, California, USA to investigate energetic ion transport and nonlinear Alfvénic fluctuations for a reversed shear, strongly beam heated DIII–D discharge continued. In 2008 the first fully nonlinear particle simulation of the reference DIII–D discharge was performed by using a multi-mode (n=0–5) simulation (thus including mode coupling [1.52]).

Some of the nonlinear dynamics are still neglected; in particular, the evolution of the (m=0, n=0) component (here, m is the poloidal mode number) of the fluctuating potentials is dropped, as well as that of the (m=1, n=0) component of the fast–ion drive. The reason for the former approximation is that the MHD model itself is not suitable for properly describing the evolution of the (m=0, n=0) equilibrium component. The aim of the latter is to avoid spurious dynamics effects due to the fact that the initial fast–ion distribution function is not expressed in terms of conserved quantities of particle motion. Figure 1.15 shows the energy content of the dominant poloidal component vs time for each simulated n. Note that, in a first purely linear growth phase, modes with n=2 and n=3 exhibit the highest growth rates. As mode-mode coupling becomes important ($t \lesssim 150\ \omega_{A0}^{-1}$ with $\omega_{A0} \equiv v_{A0}/R_0$ the on axis Alfvén frequency), interaction between n=2 and n=3 enhances the growth rate of n=5 and, especially, n=1 modes. This is easily understood in terms of three-wave nonlinear interactions. The n=2 and n=3 modes in time saturate, giving rise to fast ion displacement ($t \approx 190\ \omega_{A0}^{-1}$). The n=1 mode, once the drive due to three–wave coupling is exhausted, is still driven by the residual fast–ion pressure gradient. Then, it

[1.30] F. Zonca et al., Plasma Phys. Control. Fusion **48**, B15 (2006)

[1.31] L. Chen and F. Zonca, Nucl. Fusion **47**, S727 (2007)

[1.32] L. Chen, Plasma Phys. Control. Fusion **50**, 124001 (2008)

[1.33] F. Zonca, Int. J. Mod. Phys. A **23**, 1165 (2008)

[1.34] F. Zonca and L. Chen, *Structures of the low frequency Alfvén continuous spectrum and their consequences on MHD and micro-turbulence*, Proceeding of the Conference on Theory of Fusion Plasmas (Varenna 2008), AIP Vol. **1069**, 355-360 (2008)

[1.35] A. Hasegawa, C.G. Maclennan and Y. Kodama, Phys. Fluids **22**, 2122 (1979)

[1.36] N. Winsor, J.L. Johnson and J.M. Dawson, Phys. Fluids **11**, 2448 (1968)

[1.37] L. Chen and F. Zonca, Nucl. Fusion **47**, 886 (2007)

[1.38] L. Chen et al., Nucl. Fusion **41**, 747 (2001)

[1.39] P.N. Guzdar et al., Phys. Rev. Letts **87**, 015001 (2001)

[1.40] P.H. Diamond et al., Plasma Phys. Control. Fusion **47**, R35 (2005)

[1.41] F. Zonca et al., Nucl. Fusion **45**, 477 (2005)

[1.42] F. Zonca and L. Chen, Europhys. Lett. **83**, 35001 (2008)

[1.43] A.I. Smolyakov et al., Phys. Lett. A **372**, 6750 (2008)

[1.44] W.W. Heidbrink et al., Phys. Rev. Letts **71**, 855 (1993)

[1.45] A.D. Turnbull et al., Phys. FLuids B **5**, 2546 (1993)

[1.46] F. Zonca et al., *Collective effects and resonant excitation of electron–fishbones in FTU and HL-1M,* Presented at the 8th Easter Plasma Mtg. on Reconnection and Turbulence in Magnetically Confined Plasmas (Turin, 2003)

[1.47] L. Chen, R.B. White and M.N. Rosenbluth, Phys. Rev. Letts **52**, 1122 (1984)

[1.48] L. Chen, Phys. Plasmas **1**, 1519 (1994)

[1.49] F. Zonca and L. Chen, Plasma Phys. Control. Fusion **48**, 537 (2006)

[1.50] J.P. Graves, R.J. Hastie and K.I. Hopcraft, Plasma Phys. Control. Fusion **42**, 1049 (2000)

[1.51] G. Vlad et al., *Particle simulations of Alfvén modes in reversed–shear DIII–D discharges heated by neutral beams,* Presented at the 10th IAEA Technical Meeting on Energetic Particles in Magnetic Confinement Systems (Kloster 2007), page OT 7

[1.52] G. Vlad et al., *Particle simulation of energetic particle driven Alfvén modes*, Proceedings of the 22nd International Conference on Fusion Energy (Geneva 2008), IAEA Vienna, on line at http://www.fec2008.ch/preprints/th_5-1.pdf

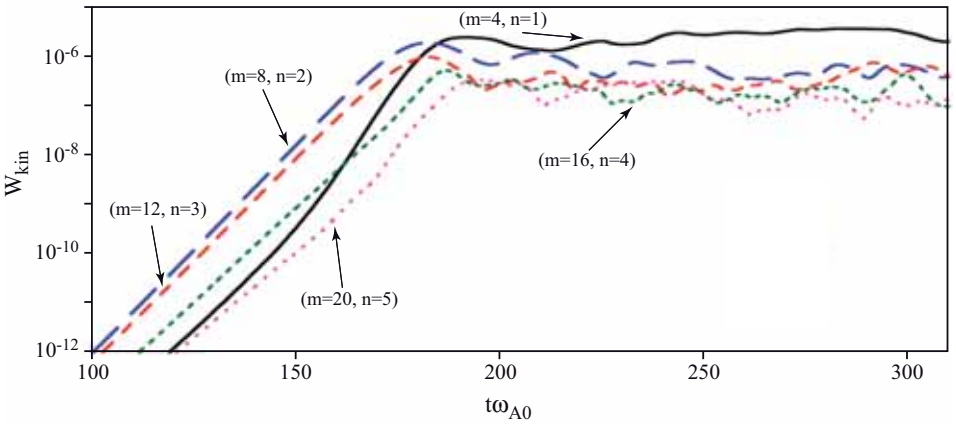

Fig. 1.15 – Fully nonlinear multi-mode simulation: time evolution of the kinetic energy content W_{kin} of the dominant poloidal harmonics for different–n values

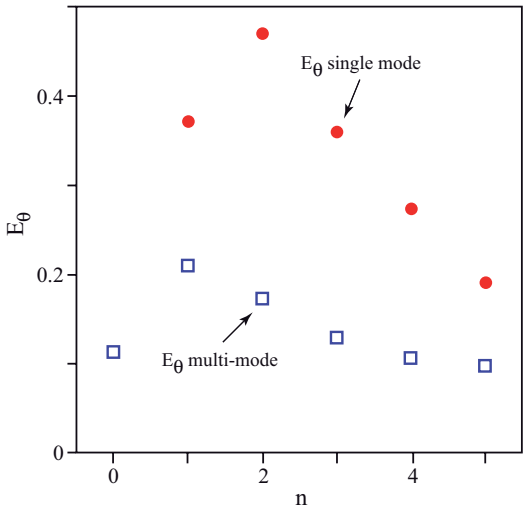

Fig. 1.16 – Saturation levels of poloidal electric field E_θ of the fully nonlinear multi–mode simulation compared with those of single–n numerical investigations

grows further ($t \geq 200\ \omega_{A0}^{-1}$) and in the end produces further ion density flattening, reaching saturation itself ($t \geq 370\ \omega_{A0}^{-1}$).

The overall effect on the fast–ion density profile is of the same order as that obtained in single–mode simulations. In the present case, both the competition of different–n modes in extracting energy from resonant particles (as expected for energetic particle driven modes), thereby flattening the fast ion profile, and the energy transfer from fast to slower growing modes by three–wave nonlinear interactions cause each toroidal mode to saturate at a lower level than that reached in the corresponding single-mode simulation.

This is shown in Figure 1.16, which compares the saturation levels obtained, in single–mode and multi–mode simulations, for the dominant poloidal harmonics of the poloidal electric field (responsible for fast–ion convective displacement) corresponding to different n values. The observed reduction in the saturation levels with respect to single–n studies indicates better agreement between perturbed field levels as predicted by numerical simulations and those inferred from linear MHD reconstruction based on experimental measurements.

A new hybrid MHD gyrokinetic code

A new hybrid MHD gyrokinetic code has been developed for the simulation of nonlinear interactions between Alfvén modes and energetic ions. Unlike the existing hybrid MHD gyrokinetic code (HMGC) [1.53], the new code is suitable for studying general high–pressure (high β) axisymmetric equilibria (perturbed electromagnetic fields fully retained). The gyrokinetic ordering, $k_\perp \rho \approx 1$ (with $k_\perp$ and ρ_H the perpendicular wave vector of the fluctuating fields and the energetic ion Larmor radius, respectively), is also assumed. The energetic ion dynamics is obtained by solving the gyrocentre equations of motion expanded up to order $O(\varepsilon^2)$ and $O(\varepsilon\varepsilon_B)$, where ε is the gyrokinetic ordering parameter ($\varepsilon \approx \rho_H/L_n$) and $\varepsilon_B \approx \rho_H/L_B < \varepsilon$ the ratio between the ion Larmor radius and the equilibrium magnetic field scale length. The code is built by interfacing an initial–value version of the original eigenvalue MHD stability code MARS [1.54] (adapted for the computation of the perturbed scalar and vector potentials, besides the perturbed magnetic and velocity fields) with a gyrokinetic particle–in–cell module (yielding the energetic ion pressure tensor back to the MHD solver). The gyrokinetic module is sufficiently general to be interfaced eventually with other different MHD field solvers. In the present version, the equilibrium quantities are yielded by the equilibrium code CHEASE [1.55] and suitably processed in order to obtain the desired objects (see, e.g., figure 1.17 for one of the Christoffel symbols needed for computing covariant derivatives).

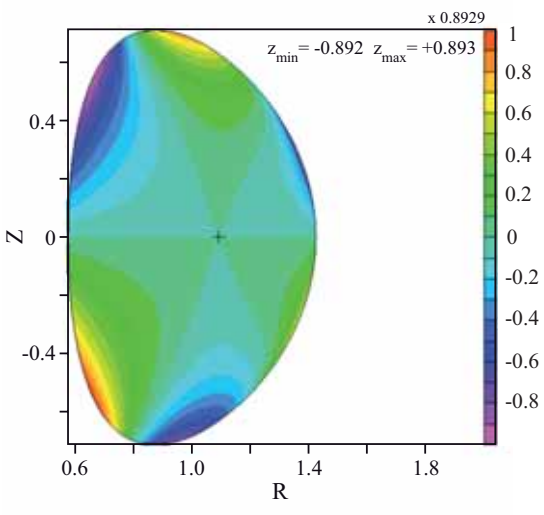

Fig. 1.17 – One of the Christoffel symbols ($\Gamma^{s}_{s\chi}$) needed for computing the covariant derivatives in curvilinear flux coordinates (σ,χ,ϕ). A JET–like equilibrium is considered

Numerical investigation of multi-scale burning plasma physics

International collaborations are crucial aspects of ENEA's theory and modelling work on multi–scale complex nonlinear behaviour of burning plasmas and of the FAST conceptual design.

Under a collaboration with the Plasma Physics Research Centre (CRPP) Lausanne the kinetic particle–in–cell module of HMGC [1.53] has been used to investigate high energetic alpha–particle interaction with micro-instability ion temperature gradient (ITG) driven turbulence and related transport processes.

A parallel version (Message Passing Interface [MPI] plus Open Multi–Processing [OpenMP]) of HMGC has been developed for hyerarchical distributed/shared architectures and ported on the EFDA Gateway, CRESCO and NERSC platforms. Porting on NERSC computers was done in the framework of the ENEA Frascati Plasma Theory Group participation in the US SciDAC project on "Gyrokinetic Simulation of Energetic Particle Turbulence and Transport" (GSEP).

Use of asymptotic techniques in the study of high–frequency (LH range) electromagnetic wave propagation

The propagation and absorption of high–frequency electromagnetic waves in laboratory plasma and in the presence of an external magnetic field is described by an integro–differential system of equations: the Maxwell–Vlasov system. Starting from this, a simplified equation was derived, based on the separation of scales in the differential operator in the parallel and perpendicular directions with respect to the equilibrium magnetic field. While the usual Wenzel, Kramer, Brillouin (WKB) approximation can be applied in the perpendicular direction, in the parallel direction the equation retains its integro–differential character. To further simplify the equation and reduce it to a more tractable form, the cold plasma wave and electrostatic approximations are used, which well apply to the propagation of the LH wave.

Hamiltonian perturbation theory for studying LH wave propagation in burning plasmas

The main objective of applying LH heating and current drive in next–generation tokamaks is to study the physics of a burning plasma and their applcation plays a crucial role in plasma profile control and internal transport barrier formation. For modelling the plasma–wave interaction correctly, a wave equation valid for the LH range of frequencies (cold plasma and electrostatic approximation) has been derived and asymptotically solved (WKB expansion) up to the second order in the expansion parameter [1.56], making the reconstruction of the electric field inside the plasma possible and allowing a critical analysis of the wave propagation in the vicinity of caustics and cut–offs. In 2008, the ray–tracing equations were solved numerically in the long–ray propagation-path case, which could be relevant for studying the parallel wave–number up–shift and, therefore, for demonstrating wave absorption in these cases, where first passage absorption is not present. It was demonstrated that the Hamiltonian ray–tracing equation system, which describes the bouncing of the wave from the central reflection to the cut-off points, is analogous to the harmonic oscillator dynamic system. The nonlinear character of the equation system and its non–integrability, due to the presence of two or more degrees of freedom,

[1.53] S. Briguglio et al., Phys. Plasmas **2**, 3711 (1995)
[1.54] A. Bondeson, G. Vlad and H. Luetjens, *Computation of resistive instabilities in toroidal plasmas*, IAEA Technical Committee Meeting on Advances in Simulation and Modeling of Thermonuclear Plasmas (Montreal 1992), pp. 306–315
[1.55] H. Luetjens, A. Bondeson and A. Roy, Comput. Phys. Commun. **69**, 287 (1992)
[1.56] A. Cardinali et al., Phys. Plasmas **14**, 112506 (2007)

leads to Hamiltonian chaos. These aspects were studied by producing phase portrait plots, Poincaré maps and computing the Liapunov exponents, etc., and thereby clarifying some interesting features of LH propagation in magnetized plasmas.

1.5 Jet Collaboration

Six experimental campaigns (C20–C25) were carried out in 2008. As in 2007, the campaigns included an integrated experimental programme organised by two main task forces (TFs S1 and S2): the experiments proposed by the other task forces (Diagnostics, Heating, Magnetics, Exhaust, Transport and DT) were integrated in the S1 (H–mode scenario) and S2 (Internal Transport Barriers and Hybrid scenarios) experimental programme. ENEA's involvement in the European Fusion Development Agreement (EFDA) JET 2008 work programme concerned participation in the JET second enhancement programme (EP2) and the realisation of experiments for C20-C25.

ENEA has provided the EFDA associated leader for JET, one TF leader (Diagnostics), one deputy TF leader (Internal Transport Barriers and Hybrid scenarios), one responsible officer (RO) in the Close Support Unit (CSU) (H–mode scenario and Transport and project "Integrated transport and MHD") and, one RO for Enhancements in the EFDA JET CSU and one RO for Contracts in the EFDA JET CSU.

ENEA's participation in orders (contracts between Euratom and EU Associations) for the JET campaigns is close to 12% of the total. The ENEA–Euratom Association unites the activity of ENEA Frascati, the CREATE consortium, the Institute of Plasma Physics CNR Milan, the Reversed Field Experiment (RFX) Padua, Turin Polytechnic (POLITO), the Universities of Catania and Rome II Tor Vergata (figs. 1.18–1.20).

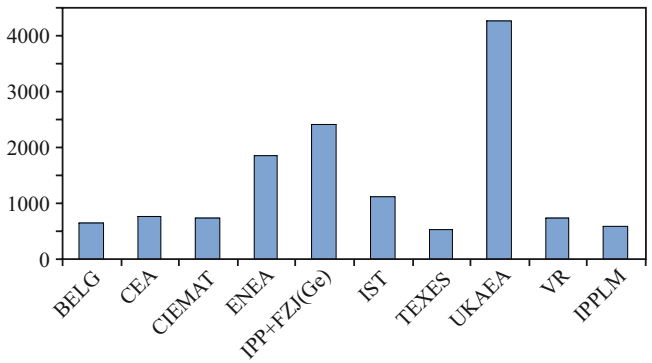

Fig.1.18 – Distribution of participation in JET C20–C25 by EU associations (with number of working days >500; vertical axis is number of working days)

Participation in JET EP2

Compact neutron spectrometers and new electronics for the neutron profile monitor. The new neutron/γ–ray digital pulse shape discrimination (DPSD) system for NE213 scintillators has been completed [1.57,1.58]. The output signal of the photomultiplier is coupled to a fast transient recorder (FPGA-based) and each single pulse is

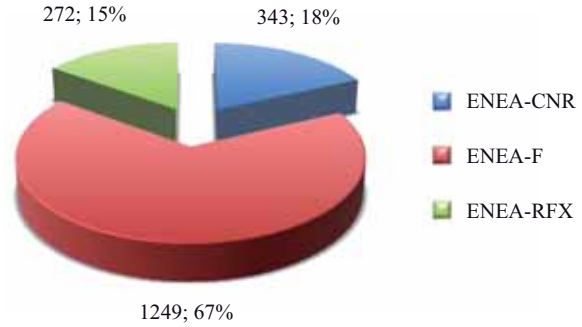

Fig. 1.19 – Distribution of working days under orders for JET C20–C25 between the institutes of ENEA–Euratom Association (ENEA F corresponds to the sum of working days related to ENEA Frascati, CREATE, POLITO, Catania, Rome II; total number of working days of EU associations is 15177)

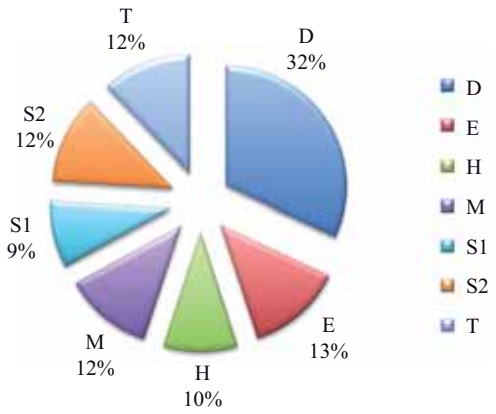

Fig. 1.20 – Distribution of manpower between TFs for JET C20–C25

digitized at 200 MSamples/s and stored. The recorded data are processed off-line for removal of low-frequency noise, discrimination between neutron and gamma-ray events, pile-up identification. The main advantages of the DPSD compared to analogue techniques are the possibility of achieving high count rate operation (MHz range) and the consequent increase in the measurement dynamic range/time resolution; raw data (i.e., pulse signals) re-processing possibility; simultaneous neutron and gamma pulse height spectra (PHS) for each line of sight (LOS) on any preset time and energy window. This new system is currently employed in two JET EP2 projects: Compact Neutron Spectrometer and New Electronics for the Neutron Profile Monitor.

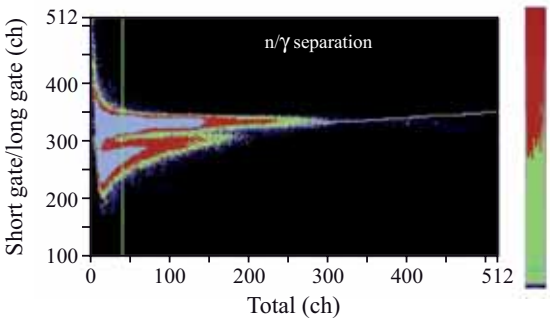

Fig. 1.21 – Acquisition example of neutron/gamma discrimination obtained by using data acquired from neutron source (Am/Be). Horizontal axis: energy (total integral of pulses); vertical axis: ratio ST/LT. The white line clearly separates gamma rays from neutrons

a) Compact neutron spectrometer. The aim of the compact neutron spectrometer (CNS) is to provide measurements of neutron spectra in the range 1.5–20 MeV with high energy resolution and post-experiment data reprocessing features. The CNS project is divided in two steps: i) realisation and calibration of a CNS unit based on a liquid organic scintillator NE213 coupled to a photomultiplier developed by Physikalisch-Technische Bundesanstalt (PTB) in Braunschweig; ii) construction of a DPSD for acquisition and data processing developed by ENEA Frascati. The DPSD system for the CNS is based on two 14-bit 100 MS/s analog-to-digital converters (ADCs), coupled in interleaved mode in order to obtain an actual sampling rate of 200 MS/s on one input channel, a field programmable gate array (FPGA) and a high-speed PCI board (maximum throughput 80 MB/s). Examples of measurements of discrimination between neutron and gamma rays are reported in figures 1.21 and 1.22. The discrimination, based on the different intensities of the slow and fast components of the light produced by neutrons and gamma rays interacting with the scintillator, is carried out using the charge comparison method, which compares two time integrals (short time integral [ST] and long time [LT]) of a pulse.

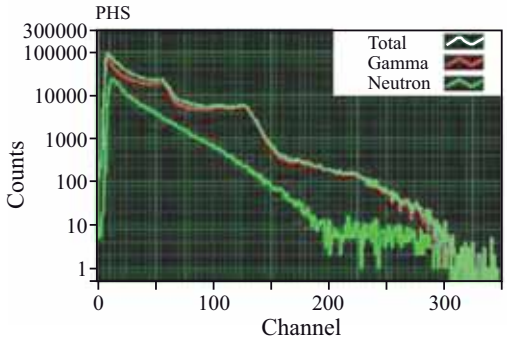

Fig. 1.22 – Pulse height spectra (log-linear plot): neutron (green), gammas (red), white (total)

b) New electronics for the neutron profile monitor. The JET neutron emission profile diagnostic (KN3) consists of two fan-shaped arrays of collimators (ten horizontal + nine vertical LOS). Each LOS has a NE213 liquid scintillator with analogue pulse shape discrimination (PSD) electronics for detecting 2.5-MeV and 14-MeV neutrons. The main goal of the JET JW7-PM-EP2-DNN-02 task is to replace the analogue PSDs and data acquisition/processing systems of the 19 neutron detectors of KN3 with a DSPS system (based on FPGA devices) similar to that used for CNS.

The results of the preliminary tests at JET are promising (see fig. 1.23).

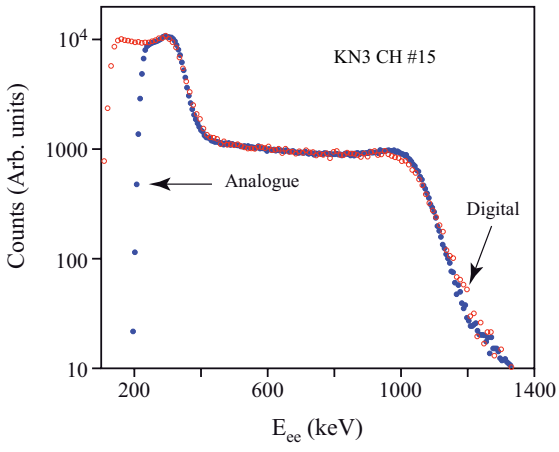

Fig. 1.23 – Comparison of digital and analog pulse height spectra (gamma rays from a ^{22}Na source)

Development of artificial diamond detectors

Artificial single crystal diamond for neutron detection. During the 2008 experimental campaigns, four single crystal diamond (SCD) detectors grown by chemical vapour deposition (CVD) were installed

[1.57] M. Riva et al., Fusion Eng. Des. **82**, 1245 (2007)
[1.58] D. Marocco et al., *High count rate neutron spectrometry with liquid scintillation detectors*, to be published in IEEE Trans. Nucl. Sci.

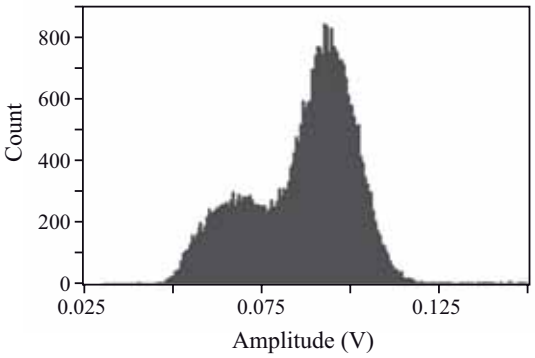

Fig. 1.24 – Pulse height spectrum measured at JET with SCD+LiF connected to FCA and fast digitizer

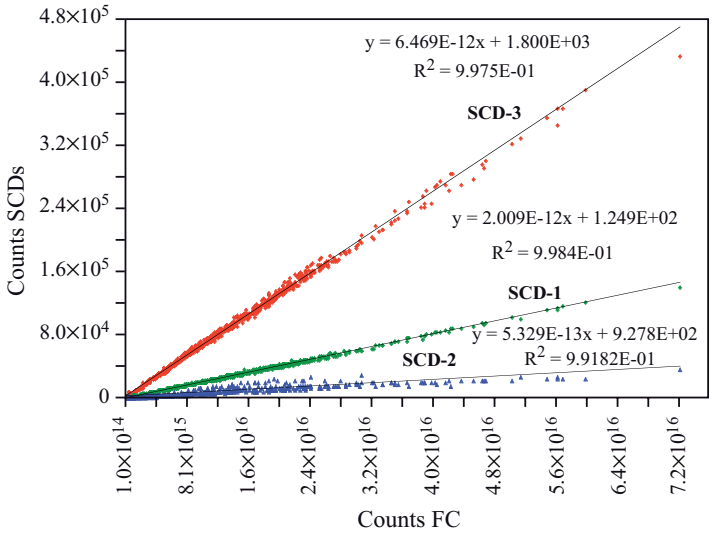

Fig. 1.25 – Correlation between the SCD–1, SCD–2 and SCD–3 detectors with the KN1 (fission chamber). Correlation coefficients and linear fit data are also reported for each SCD detector

at JET to detect neutron emission. The SCD detectors have different thickness, performance and electronics. Three detectors were covered with a thin layer of LiF enriched in ^{6}Li, which allows the detection of low-energy neutrons [1.59,1.60] via the $n+^{6}Li \rightarrow \alpha+T$ reaction. The fourth SCD is 200–μm thick and covered with a layer of polyethylene to enhance its response to 14–MeV neutrons by using the high value (1 barn) of the (n,H) scattering cross section for H. In the latter case proton recoil is used to detect neutrons. The goal is to detect both total and time-dependent neutron emission, distinguishing between DD and 14–MeV neutrons (the latter due to triton burn-up). One ambitious goal (achieved) of the present activity is to demonstrate the capability of SCD detectors to operate with the electronics connected to the detector throughout a long (100 m), low attenuation, super–screened single cable. In a second step it was demonstrated that the SCD could operate also as spectrometer using the above working scheme. An ad hoc fast charge amplifier (FCA) was developed for this purpose. With this system it is possible to get the pulse height spectrum (fig. 1.24) for one of the SCD detectors covered with LiF. Due to the presence of LiF, it is also possible to measure the peaks of α and T produced by the $n+^{6}Li \rightarrow \alpha+T$. This test is ITER–relevant as in this case only the radiation hard diamond detector is located in the radiation field to be measured, while the processing electronics is far away. Data analysis demonstrates the stability, reliability and capability of SCD diamond detectors. Comparison of the data measured by the SCD vs the JET standard neutron monitors (fig. 1.25) shows that diamond detectors are now ready for operation in a tokamak [1.61,1.62].

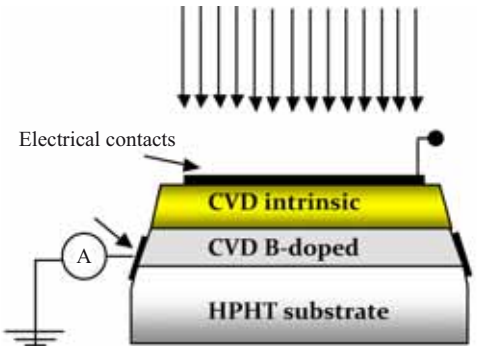

Fig. 1.26 – Schematic of the CVD detector

Artificial diamond for VUV and soft-x-ray detection. In 2008 two artificial diamond films were installed at JET under the EP2 project. The devices work as vacuum ultraviolet (VUV) and SXR radiation detectors emitted from JET plasma. The SRX detector is calibrated. Both devices are inside the KS6 chamber (Bragg rotor x–ray spectrometer, impurity survey system) with a direct horizontal view of JET plasma, without any line selection. The diamond films were grown by the CVD technique and have a layered structure. Boron-doped SCD is grown on top of commercial high–temperature high–purity diamond substrate. Subsequently a film of high–purity SCD diamond layer is grown on top of the boron layer. This layer is the true detection region of radiation. The boron–doped layer acts as a rear electrical contact, while a metal contact is deposited on top of the active layer (fig. 1.26).

The following diamond detectors were installed in the KS6 chamber:

1. VUV detector SCD476, intrinsic and active layer 1 μm, 2–nm metallic platinum contact.
2. SXR detector SCD270, intrinsic layer 26 μm, measured active layer at 0 Volts bias 3.75 μm, 100–nm metallic aluminium contact and a 10–μm polyethylene filter to cut radiation below 1 keV (50% cut–off).

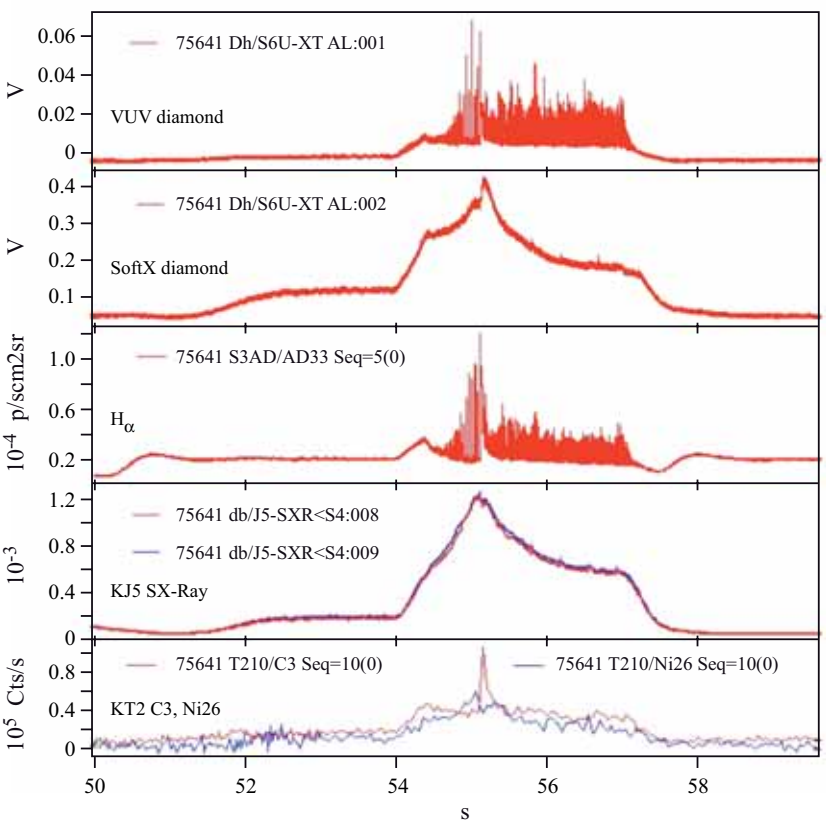

Fig. 1.27 – Example of the measured signal compared with other diagnostics

Soft–x–ray detector calibration and measurements. The responsivity of the SXR detector was determined with a calibration performed at the Diamond Light Source synchrotron facility at Harwell (UK). The monochromatic x–ray of the B16 test beamline was used. An example of the measured signals compared with other JET detectors measuring the same radiations is shown in figure 1.27 (JET pulse 75641 – ITER-like antenna [ILA] commissioning pulse, about 7.5 MW neutral beam injection). The signals demonstrate measurements with a very good signal–to–noise ratio and excellent sensitivity. The VUV diamond is excellent for measuring edge localised mode (ELM) activity (as can be seen in figure 1.27 by comparing the VUV signal with H_α). The SXR diamond appears promising for MHD studies, as can be seen by comparing the second and fourth traces from the top. The last trace in figure 1.27 is related to a measurement of impurity influxes during laser blow–off experiments in which the Ni influx is detected.

Pellet Commissioning. During 2008, ENEA contributed to the commissioning of a new high–frequency pellet injector (HFPI) designed to deliver pellets both for fuelling purposes and for ELM pacing. The new launcher has been successfully tested in the fuelling mode and the extension to full performance is still in progress.

The data taken with the HFPI will be inserted into a database created in the past, which contains information on the target plasmas and pellet injection parameters. The database includes pellets with masses corresponding to 1.9–3.8×10^{21} D atoms, speeds of 80–360 m/s and target plasmas with T_{eo}=0.7–7.0 keV and n_{eo}=1.0–7.5×10^{19} m^{-3}. The fuelling efficiency and deposition profiles are being studied with particular attention paid to quantifying the radial particle drift predicted by the theory and already observed on medium-size tokamaks such as ASDEX–U and DIII–D. Since pellet injection is expected to be used to raise and control the density in a reactor-grade plasma, it is of great importance to assess the viability and efficiency of this method in large tokamaks, such as JET, in order to gain confidence in extrapolation to ITER.

Participation in C20-C25

Advanced Tokamak Scenario: analysis of beta-limiting modes. Access to high β_N regimes with a q profile compatible with a large bootstrap current has been systematically investigated in JET H mode plasmas [1.63]. In these discharges with relatively broad pressure profiles, the achievable β_N was limited

[1.59] M. Marinelli et al., Appl. Phys. Letts **89**, 1 (2006)
[1.60] M. Marinelli et al., App. Phys. Letts **90**, 183509 (2007)
[1.61] M. Angelone et. al., Nucl. Instrum. Meth. Phys. Res. A **595**, 616 (2008)
[1.62] D. Lattanzi et. al., *Synthetic single crystal CVD diamond as neutron detectors at JET,* Presented at the 25th Symposium on Fusion Technology - SOFT (Rostock 2008) and to appear in Fus. Eng. Des.
[1.63] C.D. Challis et al., *High β_N JET H–modes for steady–state application*, Proceeding of the 34th EPS Conference on Plasma Physics (Warsaw 2007), ECA Vol **31F**, P5.124 (2007), on line at http://epsppd.epfl.ch/Warsaw/pdf/P5_124.pdf

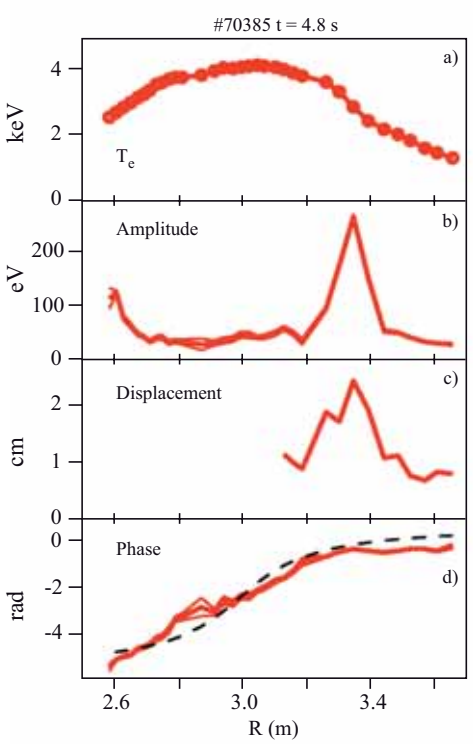

Fig. 1.28 – Profiles along the ECE sightline radial coordinate. a) Mean T_e; b) zero-to-peak oscillation amplitude; c) displacement; d) phase. Dashed line is the expected phase for m=2

by an n=1 MHD instability that resulted in a soft but significant loss of confinement. In previous experiments on DIII-D, the beta-limiting n=1 instability was identified as a neoclassical tearing mode. Analysis of JET data [1.64] has shown that the nature of this mode is different; in fact it grows initially without forming any magnetic island, i.e., it starts with a kink-like rather than tearing-like structure.

This is the conclusion of a careful analysis of the internal structure of the mode, as detailed in the following.

The radial structure of the n=1 mode was investigated using 48 temperature channels with fast data acquisition from the electron cyclotron emission (ECE) diagnostic (fig. 1.28). For each channel (k), the cross-spectral density $G_{kM}(f)$ with a reference magnetic signal (M) was calculated. Phase $\phi_k=\arg(G_{kM})$, amplitude $A_k=|G_{kM}|/\sqrt{G_{MM}}$ and coherence $\gamma_{kM}=|G_{kM}|/\sqrt{G_{kk}G_{MM}}$ were evaluated at the spectral peak corresponding to mode frequency. Amplitude and phase profiles vs major radius coordinate (R) on the ECE sightline, with confidence intervals delimited by thin lines, are shown in figures 1.28b and 1.28d. The phase profile is ideal-like in this time slice (t=4.8 s), i.e., it has no π–jumps that would reveal the presence of magnetic islands. Phase varies by 5.1 rad as R spans from 2.58 to 3.66 m, due to the fact that the ECE sightline lies at $Z_0 \approx 17$ cm below the magnetic axis plane so that the poloidal angle varies with sightline coordinate as $\theta=\tan^{-1}(Z_0/(Z-R_0))$. The phase profile is in rough agreement with the "baseline" expected for a mode with m=2 poloidal number (black dashed curve in fig. 1.28d).

The flux surface displacement (fig. 1.28c) was estimated as $\xi=A\cos\theta/(dT_e/dR)$, where A is amplitude and the $\cos\theta$ factor estimates the actual T_e gradient from the derivative along the sightline coordinate. Results are only reliable for R>3.2 m, where a broad peak can be seen. Similar displacement profiles were observed for n=1 modes in JET plasmas with internal transport barriers (ITBs) and very peaked pressure profiles [1.65], but, while in ITB experiments the mode led to disruption at $\beta_N<2.5$, in the high beta plasmas with moderate pressure peaking as described here, the mode typically saturated at displacement values below 5 cm.

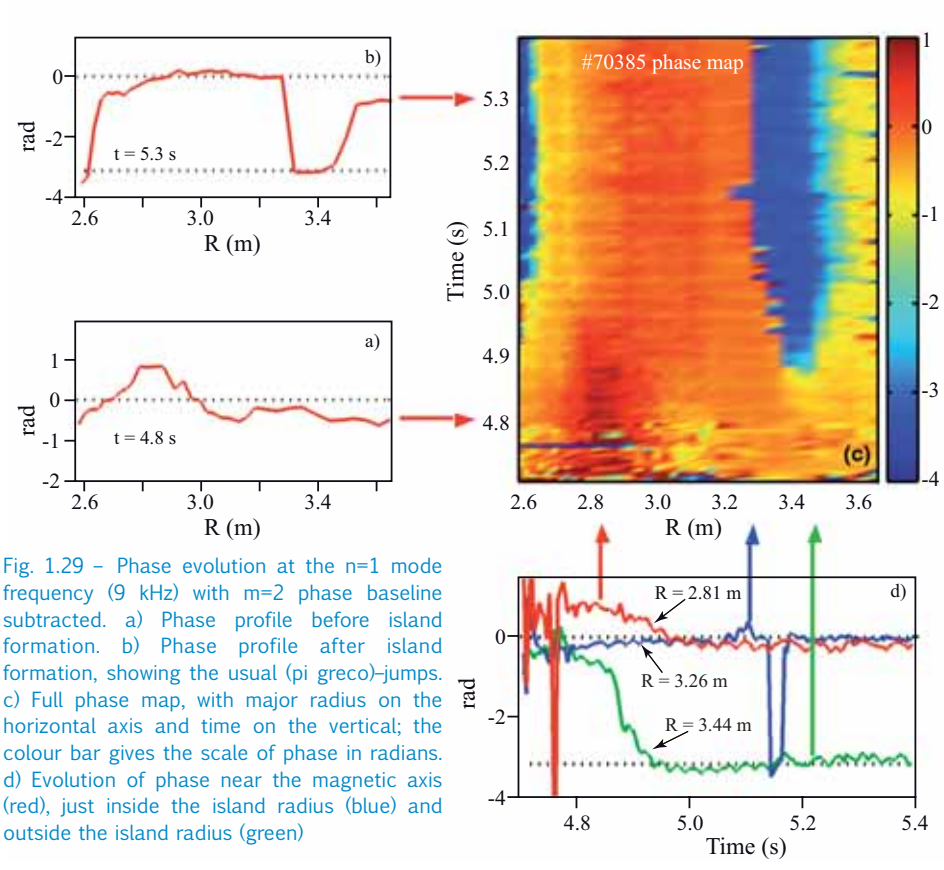

Fig. 1.29 – Phase evolution at the n=1 mode frequency (9 kHz) with m=2 phase baseline subtracted. a) Phase profile before island formation. b) Phase profile after island formation, showing the usual (pi greco)–jumps. c) Full phase map, with major radius on the horizontal axis and time on the vertical; the colour bar gives the scale of phase in radians. d) Evolution of phase near the magnetic axis (red), just inside the island radius (blue) and outside the island radius (green)

The subsequent evolution of phase is shown in figure 1.29. In figure 1.29c the horizontal (vertical) axis of the color map represents major radius (time). The m=2 baseline phase profile (dashed line in

fig. 1.28d) has been subtracted. The island appears as a π–phase jump, i.e., with the colour bar used, as a transition from red to blue. Clearly, the island appears after t=4.87 s.

Figures 1.29a and 1.29b respectively show profiles at t=4.8 s (the same time-slice with ideal–like profile as shown in fig. 1.28) and at t=5.3 s. The latter clearly features π–jumps (at R=2.6 and 3.3 m), which is the signature of the presence of an island. Time evolution for three channels is shown in figure 1.29d. For a pure m=2 mode, the traces should lie on one of the dotted lines at 0 and - π, as they actually do for t>5 s. Deviations observed at earlier times can be explained by a mode mixture involving a principal kink component, a principal tearing component (island), which lags in phase the kink component, and secondary components with m=1 or m=3.

Edge bootstrap current driving improved confinement in advanced scenarios of JET. A crucial issue of the development of steady–state tokamak regimes is optimisation of the plasma current profile evolution to avoid deleterious MHD modes while promoting the formation and sustainment of the transport barriers (TBs) that enclose a large fraction of the plasma volume.

Theory shows that a low magnetic shear (typically $s \leq 0.2$) is useful to suppress the effects of turbulent structures that contribute strongly to thermal transport in tokamak plasmas [1.66]. The role of a low magnetic shear was identified as important for determining the occurrence of the long–lasting TBs of JET [1.67] with radial foot $\rho \approx 0.6$–0.7 (ρ=normalised toroidal flux coordinate), interpreted as the effect of a low shear produced by lower hybrid current drive (LHCD) applied during both the current ramp–up and the H-mode phases [1.68].

Recently, experiments have been performed in JET at ITER–relevant conditions for fully non–inductive operation of high triangularity ($\delta \approx 0.4$) and $q_{edge} \approx 5$, at I_p=1.5 MA, B_T=2.3 T, main heating power $P_{NBI} \approx 20$ MW of neutral beam injection applied after the end of the plasma current ramp–up (prelude phase). Normalised beta $\beta_N \approx 2.8$ was obtained at H_{89}=2.2 and maintained for three seconds during an ELMy H–mode phase [1.69].

The plasma current density evolution was modelled in realistic conditions of these latter and new experiments at JET, establishing a link between bootstrap current at the edge and occurrence of the high β_N phase.

In new experiments with LHCD, but also with lower gas fuelling in prelude (i.e., before the main heating phase), a significant high β_N phase is established, which is characterised by low shear at large radii.

The proposed interpretation of these experiments is that the initial higher temperature at the edge, enhancing the local bootstrap current, allows compensation of the higher shear produced by LHCD, hence favouring the high β_N phase build-up via low shear at large radii.

Hybrid scenarios in JET experiments. The plan for the future international experiment (ITER, presently under construction in France) is to operate in three different regimes: H–mode characterised by an energy transport barrier at the plasma edge; the advanced tokamak regime characterised by an ITB; and the so–called hybrid regime, characterised by intermediate peaking of the current density profile, by the possibility to allow quite long (although not stationary) reactor operations and by good bulk

[1.64] P. Buratti et al., *Radial analysis of beta-limiting modes in JET,* Proceedings of the 35th EPS Conference on Plasma Physics (Hersonissos 2008) ECA Vol. **32D** P-1.069 (2008), on line at http://epsppd.epfl.ch/Hersonissos/pdf/P1_069.pdf

[1.65] G.T.A. Huysmans et al., Nucl. Fusion **39**, 1489 (1999)

[1.66] F. Romanelli, F. Zonca, Phy Fluids B **5**, 4041 (1993)

[1.67] J. Mailloux et al., Phys. Plasmas **9**, 2156 (2002) and C. Castaldo et al., Phys. Plasmas **9**, 3205 (2002)

[1.68] R. Cesario et al., Phys. Rev. Letts **92**, 175002 (2004)

[1.69] X. Litaudon et al., Plasma Phys. Control. Fusion **49**, B529-B550 (2007) and R. Cesario et al, *Lower hybrid current drive in experiments for transport barriers at high β_N of JET (Joint European Torus),* 17th Topical Conference on Radio Frequency Power in Plasmas (Clearwater 2007)

plasma energy confinement, without too strong a peaking of the pressure profile. Experiments have been performed to study the confinement properties of the hybrid scenario, working with plasma configurations at high triangularity of the last closed magnetic surface. Figure 1.30 reports energy confinement for a large set of these discharges vs the best scaling of the confinement time for the standard/reference H–mode. As can be observed energy confinement has better behaviour up to a factor of the order of 1.4 of the reference ITER 98y energy confinement scaling. Experiments clearly showed that this regime (with $H_{98}=\tau/\tau_{98y}$~1.4), at low plasma current (I_p) and toroidal field (B_T), is stationary on the resistive plasma time scale, at relatively high normalised beta ($\beta_N\approx3$). This can be observed in figure 1.31, where the experimental traces for some physics quantities are reported for shot #75590 (B_T=1.7 T, I_p=1.3 MA): it can be noted that the thermal β_N and the confinement parameter $H_{98}=\tau/\tau_{98y}$ are practically constant for the full duration of the experiment. The present experiments are dedicated to the extension of this scenario at higher current and magnetic field.

Plasma control. The joint activity of ENEA and CREATE on plasma magnetic control in JET was mainly focussed on the new JET enhancement project "Plasma Control Upgrade" (PCU) and its extension (PCU2). Initially aimed at an overhaul of JET plasma control capabilities, it was eventually focussed on improving the vertical stabilisation (VS) system ability to recover from large ELM perturbations. The activity was aimed principally at researching a solution that could be implemented within the timing and budget constraints. A very important task was that of improving the modelling of JET plasma, iron core and passive structures. Using dedicated experiments, the models were progressively refined until it was possible not just to explain the experimental data but to predict the VS system behaviour (fig. 1.32). The reason for undesired oscillations was identified in the coupling between VS system and shape controller (SC) or extreme shape controller (XSC). New control systems and improved plasma speed estimators and control algorithms can now be designed and tested in simulation before being tried on the machine. At the same time the project team studied the best options for power supply (PS) and control system upgrades and evaluated whether a change of turns in the stabilisation coil was desirable and possible. The activity was complemented by experimental tests in the 2008 campaigns addressed to phase margin experimental determination, VS tests with alternative estimators and control algorithms, PCU benchmark criteria, analysis of plasma oscillations and VS/SC coupling.

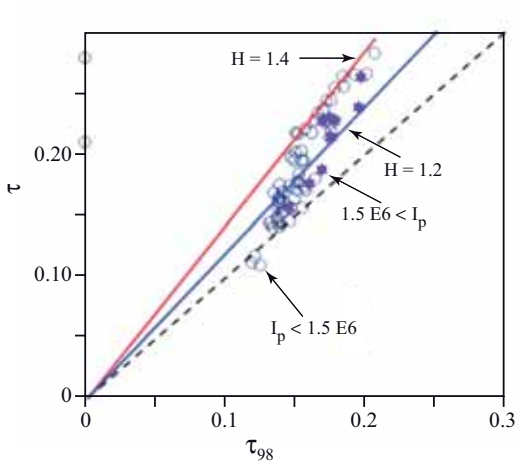

Fig. 1.30 – Experimental confinement time vs ITER 98y energy confinement scaling

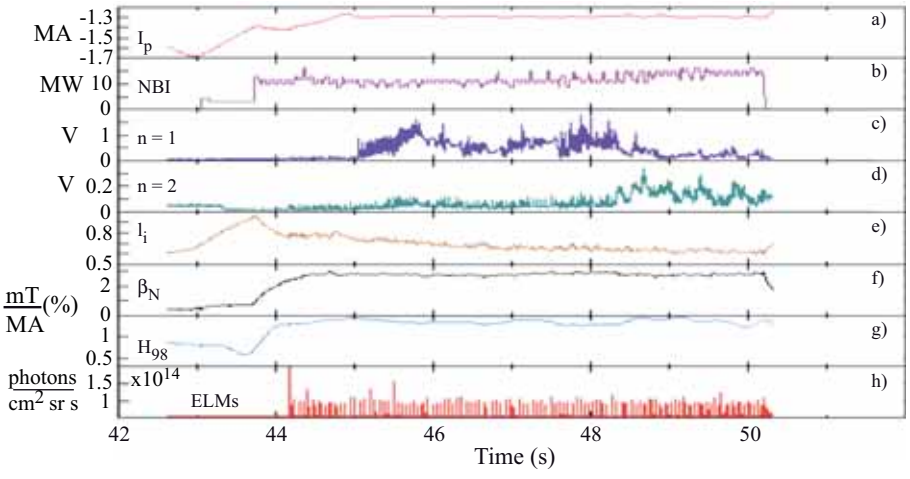

Fig. 1.31 – Experimental time traces. From top a) plasma current; b) neutral beam power; c) n=1 mode activity; d) n=2 mode activity; e) internal inductance; f) normalised beta; g) H_{98} confinement parameter; h) ELM activity

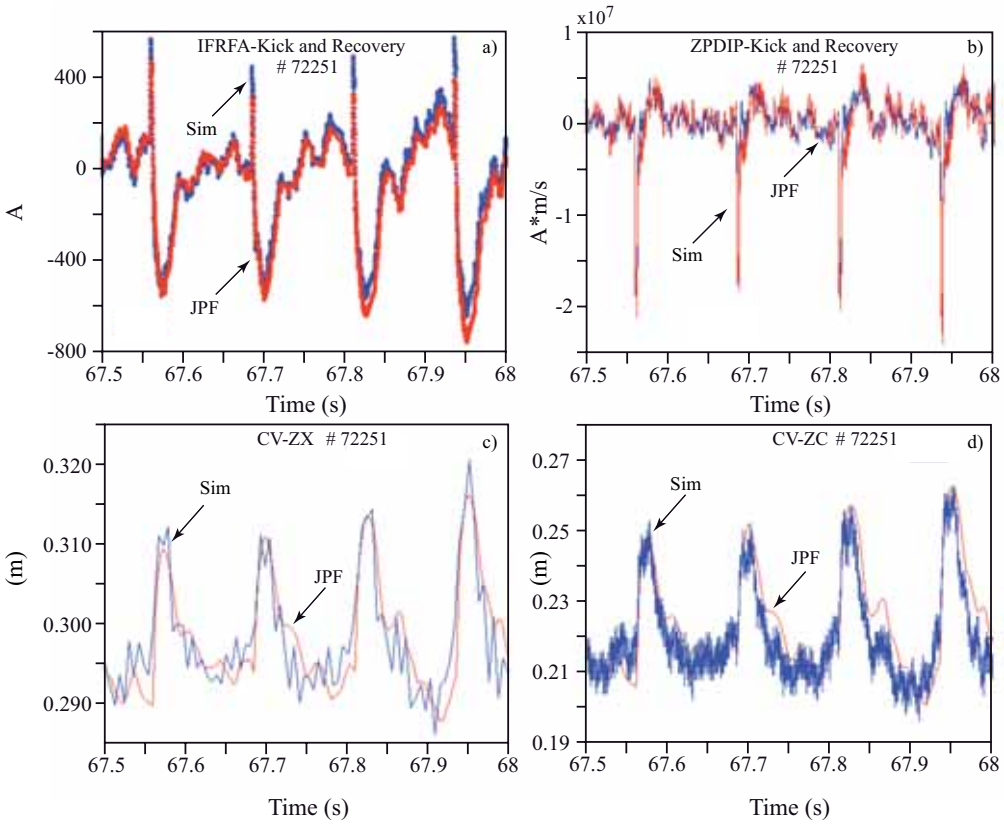

Fig. 1.32 – Kick and recovery tests in JET shot #72251. a) Simulated vs experimental values of radial field circuit current, b) ZPD–IP vertical speed estimator, and reconstructed values of the vertical positions of c) X–point and d) plasma current centroid

Analysis of experiments on fast ions: numerical simulations of fast–ion losses in JET shot #69432 t=46 s. The aim of this work was to identify the region where energetic ions, detected by the scintillator probe in the JET #69432 discharge, come from. The HAGIS code [1.70] was used to follow the ion trajectories in the reconstructed equilibrium provided by the HELENA code, in the absence of any perturbation. Three kinds of ions were considered: i) ^{3}He minority ions accelerated with ion cyclotron resonance heating (ICRH) (tail temperature 200–400 keV); ii) 3.6–MeV alpha particles (source broadening from 2 to 5 MeV); iii) 15–MeV protons. The scintillator probe locates the peak of lost ions as a function of their pitch angle (in the range $\lambda \approx 35°–85°$) and their Larmor radius (in the range $\rho_l \approx 4–13$ cm) (fig. 1.33a). The energy corresponding to these values of pitch angle and Larmor radius cannot correspond to protons with an energy of 15 MeV. Indeed, even when protons are lost close to the scintillator, the combination of their final Larmor radius and pitch angle cannot correspond to that measured by the detector. On the other hand, both passing and trapped ^{3}He ions, accelerated with ICRH, energy in the range between 200 and 400 keV and initially starting at different radial positions, cannot be lost at the edge. The fusion-born 3.6–MeV alpha particles have source broadened from 2 MeV to 5 MeV and fit the experimental measurements in the best way (fig. 1.33b). This result indicates a great opportunity to investigate losses of fusion-born alpha particles around 3.6 MeV without performing tritium experiments.

Experimental proposals

Tritium minority heating with mode conversion of fast waves. Interaction of plasma ions with ion Bernstein waves (IBWs), coupled to tokamak plasmas by mode conversion of fast magnetosonic waves, has been observed both at the 3/2 cyclotron harmonic and at the fundamental cyclotron resonance of deuterium majority ions. A new heating scenario is presented, based on IBWs: coupled by mode conversion of fast magnetosonic waves in a D(H) plasma, IBWs are damped by minority tritium ions at the first cyclotron harmonic $\omega = 2\Omega_T$. In tokamaks with aspect ratio $R_0/a > 2$, this resonant layer can be located at $R_T \approx R_0$. The mode conversion layer is located near the centre of the plasma column at $R \approx 1.06\ R_0$, provided the D/H density ratio be $n_H/n_D \approx 1$. The IBWs are expected to be the leading mode–converted waves, and they propagate in a small plasma region of width $\Delta_R \approx 0.06\ R_0$, close to the centre. The power damped on the electrons can be neglected in high beta plasmas, and the power is absorbed by the tritium ions via cyclotron damping. A specific scenario for JET has been analysed by

[1.70] S.D. Pinches et al., Computer Physics Comm. **111**, 133 (1998)

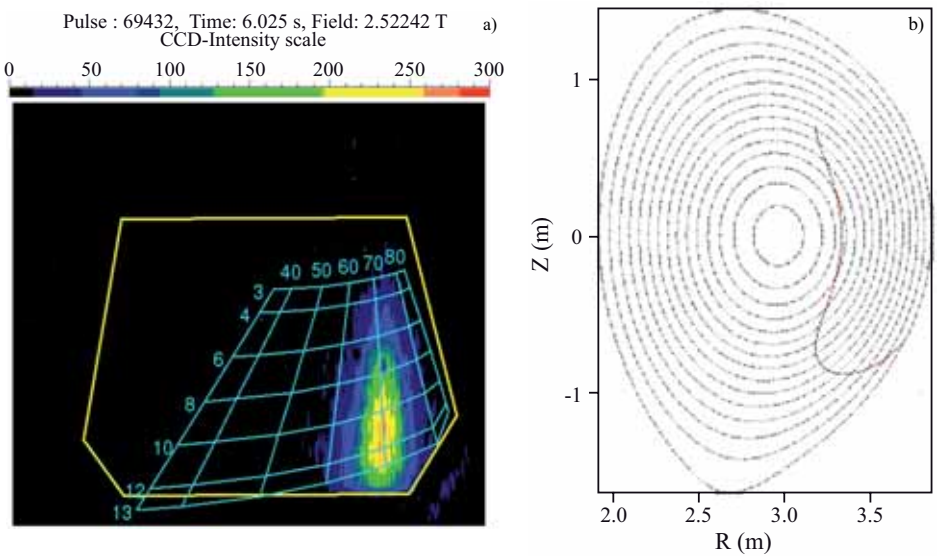

Fig. 1.33 – a) Image of ion losses detected by the scintillator probe vs ion pitch angle (in degrees, horizontal axis) and ion Larmor radius (in cm, vertical axis). The grid is reconstructed at t=46.025 s. b) Poloidal projection of a 5.1–MeV alpha particle starting at R≈3.18 m, ϑ=0.85° and detected by the scintillator

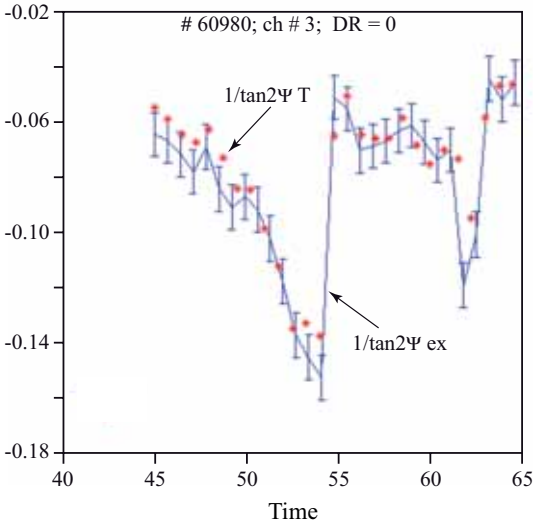

Fig. 1.34 – Measured (continuous blue line) and calculated (red stars) Faraday rotation for the shot #60980 using numerical solution of Stokes equations

the TORIC code, and the distribution function of the minority tritium ions has been evaluated by quasilinear theory.

Possible use of the LH wave in hybrid scenarios on JET. A detailed study of LHCD was performed to demonstrate the possibility of an off-axis current drive in discharges devoted to a hybrid scenario. Lower hybrid was applied at the end of the ramp-up phase in the presence of low–power NBI in order to show that the current drive produced at large radius (r/a=0.7–0.8) is able to flatten the q profile and maintain its value grater than 1 in a large domain of the plasma radius. It was shown that a non-negligible current can be produced in discharges at low (B=1.7 T) and high (B=2.3 T) magnetic fields, with an input coupled power around 1 MW. Further studies have been started to see whether in the main heating phase the LH wave is also able to maintain and sustain these specific q profiles. Iteration with the JETTO transport code has also been performed to see the evolution of the q profiles under the action of the LHCD.

Diagnostics

Modelling of polarimetry measurements. A detailed analysis of Faraday measurements and a comparison with available models were carried out. A rigorous approach to the interference between Faraday and Cotton–Mouton was also introduced. The main results are: i) the Faraday rotation can be calculated from Stokes equations [1.71] and the results are in agreement with measurements at low density and current; ii) moving to high density and current discharges, a shift of the coordinate of the lines of sights of 4 cm (in the direction of low field side) is required to reconcile the measurements with calculations: in practice the Faraday measurements give direct information about the correction to be introduced in the equilibrium. Figure 1.34 shows the measured and calculated Faraday rotation for a low-density shot, where the shift of the coordinate of the polarimeter line of sight was not necessary.

Current profile measurements by MSE. Determination of the q profile in JET is carried out using various diagnostics and equilibrium analysis constrained by the values of experimental data. In particular the constraints caused by MSE and polarimetry are used in the equilibrium fitting (EFIT) code to optimise the equilibrium evaluation. To increase the reliability of q–profile estimates, fast signals and MHD analysis can, in some cases, give precise information on the position of rational surfaces. Recent tools for MHD analysis include the corrections to the magnetic island rotation due to diamagnetic effects. The EFIT analysis, with MSE plus polarimetry, is particularly well confirmed in the hybrid regime by the systematic analysis of MHD data carried out using the new tools.

1.6 Construction of the First Phase of the PROTO–SPHERA Experiment

The PROTO–SPHERA system is a simply connected magnetoplasma configuration, composed of

- a spherical torus (ST, with external diameter $2\times R_{sph}=0.7$ m, with closed flux surfaces and toroidal plasma current $I_{ST}\leq 240$ kA) and
- a hydrogen plasma arc, taking the form of a screw pinch fed by annular electrodes (fig. 1.35): $R_{Electrode}=0.40$ m, $\Delta Z_{Electrode}=0.04$ m (SP, with length $L_{Pinch}\approx 2$ m and midplane diameter $2\times\rho_{Pinch}\approx 0.08$ m, with open flux surfaces and plasma electrode current $I_{Electrode}=60$ kA.

The central metallic conductor of a spherical tokamak will be replaced in PROTO–SPHERA by the SP acting as a plasma central column: resistive instabilities will drive magnetic reconnections, injecting magnetic helicity, poloidal flux and plasma current from the electrode–driven SP into the ST and converting into plasma kinetic energy a fraction of the injected magnetic energy (fig. 1.35).

In order to compare the plasma performance of PROTO–SPHERA with that of a spherical tokamak with a metal centre post, geometrical size and plasma currents very similar to those of the pioneering spherical tokamak experiment START, operated in Culham from 1991 to 1998, have been chosen. Under the collaboration established with UKAEA–Culham, in 2004 Culham donated to Frascati the available START equipment (in particular the vacuum vessel), see figure 1.36.

In order to clarify the breakdown conditions and pinch stability before the formation of the ST, the MULTI–PINCH test–bench has been designed as a reduced setup of the PROTO–SPHERA experiment, devoted to assessing and clarifying the most critical points of the PROTO–SPHERA experiment from the SP viewpoint: to explore the breakdown conditions and the pinch stability in the starting phase of the PROTO–SPHERA discharge, in the presence of the poloidal field (PF) shaping coils alone and therefore in the absence of the ST.

MULTI–PINCH explores the first phase of the PROTO–SPHERA discharge ($I_{Electrode}\leq 10$ kA), in the presence of the shaping subset of the poloidal field coils alone and therefore in the absence of the ST (fig. 1.37). The MULTI–PINCH cathode is the final PROTO–SPHERA cathode, only partially filled with tungsten filament modules (54 vs 378). Each filament will deliver its maximum plasma current (150 A). The screw pinch amplifier will be limited to the first unit ($I_{Electrode}\leq 10$ kA) and also the cathode heating power supply will be 1/6 of the final power (10 kA and 25 V ac).

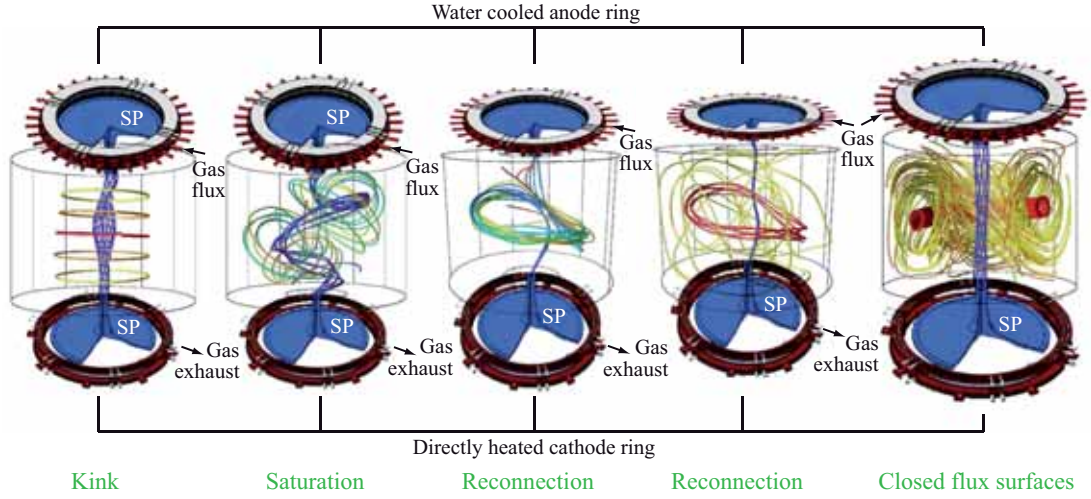

Fig. 1.35 – Sketch of the PROTO–SPHERA plasma formation

[1.71] F.P. Orsitto et al., Plasma Phys. Control. Fusion **50**, 115009 (2008)

Fig. 1.36 – The START vacuum vessel being transferred from Culham to Frascati in 2004

Fig. 1.37 – CAD model of MULTI–PINCH, showing the disassembling of the cathode group from below

Fig. 1.38 – a) Modules of the final annular anode of MULT–PINCH; b) annular cathode with 54 tungsten filaments

MULTI–PINCH will also be relevant for the main tokamak line for exploring biased divertors and plasma sources for neutral beam injectors ($P_{Electrode} \approx 20$ MW/m^2) and for high current vacuum arcs ($j_{Electrode} \approx 1$ MA/m^2) in the presence of guiding magnetic fields.

The MULTI–PINCH vacuum sealed poloidal field coils (four pairs) were completed in March 2007 by ASG Superconductors (Genoa). Like all the other load–assembly and power supply components built for MULTI–PINCH, the four pairs of PF shaping coils and their power supply will be fully reusable for PROTO–SPHERA.

A European call for tender for the remaining parts of the MULTI–PINCH load assembly was started in spring 2007 and adjudicated in November 2007 to ASG Superconductors (Genoa). In June 2008 the emptied START vacuum vessel was shipped from Frascati to ASG.

Fig. 1.39 – a) Anode group with nearby plasma shaping coils; b) cathode group

Fig. 1.40 – a) Final closure of cathode group – lower part of MULTI–PINCH; b) final closure of anode group – upper part. ASG Superconductors Genoa (October 2009)

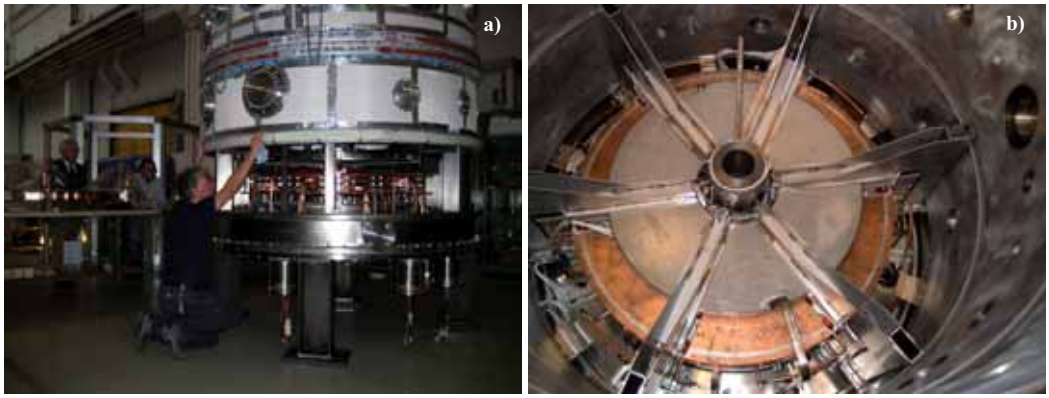

Fig. 1.41 – The cathode group: a) during assembly; b) inside the vacuum vessel

Fig. 1.42 – MULTU–PINCH at ASG Superconductors (Genoa) ready for vacuum test (October 2009)

In December 2008 ASG completed the work for the detailed design of the load-assembly and started its construction. Figures 1.38 to 1.42 show the final phases of construction at ASG Superconductors in Autumn 2009.

The machine will be delivered to Frascati within December 2009.

2. Fusion Advanced Studies Torus

The Fusion Advanced Studies Torus (FAST) conceptual study has been proposed as a possible European ITER–satellite facility for preparing ITER operation scenarios and helping early DEMO design and R&D. Insights into ITER operation regimes and the physics of reactor–relevant plasmas can be obtained from experiments for integrated studies on i) plasma–wall interaction (PWI) with a very large power load; ii) open questions concerning plasma operation, i.e., edge localised modes (ELMs), plasma control, etc., and iii) nonlinear dynamics (which are important for understanding alpha-particle behaviour in burning plasmas) by using fast ions accelerated by heating and current drive systems.

The objectives of FAST are to help the preparation of ITER scenarios and the development of new expertise for DEMO design and R&D in an integrated way; simultaneously address several aspects of nonlinear dynamics, which are relevant to understanding alpha particle behaviour in burning plasmas and their interaction with plasma turbulence and turbulent transport; exploit advanced regimes with a long pulse duration compared to the current diffusion time and up to full non–inductive current drive (NICD); test technical innovative solutions for the first wall/divertor directly relevant to ITER and DEMO; and provide a test bed for ITER and DEMO diagnostics as well as an ideal framework for model and numerical code benchmarks and verification/validation in ITER- and DEMO–relevant plasma conditions. The prerequisites to be satisfied in order to reproduce the physics of ITER–relevant plasmas yield the following set of FAST parameters: 1) plasma current I_p from 2 MA (corresponding to full NICD) up to 8 MA (corresponding to maximised performance); 2) auxiliary heating systems able to accelerate the plasma ions to energies in the range of 0.5–1 MeV; 3) major radius of about 1.8 m and minor radius around 0.65 m; 4) pulse duration from 20 s for the reference H–mode scenario, up to 170 s (~40 τ_{res}, with τ_{res} the resistive time) at 3 MA/3.5 T.

2.2 Physics

Physics basis

The possibility of investigating integrated burning plasma physics issues in an ITER–satellite facility largely relies on the similarity argument based on the existence of three dimensionless parameters in the equations governing quasi-neutral, collisional, finite–β plasmas; i.e., ρ^*, β and ν^* [2.1]. These parameters are the ion Larmor radius in units of the torus minor radius (ρ^*), the ratio of plasma to magnetic pressure (β) and the ratio of connection length to the collisional mean free path (ν^*). For fixed equilibrium geometry and profiles, the similarity argument corresponds to having one free quantity to choose from B (magnetic field), R (major radius), n (density) and T (temperature). The choice underlying the FAST [2.2] scientific rationale is to relax the idea of maintaining identical ρ^*, β, ν^* and fixing T with the consequent $\rho^* \propto R^{-1/2}$ scaling. This choice ensures systematic derivation of FAST plasma scenarios in which ρ^* differs from the ITER [2.3] value by a factor of $3^{1/2}$ at most [2.4]. For a fixed ratio of the fast particle (FP) slowing down time (τ_{SD}) to the energy confinement time (τ_E), fixing T implies fixing plasma performance, since $\tau_{SD}/\tau_E \propto T^{5/2}/N$, with $N=nT\tau_E$. Fixing T corresponds to controlling edge physics conditions and plasma wall interactions (PWIs) as well.

As anticipated in [2.2,2.4], the FP population must satisfy the following criteria: a) E_H must satisfy the condition $E_H > E_{crit} \propto T$, with E_{crit} the critical energy, corresponding to dominant electron heating by FPs (≈70% by fusion as in ITER); b) the fast–ion–induced fluctuation spectrum must be preserved in mode number ($\rho^*_H \sim \rho^*_{H,ITER}$) and normalised frequency ($(\omega_H/\omega_A) \sim (\omega_H/\omega_A)_{ITER}$, with ω_H the FP characteristic frequency [2.5] and $\omega_A = v_A/qR$ the Alfvén frequency); c) the strength of the wave-particle interaction must be conserved (given β, $\beta_H \sim \beta_{H,ITER} \Leftrightarrow (\tau_{SD}/\tau_E) \sim (\tau_{SD}/\tau_E)_{ITER}$). Selecting T≅13 keV, and by assuming the perpendicular supra-thermal ^{3}He minority tail $\propto \exp(-E_H/T_H)$ due to ion cyclotron resonance heating (ICRH) in D plasmas, it is possible to show that $T_H \cong 750$ keV [2.4] gives ≈70% of collisional power transfer from FPs to electrons. Following [2.6], one can further relate T and R imposing that $\tau_{SD}/\tau_E \sim$ const and using a confinement scaling law, such as ITER98y2, for expressing $N \propto (I_p/R^{a})^{5/2}$ with a=1/3 [2.6]. By using the standard scalings [2.6-2.8,2.1,2.2,2.4], $N \propto (T^{1/2}/R^{a-1/2})^{5/2}$ and it follows that $T \propto R^{1/3}$, $I_p \propto R^{2/3}$, $B \propto R^{-1/3}$, $\tau_{res} \propto R^{3/2}$ (resistive time), $\nu^* \propto R^{-2/3}$, $P_{ADD} \propto R^{5/6}$ (additional power) and $N \propto R^{5/6}$ [2.4]. These scalings encompass physics integration as discussed above and in [2.4]; meanwhile they allow one to elucidate how physics integration reflects on macroscopic design parameters as a function of system size. A larger device would be favoured by a moderate improvement. Note that, given wave-number spectrum invariance, normalised frequency invariance with regard to ω_A and/or ω_{Ti} (the thermal ion transit frequency) automatically implies normalised frequency invariance with regard to magnetic and diamagnetic drift frequencies close to those of ITER relevance ($\rho^* \propto R^{-1/2}$ and $\nu^* \propto R^{-2/3}$). However, in order to achieve long pulse operation, it would be more demanding as regards additional power ($P_{ADD} \propto R^{5/6}$) and discharge duration ($\tau_{res} \propto R^{3/2}$). Engineering constraints would also become increasingly severe ($B^2R^2 \propto R^{4/3}$) and cost would levitate (€$\propto B^2R^3 \propto R^{7/3}$). For instance, a device of R=3 m would be marginally closer to ITER than FAST (R=1.82 m). Meanwhile, such a device would require B=6.3 T, I_p=9.1 MA and P_{ADD}=45 MW to achieve the same integrated physics as in the FAST H-mode reference scenario, it would need to operate with a pulse length of 360 s at P_{ADD}=60 MW to reproduce the AT full NICD scenario at 170 s, and it would be more than three times as expensive.

Plasma scenarios and equilibrium configurations

The FAST equilibrium configurations have been designed in order to reproduce those of ITER with scaled plasma current, but still suitable to fulfil plasma conditions for studying operation problems, plasma–wall interaction and burning plasma physics issues in an integrated framework [2.9]. An overview of some of the possible achievable configurations is given in table 2.I.

The objective of the H–mode reference scenario is to determine the complete plasma behaviour and study plasma transport and the confinement of FP (~1 MeV) ions produced by 30 MW of ion cyclotron [2.5] minority (~1% of ^{3}He) heating. All the plasma parameters of this scenario have been fully validated by means of the JETTO code, using a semi–empirical mixed Bohm/gyro–Bohm transport model

Table 2.I – FAST plasma parameters

FAST	H–mode reference	H–mode extreme	Hybrid	AT	AT2	AT Full NICD
I_p (MA)	6.5	8	5	3	3	2
q_{95}	3	2.6	4	5	3	5
B_T (T)	7.5	8.5	7.5	6	3.5	3.5
H_{98}	1	1	1.3	1.5	1.5	1.5
$<n_{20}>$ (m^{-3})	2	5	3	1.2	1.1	1
$P_{th\ H}$ (MW)	14–18	22–35	18–23	8.5–12	5–7	5–7
β_N	1.3	1.7	2.0	1.9	3.2	3.4
τ_E (s)	0.4	0.65	0.5	0.25	0.18	0.13
τ_{res} (s)	5.5	5	3	3	5–6	2–5
T_0 (keV)	13.0	9.0	8.5	13	13	7.5
Q	0.65	2.5	0.9	0.19	0.14	0.06
$t_{discharge}$(s)	20	13	20	70	170	170
$t_{flat-top}$(s)	13	2	15	60	160	160
I_{NI}/I_p (%)	15	15	30	60	80	>100
P_{ADD}(MW)	30	40	30	30	40	40

[2.10,2.11]. Several iterations between JETTO and the TORIC code [2.12], in combination with the steady–state quasi–linear Fokker–Planck (SSQLFP) code [2.13] to deal with the coupled problem of propagation and quasi–linear absorption of ICRH, have made it possible to consistently evaluate the dynamic scenario evolution.

Linear and quasi–linear calculations of ICRH wave absorption have also been performed for the AT full NICD scenario (B_T=3.5 T, I_p=2 MA and central density n_{e0}~2.14×10^{20} m^{-3}) with a ^{3}He minority–heating scheme (7% concentration) by means of TORIC and SSQLFP used in combination. Preliminary results show that the power deposited on minority ions (50%) is completely redistributed to the bulk deuterium ions on the collisional time-scale. Assuming 6 MW of LH at 5 GHz, around 30–40% of I_{LHCD} can be driven well aligned with the foreseen bootstrap current (~60–70%) and with the assumed reversed q profile.

The finite number and toroidal extension of the toroidal field (TF) coils causes a periodic variation in the toroidal field from its nominal value (toroidal field ripple [TFR]), δ_{BT}. The two different approaches studied in order to reduce the TFR amplitude in FAST consist in using ferromagnetic inserts and active coils [2.14]. All the analyses were carried out with the 2D and 3D electromagnetic (em) Ansoft Maxwell FEM® code by assuming a magnetic field of 7.5 T (H–mode reference scenario). Ripple at the plasma

[2.1] B.B. Kadomtsev, Sov. J. Plasma Phys. **1**, 295 (1975)

[2.2] FAST-Team Technical Report ENEA/FPN-FAST-RT-07/001

[2.3] N. Holtkamp et al., *The status of the ITER design*, Presented at the 22nd IAEA Fusion Energy Conference, (Geneva 2008), IAEA Vienna, OV_2-1, on line at http://www-naweb.iaea.org/napc/physics/FEC/FEC2008/html/index.htm

[2.4] A. Pizzuto et al., *The fusion advanced studies torus (FAST): a proposal for an ITER satellite facility in support of the development of fusion energy*, Proceedings of the 22nd IAEA Fusion Energy Conference, (Geneva 2008), IAEA Vienna, on line at http://www.fec2008.ch/preprints/FT_1-5.pdf and to be published in Nucl. Fusion

[2.5] A. Cardinali et al., *Minority ions acceleration by ICRH: a tool for investigating burning plasma physics,* Proceedings of the 22nd IAEA Fusion Energy Conference, (Geneva 2008), IAEA Vienna, on line at http://www.fec2008.ch/preprints/TH_p3-6.pdf and to be published in Nucl. Fusion

[2.6] F. Romanelli et al., Fusion. Sci. Technol. **45**, 483 (2004)

[2.7] K. Lackner, Comments Plasma Phys. Control. Fusion **13**, 163 (1990)

[2.8] K. Lackner K., Comments Plasma Phys. Control. Fusion **15**, 359 (1994)

[2.9] G. Calabrò et al., *FAST plasma scenarios and equilibrium configurations*, Proceedings of the 22nd IAEA Fusion Energy Conference, (Geneva 2008), IAEA Vienna, on line at http://www.fec2008.ch/preprints/FT_p3-11.pdf and to be published in Nucl. Fusion

[2.10] G. Cenacchi and A. Taroni, *JETTO: A free boundary plasma transport code (basic version),* Report JET-IR (88) 03 (1988)

[2.11] G. Vlad et al., Nucl. Fusion **38**, 557-570 (1998)

[2.12] M. Brambilla, Plasma Phys. Control. Fusion **41**, 1 (1999)

[2.13] M. Brambilla, Nucl. Fusion **34**, 1121 (1994)

[2.14] G. Calabrò et al., *Toroidal field ripple reduction studies for ITER and FAST,* submitted to Fusion Eng. Des.

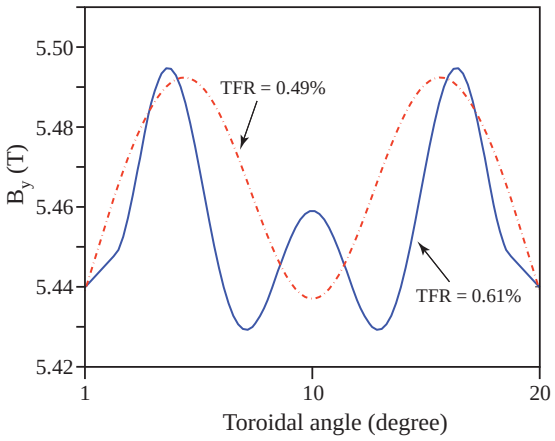

Fig. 2.1 – Toroidal field along the toroidal angle at the radial position (r=2.5 m, z=0.3 m), in the presence of the optimised Fe inserts (solid blue line) and the active coil (dash–dotted red line)

boundary (near the equatorial port) has been reduced from 2% to 0.3% with optimised Fe inserts. The analyses carried out by using active coils showed the possibility of reducing the maximum TFR for FAST at the plasma boundary, on the equatorial plane, well below 0.3%. In figure 2.1 the effect of the optimised Fe insert and active coil are compared at a different radial position, showing that the TFR reduction produced by the active coil is still good.

Preliminary analyses were performed to study control of the plasma current, shape and position during the flat-top of the reference H–mode plasma scenario [2.15]. Optimisation of a copper shell position inside the vacuum vessel slows the vertical stability growth time down to 100 ms, with a comfortable stability margin.

Minority–ion acceleration by ICRH

Minority–ion acceleration by ICRH: a tool for investigating burning plasma physics. Studies on the acceleration of minority ions by ICRH and their utilisation as a powerful tool for investigating burning plasma physics in FAST continued also in 2008. In particular, the stability analysis of collective modes excited by the ICRH–induced energetic ion tail was studied with the hybrid magnetohydrodynamic gyrokinetic code (HMGC) [2.16], once the effective temperature of the minority ion tail and the fraction of fast ions had been consistently evaluated by the 2D full-wave TORIC code coupled to SSQLFP. The resulting anisotropic ($T_\perp > T_\parallel$) Maxwellian initial fast-particle distribution function was used to simulate the nonlinear dynamics of energetic particle modes characterised by various toroidal mode numbers (n= 4, 8, 16 and 24). It is useful to recall that the same toroidal mode numbers (15 <n <25) that will be relevant in ITER are expected to dominate the Alfvén fluctuation spectrum in FAST; moreover, the relevant range of frequencies, if normalised to the Alfvén frequency, will also be the same. For n=4 and 8 [2.17, 2.5] two kinds of parametric studies were done: the first, by varying the minority fraction; the second by varying the perpendicular temperature. In both studies the parameters were changed, while the radial profiles were kept fixed. For higher toroidal mode number simulations (n=16 and 24) [2.18], which require high-performance computing resources, the new machines of the GATEWAY project recently launched by EFDA (http://www.efda-itm.eu/) were employed.

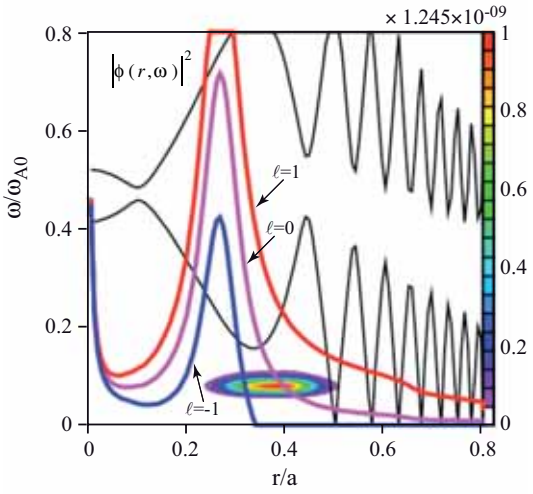

Fig. 2.2 – Mode intensity contour plots during linear destabilisation of n=8 mode. Shear Alfvén continuum (black lines); precession (ℓ=0, magenta); lowest order precession–bounce resonances (ℓ=±1, red and blue, respectively)

In all the simulations performed for the H–mode reference scenario of FAST, the occurrence of one, or more than one, energetic particle mode (EPM) was observed. Typically, the higher the toroidal mode number, the richer the spectra. Radial localisation and frequencies of the observed EPMs (fig. 2.2) are in agreement with the prediction of analytic theory [2.19-2.21]. The dominant contribution from energetic ions can be shown to be due to precession-bounce resonances ($\omega=\omega_{dH}+\ell\omega_{BH}$, with ℓ=0, ±1, and ω_{dH} and ω_{BH} the precession and bounce resonances, respectively) and at a localised radius where α_H is maximum (here $\alpha_H \equiv -Rq^2 d\beta_H/dr$ is the local drive). Low–frequency EPMs exhibit the same

bursting nature as n=1 fishbones, which are internal kink oscillations excited by a magnetically trapped population of fast particles [2.22] and characterised by the same wave-particle resonance excitation mechanism: thus, they can be referred to as high(moderate)–n fishbone–like modes [2.23].

Edge plasma Issue

Problems related to plasma-wall interaction in FAST were analysed, with particular emphasis on divertor heat loads and plasma purity. By using the COREDIV code the FAST scrape–off layer/edge plasma was modelled for both H–mode and stationary scenarios. Injection of impurities was allowed in order to increase the fraction of radiated power when intrinsic impurities were insufficient (W) or inefficient (Li). In all the examined scenarios the divertor heat load was below 18 MW/m^2, which represents the safety limit for the W monoblock technology presently accepted for the ITER divertor tiles. With W as divertor material, a small amount of extrinsic impurities (Ar, Ne) is necessary in the intermediate and in the high–density H–mode scenarios, while Li always needs impurity seeding. The divertor energy load by ELMs was also evaluated: the calculated maximum load of about 1.0 MJ·m^{-2} is believed to be well manageable by the foreseen mitigation systems. [2.24].

2.3 Design Description

Load assembly

FAST (fig. 2.3) operates at a wide range of parameters: high performance H–mode (B_T up to 8.5 T; I_p up to 8 MA), Advanced Tokamak (I_p=3 MA) and full noninductive current scenario (I_p=2 MA). The cross sections of the entire machine show the main parameters (fig. 2.4).

Helium gas at 30 K is used to cool the resistive copper magnets [2.25]. The worst thermal condition corresponds to the long-pulse advanced scenario (170 s, I_p=3 MA/B_T=3.5 T), in which the toroidal coil temperature reaches about 150 K in the inner leg region. The poloidal coil system reaches 85 K as a maximum.

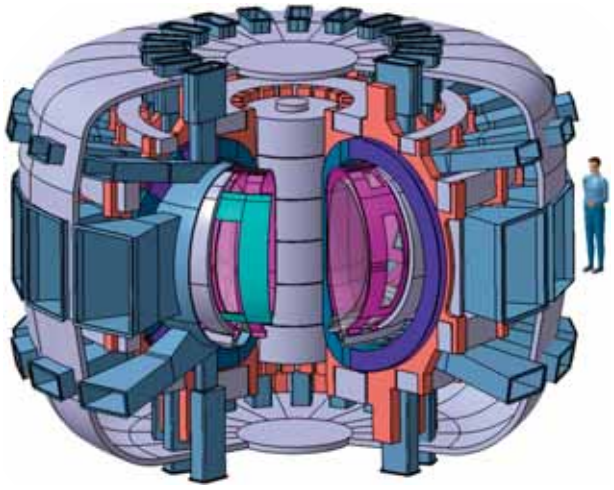

Fig. 2.3 – FAST load assembly view

[2.15] G. Ramogida et al., *Plasma scenarios, equilibrium configurations and control in the design of FAST,* submitted to Fusion Eng. Des.

[2.16] S. Briguglio et al., Phys. Plasmas **2**, 3711 (1995)

[2.17] C. Di Troia, et al., *Investigation of fast ion behavior in burning plasmas via ion cyclotron resonance heating*, Proceedings of the 35th EPS Conference on Plasma Physics (Hersonissos 2008), ECA Vol. **32D**, P5.055 (2008)

[2.18] C. Di Troia et al., *Fast ions transport and confinement in the FAST conceptual design*, Presented at the 13th EU-US TTF Workshop 2008 and 1st EFDA Transport Topical Group Meeting, (Copenhagen 2008), P–51

[2.19] F. Zonca and L. Chen, Plasma Phys. Control. Fusion **48**, 537, (2006)

[2.20] F. Zonca, L. Chen and R.A. Santoro, Plasma Phys. Control. Fusion **38**, 2011 (1996)

[2.21] F. Zonca and L. Chen, Phys. Plasmas **7**, 4600, (2000), and F. Zonca et al., Phys. Plasmas **9**, 4939 (2002)

[2.22] L. Chen, R.B. White and M.N. Rosenbluth, Phys. Rev. Letts **52**, 1122 (1984)

[2.23] L. Chen and F. Zonca, Nucl. Fusion **47**, S727 (2007)

[2.24] G. Maddaluno et al., *Edge plasma physics issues for the Fusion Advanced Studies Torus (FAST) in reactor relevant conditions*, Proceedings of the 22nd IAEA Fusion Energy Conference (Geneva 2008), IAEA Vienna, on line at http://www.fec2008.ch/preprints/TH_p4-6.pdf and to be published in Nucl. Fusion

[2.25] B. Coppi et al., *Ignitor project feasibility study,* ENEA Frascati Contract n° 24137, Status Report (Nov. 1988)

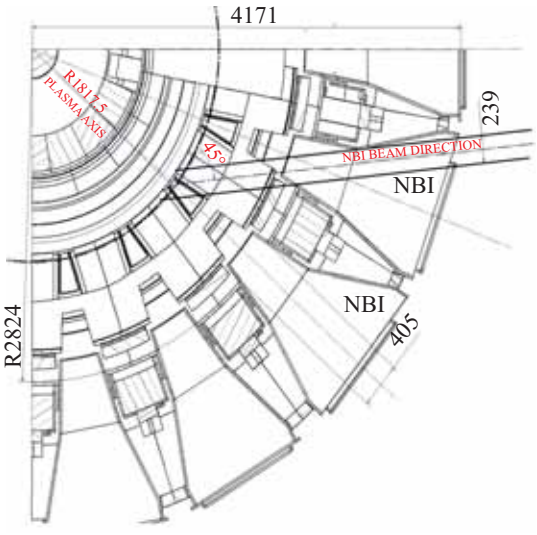

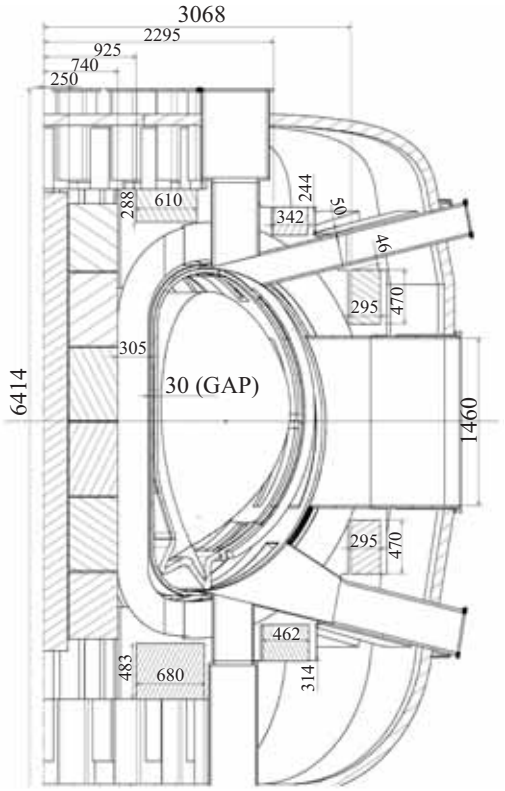

Fig. 2.4 – Cross sections of the FAST machine

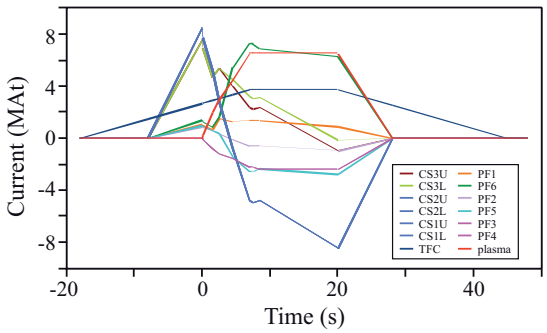

Fig. 2.5 – H-mode reference scenario equilibrium currents

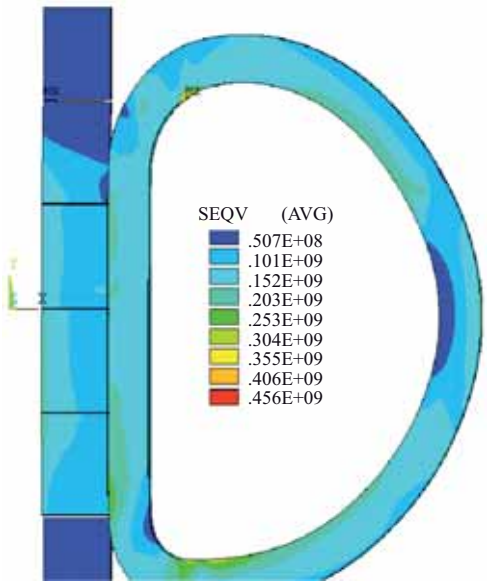

Fig. 2.6 – Von Mises stress (MPa) on copper

The toroidal field (TF) system, operating at the H–mode reference scenario (fig. 2.5) (6.5 MA/7.5 T), is supported by a combination of "wedging", in the TFCs inboard legs, with "bucking" between the toroidal field coils (TFCs) and the central solenoid (CS) (fig. 2.6). Due to the full structural cooperation, the CS and the TF coils have been modelled as a whole. The structural analysis considered the in-plane em loads acting during the plasma current flat-top (i.e., t=8 s). The CS coils were assumed as operating in two alternative states. Normal operating condition with CS coils energised with the scenario equilibrium currents, and fault condition with CS coils de–energised. The highest stresses, less than 250 MPa, were found for the de-energised coils. In normal operating conditions the stress reduces to 200 MPa.

The yield strength of copper alloy is 380 MPa at 77 K and 330 MPa at room temperature. In conclusion, the structural analysis indicates that stresses are within the allowable values for both cases.

The operating scenarios of the vacuum vessel (VV) are characterised by fairly low loads during normal plasma behaviour and rather large loads during a plasma vertical displacement event (VDE)

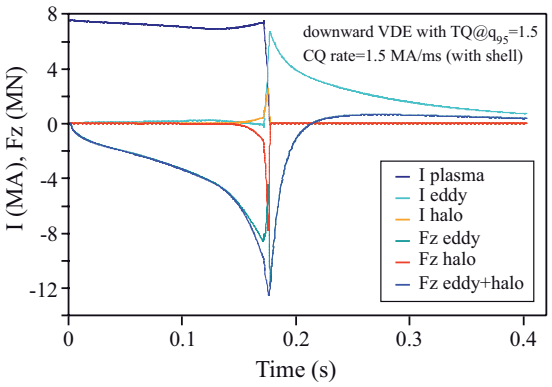

Fig. 2.7 – VDE parameters and Fz EM force

and disruptions. The worst disruption expected is a VDE (fig. 2.7) toward the divertor in the 8–MA H–mode extreme scenario. The loads were obtained by using an appropriate axisymmetric finite element model with the MAXFEA MHD code.

The stresses induced by the VDE loads were obtained by modelling a 20° VV sector with cyclic symmetry as boundary conditions. Extensive 3D finite element stress analyses of the VV performed with ABAQUS code showed average Von Mises (VM) stresses of ~250 MPa (fig. 2.8) and a maximum displacement of ~14 mm. Stresses are within the acceptable limit (Inconel 625 yield strength=420 MPa).

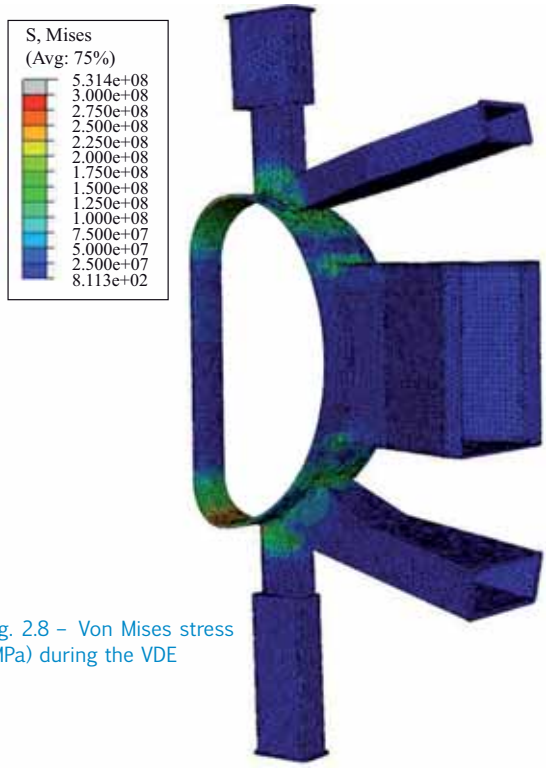

Fig. 2.8 – Von Mises stress (MPa) during the VDE

Heating systems

ICRH system. The scientific rationale of FAST is based on the use of an ICRH system that can provide useful information about the fundamental dynamics of charged fusion products in burning plasmas. The system produces a fast-ion population through the acceleration of minority species. Since the magnetic field of FAST in the H–mode scenario is B=7.5 T, the reference minority species is ^{3}He in the 70–80 MHz frequency range. In its initial configuration the system will couple 30 MW to the plasma. The main parameters of the system are summarised in table 2.II.

Table 2.II – ICRH system main parameters

Frequency range	60 – 90 MHz
Coupled peak power	30 MW
Max coupled power density	10 MW/m^2
Max pulse length	160 s
Min duty cycle	160 s/2h
RF sources (24 units)	2 MW/CW tetrodes
Bandwidth	± 2 MHz @ -1 dB
Launcher type	4 rows of 2 current straps
No. of launchers	

The eight current straps of a launcher are protected by a Faraday shield (FS) made up of a set of 30 non–tilted elements with a smoothed rectangular cross section (fig. 2.9). The main aims of the FS are to suppress the components of the emitted radiation parallel to the local B–field and to shield the electrically active components from direct contact with the plasma. All the antenna components (straps and FS rods) are water–cooled. The front part of the antenna is larger than the access port and has to be installed and connected to the coaxial cables from the adjacent ports. The performance of the launcher has been

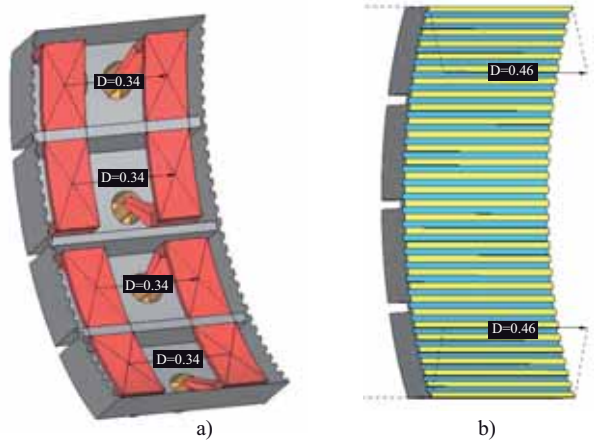

Fig. 2.9 – The ICRH launcher: a) The current straps and b) the Faraday shield

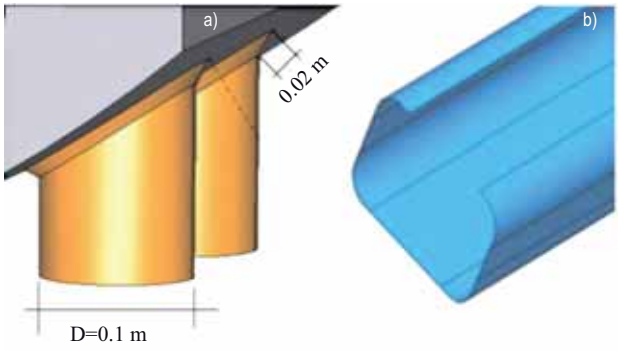

Fig. 2.10 – Launcher optimisation: a) Smoothed connections, b) Rounded rod profile

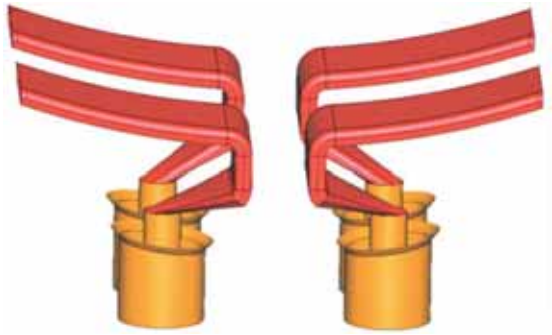

Fig. 2.11 – Bend rounding

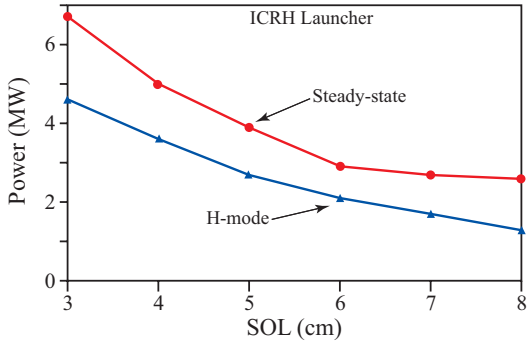

Fig. 2.12 – Coupled power vs SOL

optimised with the TOPICA code, developed by Turin Polytechnic, on the reference FAST H–mode plasma scenario at 80 MHz with 2% of ^{3}He minority. The optimised distance between straps is set to 28 cm. The connections of the straps have been smoothed (fig. 2.10a). The Faraday shield has been optimised by rounding the rod profile and by reducing the rod height to 1.5 cm (fig. 2.10b). The model of the straps has been optimised by rounding their bends (fig. 2.11). The performance of the optimised launcher is given in figure 2.12.

According to the simulation by TOPICA, in steady–state scenarios the launcher is able to couple up to 6.7 MW with a scrape–off layer (SOL) of 3 cm; with the same SOL the coupled power is reduced to 4.6 MW in H–mode plasmas. The computed launched spectra in the steady–state and H–mode scenarios are reported in figure 2.13.

In vacuum the analysis shows very low inter–strap coupling. The current distribution in the straps is very good and almost constant along their entire length. The current in the straps has a very high absolute value. The straps are independently powered in groups of two by a single high–power tetrode (i.e., the TH 526, rated for a maximum radiofrequency (rf) power output of 2 MW in the frequency range 35–80 MHz). Routine operations could be reliably foreseen at 1.5 MW or at higher frequency. A solid–state high–voltage power system (36 kV/380 A) supplies the 24 tetrodes grouped four–by–four.

LHCD system. Lower hybrid waves can be used to control the current density profile and thereby allow the generation and sustainment of advanced regime scenarios in an ITER–like range of plasma densities.

The lower hybrid current drive (LHCD) system for FAST is designed to routinely couple rf power of at least 6 MW in a pulsed regime, with a pulse length of up to 160 s. The working frequency has been set to 3.7 GHz, mainly due to high–power continuous wave (CW) sources already available

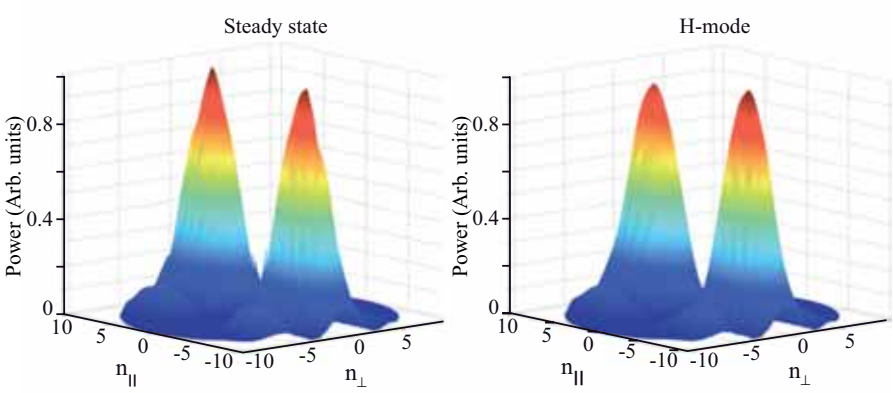

Fig. 2.13 – ICRH launcher – launched spectra

Table 2.III – TH 2103 main parameters

Frequency	3.7 GHz
Bandwidth @ -1 dB	10 MHz
Output power (CW)	500 kW
Gain	47 dB
Cathode voltage	60 kV
Beam current	20 A
Efficiency	42%
Modulating anode voltage	45 kV
Modulating anode current	50 mA

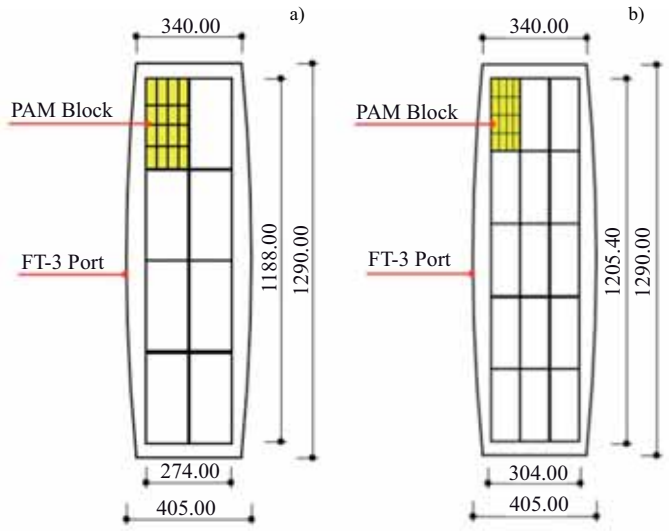

Fig. 2.14 – LHCD launcher configuration: a) 3.7 GHz Launcher, b) 5 GHz Launcher

at this frequency, i.e., the TH 2103 klystron, rated at 500 kW/CW and 650 kW/10 s (table 2.III). This klystron, used on the Tore Supra and JET LHCD systems, is to be further developed for higher performance in CW.

An ITER–relevant passive-active multijunction (PAM) launcher will be used to allow simultaneous coupling of LH waves in plasmas with severe edge conditions (H–mode) and to effectively water cool the antenna in long operations and in the presence of heavy thermal loads. The design of the launcher is based on the requirement of a peak refraction index $N_{||peak}$=1.9 and a maximum power density at the launcher mouth of about 25 MW/m^2 in matched conditions, which is comparable to the values normally achieved in JET and Tore Supra. To achieve this power density, the cross section of the FAST ports makes it necessary to split the overall LHCD power in two independent launchers located in two different equatorial ports of the machine. Each launcher (fig. 2.14a) includes eight PAM blocks arranged in four poloidal rows and two toroidal columns, with each PAM block (fig. 2.15) fed by a 500–kW klystron, so that a total of 8 MW can be installed (16 klystrons).

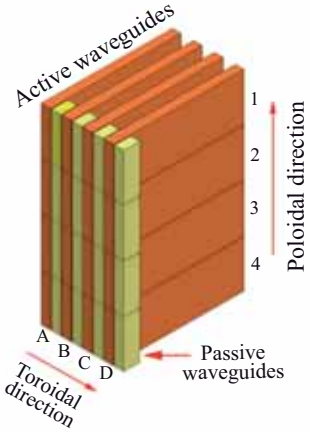

Fig. 2.15 – Computer model of the mouth of a PAM block

A back-up solution with a more suitable 5–GHz frequency has been studied. The final choice will depend on the availability of suitable rf power generators (500 kW, CW). By leaving the block geometry (4 rows × 4 columns) unmodified, the 5–GHz allows the use of a single launcher consisting of 15 PAM blocks arranged in three toroidal rows of five blocks (fig. 2.14b), to couple the minimum required 6–MW power. In this case the power density at the launcher mouth would be 43 MW/m^2 in matched conditions. The main characteristics of the two launchers are given in table 2IV.

Table 2.IV – LHCD system - main characteristics

	f = 3.7 GHz	f = 5 GHz
Pitch between active waveguides	32 mm	24 mm
Waveguide width x height	14x72.14 mm	10x58.17 mm
Wguides per PAM block (act/pass)	16/16	16/16
Overall block dimensions (h x w)	298.54x130 mm	243x98 mm
Coupled power per block	400 kW	400 kW
Power density at the block mouth (*)	25 MW	43 MW
No. of poloidal/toroidal blocks/port	2/4	3/5
Total coupled RF power	6.4 MW	6 MW

(*) In matched conditions

3. Technology Programme

The technology activities carried out by the Euratom–ENEA Association concern the continuation of the European Fusion Development Agreement as well as the ITER activities coordinated by the ITER International Office and Fusion for Energy and include design and R&D activities under the Broader Approach agreement between the EU and Japan.

In order to better contribute to the programme, a number of consortium agreements have been established between the Euratom Associations.

Collaboration with industry in view of participation in the construction of ITER was further strengthened, mainly in the field of magnet and divertor components. The latter successfully withstood severe thermal cyclic tests in the framework of the actions aimed at qualifying ITER suppliers.

Furthermore, the European Test Blanket Facility in operation at ENEA Brasimone represents an important facility for the characterisation of the test blanket module to be developed in the coming years in collaboration with other Euratom Associations. The design of the radial neutron camera has been further optimised and has passed into the wider frame of the port plug activities, also in collaboration with many other Euratom Associations. The performance achievable with the in–vessel viewing system, developed at ENEA and selected as the reference ITER system, has been further assessed by experimental trials.

Design activities for the JT–60SA magnet and power supply system as well as the design and experimental activities related to the International Fusion Materials Irradiation Facility target have been continued.

Significant work was done to define quality assurance for neutronics analyses. Mockups of the ITER pre–compression ring made in glass fibre epoxy were tested and other mockups have been realised to investigate different fabrication routes.

The activities and results documented in the following illustrate ENEA's efforts in supporting fusion development

3.2 Divertor, First Wall, Vacuum Vessel and Shield

Alternative tungsten grade for divertor monoblocks

The feasibility of using an alternative W grade to manufacture the divertor monoblocks is still under investigation (EFDA contract 05/1249). One hundred tiles have been supplied by the Efremov Institute in St. Petersburg, Russian Federation, together with a non-destructive testing report assuring defect-free copper casting. Six monoblock samples in which five W tiles are bonded to the ITER-grade copper tube were successfully manufactured at the ENEA labs by hot radial pressing (HRP) (fig. 3.1). The samples were also non-destructively examined. No joining defects were detected, so they were delivered to the Efremov Institute for thermal fatigue high heat flux testing.

Fig. 3.1 – Tungsten monoblock samples manufactured by HRP

The performance of the W monoblocks will be tested via cyclic high heat flux loading (4,000 cycles per mockup) up to the maximum incident power of 20 MW/m^2. The tests will be performed at the Efremov TSEFEY facility.

W and CFC tile analysis

The profilometric and metallo-(ceramo-)graphic analysis of W and CFC tiles exposed to ITER-relevant Type-I edge localised mode (ELM) and disruption loads was completed at the Quasi-Stationary Plasma Accelerator (QSPA) facility of the Russian research institute TRINITI (task TW4-TPP-TARCAR) [3.1]. The main final results were: in the W tile region within the footprint of the plasma beam, cracks more than 500 μm long as well as much shallower cracks (<50 μm) were visible; on the CFC tiles, erosion of the PAN fibres up to about 120 μm was found (fig. 3.2), but erosion of the pitch fibres was negligible. The PAN fibres also showed crack formation.

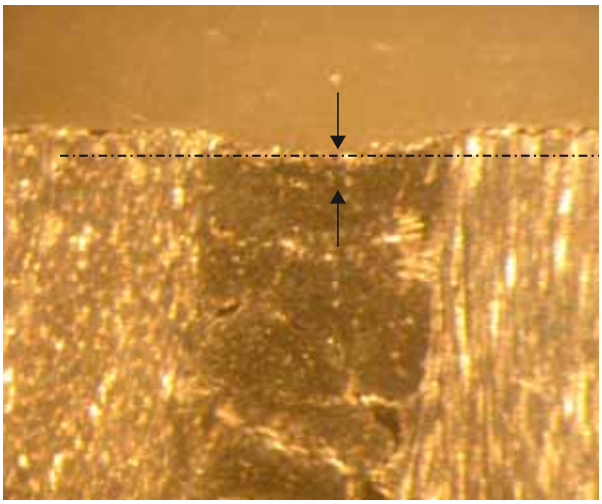

Fig. 3.2 – Ceramography of a CFC tile showing erosion of PAN fibres

Characterisation of ITER PFW panels under thermal fatigue cycles

The Engineering Design Activities (EDA) VI test campaign was completed. Two first-wall panel mockups (Be armoured PH/S 39B and PH/S 40B [fig. 3.3]) were thermal fatigue tested up to 30000 cycles in the EDA-BETA facility. Each cycle consisted of a period of 300 s with a maximum emitted heat flux of 0.8 MW/m^2.

During the whole campaign, the following test matrix was adopted:

- Steady-state tests up to 44 kW of total electrical power, corresponding to an emitted heat flux of 0.80 MW/m^2.
- Total of 11422 fatigue cycles in a power range of 10–44 kW, corresponding to an emitted heat flux of 0.18–0.80 MW/m^2.

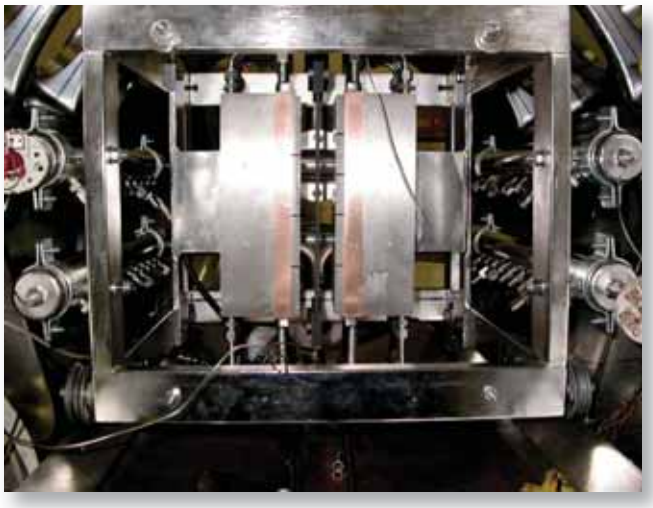

Fig. 3.3 – The two PFW panel mockups assembled in EDA–BETA apparatus

- Total of 18579 fatigue cycles (5–40 kW) corresponding to an emitted heat flux of 0.09–0.73 MW/m^2.

Calorimetric analysis showed that the absorbed heat flux was 0.12–0.67 MW/m^2 in a power range of 10–44 kW and 0.08–0.62 MW/m^2 for 5–40 kW.

Fifteen carbon fibre composite (CFC) electrical heaters were constructed and used to perform the whole thermal fatigue campaign. During the tests the experimental conditions were stable.

At the end of the campaign neither PH/S 39B nor PH/S 40B mockups showed any sign of failure, although the conditions of the Be surface and the hipped joints still have to be analysed in detail.

Hydraulic test of integrated divertor system

One of the most technically challenging components of ITER is the divertor cassette. It requires regular and scheduled maintenance which has to be performed rapidly and reliably. However prior to removing the cassette from the divertor, draining and drying operations have to be performed. Thus the activities were mainly focussed on validating the hydraulic ITER divertor cassette design and improving the remote handling (RH) procedures for the assembly of the three plasma-facing components (PFCs) on the cassette body.

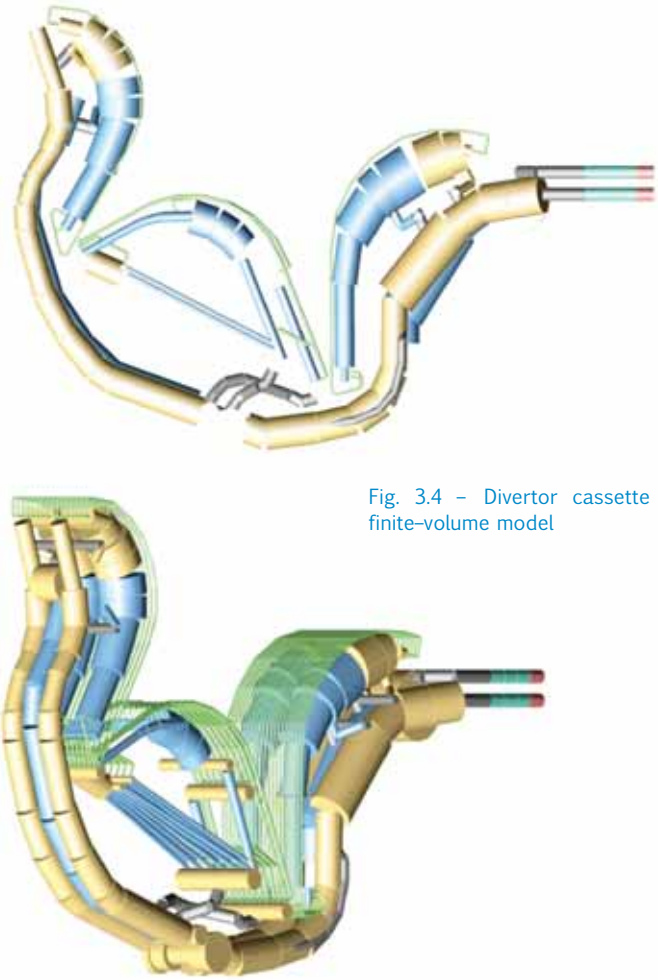

Fig. 3.4 – Divertor cassette finite–volume model

ENEA was in charge of assembling the PFCs on the cassette body (CB) and performing the hydraulic testing of the cassette prototype under both steady-state and transient conditions (EFDA contract 07–1702–1595).

During the reporting period the following activities were carried out:

- Upgrading of the ENEA Brasimone divertor refurbishment platform (DRP) to enable handling of the new ITER divertor cassette prototype.
- Modification of the existing lift frames to lift the separate components (inner/outer vertical targets and dome).
- Launching of call for tender for the procurement of the expansion tool.
- Cutting of manifolds on the PFCs.
- Pre-assembly of the PFCs on the CB with the use of dummy pins.
- Preparation of RELAP 5 model of the CB on the basis of the “as-built” drawings (fig. 3.4).
- Implementation of the existing models of the PFCs.

[3.1] G. Maddaluno, G. Giacomi, E. Serra - TW4-TPP-TARCAR_ENEA_Final report_draft

Dust detection

The previous work on dust detection in FTU by Thomson scattering has been extended (task TW6–TPP–DUSMEAS). Size estimation inferred from laser light scattering was refined by allowing for particle ablation and by searching for a correlation between the amount of detected dust and the plasma parameters just before and after a disruption.

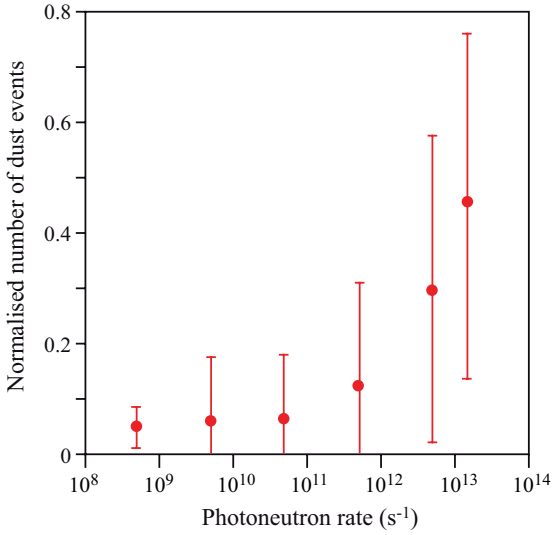

Fig. 3.5 – Amount of dust detected after disruptions vs number of photoneutrons from (γ,n) reactions

Allowing for particle ablation by laser power (indicated by the detection of black–body–like signals from dust particles), it was found that the dust particle radius estimated previously should probably be multiplied by a factor of 4 [3.2].

As for the correlation between the amount of dust detected and the plasma parameters just before a disruption, analysis of more than 1600 shots ending with a disruption and showing the presence of dust [3.3] revealed there was a clear dependence of the amount of dust on the number of detected photoneutrons. Photoneutrons are produced in (γ,n) reactions induced by bremmsthralung radiation emitted during the impact of runaway electrons on plasma–facing components (fig. 3.5). This preliminary result suggests that runaway electrons could be one of the major sources of dust in FTU.

3.3 Breeder Blanket and Fuel Cycle

Test Blanket Modules

Two test blanket module (TBM) options, helium cooled pebble bed (HCPB) and helium-cooled lithium lead (HCLL), are being developed in Europe with the aim of testing these important systems in ITER. However, the possibility of providing ITER with the European TBM systems within the time scale of ITER construction is a strong challenge. The three main milestones identified for the TBM programme are the manufacture, delivery, testing and commissioning in ITER of the systems ready for the first ITER plasma (July 2008).

To cope with the challenge, the TBM Consortium of (Euratom) Associates (TBM–CA) has been established. The objective is to have strategic and organisational cooperation among associates in order to determine the rules applicable to proposals of contracts with the European Domestic Agency (Fusion For Energy [F4E]) to develop, produce, qualify, install and operate the EU TBM systems in ITER. The consortium is made up of CEA, CIEMAT, ENEA, FZK, NRI (CR) and RMKI Hungary. The Consortium Agreement was signed in November 2008. The organisation is to have a governing board, project leader, management support team and four technical divisions. ENEA's role is prominent, with the same voting rights as CEA and FZK on the governing board and with the responsibility of one technical division (Division 3: Helium Loops and Testing).

TBM Consortium – Quality assurance

Quality assurance (QA) is a part of the TBM Consortium project management plan. ENEA has produced the QA documents related to its participation in the consortium.

European Breeding Blanket Test Facility design and construction

The European Breeding Blanket Test Facility (EBBTF), the reference European facility for TBM qualification, consists basically of the IELLLO lead–lithium loop and HEFUS3 helium loop.

In 2008 upgrading of the HEFUS3 facility was completed with the following main modifications:

- new helium/water heat exchanger of 900 kW (fig. 3.6);
- new piping in the hot and cold branches of the loop;
- upgraded electrical power supply unit capable of providing 1000 kW of thermal power (250 kW to first wall +750 kW to breeding zone) to the test section.

All the acceptance tests for the new components as requested by the European Pressure Equipment Directive (PED) and Italian regulations were successful.

Fig. 3.6 – Helium/water heat exchanger installation

The upgrading together with installation in the loop of the new helium compressor, which can provide a mass flow–rate of up to 1.4 kg/s, will render the EBBTF facility unique in terms of size, power and flexibility, and make it possible to test

- the HCLL–TBM mockup, up to 1:1 scale;
- the HCPB–TBM mockups, up to scale 1:1;
- technologies and components relevant for both TBMs as well as the DEMO reactor blanket concepts and main TBM ancillary circuits.

Given the high flexibility of the system it will be possible to test differently sized mockups of both the HCLL and the HCPB. In principle, both types could be operated in parallel at a reduced He flow–rate.

Thermomechanics for HCPB TBM

In 2008, ENEA Brasimone tested the HEXCALIBER mockup and performed the related benchmark activities to assess and validate a pebble bed constitutive model developed in collaboration with Palermo University.

During the HEXCALIBER test campaign, the feasibility of the test section design, fabrication techniques and the functionality of the flat electrical heaters were checked. In addition, issues related to beryllium pebbles were carefully studied in order to have extremely safe operation without the danger of contamination by beryllium dust. In fact, for the first time in Europe, a medium–scale mockup with both lithium orthosilicate and beryllium pebble beds was tested (fig. 3.7). An extensive set of experimental data on the thermomechanical behaviour of pebble beds was obtained during the campaign. The thermal conductivity of lithium orthosilicate and beryllium pebble beds was also investigated.

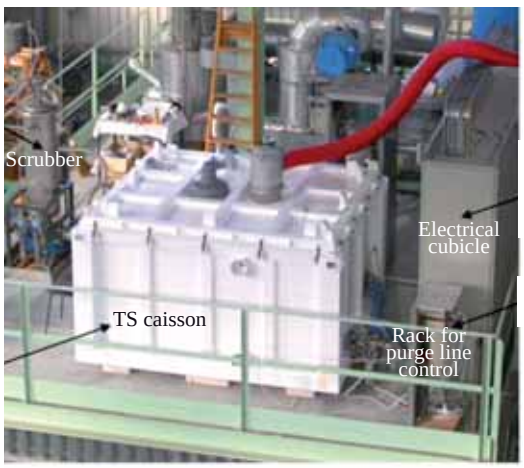

Fig. 3.7 – HEXCALIBER experimental apparatus

[3.2] E. Giovannozzi et al., *Dust in FTU with the Thomson scattering diagnostic,* presented at the 5th International Conference on the Physics of Dusty Plasmas (AZORES 2008)

[3.3] A. Rydzy, *Studio della polvere nel tokamak FTU tramite Thomson scattering*, Dottorato di Ricerca in Elettronica Quantistica e Plasmi (Università degli Studi di Tor Vergata, Facoltà di Ingegneria), in preparation

Within the framework of the benchmark exercise, a detailed 3D finite–elements model (FEM) of the mockup was set up. The helium coolant flow domain was included to appropriately simulate the convection–induced thermal coupling between the mockup and the coolant, which could severely affect the pebble–bed behaviour. Attention was focussed on the numerical prediction of temperatures at the instrumented points located within the pebble beds. Comparison with the corresponding experimental values was satisfactory, particularly for the steady–state phase of each test. The maximum relative error of about 12% was probably caused by a variation in the distance of the thermocouple from the heater, which may occur during the test as a result of pebble relocations.

Technologies of tritium extraction from Pb-17Li: TRIEX loop

To find the most promising technology for extracting tritium from lead lithium is fundamental in developing and designing the TBM auxiliary systems. With the main objective of investigating the behaviour of gas liquid contactors (GLCs) for the HCLL blanket (ITER and DEMO) a tritium extraction (TRIEX) facility was built and installed at the end of 2005 at ENEA Brasimone.

During the third year of TRIEX activity (2008), the loop was modified by adding a by–pass line between the pump inlet/outlet so that the pump would have stable operation in the foreseen experimental conditions. Tests will be started in 2009 with the aim of investigating GLCs based on packed columns: the most promising configuration of the tritium extractor will be qualified and a performance database to implement/validate modelling codes will be developed. The results will be useful for selecting the future TES for HCLL, consisting of the tritium extraction unit and the tritium removal system.

Experimental study on efficiency of oxide layers for hydrogen-permeation reduction through EUROFER and heat exchanger materials (Incoloy, Inconel)

The work to demonstrate the possibility of using natural oxides as tritium permeation barriers was concluded successfully in 2008. Permeation tests were conducted on Incoloy 800 HT. Verification of the performance of the material in terms of permeation reduction factor (PRF) when exposed to oxidant atmosphere confirmed the literature data. This means that Incoloy is naturally covered by a thin oxide layer and that this film is neither damaged nor increased in the experimental conditions. In addition, it is practically impossible to measure the permeation rate in the non–oxidised material, as oxide is immediately produced when the material is exposed to air. The permeated flux was much lower than that found in the literature data referring to virgin material and practically the same in all the tested specimens: The PRF, comparing the experimental results with literature data, was estimated to be 100 times the experimental values found in the literature. These results confirm those obtained for a different nickel alloy (Inconel 718).

Conceptual design of helium processing systems for TBM and determination of TBM–ITER tritium plant interfaces

The coolant purification system (CPS) and the tritium extraction system (TES) are the principal auxiliary circuits of any type of TBM to be tested in ITER. In the HCPB, the TES has to extract tritium from the lithizated ceramic breeder by gas purging, remove it from the purge gas and route it to the tritium plant for final processing. In the HCLL the TES has to extract tritium from the flowing lithium–lead alloy in a dedicated subsystem, which can be based on different technologies, remove it from the resulting gas stream and route it to the tritium plant for final processing.

The CPS has to process a slip stream from the helium cooling circuit in order to remove tritium and incondensable impurities, and to add H_2 and H_2O in order to control the oxygen potential in the coolant.

In 2008 the activities concerning development of the helium processing systems included a revision of the conceptual design of the HCPB–TES and CPS with a breakdown of each system into subsystems and a description of the related main features and functions (fig. 3.8); production of a 3D layout of the TES

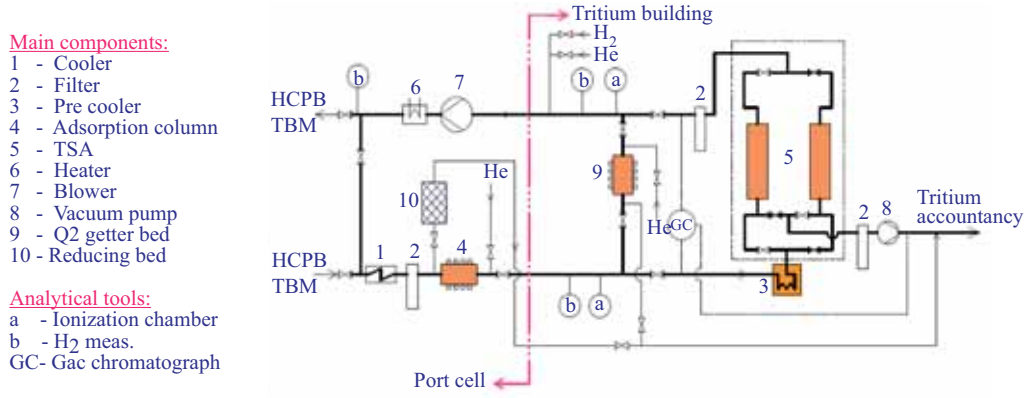

Fig. 3.8 – Tritium extraction system process flow diagram

and CPS to provide a first assessment of the required space; and determination of the flow–rate and composition of the gas stream from the TES and CPS to the ITER tritium systems, for the different operative conditions foreseen during the TBM testing in ITER.

Electromagnetic load calculations and structural analysis of DEMO HCLL blanket

In tokamak machines a plasma disruption causes the rise of eddy currents inside the conductive structures, e.g., first wall and blanket components, particularly on the high magnetic field (inboard) side. These currents, combined with the magnetic field, produce electromagnetic (em) loads, whose widths depend on plasma current, toroidal field and the size and resistivity of the conductive structures and their attachments. In DEMO the structures most involved are the breeding blanket modules, so their design has to satisfy both maintenance and structural constraints, as well as the tritium production requirements.

In this study, the em loads were evaluated for the DEMO multi–module–segment (MMS) HCLL (He coolant, lithium–lead as neutron multiplier and ceramic as breeder) configuration for the case of an accidental plasma disruption. The analysis considered different blanket options (including the vacuum vessel) and attachments of the blanket to the supporting structure. Two geometric configurations were analysed. The ANSYS code was used with appropriate FEMs, and the forces and torques on each blanket module (eight on the inboard, six on the outboard segments) and on the whole multi-module segment were evaluated. Different options of the electrical contact between blanket and manifold and different blanket toroidal segmentations were also analysed for each geometric configuration.

The blanket and vessel geometry used are consistent with the DEMO C plasma option (plasma current 19.4 MA, toroidal field 5.86 T at a major radius of 7.5 m). The em transient was simulated by a major disruption with the plasma at rest and 40–ms linear current quench.

The em body forces resulting from the em analyses were then transferred to a structural mesh for the mechanical analysis of the blanket supporting system. Two concepts of supporting structure, one from CEA and one from European Fusion and Technology (EFET), were analysed for two different em loading scenarios (with different module sizes and electrical connections to the back–plate). The FEM for structural analyses was obtained from the mesh built for the em analysis, hence allowing the em loads to be applied directly onto the structural mesh. This approach permitted a preliminary evaluation of the forces and moments acting on the supporting structure, even though a fully detailed design of the internal structure of manifolds, blanket modules and attachments was lacking. The vacuum vessel was assumed as infinitely rigid in the model.

Linear static analyses at four time points was used instead of static transient analyses which is impractical due to the complex distribution of forces in the multi-module volume. Figure 3.9 shows the time evolution of the total force (on blanket modules and manifolds, inboard and outboard) in the reference case: maximum forces on the supports were observed at the end of a disruption (time step 3).

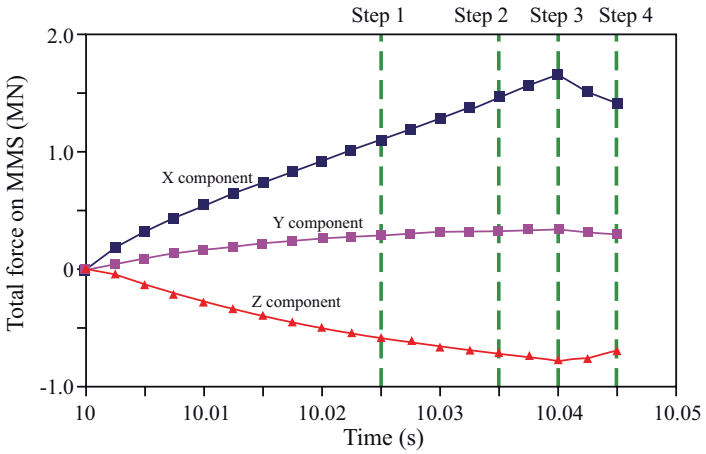

Fig. 3.9 – Time evolution of total force in DEMO during a plasma disruption (reference em loading)

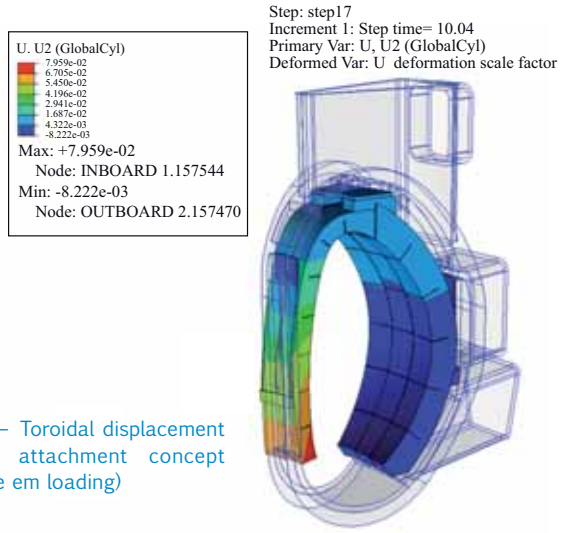

Fig. 3.10 – Toroidal displacement for CEA attachment concept (reference em loading)

Evaluation of the forces and moments acting on the multi–module–segment attachment (CEA concept) for the reference em loading scenario indicated relatively high (about 80 mm, fig. 3.10) toroidal displacement of the inboard segments and high toroidal bending stress (about 400 MPa, fig. 3.11) in the inboard flexion bars, above the minimum yield stress at operating temperature (272 MPa at 500°C).

The EFET concept of multi–module–segment attachment is similar to that of CEA, but the bending bars are lower, shorter and more inclined along the vacuum vessel shape than in the CEA attachment system. In addition there are three bending bars at the outboard instead of two. The same reference em loading was applied to this modified attachment system and showed a moderate reduction in the toroidal displacement (about 65 mm) of the inboard segments, but at the price of significantly higher toroidal bending stress (up to 1500 MPa) in the inboard flexion bars.

The EFET modified configuration was also loaded with the Option 4 em loading scenario (where the blanket toroidal segmentation is doubled and the electrical connection between module and back–plate is only at four discrete points). In this case a significant reduction in toroidal displacement (about 30 mm) in the inboard segments was obtained, while the toroidal bending stress in the inboard flexion bars doubled (up to 800 MPa).

Fig. 3.11 – Stress distribution along inboard bending bars for CEA attachment concept (reference em loading)

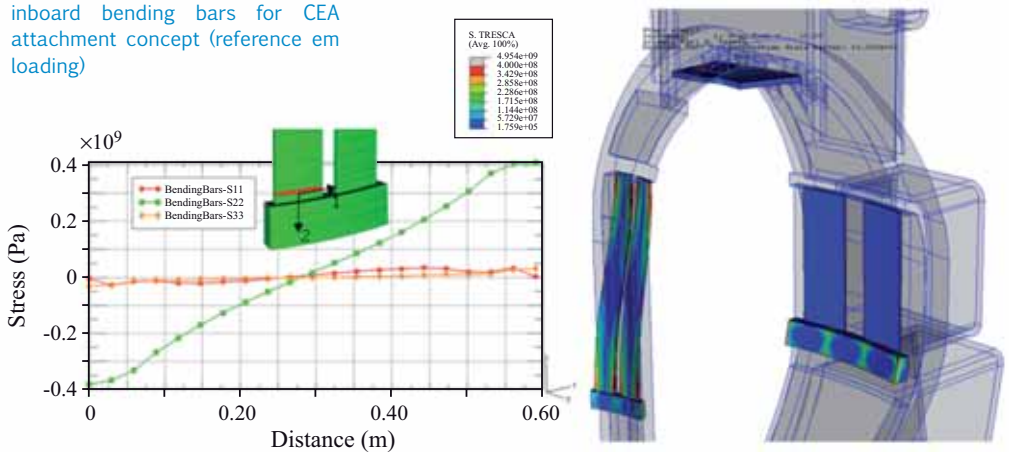

These analyses showed that a significant reduction (a factor of two) in em forces, displacements and stress intensity on the bending bars can be obtained by halving toroidally the blanket modules and connecting them to the back–plate only in the corners (HCLL Option 4 em loading). Moreover the EFET concept of multi–module-segment attachment was confirmed as being more rigid in the toroidal direction than the CEA design, but out–of–plane bending of the inboard bars is too severe even with HCLL Option 4 em loading. Therefore, the inboard attachment system in DEMO needs to be revised.

Tritium confinement

The tritium confinement strategy adopted in the ITER hot cell building was compared with the safety requirements of the applicable French safety codes and guidelines. Several features of the actual design of the hot cell confinement system are not in agreement with these safety requirements [3.4]. (Task TW6–TTFD–TR69–EFDA contract 07–1702/1551.)

The results of the analysis of vent detritiation system catalyst poisoning when exposed to combustion fumes demonstrated the effectiveness of such material [3.5]. (Task ITER TW4–TTFD–TR49.)

Under the EURATOM Research Training Network "Preparing the ITER Fuel Cycle" – (contract No. 042862 (FU 06), ENEA Frascati labs have been preparing a trainee to work in the area of the ITER fuel cycle. The trainee has been involved in studying the design, manufacturing techniques and characterisation of thin-wall permeator tubes via cold–rolling and diffusion welding of thin Pd-Ag foils.

Finally, the completed analysis of tritium diffusion through the neutral beam injector (NBI) calorimeter panel and the safety analysis of the NBI to be built in Padua showed that the diffusion has a very low impact on the environment [3.6, 3.7].

3.4 Magnet and Power Supply

NDT using ultrasonics of circle–in–square but welds for CS and PF conductor jackets

The aim of the activity is to identify a reliable non-destructive testing (NDT) ultrasonic procedure to ascertain the quality of butt welds for the central solenoid (CS) and poloidal field (PF) conductor jackets (EFDA contract 06/TW5–TVD–FABCON).

EFDA supplied ENEA with the welded jacket–mockups. ENEA will introduce artificial defects in the mockups; for example, flat–bottomed holes in one mockup with welding and in one mockup without welding, which will be used as a calibration block, and then several spark erosion notches in two mockups (one without welding), which will be used as reference blocks.

Two 300–mm–long jacket samples (fig. 3.12a) made of SS 316 LN were chosen to manufacture the reference blocks. The first will be used as a calibration block. The second has a multi–pass tungsten inert gas (TIG) welded junction (realised by Ansaldo) in the middle zone and will be used to establish the detection capability of ultrasonic techniques in the welded zone. The weld was also submitted to radiographic testing and no significant defect was found.

Eight artificial types of defect were defined in order to simulate natural welding faults. They will be inserted in both samples: two flat bottomed, 1–mm–diam, 2.5–mm–high holes to simulate porous anomalies and six 0.2–mm–wide notches with different planar size to simulate cracks. They are

[3.4] C. Rizzello, S. Tosti and T. Pinna, *Review of tritium confinement concept and atmosphere detritiation systems in the ITER Hot Cells complex*, ENEA Internal Report FUS-TN-SA-SE-R–192 (June 2008)

[3.5] F. Borgognoni, C. Rizzello and S. Tosti, Fusion Eng. Des. **83,** 1375–1379 (2008)

[3.6] F. Borgognoni et al., *Evaluation of tritium diffusion through the Neutral Beam Injector calorimeter panel*, Fusion Eng. Des., doi:10.1016/j.fusengdes.2008.12.072

[3.7] S. Sandri et al., *The first ITER NB Injector and the ITER NB Test Facility: Nuclear analysis and safety assessment - Site Specific Radiation Safety Report for NBTF*, ENEA Internal Report RTI (2008)4 (Feb. 2008)

Fig. 3.12 – a) Jacket samples for reference blocks; b) miniaturised VRUT–3 TOFD boresonic device

distributed in different circular positions and different planes inside the welded region. The most promising ultrasonic technique is time–of–flight diffraction (TOFD). An ad hoc probe and probe holder have been designed and manufactured (fig. 3.12b). A preliminary feasibility investigation on an available sample gave encouraging results, but some difficulties are expected when inspecting the welded zone.

ITER pre–compression rings

Characterisation. Work on the ITER pre–compression rings (EFDA contract 07–1702/1588) continued with tests of the second ring mockup. Based on the experience gained in testing the first ring and following a FEM analysis, the testing system was improved by applying, e.g., a new stainless steel ring spreader and a steel disc to perform long–term stress relaxation tests with constant ring deformation. Subjected to an imposed deformation corresponding to a mean hoop stress of 800 MPa for about 3000 h, the mockup showed a very contained stress relaxation (~1%) limited to the first 500 h and due mainly to settling of the glass fibres into the composite matrix [3.8]. X rays and ultrasonic surveys showed the presence of some minor delamination after the stress relaxation test.

The mockup was then loaded up to failure and showed an ultimate tensile strength of 1100 Mpa (fig. 3.13), which is a very positive and promising result considering the already tested status of the mockup and maybe some improvements to be done. ENEA commissioned the manufacture of the other five ring mockups to an industrial partner. The characterisation of the composite material of the ring will continue with creep, shear and compression tests.

Fig. 3.13 – Testing machine for ITER pre–compression rings

Characterisation of fibreglass unidirectional S–glass

In 2008 the activities relating to the long-term characterisation of the fibreglass unidirectional S glass (FUS) consisted of several tests performed at stress levels greater than 75% of the ultimate tensile strength (UTS) (2200MPa) of the material. Differences in strain behaviour were observed with increasing stress level: both in strain rate and failure time the material showed that with stresses

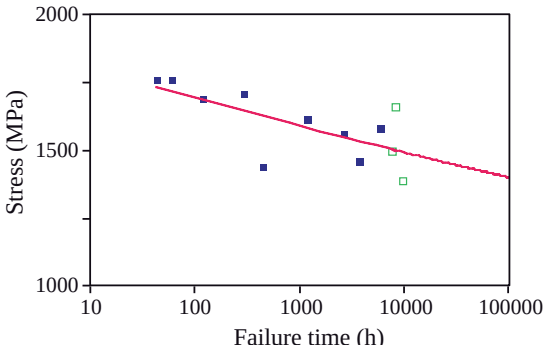

Figure 3.14 – Failure time of samples vs stress level. Open squares: tests in progress (therefore an underestimate of the failure time)

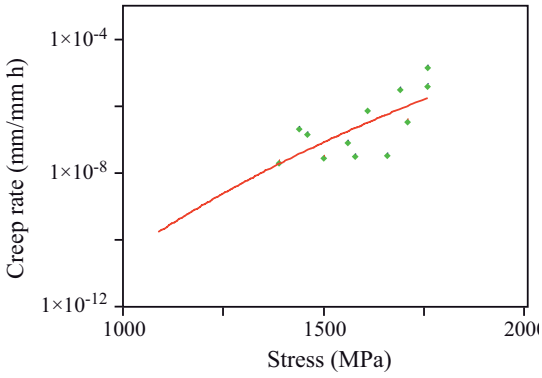

Figure 3.15 – Creep rate of the samples vs stress level

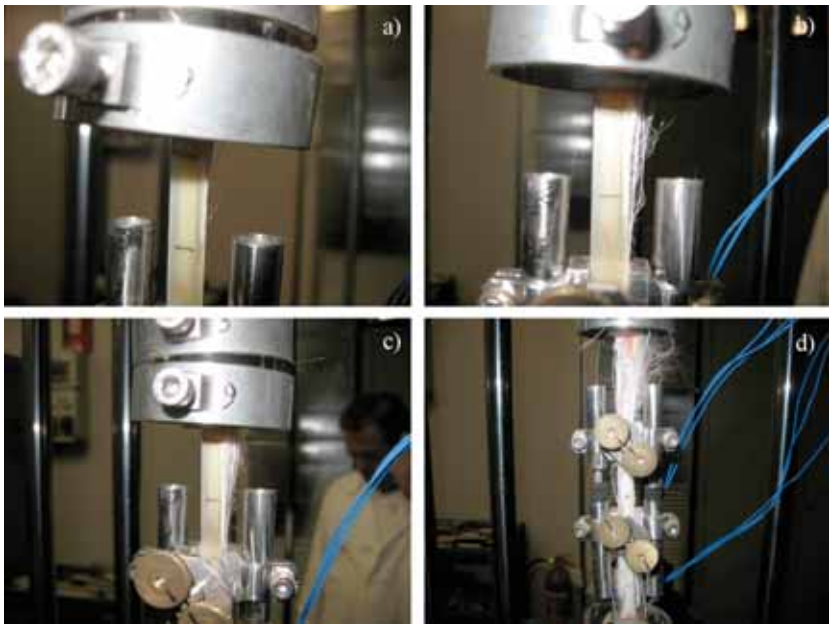

Fig 3.16 – Progress of failure in a sample a) 1217 MPa; b) 1322 MPa; c) 1426 MPs; d) failure, 1426 MPa after 464 h

higher than 75% of UTS it had a faster collapse (failure lower than 500 h) (figs 3.14, 3.15). These tests provided preliminary results on the behaviour of the material subjected to constant loads for a relatively long time. The conclusion from the present test campaign is that at a stress level of 1000 MPa (which can be envisaged for the ITER pre–compression rings), the strain and the failure rate are sufficiently low to assure that the material will have a longer duration than the ITER operating life. Figure 3.16 shows the progress of failure for a sample of VR5–1s.

TF structure closure

Work on the development and qualification of laser welding of the ITER TF structure closure (EFDA contract 07–1702/1589) started in 2008 with the specialised collaboration of the Centro Sviluppo Materiali and IPG Photonics. The activity was divided into three phases: i) Investigation of different root laser welding processes on several samples with different thickness and gaps: Two particular root welding processes, ytterbium fibre laser and hybrid (laser and gas metal arc) welding techniques, were selected and optimised. ii) Qualification phase: a 22–mm–thick root weld with 20 kW ytterbium fibre laser was carried out according to the UNI EN 15614–11 standard, hence comprising non–destructive and mechanical tests. The same standard was followed to qualify a 9–mm–thick root weld with hybrid welding

[3.8] P. Rossi et al., *Stress relaxation testing of pre–compression ring mock–up for the ITER magnet system*, presented at the 25th Symposium on Fusion Technology – SOFT (Rostock 2008), to appear in Fusion Eng. Des.

Fig. 3.17 – Typical macrosection of hybrid weld root pass

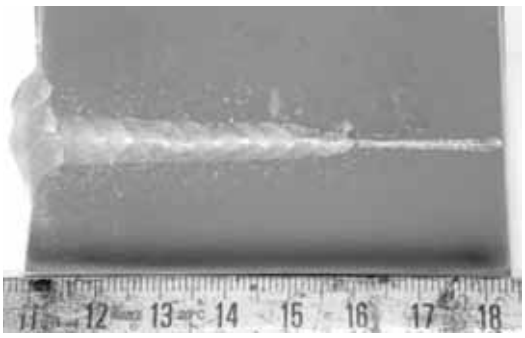

Fig. 3.18 – Typical macrosection of a completely filled groove joint

techniques (fig. 3.17). iii) Final phase: A full 75–mm–thick joint was optimised and qualified following the UNI EN 15614–1 standard, hence with a root laser weld and a filling completed with gas metal arc welding (fig. 3.18). This sample is representative of almost all the welds foreseen for the ITER TF structure closure.

High–frequency/high–voltage power supply for ITER gyrotrons

The activity in support of the manufacture of the main high–voltage (HV) power supply and the development of simulation models of the HV power supplies of the Lausanne gyrotron test facility (fig. 3.19) was successfully completed (EFDA task CCGDS5).

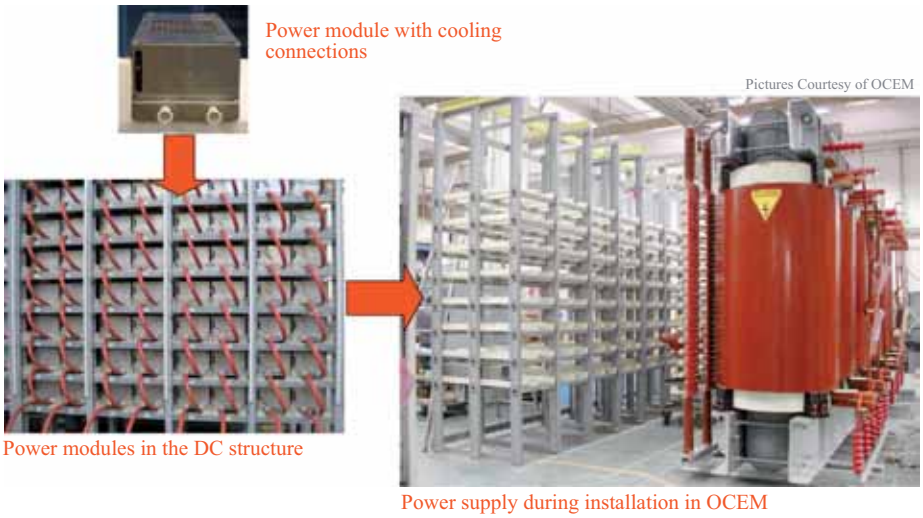

Fig. 3.19 – Main high–voltage power supply for EU EC test facility (Lausanne)

ITER steady–state electrical power network

In the framework of the "Supervision and Collaboration to the detailed Design Activities of the ITER Steady–State Electrical Power Network (SSEPN)", a new solution for the medium–voltage distribution level (22kV) was analysed (EFDA contract 06–1490). The new proposal will probably be endorsed by the International Office.

JT–60SA power supplies

Under the Broader Approach Agreement, analysis of the coil power supplies of the new tokamak JT–60SA continued. In close collaboration with Japan Atomic Energy Agency (JAEA) labs in Naka, the basic features of the coil power supplies were defined and a preliminary layout study developed.

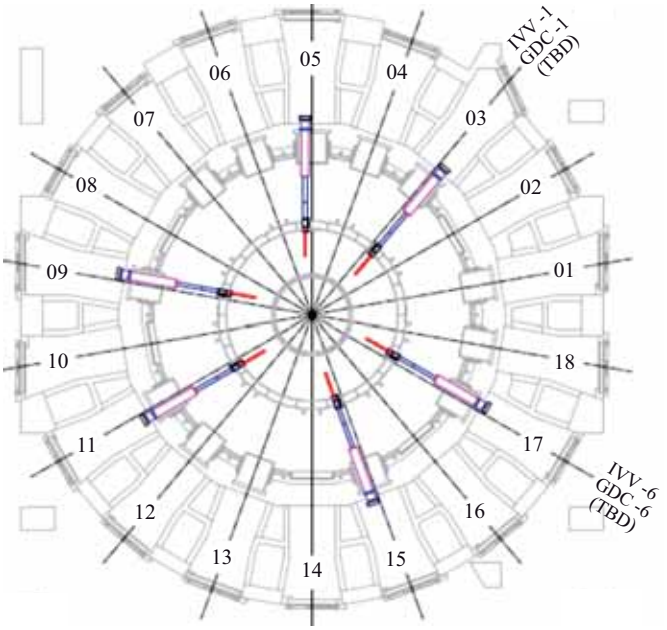

Fig. 3.20 – Top view of the ITER IVVS

3.5 Remote Handling and Metrology

ITER viewing and ranging system

The in–vessel viewing system (IVVS) conceived and developed by ENEA allows inspection of the in–vessel components of fusion machines and by generating 2D and 3D images of the in–vessel surface it is possible to detect damage and possibly measure the erosion of the in-vessel materials. The 3D images are obtained by merging viewing and distance measurements thanks to the optical radar concept used by the IVVS.

After a first test campaign the IVVS reached sub–millimetric accuracy on the principal materials used for the in–vessel components, including the carbon fibre composite (CFC) of the divertor. The system hence become the reference for ITER in–vessel inspection (figs. 3.20, 3.21). In 2008 ENEA won a grant emitted by F4E for the conceptual design of the final ITER in–vessel inspection prototype and the assessment of the present IVVS prototype, finalising the multi–year research for ITER. The activity is expected to begin in the first months of 2009.

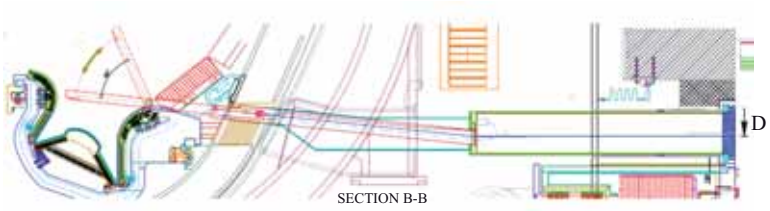

Fig. 3.21 – IVVS insertion in ITER

The target specifications for the IVVS were defined by F4E as follows:

- Metrology accuracy: 0.5 mm at 5–m distance and angle of incidence <80° on ITER–relevant materials and surfaces (sub–millimetric at any distance and angle of incidence <80°).
- Viewing capability spatial resolution: ≤1mm at target distances of 0.5 m–4 m and ≤3 mm at target distances up to 10 m.
- Blind spots close to the penetration point of one probe covered by adjacent probes.
- Environmental conditions during inspection:
  Pressure in UHV conditions –10^{-3} Pa.
  At atmospheric pressure the IVVS is to operate in dry air or nitrogen.
  Operating temperature ≤120°C; baking temperature 240°C.
  Environmental radiation dose rate up to 5 KGy/h (gamma rays).
  Environmental radiation dose: up to 10 MGy (gamma rays) and total neutron fluence 5×10^{13} n/cm^2 (neutrons are flowing to the IVVS storage position during plasma pulses).
- Magnetic field of up to 8 T (to be confirmed) – 0.3 T in storage.
- Inspection time: ≤8 h for an overnight inspection of the whole VV.
- Self–illumination (no need for external light source).

Six IVVS probes are foreseen for inspecting the whole in–vessel surface of ITER. The optimum would be nine probes, but this is not possible because of port availability (fig. 3.20).

The system will be introduced in ITER by means of an appropriate deployer through the divertor port. The last segment of the deployer system, carrying the scanning head, will be able to rotate to place

the IVVS scanning head in the optimal position to scan the divertor or the first wall of the vessel. The probe will be deployed in the vessel during night shifts or at weekends to inspect the inner vessel surface and to plan the maintenance activities [3.9].

Fig. 3.22 – 500–MHz radar electronics

Radar electronics and reflectometer

A key component of the IVVS is the radar electronic equipment (fig. 3.22), which allows vector measurements on radiofrequency signals, detecting the amplitude and the difference in phase of a signal with respect to a reference signal. ENEA patented the technology in Italy. The first release was developed using digital receivers and VME DSP boards, then a miniaturised field programmable gate array (FPGA) based system was developed. The performance of successive releases increased, starting from 80 MHz input frequency and going up to 200 MHz. A further radar electronic release in 2008 increased the frequency up to 500 Mhz with double modulation capability.

A dedicated version was developed, which allows simultaneous detection of the two 20–MHz channels of the reflectometer. The measurement rate was strongly increased from the 100 KHz needed by the IVVS to the 2 MHz needed by the reflectometer.

Fig. 3.23 – HCLL–TBM mockup in front of the FNG target

3.6 Neutronics

Neutronics experiment on HCLL–TBM mockup

A neutronics experiment was carried out on the PbLi/EUROFER steel mockup of the helium–cooled lithium–lead test blanket modules (HCLL–TBMs) in order to validate the capability of neutronics codes and nuclear data to predict the tritium production rate (TPR) and other nuclear responses with qualified uncertainties. A similar experiment had already been performed on the HCPB breeder blanket concept.

The mockup was set up in November and irradiated for two weeks by 14–MeV neutrons at the Frascati neutron generator (FNG) (fig. 3.23). As in the previous HCPB–TBM mockup experiments, the tritium production was measured with the use of Li_2CO_3 pellets (containing both natural and ^6Li–enriched lithium) located at various positions and depths inside the mockup (fig. 3.24). Three independent measuring techniques were employed by ENEA, FZK/TUD and JAEA to measure the tritium in the irradiated Li_2CO_3 pellets. Other independent techniques were also used: thermoluminescence detectors (TLDs), through distinct measurements of the absorbed dose due to the energy released in the (n,t) reaction and in the decay of tritium after irradiation, and diamond detectors covered with ^6LiF. The neutron flux attenuation in the PbLi was also measured by means of the activation foil technique.

Fig. 3.24 – TLDs and Li_2CO_3 pellets in measuring positions inside the central mockup bricks

The measured quantities will be compared with calculations, using a very detailed model of the assembly and experimental setup and nuclear data from the JEFF–3.1 and FENDL–2.1 libraries. The first results for the calculated/experimental (C/E) ratios together with the related uncertainties have been obtained. The sensitivity and uncertainty analysis of the experiment provides the most relevant elements/isotopes and nuclear reactions that contribute mainly to determining the TPR.

Design of the ITER radial neutron camera

The main function of the ITER radial neutron camera (RNC) is to provide the spatial distribution of the neutron source (emissivity profile) and the total neutron source strength (EFDA task 06–1441) [3.10]. Information on other plasma parameters can be obtained from the RNC measurements, depending on the choice of detectors and using data from other diagnostics. The task also includes design and performance analysis in the following areas: diagnostic integration in the port inter–space and port cell; optimisation of collimators for signal, signal–to–noise ratio and neutron streaming; review of the detector types, data–acquisition electronics and calibration methods; integration of the in–port collimators and detectors; update of the performance predictions of the RNC in relation to the ITER measurement requirements; analysis of the possible inclusion of gamma–ray detectors in some of the neutron camera channels. These activities were carried out with extensive use of MCNP calculations and the measurement simulation software tool (MSST) [3.11] for neutron emissivity reconstruction through Abel inversion techniques.

The RNC is composed of two parts: a) The part viewing the plasma core (ex–port) is a massive shielding structure (~30 tons) located in the region between the port and bioshield (port inter space). It is a fan–shaped array of three sets of twelve collimators located on different toroidal planes (2° separation between each couple of planes). Each collimator is equipped with a set of detectors chosen to provide the required range of sensitivity and temporal and spectral resolution. b) The part viewing the plasma edge (in–port) is located inside the port plug and consists of nine collimators subdivided in three sets located in different toroidal planes: two fan–shaped sets of four collimators for upper and lower plasma edge coverage and a single collimator located on the equatorial plane. One important result of the work carried out is that a slight poloidal rotation (±1.3°) of two of the three ex–port planes (fig. 3.25) (so that the RNC has a total of 36 interleaved ex–port lines of sight) could improve spatial resolution and reconstruction capability.

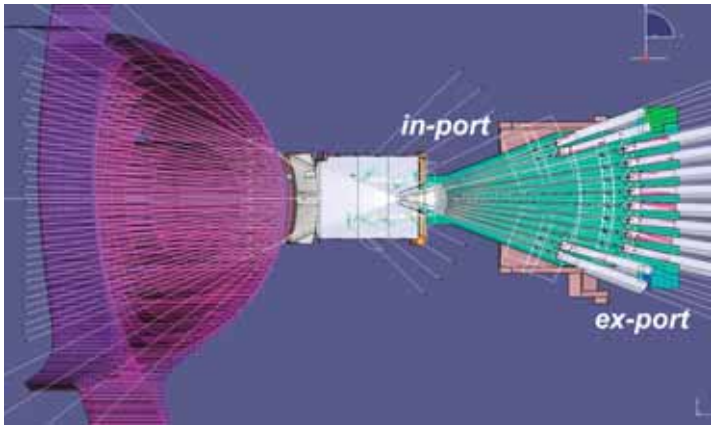

Fig. 3.25 – Updated layout of the ITER RNC including ex–port and in–port lines of sight

[3.9] C. Neri et al., *The upgraded laser in vessel viewing system (IVVS) for ITER*, Presented at the 25th Symposium on Fusion Technology - SOFT (Rostock 2008), to appear in Fusion Eng. Des.

[3.10] S. Salasca et al., *Development of equatorial visible/infrared wide angle viewing system and radial neutron camera for ITER*, Fusion Eng. Des., doi:10.1016/j.fusengdes.2008.12.088

[3.11] L. Petrizzi et al, Fusion Eng. Des. **82**, 1308–1314 (2007)

Table 3.I – Uncollided neutron flux (signal) and collided flux (noise) in the scoring regions of LOS. Neutron source yield DT 1.49×10^{20}

Ex–port LOS	Signal (n cm^{-2} s^{-1})	Noise (n cm^{-2} s^{-1})
1	3.47×10^{7}	4.76×10^{6}
2	4.75×10^{7}	1.86×10^{6}
3	2.92×10^{7}	6.86×10^{6}
4	3.36×10^{7}	1.16×10^{6}
5	3.57×10^{7}	7.59×10^{6}
6	4.00×10^{7}	7.45×10^{6}
7	4.11×10^{7}	8.35×10^{6}
8	4.04×10^{7}	8.42×10^{6}
9	3.79×10^{7}	7.15×10^{6}
10	2.89×10^{7}	6.46×10^{6}
11	5.48×10^{7}	2.57×10^{6}
12	3.94×10^{7}	2.79×10^{6}

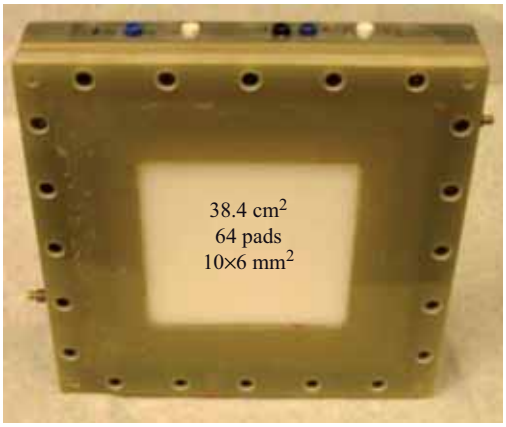

Fig. 3.26 – View of the DT_GEM

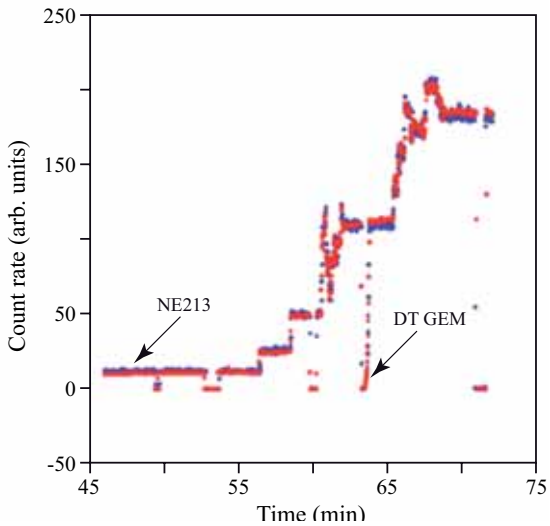

Previous work [3.12–3.14] has been further developed. The biasing technique of the source was improved. Uncollided neutron fluxes were calculated seven meters from the plasma (table 3.I). To verify the performance of a hypothetical gamma camera, the gamma background was calculated. The dose rate after shutdown was calculated outside the RNC system. It has been suggested that the design be modified and the dose lowered to a 100 microSv/hr limit. Simple parametric studies were performed to find the optimal collimator length for the best signal–to–noise ratio, with good intensity.

Development of a GEM 14–MeV neutron detector

The prototype of a new neutron flux monitor for fusion applications has been developed in the framework of an INFN Frascati and ENEA Frascati collaboration. The detector consists of a triple–gas electron multiplier (GEM), a proton recoil converter and a low energy proton absorber. Polyethylene is used as converter and an aluminium absorber sheet covers a triple 10×10 cm^2 GEM filled with an $Ar/CO_2/CF_4$ gas mixture. The detector is read out with 64 pads (10×6 mm^2) in a 4×16 matrix (fig. 3.26). MCNPX was used for the design and optimisation of the detector for 14–MeV neutrons. The results of the first tests under 14–MeV neutron irradiation at the FNG [3.15] indicate good performance at high count rates in a transient neutron flux (fig. 3.27), good efficiency, low sensitivity to gamma radiation and high voltage stability under irradiation. Further developments are foreseen, including the construction of a prototype for 2.5–MeV neutron detection.

Analysis of radiation conditions around the divertor, diagnostic and cryopump ports [3.16]

The activity entailed performing a detailed analysis of the radiation conditions around the lower ports of ITER. The main quantities requested were nuclear heating, dose rate after shutdown, integral dose accumulated during the ITER lifetime and tritium production in selected positions. The information was requested by the designers in order to confirm their assumptions based on previous calculations and to assess the new values according to the new design changes.

The analysis was performed by means of MCNP [3.17] (version 5, version 1.30) with the FENDL 2.1 nuclear data libraries. Dose rate after shutdown was calculated by means of the D1S [3.18–3.20] advanced method, which makes use of a modified code version of MCNP supplied with a special coupled n–gamma transport library. The code and library are considered the reference ITER

Fig. 3.27 – Comparison of DT_GEM (red) and NE213 (blue) signals during 14–MeV irradiation at FNG

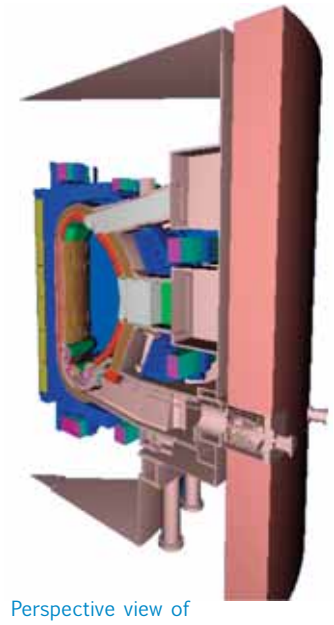

Fig. 3.28 – Perspective view of the 40° MCNP model with the two cryopumps from the outside. Image by SABRINA software

Fig. 3.29 – Map of dose rate 12 days after shutdown (μSv/h) in some zones of the upper cryopump. Behind the bioshield the dose level is lower than 10 μSv/h)

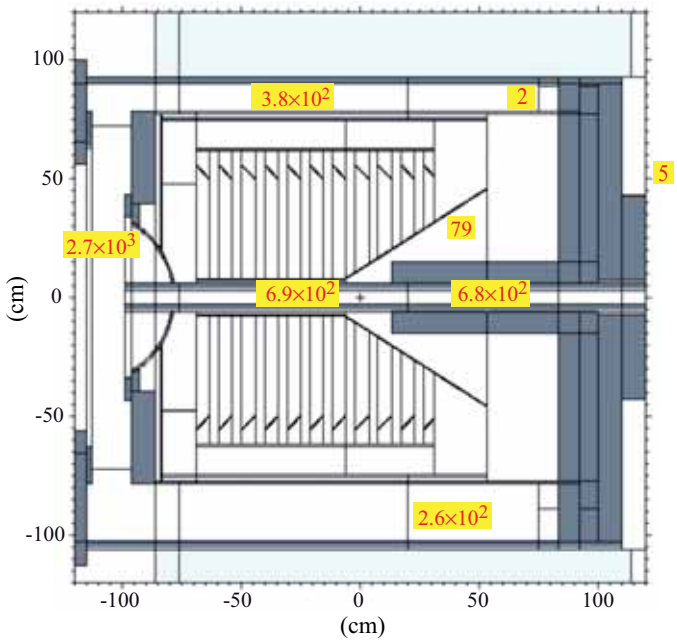

analysis tools and comply with the QA requirement. A full 3D model was developed starting from a general model in which details of the lower ports were added (fig. 3.28). Results are shown for the cryopump (fig 3.29). Compared with the previous analyses they show consistency, taking into account the design changes in the divertor cassette layout and in the cryopumps.

Neutronic analysis of JT–60SA toroidal magnets

A complete neutronic analysis was performed for the current design of the JT–60SA toroidal field coil (TFC) system [3.21]. Nuclear heating of the superconducting winding and the case and the absorbed dose of the insulation and neutron spectra were calculated by means of the MCNP5 code in a full 3D geometry for 1.5×10^{17} n/s DD neutron emission rate. In addition 1% DT due to triton burn–up were considered. The 3D geometrical model of JT60–SA was developed by describing a 20° machine sector bounded by reflecting planes. Poloidal and equatorial sections of the 3D model are shown in figure 3.30. The TFC was poloidally segmented into 14 sectors, labelled from A to N in a clockwise direction.

[3.12] B. Esposito et al., *Analysis of the ITER radial neutron camera*, Final Report on EFDA06/1441 FU06-CT-2006-00488 (Dec. 2008)

[3.13] B. Esposito et al., *Final Report on the Design Analysis of the ITER radial neutron camera,* Final Report Contract FU06–CT–2004–00172 (EFDA/04-1209)

[3.14] L. Petrizzi et al., *Neutronic design of the ITER radial neutron camera*, Presented at 24th Symposium on Fusion Technology - SOFT (Warsaw 2006)

[3.15] R. Villari et al., *Development of the DT_GEM: a gas electron multiplier detector for neutron diagnostics in controlled thermonuclear fusion,* accepted for publication in IEEE Trans. Nuclear Sci.

[3.16] L. Petrizzi et al., *Analysis of radiation conditions around the divertor RH, diagnostic and cryopump ports*, preliminary report ITER 07/028 (Nov 2008)

[3.17] X5 Monte Carlo Team, *MCNP a general Monte Carlo N-Particle transport code*, Version 5, LA-CP-03 0245, Manual Vol. **II** (2003)

[3.18] H. Iida et al., J. Nucl. Sci. Technol., Suppl. 1. pp. 235-242 (2000)

[3.19] L. Petrizzi et al., *Improvement and benchmarking of the new shutdown dose estimation method by Monte Carlo code: advanced Monte Carlo for radiation physics, particle transport simulation and applications*, Proceedings of the MC2000 Conference (Lisbon 2000), Ed. by Springer, pp. 865-870 (2001)

[3.20] P. Batistoni et al., Fusion Eng. Des. **58/59**, 613-616 (2001)

[3.21] R. Villari et al., *Neutronic analysis of the JT–60SA toroidal magnets*, Presented at the 25th Symposium on Fusion Technology - SOFT (Rostock 2008) to appear in Fusion Eng. Des.

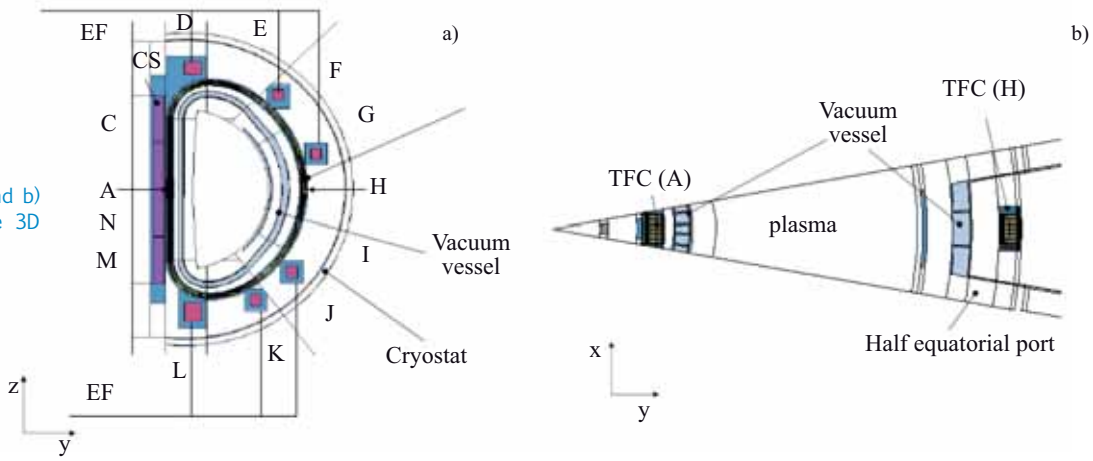

Fig. 3.30 – a) Poloidal and b) equatorial sections of the 3D MCNP model JT–60 SA

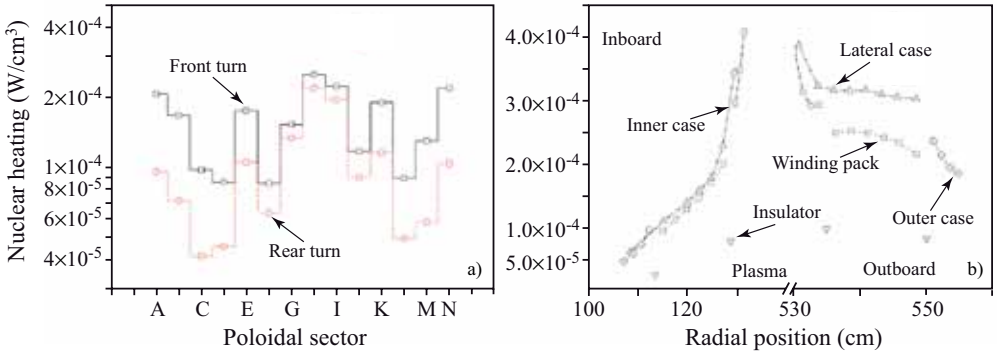

Fig. 3.31 – a) Poloidal and b) radial profiles of the nuclear heating

Table 3.II - TFC magnet system nuclear heating (kW)

Poloidal sector	WP	Case	Insulator	Total
A-B-C-M-N	0.45	0.41	0.03	0.90
F-G-H-I-J	0.92	1.69	0.06	2.66
D-E-L-K	0.64	1.05	0.04	1.73
TFC total	2.02	3.15	2.12	5.30
Total (Safety factor=1.5)	**3.03**	**4.73**	**0.19**	**7.95**

Detailed spatial distributions of the nuclear heating of the winding pack (WP), case and insulator have been calculated and the results, multiplied by the proper safety margin, will be used as input for thermohydraulic calculations. Figure 3.31 shows the a) poloidal and b) radial profiles of the calculated nuclear heating. The nuclear heating of the WP is less than 0.3 mW/cm^3. The value in the outboard innermost turn is ~20% higher than inboard because of the radiation streaming through the large equatorial port. The WP nuclear heating is distributed between the different components in the following percentages: NbTi 10.3%, Cu 43.2%, jacket SS 34.3%, He 2.4% and insulator 9.8%.

The total nuclear heating of the TFC system (for the overall 18–coil system) is summarised in table 3.II for the WP, case and insulator.

The overall power to be removed by helium flow (applying a safety factor equal to 1.5) is about 8 kW, of which less than 40% is deposited on the WP, ~2% on the insulator and the rest on the case.

The estimated absorbed dose to insulator is less than 20 kGy (including 1.8 as safety margin). This is low enough to avoid replacement during the whole life of the machine.

Neutron fluxes were used as input for a preliminary activation analysis performed with the FISPACT inventory code. Activity and contact dose rates were calculated at different cooling times, after 10 years of operation in some representative zones of the WP and case. All the TFC materials can be easily recycled within the first day after shutdown and hands–on recycling is possible within less than 30 years.

3.7 Materials

Thermal characterisation of SiC_f/SiC composites with 2D and 3D textile architecture

Thermal conductivity and particularly through–thickness conductivity play a fundamental role when using SiC_f/SiC as fusion reactor high–flux composites. In the thermal laboratory of ENEA Frascati, the thermal conductivity of chemical vapour infiltration (CVI) SiC_f/SiC was measured up to 500°C in the transverse direction. Thermal conductivity (λ) is calculated from the measured thermal diffusivity (α), the measured specific heat (C_p) and estimated density (r) through the equation:

$$\lambda = \alpha \cdot C_p \cdot \rho \qquad (1)$$

Thermal diffusivity was measured with apparatus that rapidly heats one side of the sample and measures the increase in temperature on the opposite side. The apparatus was set up by ENEA, which also developed a new control system. Figure 3.32 reports the experimental results for 2D and 3D textile architecture.

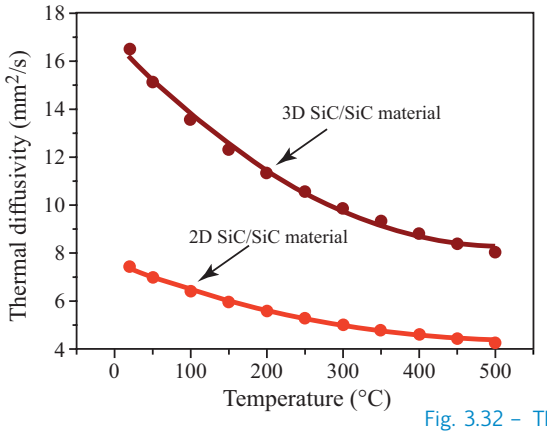

Fig. 3.32 – Thermal diffusivity vs temperature for 2D and 3D SiC_f/SiC textile architecture

The specific heat was measured with a differential thermal analyser (DTA). The method is based on comparison between the specimens to be tested and a known sample. The estimated density of the material calculated from the weight and volume of the samples was 2.53 g/cm^3 for 2D and 2.63 g/cm^3 for 3D textile architecture. The application of equation (1) is shown in figure 3.33. These results show that there is an increase of roughly 100% in thermal conductivity, passing from 2D to 3D textile architecture.

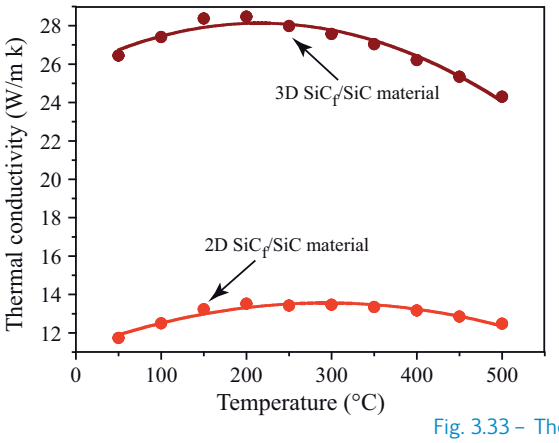

Fig. 3.33 – Thermal conductivity vs temperature for 2D and 3D SiC_f/SiC textile architecture

3.8 International Fusion Materials Irradiation Facility

Back-plate design

The functional and geometrical constraints of the back–plate bayonet option for the International Fusion Materials Irradiation Facility (IFMIF) were studied and the optimal profile to match the thermohydraulic stability requirements was designed

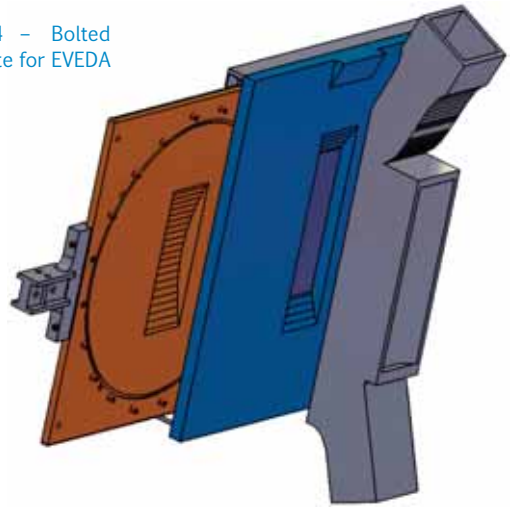

Fig. 3.34 – Bolted back–plate for EVEDA loop

Hydraulic stability analysis of the experiments at the Institute of Physics and Power Engineering (IPPE) Russian Federation pointed out the criteria for minimising flow disturbances:

- Avoid a straight path.
- Minimise curvature changes.

On the basis of these considerations, a new profile was calculated for the lithium channel. It has a central curvature radius of R=250 mm and two slightly curved branches at the inlet and outlet to replace the straight paths. The profile was mathematically traced on the basis of the approximate Bernoulli equation in order to have a linear increase/decrease in pressure along the inlet/outlet path. Starting from this fluid dynamics, the CATIA drawings of a back–plate bolted solution were produced. The engineering design of the bolted solution for the Engineering Validation and Engineering Design Activities (EVEDA) loop has been completed (fig. 3.34); the engineering design of a skate-based back-plate solution is ongoing and will be finalised in the first half of 2009.

Both design solutions can be interfaced with the Japanese (JAEA) design of the target assembly. With regard to the space required for operations, there are no differences between the two options. This is due to the fact that even the skate–based solution requires a limited number of bolts, so the use of a remotely handled wrench has to be considered in both cases.

The proposed back–plate inner profile was traced on the basis of approximate fluid dynamic considerations (the Bernoulli equation) and constancy assumptions on fluid density and viscosity in the temperature range. For these reasons it has to be qualified and validated by means of refined computational fluid dynamic code calculations. Starting from the Navier–Stokes equations and with some simplified hypothesis on the flow, several profiles that satisfied also the geometrical constraints have been calculated.

A profile capable of assuring the linear pressure gradient and satisfying the geometric requirements of the JAEA target assembly reference design geometry has been calculated and traced as function of the vertical ordinate .

Preliminary lifetime evaluation of the back–plate. In order to evaluate the expected lifetime of the present back–plate options, the interconnections between the main damaging causes were studied to find the most plausible reasons for back-plate malfunctioning. Due to a lack of knowledge in some fields and to the early stage of design, the analysis is only semi–quantitative. It accounts for erosion/corrosion, hydraulic stability, neutron damage and thermomechanical stress as the main damaging causes, and has also indicated the research areas which deserve foremost attention during the EVEDA phase. The malfunctions considered are lithium boiling, burning/piercing of the back–plate, insufficient neutron flux, brittle rupture of the back–plate, creep rupture, loss of tightness of the back–plate sealing.

The conclusions of the study were that:

- To prevent a sudden rupture of the back–plate it is necessary to control and assess the possible shift of the Bragg peak by eddy viscosity measurements in the EVEDA loop.
- The control and measurement of the lithium flow thickness also has to guarantee the constancy of the flow rate for long times.

The irradiation ductile–to–brittle transition temperature (DBTT) shift is the most probable reason for failure of the back-plate, with an expected lifetime of less than three months.

Evaluation of irradiation damage of anti-seizing material. The irradiation damage of the Dicronite® (tungsten disulfide) anti–seizing material used in the back–plate tightening mechanisms was

estimated for qualification of the bayonet option (fig. 3.35). The behaviour of the materials subjected to neutron (and gamma) radiation requires a careful calculation of neutron and gamma spectra, deposited energy, displacements per atom (dpa) and gas production. Calculations required a preliminary reconstruction of the back–plate geometry together with spatial discretization, adequate neutron source reproducing the output of the (d,n) nuclear stripping reactions, transport calculations and the production of libraries for KERMA, dpa and gas production cross sections. The calculation results are given in tables 3.III & 3.IV. The highest damage values are obtained in Dicronite® cells 6 and 16. The back–plate material is F82H steel.

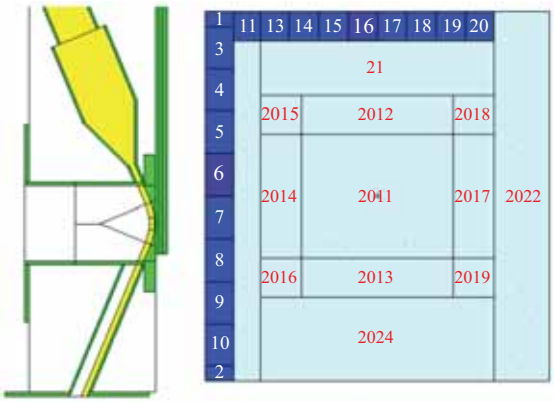

Fig. 3.35 – Model of the target assembly for the nuclear calculations and geometrical layout of the external surface (63×59 cm) of the back–plate in the X–Y plane

Thermomechanical analysis of the back-plate. Thermomechanical analysis of the bayonet bolted solution in IFMIF thermal conditions was carried out. The ANSYS code was used to evaluate the stress and deformation levels which can be achieved in operational conditions (fig. 3.36). The calculations took into account the following

Table 3.III – Total heat and dpa rate in cells 6 and 16 calculated with McEnea (c) and McDeLicious (d)

Zone	Total heat (c) (W/cm^3)	Total heat (d) (W/cm^3)	Dpa–rate (c) (dpa/y)	Dpa–rate (d) (dpa/y)
Cell 6	0.27	0.28	0.20	0.24
Cell 16	0.16	0.17	0.11	0.14

Table 3.IV – Helium and hydrogen production rates in cells 6 and 16 calculated with McEnea (c) and McDeLicious (d)

Zone	Helium production (c) (appm/y)	Helium production (d) (appm/y)	Hydrogen production (c) (appm/y)	Hydrogen production (d) (appm/y)
Cell 6	5.6	5.6	9.3	8.9
Cell 16	2.5	2.5	3.5	3.1

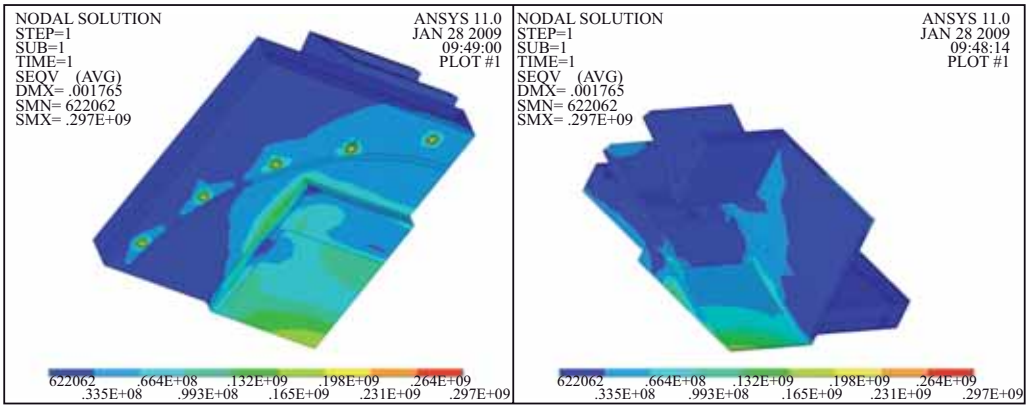

Fig. 3.36 – Von Mises stresses of the bayonet bolted solution

loads: tightening force by the bolts, elastic response of the selected gasket, thermal loads related to the IFMIF beam–on conditions. In the case of F82H material, for all the target parts, the maximum stress level (300 MPa) was reached at the bolt threads and remained well below the plastic limit for the material (463 MPa).

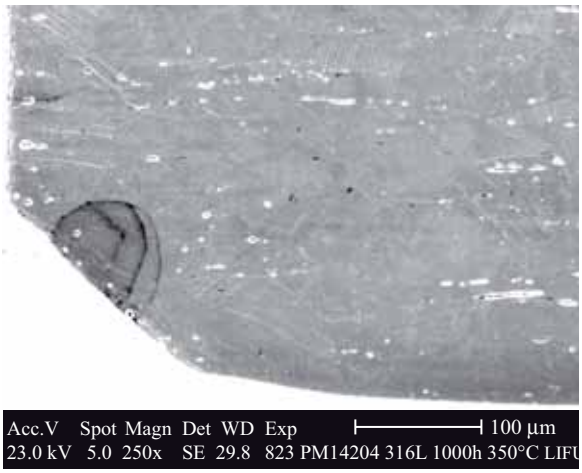

Fig. 3.37 – Material removal on specimen #1. Li flow from right to left

Erosion–corrosion of back–plate materials

The erosion/corrosion loop LIFUS3 was completely commissioned (apart from the purification system) and filled with 42 litres of lithium. The final assembly of the purification system will be finalised in the first months of 2009. A first series of 1,000–h tests with AISI 316 and EUROFER97 specimens was concluded, with the following main results:

- AISI 316 appears, as expected, more susceptible to lithium erosion/corrosion than ferritic-martensitic steels such as EUROFER97. The extrapolated corrosion/erosion rate of AISI 316 exposed at 350°C, 16 m/s flowing lithium is about 48 g/(m^2y) .
- The inlet specimens appeared more corroded than the others and examination (fig. 3.37) revealed localised erosion/corrosion at the flow inlet. This observation can be explained by considering the additional erosion effect due to enhanced turbulence at the inlet of the test section. The Reynolds number increases by 38% at the specimen inlet, which corresponds to an enhanced erosive effect.
- The corrosion/erosion rate of EUROFER97 exposed at 350°C and 16 m/s flowing lithium is about 25.4 g/(m^2y). It is evident that for ferritic–martensitic steels the role played by lithium velocity is more intense than for the austenitic steels.

Remote handling of target assembly system

During 2008, the remote handling (RH) activities under the IFMIF EVEDA phase of the Broader Approach were aimed at validating the back–plate bayonet concept design under IFMIF–relevant environmental conditions, devising a suitable RH strategy for refurbishment of the target assembly system and developing preliminary RH procedures for the target itself. The activities and results are reported below.

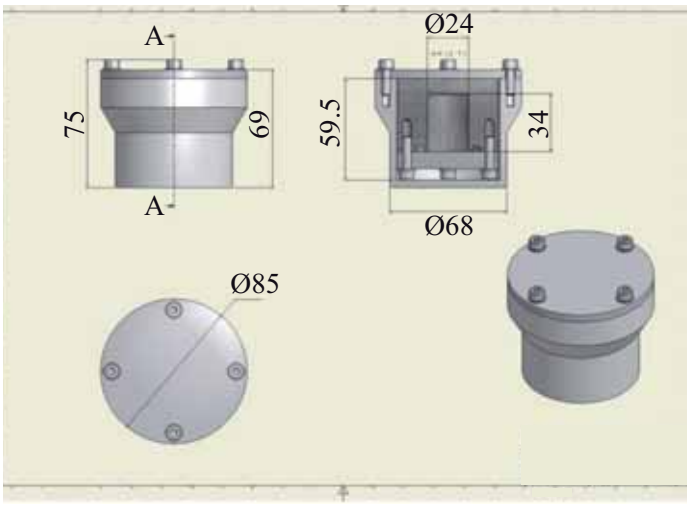

Evaluation of the sealing capability of the proposed Helicoflex gasket. The aim is to verify the sealing performance against Li infiltration and corrosion–induced damage of the Helicoflex HNV 200 type gasket under IFMIF–relevant operating conditions. The design and manufacturing of the test rigs has been completed (figs. 3.38 and 3.39). Each test rig has a capacity of 7–8 g of lithium and will be equipped with a metallic gasket (i.e., Helicoflex HNV200 soft iron/Nimonic 90/SS 304L; cross section=3.3 mm; diameter=34.20 mm).

Fig. 3.38 – Design of the test rigs

Fig. 3.39 – The manufactured test rigs

Dicronite assessment. So far work has been focussed on defining the experimental conditions and the design of the rigs to be tested. To define the experimental conditions (i.e., set up the heavy ion beam accelerator, selection of the ion type and the energy required), the neutron flux distribution on the back–plate and on the tightening mechanisms of the back–plate itself was calculated in the ambit of the neutron analysis task of the Engineering Design Support Activity. A preliminary simulation to select the ion type to be accelerated within the required energy range (i.e., silicon ion at 2–8 MeV) to reproduce similar damage on the rigs was completed in May 2008 (CNR Bologna Italy). The design and manufacturing of the rigs has been completed. Each rig consists of a plate (15×15 mm) made of 100 Cr6 steel covered with a substrate of 0.5–μm–thick Dicronite. The test rigs were manufactured at ENEA. The samples were treated by Dicronite Italia. The test campaign will include complete characterisation of the Dicronite behaviour within a range of 0.5–5 dpa with a step of 0.5 dpa and at high temperature (i.e., ~250°C).

The post-analysis programme includes:

- Measurement of the residual friction capability: friction measurement will be carried out by means of the inclined plane technique. The device to measure this property was designed by ENEA.
- Micro-hardness measurement of the coating and SEM analyses to be performed at the ENEA laboratories.

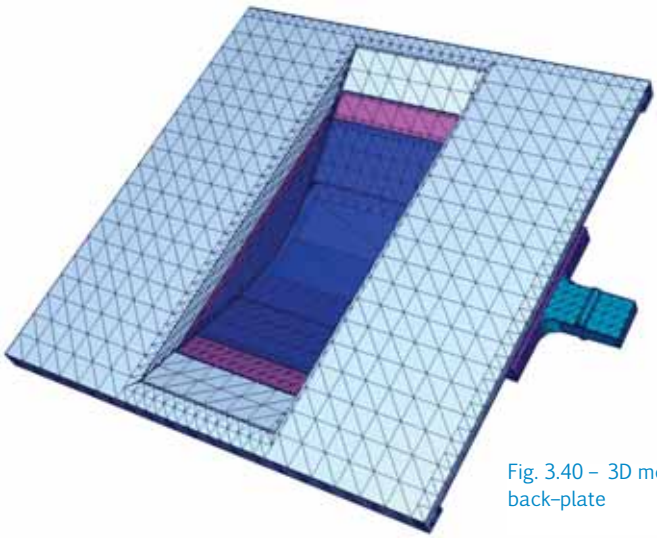

Fig. 3.40 – 3D model of the back–plate

Swelling phenomena. Preliminary analysis of the swelling issue on the locking system of the back–plate was carried out in collaboration with the University of Palermo. Based on the neutron calculation mentioned above, the analysis was aimed at defining the experimental parameters to be used as input for the simulation of swelling phenomena. In particular, the helium and hydrogen production rates inside the structural material will be analysed by adopting a computational stochastic approach and using the Monte Carlo N–Particle (MCNP) code, version 5. In the bolt area of the back–plate the expected damage rate is about 0.3 dpa/year. To assess the upper limit of the bolt working conditions and the holes on the frame of the back–plate support structure, the simulation of these phenomena will be performed within a damage rate range of 0.3–5 dpa. The University of Palermo has already completed the 3D modelling of the back–plate (fig. 3.40); the calculations should be completed by the end of July 2009.

Qualification of the Hicoflex gasket HNV200. A R&D programme between the ENEA and Garlock Company for the qualification of the Gasket Helicoflex HNV200 was defined at the end of 2008. The programme will include full testing of the designed gasket to verify its capability to fulfil all the operating conditions (e.g., vacuum and leak rate) and testing of the gasket materials under irradiation.

The feasibility of the irradiation test campaign, which could be carried out in the ENEA Casaccia Triga reactor, is under study. The following gasket materials will be tested: soft iron, SS AISI 304L, Inconel X 750 and Inconel 718. Samples of 100 Cr6 (bearing material) covered with Dicronite will also be included. Irradiation will be performed in two phases: the first up to a damage rate of 0.5 dpa; the second up to 1 dpa.

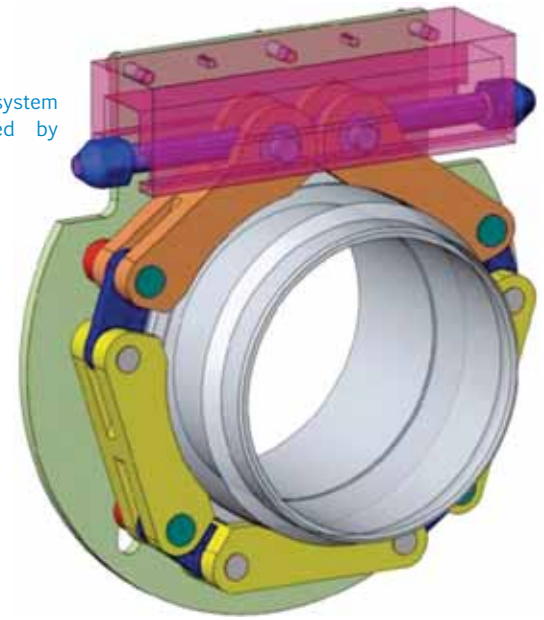

Fig. 3.41 – QDS system (Image provided by Garlock Gmbh.)

Post–analysis of the samples irradiated is under discussion, but it will include at least measurements of the main mechanical properties of the materials.

Design and test of the quick disconnecting system (bayonet concept). The agreement with Garlock includes also the design and testing of the quick disconnecting system (QDS), see figure 3.41. The QDS is the most promising flange connecting system to be implemented for the target assembly.

Lithium cleaning process. Solid lithium deposition on the frame surface of the target assembly could compromise the tightness of the target itself. Hence a suitable and effective lithium cleaning procedure is required to remove the lithium stuck on the target surface. ENEA has experience in the use of a lithium cleaning technique based on a mixed low acidic solution of acetic acid [1N] (CH_3COOH)+hydrogen peroxide (H_2O_2) +ethanol (CH_3CH_2OH) with the same ratio (1:1:1).

This cleaning solution was used at room temperature, for Li, PbLi, Pb, LBE and, according to the measurements and electronic microscopy, no steels (ferritic, martensitic or austenitic) were ever attacked, modified or corroded due to the treatment. This cleaning solution can be used both by immersion or by spraying over a dirty surface.

Remote handling procedures (bayonet concept). So far the RH activity for refurbishment of the target assembly has been focussed mainly on the back–plate replacement. The feasibility of this replacement operation within the time required (i.e., 2 days) had already been assessed. However, in the real environment (i.e., lithium) for this operation, a number of additional tasks could be required:

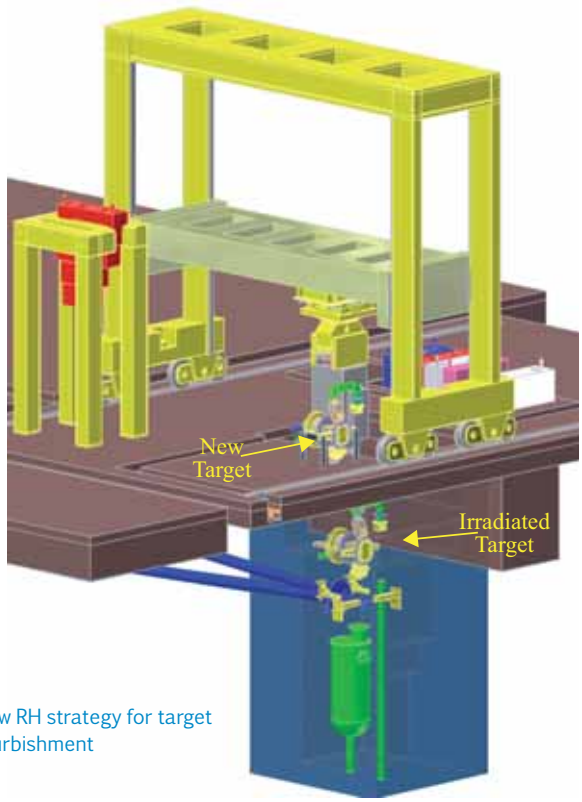

Fig. 3.42 – New RH strategy for target assembly refurbishment

1) Avoidance of back–plate sticking onto the target structure because of solid lithium deposition;
2) inspection of the target structure (nozzle, skate mechanisms, bolts and holes);
3) testing for the assembled back–plate.

In 2008 an alternative RH approach for refurbishment of the target assembly equipped with the back–plate bayonet concept was proposed by ENEA. This new strategy relies on the possibility to perform all the refurbishment operations of the target assembly offline in a hot cell, and on the availability of a new target (previously refurbished) in the access cell ready to be installed (fig 3.42). This approach allows all the RH operations to be performed in a more relaxed and safer way.

A preliminary study highlighted that the intervention time for the in situ back–plate exchange is comparable with the time required for the target replacement if it is attached to the main pipes by means of QDSs.

A preliminary list of RH operations for refurbishment of the target assembly, taking into account various scenarios, and the specifications of the main RH requirements have been prepared.

3.9 Safety and Environment, Power Plant Conceptual Studies and Socio–Economics

Computer code validation

CONSEN. Cryogenic experiments have been carried out in the CEA EVITA facility to validate computer codes for safety purposes. The goal was to simulate correctly loss–of–coolant accidents in the presence of cryogenic panels, which are similar to the surfaces of the superconducting coils in ITER. Experiments performed in the EVITA facility to highlight the mechanism of ice formation and ice–layer growth were in some cases controversial and they will have to be studied in detail to discover why. Figure 3.43 shows similar tests presenting different pressure behaviour. Hence, 15 tests were selected to be thoroughly analysed and simulated again by means of the CONSEN code [3.22]. The outcome of the study confirmed one of the theses of the CEA team, which attributed the differences in the similar test groups to the cryogenic loop not behaving as a constant heat sink. This is the main cause of the unexpected results. In addition, for some cases, the effective flow rates were different from the reference flow rates, which changed the way of interpreting the results, because what seemed incongruent was, instead, congruent. Effects such as the steam condensation around the nozzle for some groups of tests, which had been discussed as possible explanations, can now be excluded as a source of discrepancies because the nozzle temperatures are normally not too dissimilar in the domain of the same group.

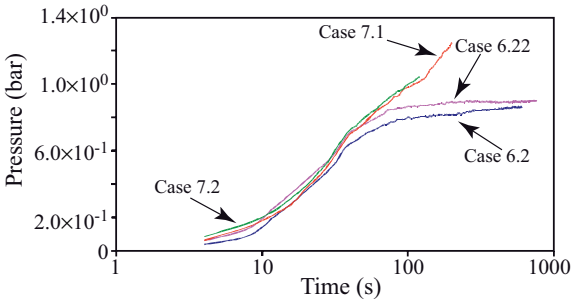

Fig. 3.43 – Pressure trends in tests 6.2, 6.22, 7.1 and 7.2 in the domain of the same group

In the light of the results of the thorough data–analysis and verification by means of CONSEN simulations, a physical justification for all the experiments has been found. The small amount of ambiguous cases is not sufficient to invalidate the quality of the EVITA experimental campaigns.

PACTITER. The new version (3.3) of the PACTITER code was acquired and set up in an ENEA Frascati Server (Linux environment) (September 2008). Preliminary tests were carried out in view of assessing the activation corrosion product (ACP) inventory of the ITER primary heat transfer system (PHTS) for the vacuum vessel (VV) loop, taking into account the most updated design data, and with/without the presence of the chemical volume control system (CVCS). The aim of the tests was to get an independent verification of PACTITER v3.3 and to check the code documentation and the user's manual.

Calculations in support of the ITER DCR-110 “Vacuum Vessel CVCS” were performed by using the old version of PACTITER [3.23]. The possibility to install high–temperature mechanical filters (MF) on the bypass line of the VV PHTS during baking operations was analysed. Three different operative scenarios related to the fraction of the main flow rate coming from the MF were analysed. Raising the filtered fraction has no positive influence in terms of reducing the ion and activity coolant concentration, while it increases the activity captured by the filters.

Implications for Preliminary Safety Report of an increase in the ITER first-wall fluence and of an "all tungsten machine"

The material activation referred to the three cases described below was assessed in 2007 with the use of the EASY–2005.1 activation code package from the United Kingdom Atomic Energy Authority (UKAEA). In 2008, the EASY–2007 (with the EAF–2007 neutron activation library) was used to perform the calculations. All the activation data results obtained and the related analysis and discussion were

[3.22] M.T. Porfiri, *Complementary CONSEN calculations for EVITA cryogenic tests type 5, 6 and 7*, ENEA Internal Report FUS-TN-SA-SE-R-184 (Dec 2008)

[3.23] L. Di Pace, *Influence of increased flow rate to mechanical filter, by-passing ion exchange resin, during VV PHTS baking*, Memo 1/2008/ENEA/FPN FUSTEC S+E

reported [3.24] and included in a DVD (DVD–ROM–3 [3.25]). A readme file [3.26] describes the DVD–ROM–3 content and its use.

- Case 1) Increase in neutron fluence on the first wall (FW) from 0.5 (i.e., the Generic Site Specific Safety Report [GSSR] value) to 1.0 MWa/m^2. Beryllium as first–wall protective layer.
- Case 2) Tungsten instead of beryllium for FW plasma-facing components (PFCs). The ITER FW fluence is 0.5 MWa/m^2.
- Case 3). Tungsten as FW protective layer and a total fluence of 1 MWA/m^2 on the FW equatorial plane.

The new analyses gave the following results. The increase in steel activation observed when EASY–2005.1 was used practically disappears when the EASY–2007 code package is applied because of the correction on the cross section data for the n, p nuclear reactions of the Ni^{58} producing Co^{58}.

Case 1) - Beryllium as PFC; FW average neutron fluence 1.0 MWa/m^2. The materials activity (except for beryllium) is about 30% higher than the corresponding Generic–site Specific Safety Report (GSSR) values up to about ten years' cooling time and increases and doubles (or triplicates) for longer cooling times. As an example (fig. 3.44), for beryliium the activity is double that of the GSSR for all the cooling times. A similar trend vs time is observed also for the materials decay heat. The materials contact dose rates are now higher than the corresponding GSSR rates (by a factor that reaches a maximum value of two), starting from a few hours after plasma shutdown. The materials unconditional clearance indexes are significantly higher than the corresponding GSSR indexes, due to the new data library used for their calculation.

Case 2) - Tungsten as PFC; FW average neutron fluence 0.5 MWa/m^2. The materials (except for tungsten) activity and decay heat are slightly lower than those of the GSSR, from plasma shutdown up to about 10 years' cooling time. After, they become modified by about ±50% (with respect to the GSSR values), depending on the material/zone. The materials (except for tungsten) contact dose rates are lower than the GSSR values by about 20%. The materials unconditional clearance indexes are significantly higher than those of the GSSR, due to the new data library used for their calculation.

For the protective layers (here tungsten, while beryllium for GSSR), the activity, decay heat, contact dose rate and clearance index reach significantly high values up to about one year's cooling time.

Case 3) - Tungsten as PFC; FW average neutron fluence 1.0 MWa/m^2. The materials (except for tungsten) activity, decay heat and contact dose rate are slightly lower than those of the GSSR in the first days after plasma shutdown; then they start to increase by up to a factor of about two. The materials unconditional clearance indexes are significantly higher than the corresponding GSSR indexes, due to the new data library used for their calculation.

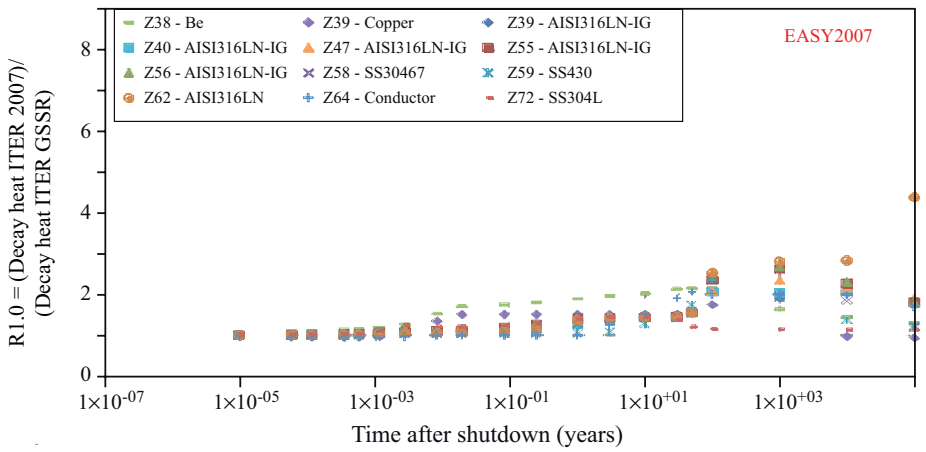

Fig. 3.44 - Comparison of ITER case 1) with ITER-GSSR decay heat for some materials/zones

For the protective layers (here tungsten while beryllium for GSSR), the activity, decay heat, contact dose rate and clearance index reach significant high values up to about one year's cooling time.

ENEA contribution to Tritium Manual

The ITER project is international, so it is very important to have a document such as the Tritium Manual that can be used to ensure a certain level of consistency in the design of the tritium systems.

The Tritium Manual currently consists of two volumes. The first contains valuable information on tritium and its various properties. The second is intended as a handbook of engineering data for tritium–handling systems, but it is not entirely in this format at present. In 2008 the results of a detailed review of Volume 2 and suggestions for its revision to make it consistent with the original intent were documented [3.27]. A third volume of the Tritium Manual would be necessary to contain the safety design guidelines requested as part of this study, so a chapter entitled "Safety Design Guidelines" was also produced. Part of the work gives information on "Safety Analysis", which is not part of the actual safety guidelines but provides the tritium system designers with useful background information.

It is always easier to get the right safety design philosophy at a general rather than a detailed level; but it is at the detailed level that it is essential to strive for a balance between the defined hazard and the defined solution. Failure to achieve a proper balance can have significant cost impacts on the project. In this respect, it should be noted that the current ITER safety approach, which pilots the safety requirements, is not properly balanced, particularly when applied to the design of tritium systems. It is believed that this imbalance (high safety demand vs low hazard level) could lead to expensive systems and components in areas where the benefit–to–cost ratio is small. The recommendation is that the tritium release limits derived from the ITER General Safety Objectives, which are higher than the design target limits recommended by the ITER project, should be used in generating safety design requirements for tritium systems. As the design targets were arbitrarily chosen a long time ago, this would be an appropriate time to review them, with the knowledge that there may be a significant cost associated with the excess level of conservatism.

IEA Co-operative programme on environmental, safety and economic aspects of fusion power

Under the International Energy Agency [IEA], an international collaborative study on fusion radioactive waste [3.28] was performed to examine "the back end" of the materials cycle as an important stage in maximising the environmental benefits of fusion as an energy source. The study addressed the management procedures for radioactive materials following the change–out of replaceable components and decommissioning of fusion facilities. This is termed as "the back end" of fusion materials, including all the procedures required to manage spent radioactive materials from fusion facilities – from the removal of components from the device to their reuse through recycling/clearance, or to the disposal of waste in dedicated repositories. Fusion devices have certain characteristics that make them environmentally friendly; minimisation of long–lived waste that could be a burden for future generations is one such characteristic. Recycling, clearance procedures and regulations have been recently revised,

[3.24] G. Cambi and D.G. Cepraga, *ITER 2007 activation calculations: understanding comparison with GSSR and implication on RPrS writing*, EFDA Task TW6-TSS-SEA4.1, Deliverable D6 – Final Report, ENEA Internal Report FUS-TN-SA-SE-R-187 (April 2008)

[3.25] G. Cambi, D.G. Cepraga, *DVD-ROM-3 containing activation calculation inputs and results in addition to those included into the CD-ROM-1 (edited in November 2007) and into the CD–ROM–2 (edited in February 2008),* transmitted to N. Taylor (ITER–Cadarache), J. Furlan (F4E-Barcelona) and R. Villari (ENEA-Frascati) on March 31, 2008

[3.26] G. Cambi, D.G. Cepraga and R. Villari, *README file for the DVD-3 containing activation calculation inputs and results in addition to those included into the CD–ROM–1 (edited in November 2007) and into the CD–ROM–2 (edited in February 2008)*, EFDA Task TW6-TSS-SEA4.1, Memo 2/2008/ENEA/FPN/FUS (Feb. 2008)

[3.27] A. Natalizio, T. Pinna and C. Rizzello, *ENEA contribution to Tritium Manual*, ENEA Internal Report FUS-TN-SA-SE-R-189 (Feb. 2008)

[3.28] M. Zucchetti et al., *The back end of the fusion materials cycle,* to appear in Fusion Sci. Technol.

Table 3.V – Integrated approach to the management of back–end fusion materials

Regulatory route	Management route	
	Recycling/reuse	Disposal
Clearance (unconditional)	Outside the nuclear industry. All final destinations are feasible [can be after a certain decay storage time; can happen within a licensed facility until specific conditions are met to allow clearance (i.e., in melting facilities to produce metal ingots)].	In non-nuclear landfill (for urban, special, or toxic waste, depending on chemical toxicity of the waste)
Conditional clearance	Within the nuclear industry or in general industry for specific applications. Materials must be subject to continuing regulatory control. Examples include building concrete rubble for base road construction or as an additive for manufacturing new concrete buildings, or metal used for making shielding blocks and containers.	In special industrial (and/or toxic) landfill
No clearance (no release)	Within the nuclear industry (can be direct reuse or after processing; the former is defined as refurbishment).	In a licensed repository for radioactive waste (after interim storage if applicable)

and the effects of these revisions on back end fusion materials were examined in the study. Finally, an integrated approach to the management of back–end fusion materials was proposed, and its application to three fusion reactor designs was analysed. The integrated approach is summarised in table 3.V.

Shutdown dose rate at JET

Code benchmark: ANITA–2000 and SCALENEA–1 validation. The deterministic, discrete ordinates technique, radiation transport assessment Scalenea–1 system (with the Anita–2007 activation code) was used to evaluate the shutdown dose rates in the same two JET positions (P1, close to the vessel, with high–sensitivity TLDs, and P2, external, with an active Geiger-Mueller [GM] type detector [fig. 3.45]) where dose rates were measured (with TLDs and GMs) at various times between September 2005 and May 2007.

The following steps were considered in applying the methodological approach:

- 1D geometry model of JET for shutdown dose rate evaluation.
- Neutron source (from D–D and D–T reactions) definition. The DD and DT neutron sources used for the 1D Sn calculations were defined according to data from a 3D MCNP calculation (performed by ENEA Frascati) and to DD and DT neutron yields from JET.
- Neutron transport calculation using the updated Scalenea–1, with the Vitenea–J 175n–42γ transport library (based on FENDL/E–2 data file), to obtain the neutron irradiation spectra in two selected JET radial directions l1 and l2, crossing the P1 and P2 positions, respectively (fig. 3.45).

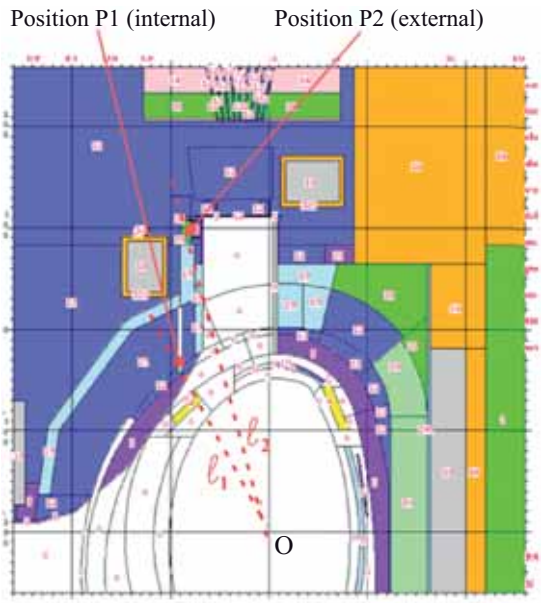

Fig. 3.45 – Section of MCNP model of JET showing the two directions l1 and l2 selected for 1D model definition (geometry and material)

- Material activation calculation using ANITA–2007, with a neutron activation library based on EAF–2007 data and with the neutron spectra previously obtained to calculate the decay gamma sources in the various material zones, along the l1 and l2 JET radial directions for various irradiation scenarios and cooling times.
- Decay–gamma transport performed with the updated Scalenea–1 to evaluate the (shutdown) dose rates in the P1 and P2 positions where TLDs and GMs were positioned for experimental dose rate measurements.

Comparison with experimental data. Comparison between calculation and experiment shows that the calculated values differ from the experimental results by about –7% to +11% for P1 and that they are all within the experimental uncertainty ranges; for P2 all the calculated results are under–estimated with respect to the experimental by about 50% to 11% and beyond the experimental uncertainty ranges (fig. 3.46).

The results confirm that the proposed approach represents a useful tool for scoping studies, providing fast and quite reliable results, e.g., when minor modifications are introduced in the reference design. This is particularly valid for the materials/zones not far from the plasma region, i.e., when the decay gamma source is not negligible.

The irradiation scenarios used and all the results are included in the ENEA report [3.29].

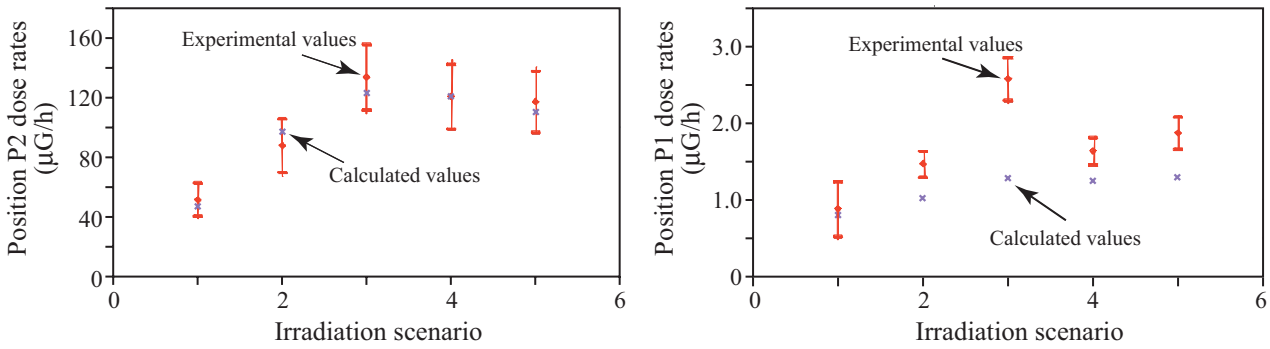

Fig. 3.46 – JET shutdown dose rate calculation-experiment comparison for internal (P1) and external (P2) positions and for various irradiation scenarios

[3.29] G. Cambi, D.G. Cepraga, *JET tokamak shutdown dose rate evaluation with ANITA-2007/Scalenea-1. Data analysis and comparison with experimental results for codes benchmark,* FT Task at JET JW5-FT-5.24, Deliverable D2 – Final Report, ENEA Internal Report in preparation

JET operating experience: global analysis of tritium plant failure

The objective of the activity was to build up an overall data collection about the existing experience on the performance and management of the JET tritium systems [3.30].

As a first step, the analysis performed in 2002 on data from the JET active gas handling system (AGHS) failures was reviewed in 2008: the failures and the system updating occurring between September 2002 and September 2006 were considered. Failed components, failure modes and, where possible, causes and consequences of the failures were investigated. For the statistical analysis, whole sets of

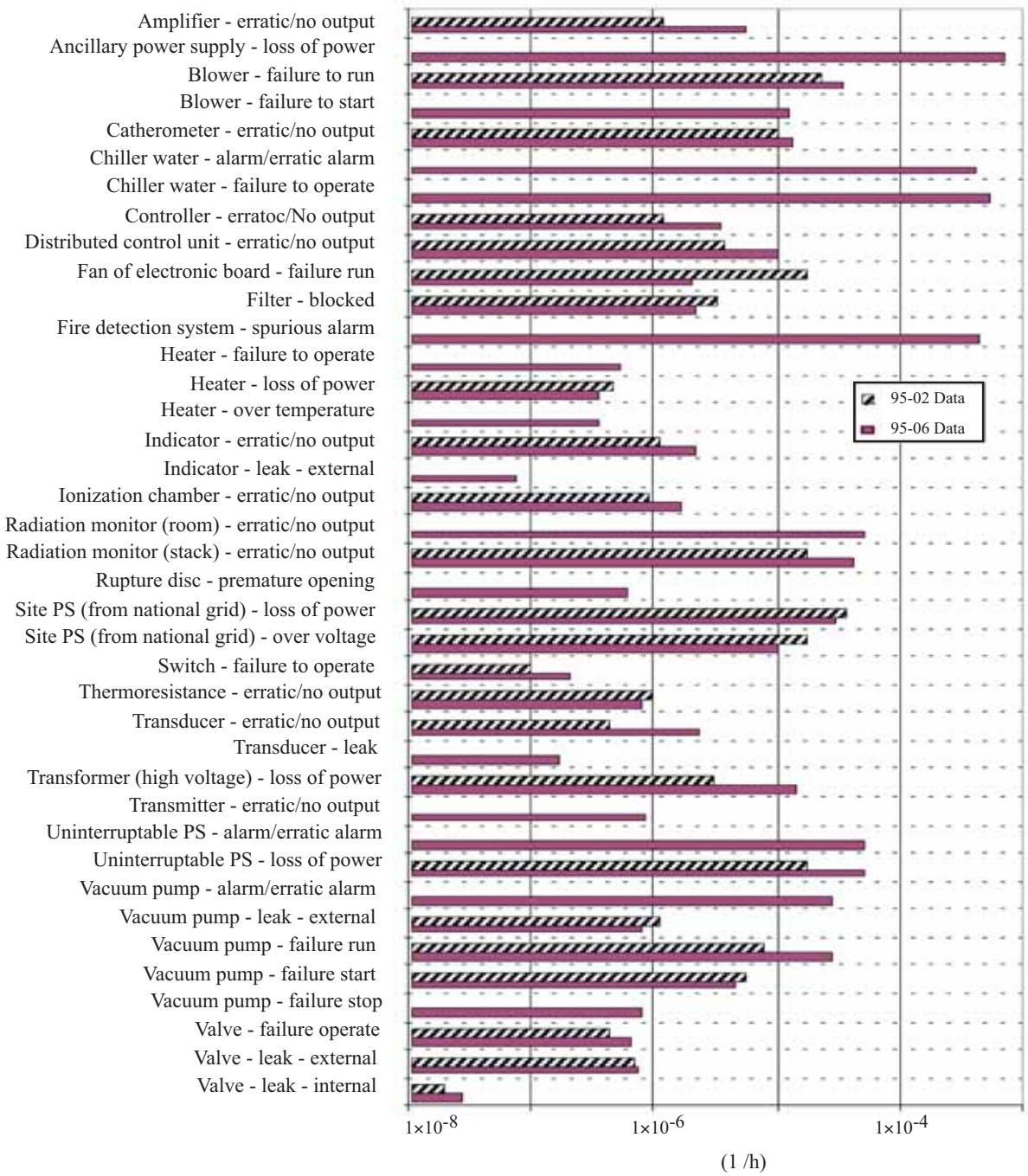

Fig. 3.47 – Failure rates for failure modes of AGHS components – Comparison between two periods of operating experience

components affected by failures/malfunctions were also identified. Components were classified and counted in terms of number, operating hours and demands to operate (for components operating intermittently). The main reliability parameters associated with the components, such as failure rate and the corresponding standard errors and confidence intervals, were estimated. It was found that about 460 failures/malfunctions on a set of more than 6200 components, operating for about 215,000,000 hours occurred from 1995 to September 2006.

Comparison between this statistical assessment and the 2002 assessment points out (fig. 3.47) that, apart from a few cases, the slight increase in failure rate values is due to a slight deterioration of components because of ageing. Comparison of the evaluated failure rates and the failure rates existing in the literature for similar applications (e.g., nuclear power plants, tritium processing laboratories) showed good agreement between the values from the different sources. This enforces the usefulness of the obtained data in evaluating reliability parameters to support the safety assessment and to analyse the availability/reliability of fusion machines/plants and tritium laboratories.

The second step of the work was a detailed analysis of some relevant maintenance operations carried out to repair some significant failures in the plant. Unavailability of components and systems, possible impact on workers' doses and possible environmental releases related to the maintenance activities were investigated. The outcome highlights the very low consequences for workers in terms of doses and the negligible effects on environmental releases, and also the key elements of procedures undertaken to perform maintenance on the AGHS.

[3.30] T. Pinna, G. Cambi and S. Knipe, *JET operating experience: global analysis of tritium plant failure,* ENEA Internal Report FUS-TN-SA-SE-R-193 (June 2008)

4. Superconductivity

In 2008, a lot of work was again devoted to R&D on conventional low–temperature superconducting (LTS) material, MgB_2 bulk samples/wires, and coated conductors, i.e., YBCO high–temperature superconductor. The manufacture and testing of LTS conductor samples for ITER and related projects are still in progress; whereas the production of the final conductor lengths for the EFDA Dipole (EDIPO) facility was completed. Research activities for a better and wider knowledge of superconducting material properties continued, with particular attention focussed on Nb_3Sn strands and MgB_2. For the studies on NbTi multi–filamentary strands, a two–component model for a new fitting/scaling formula was developed. The formula is able to predict NbTi transport current in a very wide operating range, thereby improving the applicability of the conventional fitting formula adopted in the design of superconducting magnets.

The activities concerning high-temperature superconductors (HTSs) were focussed on developing and characterising coated conductor (CC) tapes based on $YBa_2Cu_3O_{7-X}$ (YBCO) films; in particular, YBCO film deposition, tape manufacture and current transport characterisation. In this framework, several national and international collaborations were undertaken: a new method in chemical approaches for YBCO film deposition was developed in cooperation with the Technical University of Cluj-Napoca, Romania; spectroscopic characterisation of chemical–solution–deposited YBCO film was performed in collaboration with the University of Rome Tor Vergata; characterisation of YBCO properties in films with artificially added pinning centres was the main focus of the activity with the University of Rome Roma Tre.

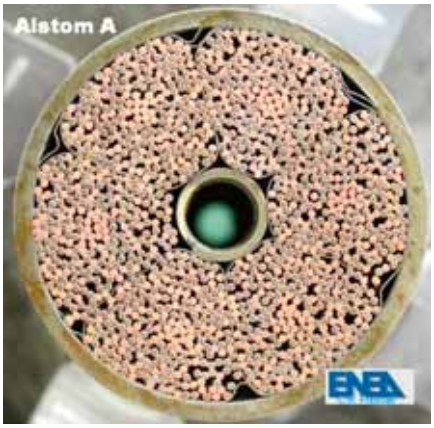

Fig. 4.1 – Cross–section of one of the ITER TF performance samples

4.2 Conductor Manufacturing and Testing

ITER toroidal field coils

Following the very good results obtained during the measurement campaign for the toroidal field (TF) prototype conductors, Fusion For Energy launched the conductor performance qualification phase in order to confirm the final ITER TF conductor design. Each of the conductor lengths was cabled by a different Nb_3Sn strand type manufactured by various producers: LUVATA Pori, Oxford Instruments Superconducting Technology (OST), ALSTOM (fig. 4.1), for two different strand layouts, and European Advanced Superconductors (EAS).

ENEA was in charge of performing quality assurance and monitoring activity during the conductor production and then carried out visual/destructive tests over some spare lengths of the samples in order to get a detailed characterisation of the conductors after production. The conductor unit lengths were successfully manufactured and will be tested in the SULTAN facility in 2009.

ITER poloidal field conductor insert

As a member of the international testing group for the ITER magnet R&D, ENEA participated in the definition and preparation of the ITER poloidal field coil insert (PFCI) test. The experimental campaign was carried out at the CSMC facility of the Japan Atomic Energy Agency (JAEA) at Naka in mid–2008; ENEA attended the first part of the test campaign, together with the European partners involved.

During the preparatory phase of the experiment, ENEA was in charge of the design of the pick–up coil measuring system for alternating current (ac) loss characterisation of the conductor and intermediate joint. Hence, during the first tests, ENEA monitored the signals from the pick–up coils and performed preliminary data analysis. Thanks to this activity, the data acquisition system for the pick–up coil signals was adjusted to its proper setting for the successive measurements.

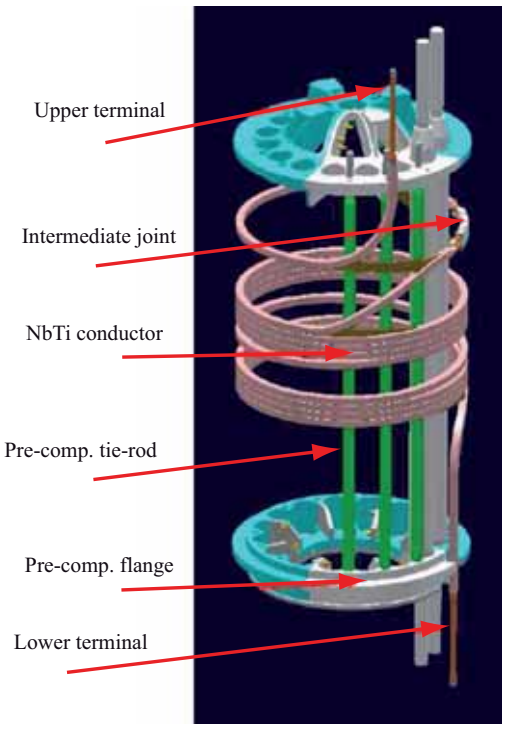

Fig. 4.2 – Representation of the ITER poloidal field coil insert

Following the first current cycles of the sample it was found that several thermometers were showing incorrect readings because of bad contacts and high voltage during previous insulation tests. An on–the–run recalibration of some temperature sensors was therefore mandatory. Using cool–down data and first–run analyses, ENEA provided the testing group with a set of parameters to correct temperature readings and carry on with the measurements within a reasonable error bar (fig. 4.2).

JT-60SA

In the framework of the JT–60SA design activities, the EU home team defined a reference layout for the TF conductor, i.e., a slightly rectangular cable–in–conduit NbTi conductor with 18 mm×22 mm internal dimensions, operating at 25.7 kA with a peak field of 5.65 T. The production of the strands and the cabling was assigned to LUVATA Fornaci di Barga, while the jacketing and compaction were carried out by ENEA. Figure 4.3 shows a cross section of the final conductor after cutting by electro–erosion.

A sample to be tested at the SULTAN facility was taken from the manufactured conductor lengths in such a way as to avoid the bottom joint between the two legs (hairpin–type sample), thus giving a single conductor length of about 7 m. To restrain the U–bent

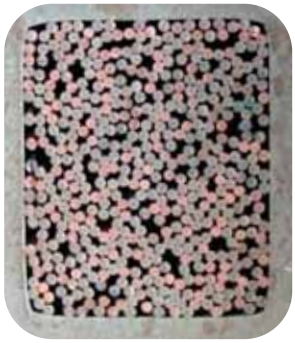

Fig. 4.3 – JT–60SA TF conductor sample cross section

Fig. 4.4 – U–bent unjacketed JT–60SA TF conductor sample in the box substituting the bottom joint in the hairpin SULTAN sample

conductor section (where there is no jacket), a stainless steel He–leak–tight box with an inner structure that completely blocks the cable was developed and manufactured at ENEA, where the sample was assembled (fig. 4.4). To get as much information as possible from the test, the two sample legs were arranged to face either the large or the small side of the rectangular conductor. This is a different orientation to that of the SULTAN field and was done in order to check any effects, caused by the different magnetic field gradients across the conductor cross section, on the critical (T_{cs}, I_c) and quench (T_q, I_q) properties.

PITSAM5: experimental evidence of cable parameter effect on performance

Cable parameters such as void fraction (VF) and twist pitch (TP) have to be carefully selected to obtain a sound conductor design as they strongly affect performance, particularly when Nb_3Sn strands are involved. Therefore a special conductor sample was prepared and tested in the SULTAN facility in order to clarify the role of the parameters. For a start a significant improvement in performance was obtained in the low–field EFDA Dipole square conductor after extra compaction (VF reduced from 37% to 30%). To evaluate the TP impact, ENEA suggested preparing a hairpin–type sample (PITSAM5), therefore no lower joint, with the two legs differentiated only by the twist pitch length (see table 4.I).

Figure 4.5 reports the T_{cs} value evolution with cycling. As can be seen, compared to the short TP leg, the long TP leg had a much better performance from the start and degraded less with increased cycling by about 1 K. The difference increases to about 2 K after the warm–up cycle because of the severe degradation of the short TP leg.

The experimental results obtained on this sample provide evidence that long twist pitch and low void fraction lead to conductor performance improvement.

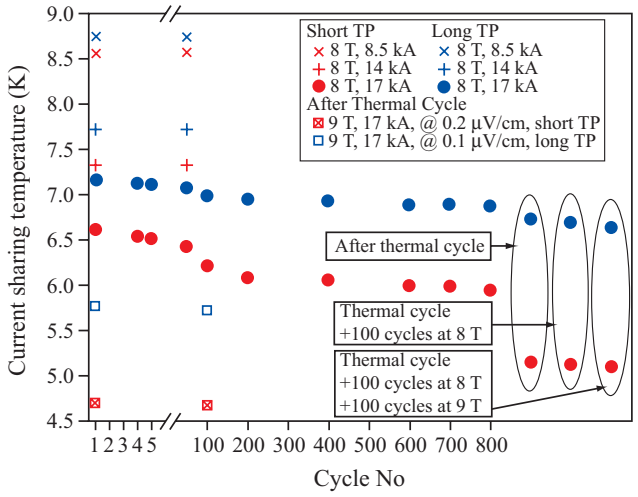

Fig. 4.5 – PITSAM5 sample performance in SULTAN facility

Table. 4.I - PITSAM5 sample characteristics

Sample	PITSAM5	
Cable pattern	(3x3)x3x4	
Cu/non Cu strand	(5/4)x3x4 triplet 1: 1 Cu/2 sc triplet 2&3: 2 Cu/1 sc	
Sc strand number	48	
Cu strand number	60	
Strand diameter	0.81 mm Cr plated	
Twist pitch ref TP: 58 mm 65 mm 139 mm 213 mm	 Short TP 33.6 mm 94.6 mm 139 mm 213 mm	 Long TP 83 mm 140 mm 192 mm 213 mm
Outer dimensions (mm)	12.6x12.6	
Void fraction (%)	30	

EFDA Dipole

ENEA has been charged with supplying the cable and following the manufacture of the entire cable–in–conduit–conductor (CICC) needed to wind the new EDIPO coil (EFDA contract 05–1316, task TMSC–DIPCON). Fabrication of the Nb3Sn CICC was carried out in collaboration with EFDA and the Italian company of Luvata Fornaci di Barga S.p.A.

Following the positive results of the PITCON task in 2007 (EFDA contract 06–1493, task TMSC–PITCON) and the manufacture of the dummy conductor for the EDIPO, in 2008 the final conductor lengths were produced and tested.

The full set of cables, four high–field (HF) and ten low–field (LF) region, for a total length of about 2.5 km, was manufactured. The process started with the cabling of the OST Nb_3Sn strands according to the different layouts defined by EFDA for each section of the dipole, followed by jacketing and compaction. The required lengths of tubes were welded by CRIOTEC Impianti S.r.l., under ENEA supervision. ENEA carried out the conduit test through gas–flow and helium–leak measurements, and developed and installed special terminations for tight sealing at both ends of each conductor. Manufacture of the EDIPO conductor started in February 2008 and was concluded successfully in July 2008, in agreement with the EFDA time schedule. In August 2008 seven large spools carrying the cables were delivered to Babcock Noell GmbH for final assembly and magnet fabrication.

ITER strand benchmarking

ENEA has been involved in the first round of ITER strand benchmarking by performing the characterisation tests of the Nb_3Sn reference strand, as provided by the ITER International Office. Unless otherwise stated, sample preparation and testing procedures followed the guidelines of the document "Procedure of I_c Sample Preparation and Test in the ITER Strand Benchmarking, Version 1.2, by Kazutaka Seo, 21 Nov. 2008". The scope of the task was to test the performance and layout of a bronze–route Nb_3Sn strand produced for ITER by the European company EAS, as benchmarking of different test facilities.

After mounting the sample on appropriate holders and following the recommended procedures, the Nb_3Sn reaction heat treatment was carried out in–house. Characterisation of the wires was performed in terms of:

- strand layout (diameter, thickness of Cr coating, Cu:nonCu ratio, twist pitch length);
- transport critical current and n-value at liquid helium;
- residual resistivity ratio (RRR);
- hysteresis losses by magnetization technique;
- critical current as a function of temperature, by the magnetization technique.

4.3 JT–60SA

During 2008, the collaborative activity of ENEA, the EU Home Team and CEA led to a very important milestone in the development of the JT–60SA project, i.e., the design of the conductor for the TF magnet was fixed according to the requirements of the latest magnet re–design.

In this framework, besides manufacturing the conductor for design qualification (see section 4.2), ENEA carried out diverse analyses. First of all, an algorithm was implemented to compute the conductor peak temperature Thotspot at quench, within the local adiabaticity approximation and within a zero–dimensional model, but including the time–dependent Cu magneto–resistance effect. As a result, it was shown that copper magneto–resistance effects have to be included in such computations, and that the conductor design also fulfils the two requirements for a CICC undergoing quench, as specified by the ITER design criteria [4.1]:

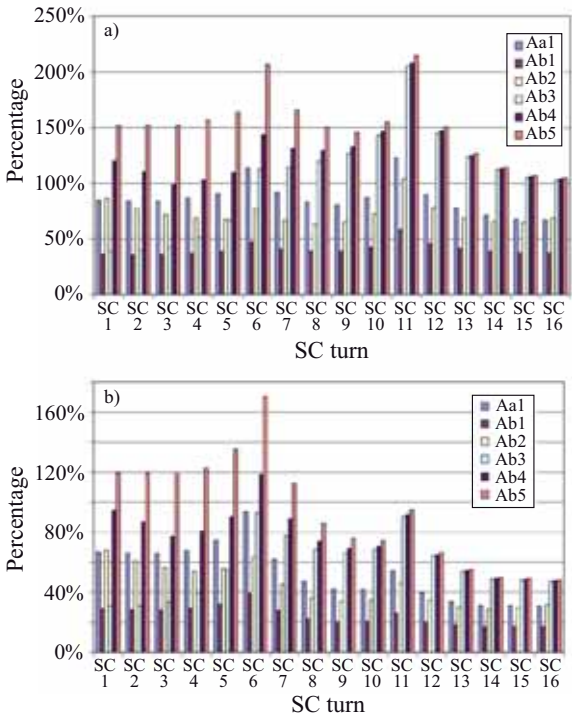

Fig. 4.6 – Heat due to casing vs heat due to neutrons for the 18 SC turns adjacent to the casing in the inboard a) and outboard b) legs

$T_{hotspot}$ = 74 K < 150 K if including all conductor components

$T_{hotspot}$ = 156 K < 250 K if only cable materials are considered

The effect of nuclear heating on the new conductor and winding pack design was also checked. On the one hand, the effect of heat transfer from the stainless steel casing to the winding pack was computed by FEM analysis; on the other, the overall heat load to the conductor was implemented in a Gandalf model and the minimum expected temperature margin was thus estimated.

Regarding computation of the heat deposited in the casing and transferred to the conductor, a 2D sensitivity analysis at the equatorial plane was performed to evaluate the effect of the number and position of the helium cooling channels in the stainless steel casings. The analysis showed that in the most critical configuration, i.e., without any He channel, the heat flux from the casing would at most double the direct heat load because of neutron deposition in the first winding pack turn. As an overall result, considering that in the analysis a 1.8 safety factor was assumed and that in the final design a more performing insulating material such as polyamide instead of epoxy resin could be used as ground insulation, one is led to the conclusion that the He channels could, in principle, be removed from the coil case design.

Figure 4.6 shows the results of the analysis in terms of percentage heat due to the casing vs heat due to neutrons for the 32 superconducting (SC) turns adjacent to the casing in the inboard and outboard legs of the TF coil (only half of the turns was considered for symmetry reasons). For each SC turn, six cooling configurations were envisaged: the first (Aa1 in the figure) considers a cooling channel for each SC turn adjacent to the casing filled with helium at rest; the remaining (Ab1–Ab5 in the figure) refer to five different configurations where a convective film condition was applied in the channel regions. Specifically, Ab1 corresponds to a configuration with the complete set of cooling channels filled with 1.5 g/s of flowing helium; whereas Ab5 corresponds to the most critical configuration without flow coolant and the remaining cases are intermediate between the two. It is apparent that the Ab5 configuration is the most critical and that the innermost conductor turn is the one most subjected to heat loading during normal machine operation.

The result of the computations was used as input in the Gandalf code, for evaluation of the minimum conductor temperature margin to be expected in normal operation. The time evolution of the heat load and its space distribution over the conductor hydraulic length was explicitly introduced in the model and, besides the central pancake, subjected to the highest magnetic field, the lateral pancake was also systematically observed. As a result, it was shown that the peak field region has a minimum ΔT_{margin}=1.2 K, even if no cooling channel is placed in front of it. The lateral pancake could instead become critical when no cooling channel is inserted at the edge of the winding pack corner.

In addition to these analyses, the conductor quench evolution was computed using Gandalf (table 4.II) to assess whether the design value for the magnet delay time constant for fast

Table 4.II – JT-60SA TF conductor: results of Gandalf code simulation

Disturbance length ΔL (m)	Disturbance duration Δt (s)	Input power for quench Q(W/m)	Time to reach quench detection threshold (V=100 mV) t(ms)
1	1	200	350
10	1	200	400
0.1	1	200	800
1	0.01	10000	200
10	0.01	10000	<100

discharge τ_{delay}=2 s was compatible with the foreseen quench detection time and characteristic intervention time of switches and breakers. Several quench scenarios were investigated, and the maximum time required to reach the quench detection voltage was estimated to be ~800 ms. Then the design value τ_{delay}=2 s was considered to be a reasonable target value for the magnet delay time constant.

4.4 Characterisation of Superconducting Materials

Study on Nb_3Sn strands

Magnetic and transport characterisation of internal tin Nb_3Sn technological strands was carried out. The Kramer upper critical field B_{c2K} and the zero–field critical temperature $T_c(0)$ with its distribution were extrapolated by measuring the magnetic moment with a vibrating sample magnetometer. To compare the properties of a sample under different strain conditions it was tested under compression (fig. 4.7), obtained by inserting and compacting it into a thin stainless steel tube before heat treatment, as well as in strain–free conditions, i.e., after removing the Cu matrix by chemical etching. Good agreement was found between theoretical predictions (through uni–axial models) and measured critical temperature T_c and B_{c2K} values (fig. 4.8), with an appropriate choice of fit parameters. However, the observed broadening of the T_c transition can only be explained as the effect of a transverse stress component. The transport properties of Nb_3Sn strands were investigated by studying the effect of bending strain on reinforced strands in stainless steel tubes. Measurements of the critical current and the n–index of internal tin Nb_3Sn wires with different values of the filament twist pitch showed that the transport properties under bending underwent decreasing degradation with increasing twist pitch. In addition, differential analysis through the second derivative of the V–I curve indicated a peaked critical current distribution for strands with untwisted filaments; whereas strands with twisted filaments showed a higher degree of non–homogeneity under bending, as confirmed by broader distributions. The reversibility of the critical current after relaxing the mechanical load was also checked, and an improvement in performance was verified after pre-bending applications, presumably due to the strain relaxation.

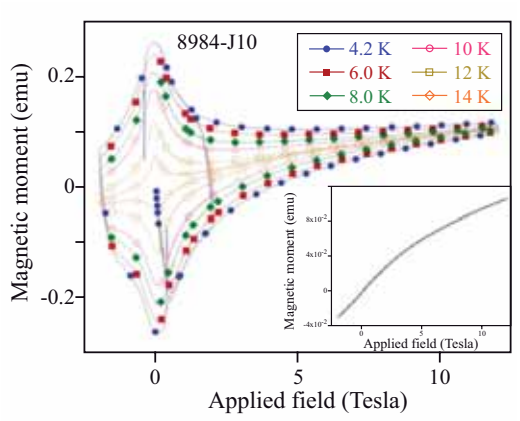

Fig. 4.7 – Magnetic moment of Nb_3Sn strand pre–compressed in stainless steel tube, as a function of applied field at different temperatures. Lines are visual guides only. The magnetic background (see inset, recorded at 20 K) is responsible for the counter–clockwise curve tilting

The current distribution in Nb_3Sn strand subjected to pure bending strain was obtained by resolving the implicit diffusion equations with the finite difference algorithm in Mathworks environment and was then compared with experimental data (fig. 4.9) The critical current dependence on bending, temperature, and magnetic field is used in the power law electric field dependence across the superconductor cross section. The strand is discretized in elements representing groups of twisted filaments embedded in the stabilisation matrix and a distributed constant circuit model is applied for current transfer among filament bundles. Transverse matrix resistivity and twist–pitch values are crucial elements for matching numerical results with experimentally measured critical currents. Very good agreement between model predictions and experimental data was obtained with fully uni–axial modelling of the Nb_3Sn critical current density with strain.

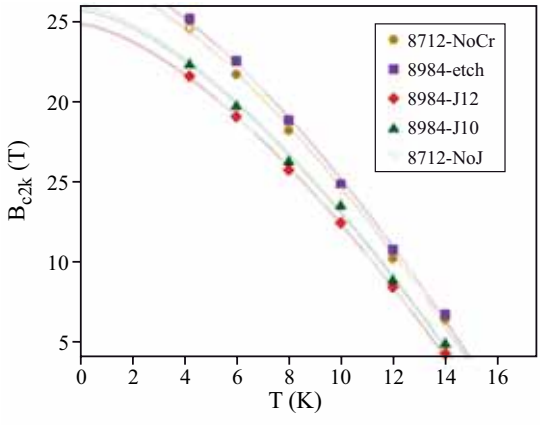

Fig. 4.8 – Extrapolated Kramer fields B_{c2K} vs temperature for different representative samples, subjected to different pre–compression conditions. Lines are theoretical fits based on an improved deviatoric model. The error of B_{c2K} is ±0.3 T, comparable with the size of the symbols

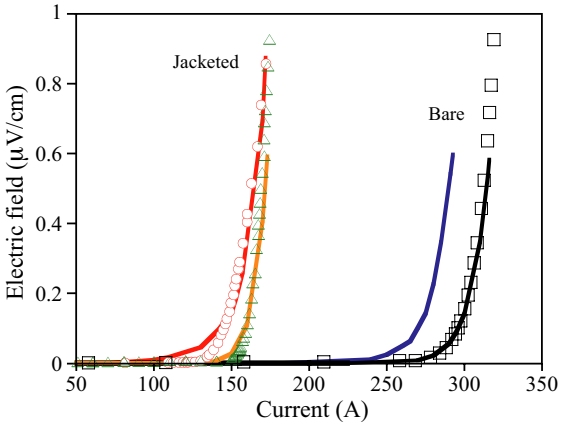

Fig. 4.9 – Electric field vs operating current at 12 T and 4.2 K. Lines represent simulation results. Symbols represent experimental data: squares – bare unbent strand; triangles – unbent jacketed strand; circles – bent jacketed strand (ε_{peak}=0.5%)

Study on NbTi

An extended measurement campaign was carried out on commercially available NbTi strands to be used in the design of fusion reactor magnets and as candidate strands for the ITER high-field poloidal coils (PF1/6) and for the TF coils of JT-60SA. Magnetic and transport measurements were carried out at variable temperature and magnetic field. From the magnetization cycles it was possible to extract information about ac hysteretic losses and to extend the critical current density J_c measurement to lower fields, thus enabling optimisation of numerical fits in a wider magnetic field range than in the past.

From the current densities, the normalised bulk pinning force was calculated as a function of the reduced magnetic field (fig. 4.10) for the whole JT-60SA TF strand dataset. In spite of a very good temperature scaling, the entire curve cannot be precisely described by a single function of the type $b^{\alpha}(1-b)^{\beta}$. An alternative approach was therefore proposed in order to obtain a practical data fitting formula for conventional NbTi strands, valid over a wider B, T range. It is assumed that two phases might coexist in the superconductor, characterised by two different pinning mechanisms or, alternatively, that two distinct regimes of the same pinning mechanism might set in, with a factorable temperature dependence. Hence the reduced bulk pinning force is defined as the full sum of two contributions of the type $b^{\alpha}(1-b)^{\beta}$, each dominating in a different magnetic field range, as follows:

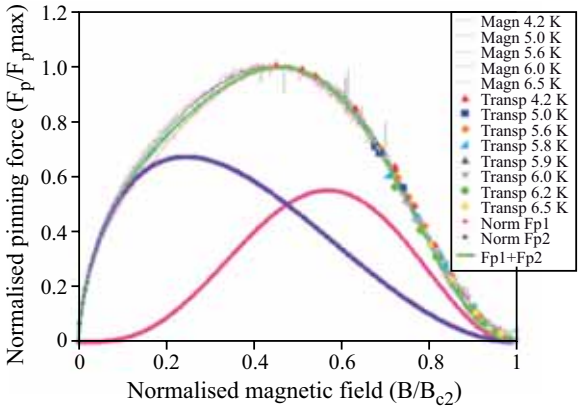

Fig. 4.10 – Normalised bulk pinning force vs reduced magnetic field for the whole JT-60SA TF strand dataset. Symbols and thin lines refer to transport and magnetization data respectively. Fp1 and Fp2 are obtained within the two-component model and their sum is plotted as a thick continuous green line

$$\frac{F_P}{F_{P\_max}} = F_P^{(1)} + F_P^{(2)} = C_1\left[\delta \cdot \frac{b^{\alpha_1}(1-b)^{\beta_1}}{g(\alpha_1,\beta_1)} + (1-\delta)\cdot\frac{b^{\alpha_2}(1-b)^{\beta_2}}{g(\alpha_2,\beta_2)}\right] \qquad (1)$$

$$g(\alpha,\beta) = \left(\frac{\alpha}{\alpha+\beta}\right)^{\alpha}\left(\frac{\beta}{\alpha+\beta}\right)^{\beta} \qquad (2)$$

The bulk pinning force parameters ($\alpha_{1,2}$, $\beta_{1,2}$) and the relative weight of the two contributions (δ) should be obtained as fit parameters. The comparison with experimental data (see fig. 4.10) demonstrates the very satisfactory result obtained. The two pinning contributions are also plotted separately to show that they are dominant in a different b range.

In complete analogy to Bottura's fitting model, the critical current density expression can be formulated within the two-component model, starting from the bulk pinning force expression (1), and with factorable temperature dependence:

$$J_c(B,T) = \frac{C_0}{B}(1-t^n)^{\gamma}\cdot\frac{F_P}{F_{P\_max}} = \frac{C_0}{B}(1-t^n)^{\gamma}\cdot\left[F^{(1)}{}_P + F^{(2)}{}_P\right] \qquad (3)$$

Using this formulation, the $J_c(B,T)$ are computed in the whole B, T range. The result is shown in figure 4.11. As one can see, the two-component model makes it possible to predict the critical current data with very good accuracy in the whole T and B range explored.

Fig. 4.11 – 2 Non–Cu J_c of the JT–60SA strand, from magnetization (lines) and transport (symbols) measurements, in the entire B, T range. Dotted lines are fits using the two–component model, with the parameters listed in the inset

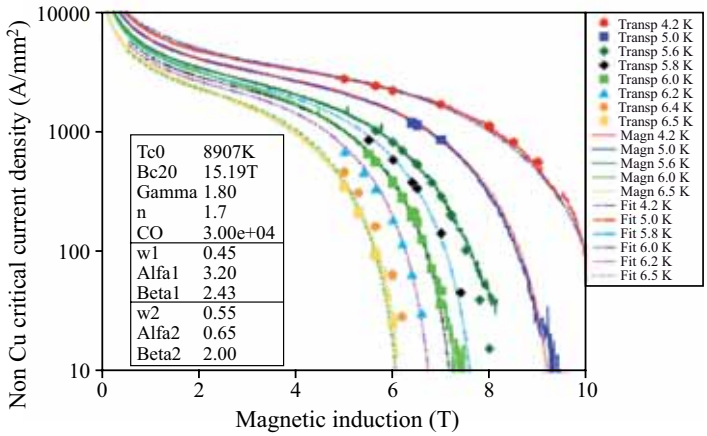

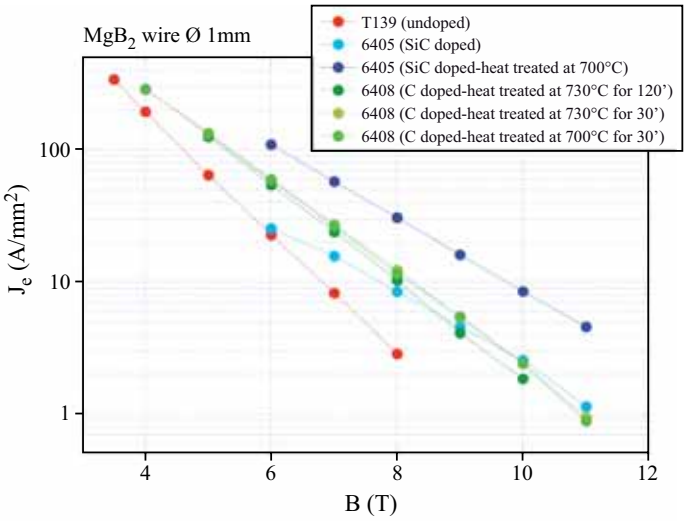

Fig. 4.12 – Summary of transport measurement on a set of 1–mm–diam MgB_2 wires with different doping and/or heat treatment

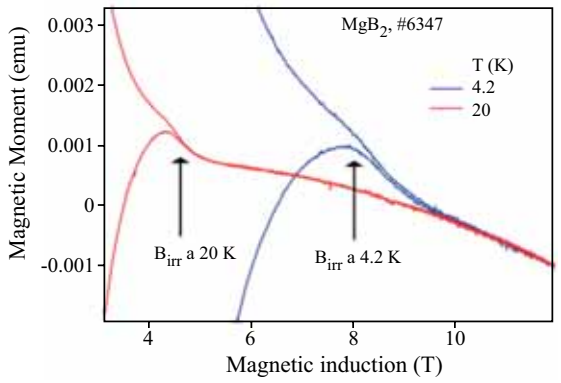

Fig. 4.13 – Magnetization loop closures at different temperatures for a MgB_2 sample

The collected database on the performance of commercially available strands, especially in the range of relatively high temperatures (T >5.5K) and magnetic fields (B ~6T) typical of applications in large coils for fusion reactors, constitutes a sound basis for magnet design, which should be based on strand properties measured in the operation–relevant temperature and magnetic field range.

Study on MgB_2

Collaboration with EDISON to optimise MgB_2 production continued. Transport and magnetic measurements were performed on samples with different shapes, production procedures and doping.

Figure 4.12 reports a summary of the transport characterisation measurement results for a set of 1–mm–diam wires. It is clear that the best performance was obtained in a SiC doped MgB_2 strand, which underwent heat treatment at 700°C. Further investigations are being carried out to assess the best wire production route and the optimal doping dosage.

The doping of bulk MgB_2 superconductor, to improve its superconducting performance, was approached by adding metallic elements (i.e., Zn,Cu,Co) to the Mg sites. The Mg–reactive liquid infiltration process was used by EDISON to promote the dopant insertion, either by using Mg based alloys or mixing the dopants with boron powders. Zn, Cu and Co ions were selected because their ionic radius is similar to that of Mg (2+).

The insertion of dopants in the MgB_2 crystal lattice can change the critical parameters of the superconductor considerably. The investigation was focussed particularly on the changes in the irreversibility field B_{irr}, which is an important engineering parameter for all superconducting applications, i.e., magnet design. A common way to characterise the B_{irr} of type–II superconductors is to use their magnetization cycle and find – at any given temperature – the magnetic field at which the irreversible magnetization, in ascending and descending fields, M+ and M-, becomes coincident. As an example, figure 4.13 reports the closure of the magnetization loops for a MgB_2 sample at two representative temperatures (4.2 K and 20 K).

The rapid decrease in B_{irr} with increasing temperature is similar to the well-known behaviour

Fig. 4.14 – B_{irr} values for different MgB_2 doped samples, extrapolated from measurements of figure 4.13, as indicated in the text

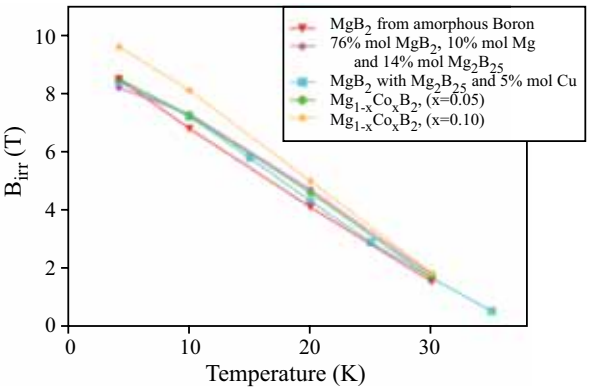

of the other HTSCs. Figure 4.14 shows that at different temperatures metallic doping increases the corresponding B_{irr} values. The increase in B_{irr} means that the superconducting currents can be maintained at higher applied magnetic fields.

Table 4.III reports T_c and B_{irr}, at various temperatures, for Cu and Co. Only the sample doped with nominal Co 10% shows a measurable decrease in T_c and a substantial increase in the B_{irr} value with respect to pure MgB_2.

Comparison of the effects of the different elements on the increase in the irreversibility field shows that Zn and Co are better than Cu, although not outstanding at the moment because of lack of optimisation of the reaction conditions and of the boron powders used. Thus, Co appears to be the best among the dopants studied and better results should be obtained with this element when micro-grains of B are used.

Table 4.III - T_c and B_{irr}, measured by magnetization cycles

Doping	T_c (K)	B_{irr} (T)			
		4.2 K	10 K	20 K	30 K
Pure MgB_2	38.5	8.3	7.2	4.6	1.7
Cu 5%	38.5	8.7	7.5	4.7	1.8
Cu 5%	38.0	8.7	7.5	4.7	1.7
Co 10%	37.0	10	8.4	5.1	1.9

4.5 High-Temperature Superconducting Materials

Ni-Cu-Co alloy as textured substrates for YBCO coated conductors

Ni-Cu based alloys have recently been widely investigated as alternative substrates for YBCO-coated conductors. Therefore, the structural, mechanical, magnetic and electrical properties of Ni 48.5 at% Cu 3 at% Co alloy (Ni-Cu-Co) were studied and compared with those exhibited by other Ni-based alloys. As already reported, this alloy exhibits tensile strength, microstructure and texture suitable for YBCO-coated conductors [4.2]. Further improvements in the substrate texture can be achieved with re-crystallization heat treatment at temperatures as high as 1050°C. No secondary re-crystallization is observed while the cube texture fractional area reaches a value of 97.7% (fig. 4.15). The out-of-plane distribution of (00l) orientation is present with full width at half maxima (FWHM) of 7.8° and 5.4° when rocking around the transverse and the rolling direction, respectively. The resistivity ρ of a re-crystallized Ni-Cu-Co substrate as a function of temperature is shown in figure 4.16. As can be seen, ρ decreases monotonically, but according two different slopes. The kink is associated with the ferromagnetic transition. In fact, from magnetization measurements, the Curie temperature was estimated to be 157 K. The ρ values are about twice as large as those measured for NiW5 substrate. YBCO films were deposited on Ni-Cu-Co substrates using the standard CeO_2/YSZ/CeO_2 buffer layer architecture with the interposition of an additional Pd layer. The YBCO film is mainly c-axis oriented and presents a critical temperature of about 87 K and a critical current density of 1.1 MA/cm^2 at 77 K in self-field. The results obtained demonstrate that this alloy tape is a good candidate for the production of YBCO based coated conductors.

Fig. 4.15 – Electron back-scattered diffraction misorientation map for Ni-Cu-Co re-crystallized for 30 min at 1050°C. The cube area fraction is 97.7%. Black points are unacquired

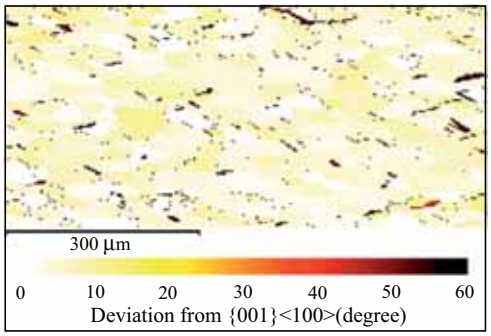

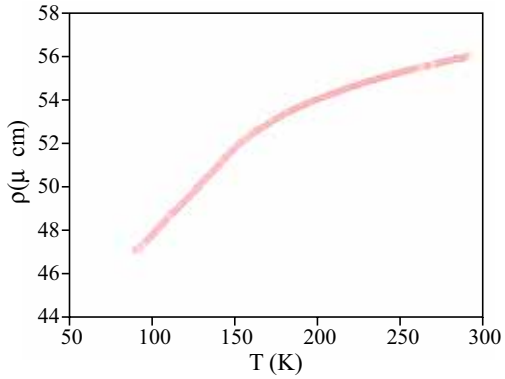

Fig. 4.16 – Resistivity ρ of a re-crystallized Ni-Cu-Co substrate as a function of temperature T

[4.2] 2007 Progress Report, ENEA - Nuclear Fusion and Fission, and Related Technologies Department, Sect. 4.8

Fig. 4.17 – X–ray photoemission spectra measured on modified TFA-MOD YBCO films on STO substrate. Energy distribution curves for the core levels of a) O 1s, b) Ba 3d, c) Ba 4d, d) Cu 2p, e) Y 3d and f) C 1s are reported at both normal (solid line) and 20° glancing (dot–dashed line with circles) electron emission angles

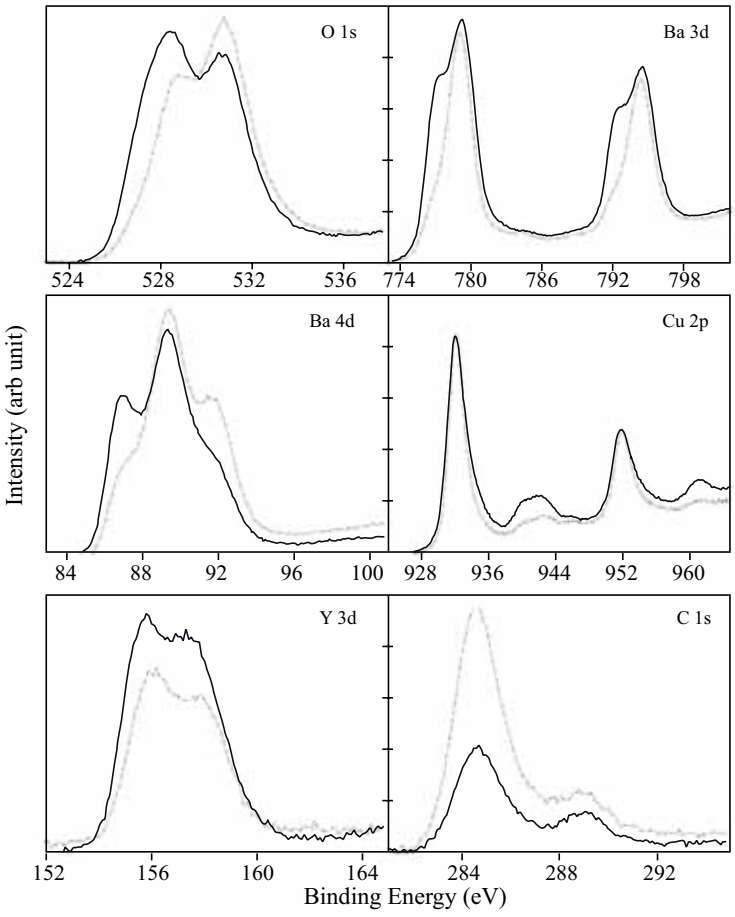

Metal propionate YBCO MOD–coated conductors

In the framework of coated conductor development, chemical solution deposition (CSD) has recently gained sustained scientific interest, particularly because of its high versatility in regard to process parameters and stoichiometric control. In addition, CSD methods are regarded as promising low–cost and industrially scalable approaches, especially for long–length YBCO tape fabrication. To date, metal–organic deposition (MOD) techniques using trifluoro-acetate (TFA) precursors routinely provide high J_c YBCO films. The removal of the fluorine content in the precursors, through its conversion into fluoridric acid, takes a long time. Modified TFA–MOD YBCO precursors with low fluorine content have been successfully proposed. Cu and Y trifluoroacetates were replaced by alcoholic solutions of acetates dispersed in propionic acid, while preserving the Ba TFA. In this way it is possible to reduce the pyrolysis process time by a factor of four. The surface chemical composition of the film deposited on STO substrate was analysed through x-ray photoemission spectroscopy (XPS). Figure 4.17 reports XPS data of a fully processed YBCO film at both normal and 20° glancing electron emission angle. The signals are in general agreement with data reported in the literature for superconducting high–quality YBCO film deposited with different techniques. The x–ray diffraction spectra reveal that epitaxial YBCO films with a sharp orientation distribution were grown on both monocrystalline STO substrate and metallic tape buffered with $Pd/CeO_2/YSZ/CeO_2$ multilayer. The direct current (dc) resistive curves exhibit a linear temperature dependence and very low residual resistance (fig. 4.18). Critical temperature values of about 91 K were obtained. The low normal state resistivity (about 300 μΩ cm at 300 K) is indicative of high–quality c–axis oriented samples. Figure 4.19 reports the dependence of $J_c(H)$, determined from dc transport measurements, on YBCO film deposited on buffered Ni–W substrate. At 77 K and self-field the critical current density is about 1.2 MA cm^{-2}.

Fig. 4.18 – Temperature dependence of the resistance of YBCO films grown on STO (black circle) and cube–textured buffered Ni–W (red cross). The curves are normalised to their respective values at 100 K. Inset: magnified transition region

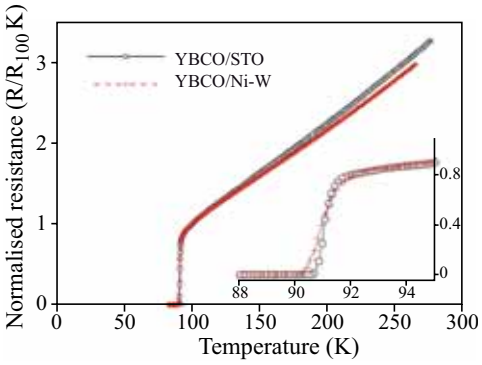

Fig. 4.19 - Magnetic field dependence of critical current density J_c measured from I–V curves, at 77 K for H perpendicular to the tape surface (H // c–axis) for a 450–n–thick YBCO film deposited on cube–textured buffered Ni–W

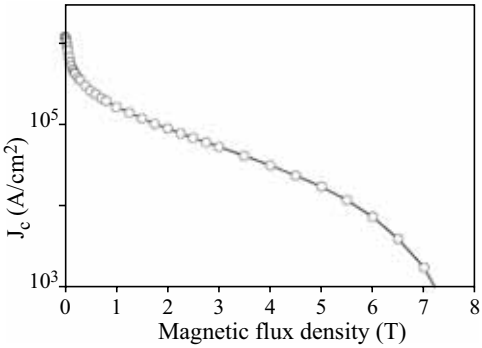

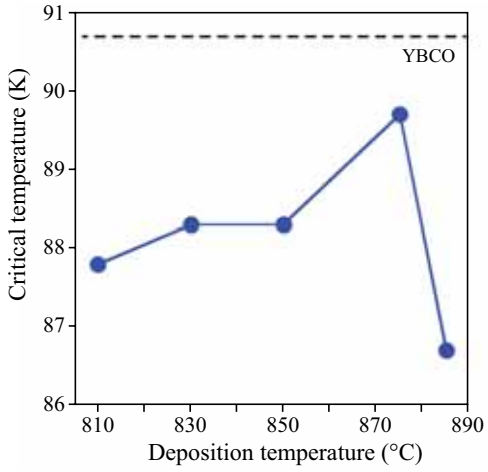

Fig. 4.20 – Critical temperature as a function of the deposition temperature recorded for 7 mol % BZO–YBCO films

YBCO films J_c in–field enhancement through introduction of artificial pinning sites

The in–field critical current density enhancement in YBCO thin film can be achieved, despite a slight T_c reduction, by introducing artificial pinning sites (APSs). YBCO thin films with $BaZrO_3$ (BZO) nano–inclusions (BZO–YBCO) were successfully grown by pulsed laser deposition (PLD) at ENEA. The films showed enhanced pinning forces and irreversibility field values.

During 2008 an extended measurement campaign was carried out on BZO–YBCO films grown on $SrTiO_3$ single crystal substrate with different BZO concentrations. YBCO samples with 2.5, 5 and 7 mol.% of BZO inclusions were grown by PLD, changing the substrate temperature (T_d) and the background oxygen pressure. The increase in the deposition temperature leads to an almost complete recovery of the T_c reduction typical of YBCO films with APSs (fig. 4.20). T_c values for samples grown at 875 °C are in the range 89.7–90.6 K, close to the 90.7 K value shown by standard YBCO films deposited at 850°C. Flux dynamics and pinning mechanisms acting in BZO–YBCO samples with different BZO concentration were investigated by means of dc transport property measurements and ac microwave measurements. Figure 4.21 shows the field dependence of the change in the thin film surface resistance for 5 mol.% BZO–YBCO and pure YBCO films. BZO–YBCO films present a dramatically reduced dissipation as a function of the applied field with respect to pure YBCO. Very interestingly, this reduction extends to temperatures close to T_c, indicating that the presence of pinning centres has an exceptionally strong effect subsequent to the introduction of BZO particles. It is a nontrivial finding that BZO inclusions originate pins that are effective at frequencies so high that the shaking of vortices around their equilibrium position is the dominating mechanism. Hence, it can be argued that BZO induces very steep and deep pinning wells. Analyses of the microwave properties of BZO–YBCO films with different BZO concentrations confirm increasing pinning efficiency with increasing BZO content in YBCO. Additional insight can be gained by investigating U_{min}, the minimum height of the vortex energy landscape. Figure 4.22 reports U_{min} calculated at $\mu_0 H$=0.5 T as a function of BZO content at three selected temperatures. It is clear that the minimum height of the potential wells increases as the BZO content increases and saturates at 5 mol % BZO. This implies that the minimum allowed value for the energy barriers increases with the introduction of BZO. A natural explanation for these findings is that each vortex finds a preferential position on a single BZO particle. At intermediate BZO content there are still fluxons pinned by natural, weak defects. With increasing BZO content each flux line finds a pinning well corresponding to a BZO particle.

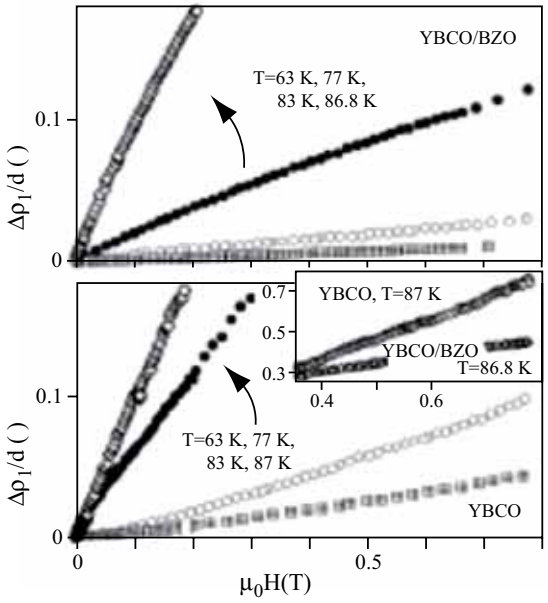

Fig. 4.21 – Field dependence of the thin film surface resistance changes, $\Delta R_s(H)=\Delta\rho_1(H)/d$, in YBCO/BZO and in pure YBCO

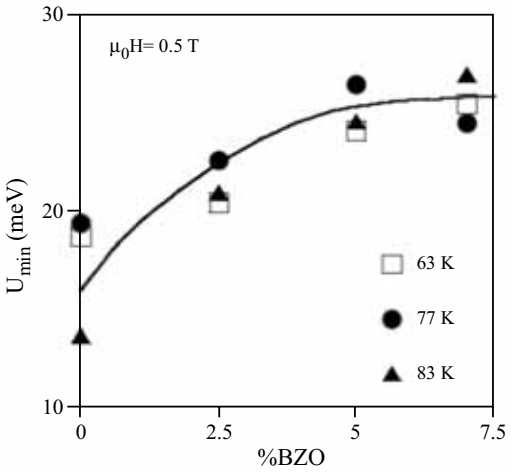

Fig. 4.22 – Minimum allowed values for the barrier height of the vortex potential landscape U_{min} calculated at $\mu_0 H$ =0.5 T as a function of BZO content and at T=63, 77 and 83 K

5. Inertial Fusion

5.1 Basic Science of Inertial Fusion Energy

Promising unconventional approaches to inertial fusion energy (IFE) based on two drivers, a laser compressor associated to a heavy–ion beam ignitor, proposed and studied through 1994–2002 in the framework of the IFE KIT activity at ENEA Frascati, were reconsidered in the present more advanced technological context. At that time the required spot diameters of heavy–ion beam (from tens of μm to a few hundred) and pulse duration (from tens of ps to a few hundred) were considered a technological challenge by the particle accelerator community [5.1,5.2].

In the present scenario a project of the High–Power Laser Energy Research Roadmap (HiPER) class, arising as reference installation for fast–ignition demonstrative experiments and multidisciplinary studies, can be expected to have provided laser pulse durations in a wider range (up to few hundred ps) than those now featuring the short pulse FI class drivers. Such a facility could represent, in perspective, an important tool to test an extended class of IFE–relevant approaches based on two laser drivers with a specialised role (compression, ignition).

Fast ignition by 1–GeV Bi–ion beams (spot diameters 30–150 μm and pulse duration 30–50 ps) in a DT fuel imploded by a –MJ laser (1994–1998), and ignition assisted by a 9–GeV Bi-ion pulse (duration ≈300 ps, diameter ≈450 μm FWHM beam energy ≈35 kJ) according to the injected entropy method (1999–2002) were reconsidered, taking as reference for this analysis experimental results obtained by the Fast Ion Generation Experiment (FIGEX–2006) [5.3] where two different multi–MeV/nucleon ion–sources were dimensioned and studied to be scaled, in perspective, to a context of thermonuclear interest.

Taking as reference the above–mentioned IFE schemes and the encouraging results obtained in the FIGEX experiment, studies were performed to design laser–generated heavy–ion sources having energy of the order of 10 GeV with a duration in the range of tens to thousands of picoseconds.

Two classes of experiment were performed in FIGEX, corresponding to different target parameters (disks with diameter/thickness >>1) and laser power densities. The ions produced were collected around the target by six Thomson spectrometers, the total energy in the channels corresponding to different charge–to–mass ratios was estimated and the related distribution functions were determined. In the case where targets of 32 μm diameter and 40 nm thickness were irradiated by 2×10^{19} W/cm^2 ≅ λ=1.054 μm most of the ions (≈70%) were detected in the forward direction around the normal, within a cone of ≈40° FWHM. The net forward momentum associated with this distribution was attributed to the electro–dynamic effects (radiation pressure) induced by the laser electromagnetic field that can overcome the thermo–kinetic effects in regimes of poor absorption (≈10–15%, as estimated from the experimental results).

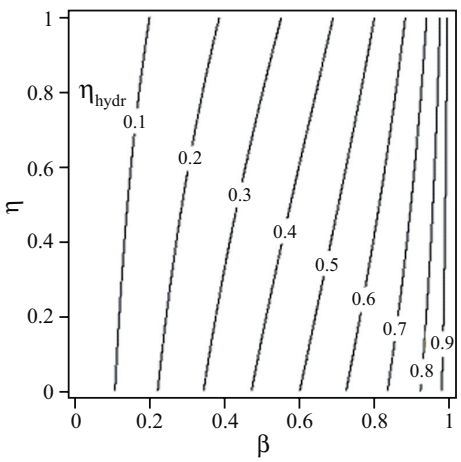

Fig. 5.1 – The hydrodynamical transfer efficiency η_{hydr} for a foil accelerated by electro–dynamic effects acting through an imperfect plasma mirror (η is the laser absorption efficiency and β the ratio aimed target velocity/light speed)

A theoretical model for the acceleration of thin foils by radiation pressure was developed to fit the experimental results and then used to design heavy–ion sources of potential interest for thermonuclear applications such as heavy ion fast ignition and inject entropy. Figure 5.1 shows the

[5.1] A. Caruso and V.A. Pais, Phys. Lett. A **243** 319-324 (1998)
[5.2] A. Caruso and C. Strangio, Laser Part. Beams **18,** 35–47 (2000)
[5.3] C. Strangio et al., Laser Part. Beams **25**, 1–7 (2007)

Table 5.I – Reference parameters for the heavy-ion source considered in the study. The ion source is obtained by irradiating a thin solid by a short laser pulse in the near field

Solid disk initial parameters	
Geometry	Disk with diameter/thickness >>1
Radius	50 (μm)
Thickness	57 (nm)
Material	Bi
Density	9.8 (g/cm^3)
Laser beam and focussing	
Energy	100 (kJ)
Wavelength	0.527 (μm)
Duration	0.5 (ps)
On solid disk spot diameter	100 (μm)
On solid disk power density	2.5×10^{21} W/cm^2
Laser generated ion beam	
Aimed MeV/nucleon	72 (Ion speed/light speed, β=0.372)
Photon absorption probability (η)	0.15

relationships between the process–relevant efficiencies and a non–dimensional parameter related to the target velocity aimed for.

It has been shown that, in these regimes (table 5.I), it is possible to obtain the efficient generation (30–45%) of all–forward ejected high–energy ions (20–150 MeV/nucleon) with the highest energy part of the spectrum well collimated within a half angle ≈2°. Also the velocity spreads are amply compatible with the ion pulse durations required for both the IFE applications, namely fast ignition and injected entropy by heavy ions.

These studies were presented at the 30th European Conference on Laser Interaction with Matter (ECLIM), Darmstadt 2008 and then a more complete version was accepted for publication in Laser and Particle Beams.

5.2 Laser–Matter Interaction

A programme to measure the astrophysical factor for nuclear fusion reactions has been set up in collaboration with the National Laboratories (LNS) of INFN Frascati.

In a first step to test the efficiency of the adopted method, encouraging results were obtained through a preliminary experiment performed with the Frascati ABC facility. The experimental results are now being analysed to establish, out of the possible available solutions found in the framework of the experiment design activities, the most suitable choice of target features and laser irradiation layout for the forthcoming final experiment. The energy distribution function of the produced ions represents a most important tool to explain the results obtained in this experiment. Thus the system of routine particle diagnostic on ABC (Faraday cups for flight time and angular dependence of the ion measurement) will be implemented by a pair of miniature Thomson spectrometers designed and constructed in collaboration with LNS-INFN and Kore University of Enna.

Experiments with the ABC installation implemented by optical shadowgraph, interferometry, transmitted light through the target, x–ray and charged particle diagnostics are also ready to start for studies on non-equilibrium processes generated in structured materials (e.g., foams) by laser–induced hydrodynamics. Part of this experiment will be performed in co–operation with the Lebedev Institute of Moscow, provider of foam targets.

5.3 Laser Technology

In the framework of the laser design activity for upgrading the ABC installation to be recognised in the Italian Roadmap of Relevant Research Infrastructures, the final analysis (also in co–operation with the

Central Laser Facility of the Rutherford Appleton Laboratories [CLF–RAL] UK, costs and time schedule included) was carried out for a control of the laser pulse time-dependence and for an optimal extraction of the energy stored in the ABC active elements by a rearrangement of the final amplification stages, passing from a master oscillator power amplifier (MOPA) to a multi–pass architecture.

5.4 HiPER Activities

A programme of coordinated activities on Safety, Environment and Fusion Technology, of interest to the IFE experimental chamber is in preparation as ENEA's contribution to the HiPER preparatory phase. The outline of a Preliminary Safety Report (PrSR) for the HiPER facility has already been prepared. Two young scientists will be engaged for the activities related to the HiPER participation, which will be performed in the framework of a consortium agreement, outside the Euratom–ENEA Association.

6. Communications and Relations with Industry

6.1 ITER & Industry

The Fusion for Energy Network of national Industrial Liaison Officers (ILO) for ITER was set up in April 2008 with the following objectives:

- Raise awareness and transmit information to potential contractors about forthcoming calls to be launched by F4E or ITER.
- Assist potential contractors in their understanding of the requirements of F4E within the frame of the above-mentioned calls.
- Advise the potential contractors, upon request on technical, contractual and financial aspects of F4E.
- Foster the registration of potential contractors in the databases of F4E.
- Act as a forum to exchange information on matters of F4E industrial policy and related subjects.
- Encourage the long-term participation of industry in fusion in view of realising DEMO.

Dr. Paola Batistoni of ENEA – FPN was formally nominated ILO for Italy. Although ENEA had already been active for several years in this field, the official start of the ILO Network triggered a number of new activities, such as,

- establishment of a mailing list of companies interested in working for ITER, including also associations and institutions with a significant outreach towards different categories of industry;
- creation of an information service announcing all calls for tender published by F4E;
- realisation of a dedicated website (http://www.iterforum.enea.it);
- organisation of an Italian network of ILOs;
- technical assistance to a growing number of companies participating in F4E bids;
- active participation in the ILO meetings and in discussions on improvements to the contractual terms foreseen by the F4E contracts.

A network of Italian ILOs was established for the large international scientific projects (CERN – Large Hadron Collider [LHC]; F4E – ITER & Broader Approach; ESO – European Extremely Large Telescope [EELT] and Atacama Large Millimeter/submillimeter Array [ALMA]) with the purpose of coordinating common actions devoted to the promotion of Italian industry in international projects.

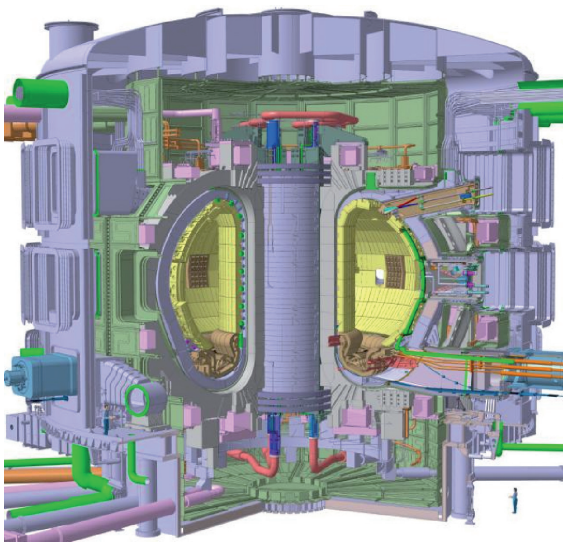

Fig. 6.1 - ITER device

Several workshop were organised or contributed to (Il reattore a fusione ITER – Opportunità per le aziende in collaboration with the Camera di Commercio Industria Artigianato Agricoltura di Torino, February 14 2008; Seminario per le Camere di Commercio Italiane ITER: Un'opportunità per le imprese, ENEA Centro Ricerche Frascati, 21 novembre 2008; European Extremely Large Telescope: Una sfida tecnologica, una opportunità per l'industria, with F4E ILO participation).

7. Publications and Events

7.1 Publications

Articles

A. MANCINI, A. AUGIERI, G. CELENTANO, L. CIONTEA, V. GALLUZZI, U. GAMBARDELLA, G. LONGO, T. PETRISOR, A. RUFOLONI, A. VANNOZZI, A. CRICENTI: *Pd layer on cube–textured substrates for MOD–TFA and PLD YBCO coated conductors*
Supercond. Sci. Technol. **21**, 015003, 1–9 (2008)

L. EL–GUEBALY, M. ZUCCHETTI, L. DI PACE, B.N. KOLBASOV, V. MASSAUT, R. PAMPIN, P. WILSON: *An integrated approach to the back–end of the fusion materials cycle*
Report UWFDM–1340 (Fusion Techology Inst. – Madison)

F. ZONCA: *The physics of burning plasmas in toroidal magnetic field devices*
Int. J. Modern Phys. A **23**, 8, 1165–1172 (2008)

B. ESPOSITO, G. GRANUCCI, P. SMEULDERS, S. NOWAK, J.R. MARTIN–SOLIS, L. GABELLIERI and the FTU and ECRH TEAMS: *Disruption avoidance in FTU by means of MHD mode stabilization using ECRH*
Phys. Rev. Letters **100**, 045006 (2008)

S. ALMAVIVA, M. MARINELLI, E. MILANI, G. PRESTOPINO, A. TUCCIARONE, C. VERONA, G, VERONA–RINATI, M. ANGELONE, D. LATTANZI, M. PILLON, R.M. MONTEREALI, M.A. VICENTI: *Thermal and fast neutron detection in chemical vapor deposition single–crystal diamond detectors*
J. Appl. Phys. **103**, 054501 (2008)

D. CIAZYNSKI, L. ZANI, P. BRUZZONE, B. STEPANOV, R. WESCHE, L. SAVOLDIRICHARD, R. ZANINO, A. NIJHUIS, Y. ILYN, S. TURTU', V. CORATO, G. DE MARZI: *Influence of cable layout on the performance of ITER–type Nb_3Sn conductors*
J. Phys.: Conf. Series **97**, 012027 (2008)

A. VANNOZZI, G. CELENTANO, A. ANGRISANI, A. AUGIERI, L. CIONTEA, I. COLANTONI, V. GALLUZZI, U. GAMBARDELLA, A. MANCINI, T. PETRISOR, A. RUFOLONI, G. THALMAIER: *Nickel–copper alloy tapes as textured substrates for YBCO coated conductors*
J. Phys.: Conf. Series **97**, 012188 (2008)

A. AUGIERI, V. GALLUZZI, G. CELENTANO, F. FABBRI, A. MANCINI, A. RUFOLONI, A. VANNOZZI, U. GAMBARDELLA, G. PADELETTI, A. CUSMË, T. PETRISOR, L. CIONTEA: *Critical current density of $YBa_2Cu_3O_{7-x}$ films with $BaZrO_3$ inclusions on $SrTiO_3$ and Al_2O_3 substrates*
J. Phys.: Conf. Series **97**, 012209 (2008)

L. CIONTEA, A. ANGRISANI ARMENIO, G. CELENTANO, T. PETRISOR jr., A. RUFOLONI, A. VANNOZZI, A. AUGERI, V. GALLUZZI, A. MANCINI, T. PETRISOR: *Metal propinate synthesis of epitaxial $YBa_2Cu_3O_{7-x}$ film*
J. Phys.: Conf. Series **97**, 012302 (2008)

L. CIONTEA, G. CELENTANO, A. AUGIERI, T. RISTOIU, R. SUCIU, M.S. GABOR, A. RUFOLONI, A. VANNOZZI, V. GALLUZZI, T. PETRISOR: *Chemically processed $BaZrO_3$ nanopowders as artificial pinning centres*
J. Phys.: Conf. Series **97**, 012289 (2008)

N. POMPEO, V. GALLUZZI, A. AUGIERI, F. FABBRI, G. CELENTANO, T. PETRISOR, R. ROGAI, E. SILVA: *Strong reduction of the field–dependent microwave surface resistance in YBCO with $BaZrO_3$ inclusions*
J. Phys.: Conf. Series **97**, 012173 (2008)

L. MUZZI, V. CORATO, R. VIOLA, A. DELLA CORTE: *Performance enhancement under bending of NB_3Sn strands with untwisted filaments*
J. Appl. Phys. **103**, 073915 (2008)

L. AFFINITO, S. CHIARELLI, V. CORATO, A. DELLA CORTE, G. DE MARZI, A. DI ZENOBIO, C. FIAMOZZI ZIGNANI, G. MESSINA, L. MUZZI, M. NAPOLITANO, S. TURTU': *Variable–temperature characterization of NbTi strands in the low critical–current density range*
J. Phys.: Conf. Series **97**, 012306 (2008)

A. PIZZUTO, L. SEMERARO, L. ZANI, P. BAYETTI, A. CUCCHIARO, P. DECOOL, A. DELLA CORTE, A. DI ZENOBIO, N. DOLGETTA, J.L. DUCHATEAU, W.H. FIETZ, R. HELLER, P. HERTOUT, M. KIKUCHI, K. KIZU, B. LACROIX, L. MUZZI, S. NICOLLET, G.M. POLLI, C. PORTAFAIX, L. RECCIA, S. TURTU', J.–M. VERGER, R. VILLARI, K. YOSHIDA: *JT–60SA toroidal field magnet system*
IEEE trans. Appl. Supercond. **18**, 2, 505–508 (2008)

L. ZANI, A. PIZZUTO, L. SEMERARO, D. CIAZYNSKI, A. CUCCHIARO, P. DECOOL, A. DELLA CORTE, A. DI ZENOBIO, N. DOLGETTA, J.L. DUCHATEAU, P. HERTOUT, M. KIKUCHI, B. LACROIX, F. MOLINIE, L. MUZZI, L. PETRIZZI, C. PORTAFAIX, G. RAMOGIDA, S. ROCCELLA, B. TURCK, S. TURTU', J.–M. VERGER, R. VILLARI, K. YOSHIDA: A *new design for JT–60SA toroidal field coils conductor and joints*
IEEE Trans. Appl. Supercond. **18**, 2, 216-219 (2008)

K. YOSHIDA, K. KIZU, K. TSUCHIYA, H. TAMAI, M. MATSUKAWA, M. KIKUCHI, A. DELLA CORTE, L. MUZZI, S. TURTU', A. DI ZENOBIO, A. PIZZUTO, C. PORTAFAIX, S. NICOLLET, P. DECOOL, J.L. DUCHATEAU, L. ZANI : *Conceptual design of superconducting magnet system for JT–60SA*
IEEE Trans. Appl. Supercond. **18**, 2, 441–446 (2008)

K. KIZU, K. TSUCHIYA, K. YOSHIDA, M. EDAYA, T. ICHIGE, H. TAMAI, M. MATSUKAWA, A. DELLA CORTE, L. MUZZI, A. DI ZENOBIO, S. TURTU', J.L. DUCHATEAU, L. ZANI: *Conductor design of CS and EF coils for JT–60SA*
IEEE Trans. Appl. Supercond. **18**, 2, 212-215 (2008)

A. DI ZENOBIO, A. DELLA CORTE, L. MUZZI, S. TURTU', W. BAKER, P. BAUER, A. PORTONE, E. SALPIETRO, J. AMEND, E. THEISEN: *Joint design for the EDIPO*
IEEE Trans. Appl. Supercond. **18**, 2, 192–195 (2008)

P. BRUZZONE, M. BAGNASCO, M. CALVI, F. CAU, D. CIAZYNSKI, A. DELLA CORTE, A. DI ZENOBIO, L. MUZZI, A. NIJHUIS, E. SALPIETRO, L. SAVOLDI RICHARD, S.TURTU', A. VOSTNER, R. WESCHE, R. ZANINO: *Test results of two European ITER TF conductor samples in SULTAN*
IEEE Trans. Appl. Supercond. **18**, 2, 1088-1091 (2008

U. BESI VETRELLA, A. DELLA CORTE, G. DE MARZI, A. DI ZENOBIO, L. MUZZI, L.RECCIA, S. TURTU', A. BALDINI, P. BRUZZONE, E. SALPIETRO, A. VOSTNER: *Manufacturing of the ITER full size prototype conductor*
IEEE Trans. Appl. Supercond. **18**, 2, 1105–1108 (2008)

A. ANGRISANI ARMENIO, A. AUGERI, G. CELENTANO, V. GALLUZZI, A. MANCINI, A. RUFOLONI, A. VANNOZZI, U. GAMBARDELLA, A. SAGGESE, P. SESSA, S. PACE: *Stability measurements on YBCO coated conductor*
IEEE Trans. Appl. Supercond. **18**, 2, 1293–1296 (2008)

A. PORTONE, W. BAKER, E. SALPIETRO, A. VOSTNER, P. BRUZZONE, F. CAU, A. DELLA CORTE, A. DI ZENOBIO, E. THEISEN, A. BALDINI, P. TESTONI, J. LUCAS, M. PINILLA, G. SAMUELLI: *Design and procurement of the European Dipole (EDIPO) superconducting magnet*
IEEE Trans. Appl. Supercond. **18,** 2, 499–504 (2008)

A. PIZZUTO, S. MONTI, F. TROIANI: Dossier "ENEA e la ricerca sul nucleare"
Ambiente Energia e Innovazione (2008)

F. ZONCA, LIU CHEN: *Radial structure and non linear excitation of geodesic acoustic modes*
European Phys. Letts **83**, 35001 (2008)

M. PILLON, M. ANGELONE, G. AIELLI, S. ALMAVIVA, M. MARINELLI, E. MILANI, G. PRESTOPINO, A. TUCCIARONE, C. VERONA, G. VERONA–RINATI: *Radiation tolerance of a high quality synthetic single crystal chemical vapor deposition diamond detector irradiated by 14.8 MeV neutrons*
J. Appl. Phys **104**, 054513 (2008)

M. ANGELONE, D. LATTANZI, M. PILLON, M. MARINELLI, E. MILANI, A. TUCCIARONE, G. VERONA-RINATI, S. POPOVICHEV, R.M. MONTEREALI, M.A. VINCENTI, A. MURARI and JET–EFDA CONTRIBUTORS: Development of single crystal diamond neutron detectors and test at JET tokamak
Nucl. Instrum. Method A **595**, 616–622 (2008)

F. ORSITTO, A. BOBOC, C. MAZZOTTA, E. GIOVANNOZZI, L. ZABEO and JET EFDA CONTRIBUTORS: *Modelling of polarimetry measurements at JET*
Plasma Phys. Control. Fusion **50**, 115009 (2008)

S.E. SEGRE, V. ZANZA: *Plasma polarimetry with retroreflection*
Plasma Phys. and Controll. Fusion **50**, 105006 (2008)

F. ZONCA, L. CHEN: *Nonlinear dynamics and complex behaviors in magnetized plasmas of fusion interest*
"Frontiers in Modern Plasma Physics", Ed. by P.K. Shukla, B. Eliasson, and L. Stenflo – AIP CP **1061**, 34 (2008)

A. MURARI, T. EDLINGTON, M. ANGELONE, L. BERTALOT, I. BOLSHAKOVA, G. BONHEURE, J. BRZOZOWSKI, V. COCCORESE, R. HOLYAKA, V. KIPTILY, I. LENGAR, P. MORGAN, M. PILLON, S. POPOVICHEV , P. PRIOR, R. PROKOPOWICZ, A. QUERCIA, M. RUBEL, M. SANTALA, A. SHEVELEV, B. SYME, G. VAGLIASINDI, R. VILLARI, V.L. ZOITA, JET–EFDA CONTRIBUTORS: *Measuring the radiation field and radiation hard detectors at JET: recent developments*
Nucl. Instrum. Meth. Phys. Res A **593**, 492-504 (2008)

F. ALLADIO, A. MANCUSO, P. MICOZZI: *Rotating twisted filaments buoyancy: comparison between the convective region of the sun and the edge of a tokamak plasma*
Plasma Phys. Control. Fusion 50, 124019 (2008)

S. RATYNSKAIA, C. CASTALDO, E. GIOVANNOZZI, D. RUDAKOV, G. MORFILL, M. HORANYI, J.H. YU, G. MADDALUNO: *In situ dust detection in fusion devices*
Plasma Phys. Control. Fusion **50**, 124046-124057 (2008)

C. STRANGIO, A. CARUSO: *ICF applications of FAST ions generated by focusing short laser pulses on ultra–thin causally isolated targets*
J. Physics: Conference Series **112**, 042043–46 (2008)

A. ANGRISANI ARMENIO, A. AUGIERI, G. CELENTANO, V. GALLUZZI, A. MANCINI, A. RUFOLONI, A. VANNOZZI, U. GAMBARDELLA, A. SAGGESE, P. SESSA, S. PACE: *Stability measurements on YBCO coated conductors*
IEEE Trans. Appl. Supercond. **18**, no 2, 1293–1296 (2008)

A. VANNOZZI, A. DI ZENOBIO, G. CELENTANO, G. GIUNCHI, C. ORECCHIA, A. RUFOLONI: *High–temperature stability of Ag film grown on Ni–Cr substrate*
Philos. Mag. **85,** 1-14 (2008)

N. POMPEO, V. GALLUZZI, R. ROGAI, G. CELENTANO, E. SILVA: *Change of strength and nature of vortex pinning in YBCO due to $BaZrO_3$ inclusions*
Physica C **468**, issue 7-10, 745-748 (2008)

E. GIOVANNOZZI, C. CASTALDO, G. APRUZZESE, G. MADDALUNO, S. RATYNSKAIA, A. RYDZY: *Dust in FTU with the Thomson scattering diagnostic*
Multifacets of Dusty Plasmas: 5th Intern. Conf. on Physics of Dusty Plasmas, Eds. J.T. Mendonca, D.P. Resendes, P.K. Shukla, AIP Vol. **1041**, 213-214 (2008)

D. MOREAU, D. MAZON, M. ARIOLA, G. DE TOMMASI, L. LABORDE, F. PICCOLO, F. SARTORI, T. TALA, L. ZABEO, A. BOBOC, E. BOUVIER, M. BRIX, J. BRZOZOWSKI, C.D. CHALIS, V. COCILOVO, V. CORDOLIANI, F. CRISANTI, E. DE LA LUNA, R. FELTON, N. HAWKES, R. KING, X. LIAUDON, T. LOARER, J. MAILLOUX, M. MAYORAL, I. NUNES, E. SURREY, O. ZIMMERMAN and JET EFDA CONTRIBUTORS: A *two–time–scale dynamic–model approach for magnetic and kinetic profile control in advanced tokamak scenarios on JET*
Nucl. Fusion **48**, 106001 (2008)

M.N.A. BEURSKENS, G. ARNOUX, A.S. BREZINSEK, C.D. CHALLIS, P.C. DE VRIES, G. GIROUD, A. HUBER, S. JACHMICH, K. MCCORMICK, R.A. PITTS, F.G. RIMINI, A. ALFIER, E. DE LA LUNA, W. FUNDAMENSKI, S. GERASIMOV, E. GIOVANNOZZI, E. JOFFRIN, M. KEMPENAARS, X. LITAUDON, T. LOARER, P. LOMAS, J. MAILLOUX, R. PASQUALOTTO, V. PERICOLI-RIDOLFINI, R. PUGNO, E. RACHLEW, S. SAARELMA, E. SOLANO, M. WALSH, L. ZABEO, K.–D.ZASTROW and JET–EFDA CONTRIBUTORS: *Pedestal and ELM response to impurity seeding in JET advanced scenario plasmas*
Nucl. Fusion **48**, 095004 (2008)

P. BATISTONI, U. FISHER, K. OCHIAI, L. PETRIZZI, K. SEIDEL. M. YOUSSEF: *Neutronics and nuclear data issues in ITER and their validation*
Fusion Eng. Des. **83**, 834-841 (2008)

L. BONCAGNI, C. CENTIOLI, F. IANNONE, C. NERI, M. PANELLA, L. PANGIONE, M. RIVA, M. SCAPPATICCI, V. VITALE, L. ZACCARIAN: *Synchronous databus network in ITER: open source real-time network for the next nuclear fusion experiment*
Fusion Eng. Des **83**, 504–510 (2008)

F. SANTORI, F. CRISANTI, R. ALBANESE, G. AMBROSINO, V. TOIGO, J. HAY, P. LOMAS, F. RIMINI, S.R. SHAW, A. LUCHETTA, J. SOUSA, A. PORTONE, T. BONICELLI, M. ARIOLA, G. ARTASERSE, M-. BIGI, P. CARD, M. CAVINATO, G. DE TOMMASI, E. GAIO, M. JENNISON, M. MATTEI, F. MAVIGLIA, F. PICCOLO, A. PIRONTI, S. SOPPELSA, F. VILLONE, L. ZANOTTO: *The JET PCU project: an international plasma control project*
Fusion Eng. Des. **83**, 202–206 (2008)

L. PETRIZZI, L. AUDITORE, D. CEPRAGA, G. CAMBI, R. VILLARI: *Helium cooled lithium lead: activation analysis of the test blanket module in ITER*
Fusion Eng. Des. **83**, 1244–1248 (2008)

P.P.H. WILSON, R. FEDER, U. FISCHER, M. LOUGHLIN, L. PETRIZZI, Y. WU, M. YOUSSEF: *State–of–the–art 3–D radiation transport methods for fusion energy systems*
Fusion Eng. Des. **83**, 824–833 (2008)

T. PINNA, G. CAMBI, M. ANGELONE and JET–EFDA CONTRIBUTORS: *Data collection on component malfunctions and failures of JET ICRH system*
Fusion Eng. Des. **83**, 1874–1877 (2008)

T. PINNA, L.V. BOCCACCINI, J.F. SALAVY: *Failure mode and effect analysis for the European test blanket modules*
Fusion Eng. Des. **83**, 1733-1737 (2008)

L. DI PACE, E. LETELLIER, H. MAUBERT, W. RASKOB: *Biological hazard issues from potential releases of tritiated dust from ITER*
Fusion Eng. Des. **83**, 1729–1732 (2008)

T. PINNA, R. CAPORALI, A. TESINI: *Failure mode and effect analysis for remote handling transfer systems of ITER*
Fusion Eng. Des. **83,** 1710-1714 (2008)

M. ZUCCHETTI, L. DI PACE, L. EL–GUEBALY, B.N. KOLBASOV, V. MASSAUT, R. PAMPIN, P. WILSON: *An integrated approach to the back-end of the fusion materials cycle*
Fusion Eng. Des. **83**, 1706-1709 (2008)

S. ROSANVALLON, C. GRISOLIA, G. COUNSELL, S.H. HONG, F. ONOFRI, J. WORMS, J. WINTER, B.M. ANNARATONE, G. MADDALUNO, P. GASIOR: *Dust control in tokamak environment*
Fusion Eng. Des. **83**, 1701–1705 (2008)

A. PORTONE, M. ROCCELLA, R. ROCCELLA, F. LUCCA, G. RAMOGIDA: *The ITER TF coil ripple: evaluation of ripple attenuation using Fe insert and of ripple enhancement produced by TBM*
Fusion Eng. Des. **83**, 1619-1624 (2008)

S. PACI, M.T. PORFIRI: *Experimental and numerical analysis of the air inflow technique for dust removal from the vacuum vessel of a tokamak machine*
Fusion Eng. Des. **83**, 151-157 (2008)

A. ANGRISANI ARMENIO, A. AUGIERI, L. CIONTEA, G. CONTINI, I. DAVOLI, V. GALLUCCI, A. MANCINI, A. RUFOLONI, T. PETRISOR, A. VANNOZZI, G. CELENTANO: *Characterization of epitaxial $YBa_2Cu_3O_{7-\delta}$ films deposited by metal propionate precursor solution*
Supercond. Sci. Technol. **21**, 125015 (2008)

F. BORGOGNONI, C. RIZZELLO, S. TOSTI: *Experimental study of the detritiation system catalyst poisoning*
Fusion Eng. Des. **83**, 1375–1379 (2008)

R. VILLARI, M. ANGELONE, P. BATISTONI, U. FISCHER, P. PERESLAVTSEV, L. PETRIZZI, S. POPOVICHEV, JET–EFDA CONTRIBUTORS: *Validation of shutdown dose rate Monte Carlo calculations through a benchmark experiment at JET*
Fusion Eng. Des. **83**, 10-12, 1782-1787 (2008)

A. VANNOZZI, A. DI ZENOBIO, G. CELENTANO, G. GIUNCHI, C. ORECCHIA, A. RUFOLONI: *High temperature stability of Ag film grown on Ni–Cr substrate*
Philosoph. Magaz **88**, 9, 1277–1290 (2008)

D. PACELLA, D. MAZON, A. ROMANO, P. MALARD, G. PIZZICAROLI: *Characterization of detection efficiency as function of energy for soft x-ray detectors*
Rev. Sci. Instrum. **79**, 10E322 (2008)

D. MAZON, D. PACELLA, P. MALARD, D. GARNIER, A. ROMANO, and C. BOUCHAND: *An original calibration technique for soft x-ray detectors and its use in the Tore Supra tomographic system*
Rev. Sci. Instrum. 79, 10E321 (2008)

M. MATSUKAWA, M. KIKUCHI, T. FUJII, T. FUJITA, T. HAYASHI, S. HIGASHIJIMA, N. HOSOGANE, Y. IKEDA, S. IDE, S. ISHIDA, Y. KAMADA, H. KIMURA, K. KIZU, K. KURIHARA, G. KURITA, K. MASAKI, G. MATSUNAGA, N. MIYA, S. MORIYAMA, A. SAKASAI, S. SAKURAI, Y.K. SHIBAMA, K. SHIMADA, A. SUKEGAWA, T. SUZUKI, Y. SUZUKI, Y. TAKASE, M. TAKECHI, H. TAMAI, K. TSUCHIYA, H. URANO, T. YAMAMOTO, K. YOSHIDA, R. ANDREANI, J. ALONSO, P. BARABASCHI, J. BOTIJA, P. CARA, A. COLETTI, R. COLETTI, P. COSTA, A. CUCCHIARO, P. DECOOL, A. DELLA CORTE, N. DOLGETTA, J.–L. DUCHATEAU, W.H. FIETZ, E. GAIO, A. GROSMAN, O. GRUBER, R. HELLER, D. HENRY, P. HERTOUT, J. HOURTOULE, B. LACROIX, R. MAGNE, M. MEDRANO, F. MICHEL, L. MUZZI, S. NICOLLET, L. NOVELLO, L. PETRIZZI, R. PIOVAN, A. PIZZUTO, C. PORTAFAIX, E. RINCON, S. ROCCELLA, L. SEMERARO, S. TURTU', J.–M. VERDER, S. VILLARI, L. ZANI, A. DI ZENOBIO: *Status of JT–60SA tokamak under the EU–JA broader approach agreement*
Fusion Eng. Des **83**, 795–803 (2008)

GY. THALMAIER, I. VIDA-SIMITI, A. RUFOLONI, G. CELENTANO, A. VANNOZZI, A. ANGRISANI, T. PETRISOR: *Ni–Cu–Co biaxially textured substrates for YBCO tape fabrication*
J. Optoelectron. Adv. Mater. **10**, 4, 913–915 (2008)

F. BELLI, B. ESPOSITO, D. MAROCCO, M. RIVA, A. ZIMBAL: *Application of a digital pileup resolving method to high count rate neutron measurements*
Rev. Sci. Instrum **79**, 10E515 (2008)

R. DE ANGELIS, M.G. VON HELLERMANN, F.P. ORSITTO, S. TUGARINOV: *Investigating the possibility of a survey fast ion diagnostic for ITER*
Rev. Sci. Instrum. **79** 10E517 (2008)

C. DI TROIA, S. BRIGUGLIO, G. CALABRÒ, A. CARDINALI, F. CRISANTI, G. FOGACCIA, M. MARINUCCI, G. VLAD, F. ZONCA: *Investigation of fast ion behavior in burning plasmas via ion cyclotron resonance heating*
ECA **32D**, P–5.055 (2008)

P. BURATTI, C.D. CHALLIS, M. GRYAWNEVICH, T.C. HENDER, E. JOFFRIN, T. LUCE, P. SMEULDERS and JET–EFDA CONTRIBUTORS: *Radial analysis of beta–limiting modes in JET*
ECA **32D**, P–1.069 (2008)

V. PERICOLI RIDOLFINI, YU. BARANOV, M. BEURSKENS, M.- BRIX, P. BURATTI, G. CALABRÒ, C. CASTALDO, R. CESARIO, C.D. CHALLIS, R. DE ANGELIS, P.C. DE VRIES, J. FERRON, E. GIOVANNOZZI, C. GIROUD, M. GRYAZNEVISH, T.C. HENDER, D. HOWWELL, E. JOFFRIN, T. LUCE, P. LOMAS, J. MAILLOUX, D.C. MAC DONALD, J. MENARD, M. MURAKAMI, F. ORSITTO, F. RIMINI, G. SAIBENE, S. SHARAPOV, P. SMEULDERS, I. VOITSEKOVITCH, O. ZIMMERMANN, and JET–EFDA CONTRIBORS: *High β_N experiments at JET in ITER–like plasmas in support of the ITER steady state scenario*
ECA **32D**, O–2.006 (2008)

A. BIANCALANI, L. CHEN, F. PEGORARO, F. ZONCA: *Continuous spectrum of shear Alfvén waves in the presence of a magnetic island*
ECA **32D**, O–2.051 (2008)

C.D. CHALLIS, E. JOFFRIN. T. LUCE, P. BURATTI, P. DE VRIES, J. HOBIRK, B, ALPER, M. BRIX, R. FELTON, J. FERRON, C. GIROUD, M. GRYAZNEVICH, N. HAWKES, T.C. HENDER, D. HOWELL, J. MENARD, M. MURAKAMI, E. RACHLEW, S. SAARELMA, S. SHARAPOV, O. TUDISCO, I. VOITSEKHOVITTCH, O. ZIMMERMANN and JET EFDA CONTRIBUTORS: *High β_N JET H–modes for steady–state application*
ECA 32D, P-5.124 (2008)

G. MAZZITELLI, M.L. APICELLA. V.PERICOLI-RIDOLFINI, A. ALEKSEYEV, G. APRUZZESE, W. BIN, P. BURATTI, R. CESARIO, S. CIPICCIA, G. CALABRÒ, R. DE ANGELIS, L. GABELLIERI, F. GANDINI, E. GIOVANNOZZI, R. GOMES, G. GRANUCCI, B. ESPOSITO, H. KROEGLER, I. LYUBLINSKI, M. MARINUCCI, C. MAZZOTTA, A. ROMANO, O. TUDISCO, A. VERTKOV, FTU TEAM, ECRH TEAM: *Experiments on FTU with a liquid lithium limiter*
ECA **32D**, O–2.001 (2008)

P. SMEULDERS: *Tomography on Lao-Hirschman type of equilibria using mode rotation*
ECA **32D**, O–2.069 (2008)

I. RICAPITO, A. CIAMPICHETTI, P. AGOSTINI, G. BENAMATI: *Tritium processing systems for HCPB–TBM*
Fusion Eng. Des. **83** 1461-1465 (2008)

RICAPITO, A. CIAMPICHETTI, G. BENAMATI, M. ZUCCHETTI: *Tritium extraction systems for the European HCLL/HCPB TBMs*
Fusion Sci. Technol. **54**, 107–112 (2008)

A. AIELLO, G. BENAMATI, R. MELDER, A. POVSTYANKO: *Mechanical properties of Eurofer 97 in Pb–16Li and irradiation effect*
J. Nucl. Mater. **376**, 396–400 (2008)

E. MAS DE LES VALLS, L. SEDANO, L. BATET, I. RICAPITO, A. AIELLO, O. GASTALDI, F. GABRIEL: *Lead–lithium eutectic material database for nuclear fusion technology*
J. Nucl. Mater. **376**, 353–357 (2008)

P. AGOSTINI, G. MICCICHÈ, A. GESSI, D. GIUSTI, F.S. NITTI, G. MERCURIO, A. ZUCCHINI, M. FRISONI: IFMIF T*arget design: development of the european concept*
Proceedings of the 3rd High Power Targetry Workshop, ISSN 1019-0643 pag. 49–53 (2008)

H. NAKAMURA, P. AGOSTINI, K. ARA, S. CEVOLANI ET al.: *Latest design of the liquid lithium target in IFMIF*
Fusion Eng. Des. **83**, 1007–1014 (2008)

Articles in course of publication

D. PACELLA, G. PIZZICAROLI, D. MAZON, P. MALARD: *An original method for measuring thickness or composition of deposition layers on tokamak surfaces*
Plasma Phys. Control Fusion

C. RIZZELLO, F. BORGOGNONI, T. PINNA, S. TOSTI: *Review of tritium confinement and atmosphere detritiation system in hot cells complex*
Fusion Eng. Des

A. CARDINALI, S. BRIGUGLIO, G. CALABRO', F. CRISANTI, C. DI TROIA, G. FOGACCIA, M. MARINUCCI, G. VLAD, F. ZONCA: *Minority ions acceleration by ICRH: a tool for investigating burning plasma physics*
Nucl. Fusion

G. VLAD, S. BRIGUGLIO, G. FOGACCIA, F. ZONCA, C. DI TROIA, W.W. HEIDBRING, M.A. VAN ZEELAND, A. BIERWAGE, X. WANG: *Particle simulation of energetic particle driven Alfvén modes in NBI heated DIII-D experiments*
Nucl. Fusion

A. PIZZUTO, F. GNESOTTO, M. LONTANO, R. ALBANESE, G. AMBROSINO, M.L. APICELLA, A. BRUSCHI, G. CALABRO', A. CARDINALI, R. CESARIO, F. CRISANTI, V. COCILOVO, A. COLETTI, R. COLETTI, P. COSTA, S. BRIGUGLIO, P. FROSI, F. CRESCENZI, V. COCCORESE,A. CUCCHIARO, C. DI TROIA, B. ESPOSITO, G. FOGACCIA, G. GRANUCCI, G. MADDALUNO, R. MAGGIORA, M. MARINUCCI, P. MARTIN, G. MAZZITELLI, F MIRIZZI, L. PANACCIONE, G. L. RAVERA, F. ORSITTO, V. PERICOLI RIDOLFINI, G. RAMOGIDA, C. RITA, A. TUCCILLO, R. ZAGORSKI, M. VALISA, G. VLAD, F. ZONCA: *The Fusion Advanced Studies Torus (FAST): a proposal for an ITER satellite facility in support of the development of fusion energy*
Nucl. Fusion

R. CESARIO, L. PANACCIONE, P. SMEULDERS, A. BOTRUGNO, G. CALABRO', A CARDINALI, C. CASTALDO, M. MARINUCCI, A. ROMANO, V. PERICOLI, A.A. TUCCILLO, F. ZONCA: *Lower hybrid wave produced supra–thermal electrons and fishbone-like instability in FTU*
Nucl. Fusion

E. VISCA, F. ESCOURBIAC, S. LIBERA, A. MANCINI, G. MAZZONE, M. MEROLA, A. PIZZUTO: *Testing of high heat flux components manufactured by ENEA for ITER divertor*
Fusion Eng. Des

G. MADDALUNO, R. ZAGORSKI, V. PERICOLI RIDOLFINI, M.L. APICELLA, G. CALABRO', F. CRISANTI, A. CUCCHIARO, A. PIZZUTO, G. RAMOGIDA: *Edge plasma physics issues for the fusion advanced studies torus (FAST) in reactor relevant conditions*
Nucl. Fusion

L. MUZZI, V. CORATO: *Direct measurement of inter–filament resistance in Nb_3Sn multi–filamentary strands*
Cond–Mat

Contributions to conferences

R. DE ANGELIS, M.G. VON HELLERMANN, F.P. ORSITTO, S. TUGARINOV: *Investigating the possibility of a survey fast ion diagnostic for ITER*
17th Topical Conference on High–Temperature Plasma Diagnostics, Albuquerque (New Mexico), May 11–15, 2008

D. PACELLA, D. MAZON, A. ROMANO, P. MALARD, G. PIZZICAROLI: *Characterization of detection efficiency as function of energy for soft x–ray detectors*
17th Topical Conference on High–Temperature Plasma Diagnostics, Albuquerque (New Mexico), May 11–15, 2008

F. BELLI, B. ESPOSITO, D. MAROCCO, M. RIVA, A. ZIMBAL: *Application of a digital pile–up resolving method to high count rate neutron measurements*
17th Topical Conference on High–Temperature Plasma Diagnostics, Albuquerque (New Mexico), May 11–15, 2008

D. MAZON, D. PACELLA, P. MALARD, D. GARNIER, A. ROMANO, C. BOUCHAND: *An original calibration technique for soft x–ray detectors and its use in the tore–supratomographic system*
17th Topical Conference on High–Temperature Plasma Diagnostics, Albuquerque (New Mexico), May 11–15, 2008

M. ANGELONE, G. AIELLI, D. LATTANZI, M. PILLON, S. ALMAVIVA, M. MARINELLI, E. MILANI, G. PRESTOPINO, A. TUCCIARONE, C. VERONA, G. VERONA–RINATI, R. CARDARELLI, R. SANTONICO: *Neutron detectors based upon artificial single crystal diamond*
SORMA West, Berkeley, CA (USA), June 2–5, 2008

D. MAROCCO, F. BELLI, B. ESPOSITO, M. RIVA: *High count rate neutron spectrometry with liquid scintillation detectors*
SORMA West, Berkeley, CA (USA), June 2–5, 2008

L. AFFINITO, A. DELLA CORTE, M. NAPOLITANO, G.M. POLLI: *An optimized bipolar current lead for the ENEA variable temperaure insert test facility for critical current measurements*
2008 Applied Superconductivity Conference, Chicago, Ill (USA), August 17–22, 2008

L. MUZZI, L. AFFINITO, V. CORATO, G. DE MARZI, A. DI ZENOBIO, C. FIAMOZZI ZIGNANI, M. NAPOLITANO, S. TURTU', R. VIOLA, A. DELLA CORTE: *Magnetic and transport characterization of NbTi strands as a basic for the design of fusion magnets*
2008 Applied Superconductivity Conference, Chicago, Ill (USA), August 17–22, 2008

V. CORATO, L. MUZZI, A. DELLA CORTE, A. DI ZENOBIO, S. TORTU', R. VIOLA: *The influence of bending strain on the*

critical current of Nb_3Sn strands with different filament twist pitch
2008 Applied Superconductivity Conference, Chicago, Ill (USA), August 17–22, 2008

A. DI ZENOBIO, U. BESI VETRELLA, V. CORATO, A. DELLA CORTE, G. GIORGI, F. MAIERNA, G. MESSINA, L. MUZZI, S. TORTU': *Application of the ENEA joint concept to NbTi CIC conductors*
2008 Applied Superconductivity Conference, Chicago, Ill (USA), August 17–22, 2008

A. DELLA CORTE, A. DI ZENOBIO, L. MUZZI, G. PASOTTI, G.M. POLLI, L. RECCIA, S. TORTU': *ENFASI: conceptual design of a 15 T large bore superconducting test facility*
2008 Applied Superconductivity Conference, Chicago, Ill (USA), August 17–22, 2008

C. FIAMOZZI ZIGNANI, V. CORATO, A. DELLA CORTE, A. DI ZENOBIO, G. MESSINA, L. MUZZI: *Simulation by finite difference numerical method of Nb_3Sn strand under bending strain*
2008 Applied Superconductivity Conference, Chicago, Ill (USA), August 17–22, 2008

A. VANNOZZI, G. CELENTANO, A. ANGRISANI ARMENIO, A. AUGIERI, V. GALLUZZI, U. GAMBARDELLA, A. MANCINI, T. PETRISOR, A. RUFOLONI, G. THALMAIER: *Ni-Cu-Co alloy textured substrate for YBCO coated conductors*
2008 Applied Superconductivity Conference, Chicago, Ill (USA), August 17–22, 2008

G. CELENTANO, G.M. POLLI, A. ANGRISANI ARMENIO, A. AUGIERI, V. GALLUZZI, A. MANCINI, A. RUFOLONI, A. VANNOZZI, U. GAMBARDELLA, A. SAGGESE, S. PACE: *Hot spot stimulated transition in YBCO coated conductors: experiments and simulations*
2008 Applied Superconductivity Conference, Chicago, Ill (USA), August 17–22, 2008

A. AUGIERI, V. GALLUZZI, G. CELENTANO, A.A. ANGRISANI, A. MANCINI, A. RUFOLONI, A. VANNOZZI, E. SILVA, N. POMPEO, T. PETRISOR, L. CIONTEA, U. GAMBARDELLA, S. RUBANOV: *Transport properties improvement by means of BZO inclusions in PLD grown YBCO thinfilms*
2008 Applied Superconductivity Conference, Chicago, Ill (USA), August 17–22, 2008

A. ANGRISANI ARMENIO, G. CELENTANO, A. RUFOLONI, A. VANNOZZI, A. AUGIERI, V. GALUZZI, A. MANCINI, L. CIONTEA, T. PETRISOR, G. CONTINI, I. DAVOLI: *Deposition and characterization of metal propionate derived epitaxial $YBa_2Cu_3O_{7-x}$ films for coated conductor fabrication*
2008 Applied Superconductivity Conference, Chicago, Ill (USA), August 17–22, 2008

A. PORTONE, W. BAKER, E. FERNANDEZ-CANO, E. SALPIETRO, P. TESTONI, A. VOSTNER, P. BRUZZONE, A. DELLA CORTE, A. BALDINI, E. THEISEN: *Status of the EDIPO project*
2008 Applied Superconductivity Conference, Chicago, Ill (USA), August 17–22, 2008

P. BRUZZONE, B. STEPANOV, R. WESCHE, A. DELLA CORTE, L. AFFINITO, M. NAPOLITANO, A. VOSTNER: *Test results of a Nb_3Sn cable–in–conduit conductor with variable pitch sequence*
2008 Applied Superconductivity Conference, Chicago, Ill (USA), August 17–22, 2008

N. POMPEO, R. ROGAI, V. GALLUZZI, A. AUGIERI, G. CELENTANO, L. CIONTEA, T. PETRISOR, E. SILVA: *Effect of $BaZrO_3$ inclusions on the microwave surface impedance of YBCO films in a magnetic field*
2008 Applied Superconductivity Conference, Chicago, Ill (USA), August 17–22, 2008

M.L. APICELLA, F. CRISANTI, G. MADDALUNO, V. PERICOLI-RIDOLFINI, R. ZAGORSKI: *Edge plasma issues of the tokamak FAST (Fusion Advanced Studies Torus) in reactor relevant conditions*
22nd IAEA Fusion Energy Conference "Celebrating fifty years of fusion.....entering into the burning plasma era", Geneva (Switzerland), October 13–18, 2008

A. CARDINALI, S. BRIGUGLIO, G. CALABRO', F. CRISANTI, C. DI TROIA, G. FOGACCIA, M. MARINUCCI, G. VLAD and F. ZONCA: *Minority ions acceleration by ICRH: a tool for investigating burning plasma physics*
22nd IAEA Fusion Energy Conference "Celebrating fifty years of fusion.....entering into the burning plasma era", Geneva (Switzerland), October 13–18, 2008

A. CUCCHIARO, R. ALBANESE, G. AMBROSINO, G. BROLATTI, G. CALABRO', V. COCILOVO, A. COLETTI, R. COLETTI, P. COSTA, P. FROSI, F. CRESCENZI, F. CRISANTI, G. GRANUCCI, G. MADDALUNO, V. PERICOLI RIDOLFINI, A. PIZZUTO, C. RITA, G. RAMOGIDA: *Load assembly design of the fast machine (rev 1)*
22nd IAEA Fusion Energy Conference "Celebrating fifty years of fusion.....entering into the burning plasma era", Geneva (Switzerland), October 13–18, 2008

A.A. TUCCILLO, A. ALEKSEYEV, B. ANGELINI, S. V. ANNIBALDI, M. L. APICELLA, G. APRUZZESE, J. BERRINO, E. BARBATO, A. BERTOCCHI, A. BIANCALANI, W. BIN, A.BOTRUGNO, G. BRACCO, S. BRIGUGLIO, A. BRUSCHI, P. BURATTI, G. CALABRO', A. CARDINALI, C. CASTALDO, C. CENTIOLI, R. CESARIO, L. CHEN, S. CIRANT, V. COCILOVO, F. CRISANTI, R. DE ANGELIS, U. DE ANGELIS, L. DI MATTEO, C. DI TROIA, B. ESPOSITO, G. FOGACCIA, D. FRIGIONE, L. GABELLIERI, F. GANDINI, E. GIOVANNOZZI, G. GRANUCCI, F. GRAVANTI, G. GROSSETTI, G. GROSSO, F. IANNONE, H. KROEGLER, V. LAZAREV, E. LAZZARO, I. E. LYUBLINSKI, G. MADDALUNO, M. MARINUCCI, D. MAROCCO, J. R. MARTIN SOLIS, G. MAZZITELLI, C. MAZZOTTA, V. MELLERA, F. MIRIZZI, S. MIRNOV, G. MONARI, A. MORO, V. MUZZINI, S. NOWAK, F. P. ORSITTO,

L. PANACCIONE, D. PACELLA, M. PANELLA, F. PEGORARO, V. PERICOLI RIDOLFINI, S. PODDA, S. RATYNSKAIA, G. RAVERA, A. ROMANO, A. RUFOLONI, A. SIMONETTO, P. SMEULDERS, C. SOZZI, E. STERNINI, B. TILIA, O. TUDISCO, A.VERTKOV, V. VITALE, G. VLAD, R. ZAGîRSKI, M. ZERBINI, F. ZONCA: *Overview of the FTU results*
22nd IAEA Fusion Energy Conference "Celebrating fifty years of fusion.....entering into the burning plasma era", Geneva (Switzerland), October 13–18, 2008

G. MAZZITELLI, M.L. APICELLA, M. MARINUCCI, A. ALEKSEYEV, G. APRUZZESE, P. BURATTI, R. CESARIO, L. GABELLIERI, V. LAZAREV, I. LYUBLINSKI, C. MAZZOTTA, S. MIRNOV, V. PEPRICOLI RIDOLFINI, A. ROMANO, O. TUDISCO, A. VERTKOV, R. ZAGORSKI, FTU TEAM, ECRH TEAM, R.B. GOMES, H. FERNANDES, C. SILVA, C. VARANDAS, O. LIELAUSIS, A. KLYUKIN, E. PLATACIS: *Status and perspectivs of the liquid material experiments in FTU and ISTTOK*
22nd IAEA Fusion Energy Conference "Celebrating fifty years of fusion.....entering into the burning plasma era", Geneva (Switzerland), October 13–18, 2008

G. VLAD, S. BRIGUGLIO, C, DI TROIA, G. FOGACCIA, F. ZONCA, K. SHINOHARA, M. ISHIKAWA, M. TAKECHI, W.W. HEIDBRING, M.A. VAN ZEELAND, A. BIERWAGE, X WANG. *Particle simulation of energetic particle driven Alfvén modes*
22nd IAEA Fusion Energy Conference "Celebrating fifty years of fusion.....entering into the burning plasma era" Geneva (Switzerland), October 13–18, 2008

U. FISCHER, P. BATISTONI, A. KLIX, I. KODELI, R.L. PEREL: *Neutronics R&D efforts in support of the European breeder blanket development programme*
22nd IAEA Fusion Energy Conference "Celebrating fifty years of fusion.....entering into the burning plasma era", Geneva (Switzerland), October 13–18, 2008

G. CALABRO', F. CRISANTI, G. RAMOGIDA, R. ALBANESE, A. CARDINALI, A. CUCCHIARO, G. GRANUCCI, G. MADDALUNO, S. NOWAK, A. PIZZUTO, V. PERICOLI RIDOLFINI, A.A. TUCCILLO, F. ZONCA: *FAST plasma scenarios and equilibrium configurations*
22nd IAEA Fusion Energy Conference "Celebrating fifty years of fusion.....entering into the burning plasma era", Geneva (Switzerland), October 13–18, 2008

A. PIZZUTO: *The Fusion Advanced Studies Torus (FAST): a proposal foran ITER satellite facility in support of the development of fusion energy*
22nd IAEA Fusion Energy Conference "Celebrating fifty years of fusion.....entering into the burning plasma era", Geneva (Switzerland), October 13–18, 2008

A. BIANCALANI, L. CHEN, F. PEGORARO, F. ZONCA, S. V. ANNIBALDI, A. BOTRUGNO, P. BURATTI, P. SMEULDERS: *Shear Alfvén wave continuous spectrum in the presence of a magnetic Island*
22nd IAEA Fusion Energy Conference "Celebrating fifty years of fusion.....entering into the burning plasma era", Geneva (Switzerland), October 13–18, 2008

C. CASTALDO, E. GIOVANNOZZI, S. RATYNSKAIA, G. CAPOBIANCO, M. DE ANGELI, U. DE ANGELIS, M. KRETSCHMER, G. MADDALUNO, C. MARMOLINO, G.E. MORFILL, V. PERICOLI-RIDOLFINI, L. PIERONI, K. RYPDAL, A. RUFOLONI, A.A. TUCCILLO, A. VANNOZZI: *Detection of dust particles in FTU*
22nd IAEA Fusion Energy Conference "Celebrating fifty years of fusion.....entering into the burning plasma era", Geneva (Switzerland), October 13–18, 2008

R. CESARIO, L. PANACCIONE, M. MARINUCCI, P. SMEULDERS, A. BOTRUGNO, G. CALABRO', C. CASTALDO, A. ROMANO, V. PERICOLI, A.A. TUCCILLO, F. ZONCA: *Fishbone–like internal kink instability driven by supra–thermal electrons on FTU generatedby lower hybrid radiofrequency power*
22nd IAEA Fusion Energy Conference "Celebrating fifty years of fusion.....entering into the burning plasma era", Geneva (Switzerland), October 13–18, 2008

B. ESPOSITO, G. GRANUCCI, S. NOWAK, J.R. MARTIN–SOLIS, L. GABELLIERI, E. LAZZARO, P. SMEULDERS, M. MARASCHEK, G. PAUTASSO, J. STOBER, L. URSO, H. ZOHM, FTU, ECRH and ASDEX–U TEAMS: *Disruption control on FTU and ASDEX upgrade with ECRH*
22nd IAEA Fusion Energy Conference "Celebrating fifty years of fusion.....entering into the burning plasma era", Geneva (Switzerland), October 13–18, 2008

F. ZONCA, L. CHEN, Z. QIU: *Kinetic theory of Geodesic Acoustic Modes: radial structures and nonlinear excitations*
22nd IAEA Fusion Energy Conference "Celebrating fifty years of fusion.....entering into the burning plasma era", Geneva (Switzerland), October 13–18, 2008

F. ALLADIO, A. MANCUSO, P. MICOZZI: *Rotating twisted filaments buoyancy: comparison between the convective region of the sun and the edge of a tokamak plasma (Invited Paper)*
35th Europ. Physical Society Conference on Plasma Physics, Hersonissos, Crete (Greece), June 9–13, 2008

A. BIANCALANI, L. CHEN, F. PEGORARO, F. ZONCA: *Continuous spectrum of shear Alfvén waves in the presence of a magnetic island*
35th Europ. Physical Society Conference on Plasma Physics, Hersonissos, Crete (Greece), June 9–13, 2008

P. BURATTI, C.D. CHALLIS, M. GRYAWNEVICH, T.C. HENDER, E. JOFFRIN, T. LUCE, P. SMEULDERS, and JET–EFDA CONTRIBUTORS: *Radial analysis of beta-limiting modes in JET*
35th Europ. Physical Society Conference on Plasma Physics, Hersonissos, Crete (Greece), June 9–13, 2008

R. CESARIO, A. CARDINALI, C. CASTALDO, D. DE ARCANGELIS, B. EUSEPI, A.A. TUCCILLO: *Lower hybrid current drive at high densities of ITER*
35th Europ. Physical Society Conference on Plasma Physics, Hersonissos, Crete (Greece) ,June 9–13, 2008

C. DI TROIA, S. BRIGUGLIO, G. CALABRO', A. CARDINALI, F. CRISANTI, G. FOGACCIA, M. MARINUCCI, G. VLAD, F. ZONCA: *Investigation of fast ion behavior in burning plasmas via Ion Cyclotron Resonance Heating*
35th Europ. Physical Society Conference on Plasma Physics, Hersonissos, Crete (Greece), June 9–13, 2008

C. MAZZOTTA, M. ROMANELLI, O. TUDISCO, L. CARRARO, S. CIRANT, E. GIOVANNOZZI, L. GABELLIERI, G. GRANUCCI, M. MARINUCCI, S. NOVAK, V. PERICOLI, M.E. PUIATTI, A. ROMANO, L. LAURO TARONI, and FTU TEAM: *Particle density behavior in FTU electron heated plasmas*
35th Europ. Physical Society Conference on Plasma Physics, Hersonissos, Crete (Greece), June 9–13, 2008

G. SONNINO, PH. PEETERS, F. ZONCA, G. BREYANNIS: *A kinetic model for the diffusion coefficients of magnetically confined plasmas in the low-collisional regime*
35th Europ. Physical Society Conference on Plasma Physics, Hersonissos, Crete (Greece), June 9–13, 2008

F. ZONCA, LIU CHEN: *Self-consistent energetic particle nonlinear dynamics due to shear Alfvén wave excitations*
35th Europ. Physical Society Conference on Plasma Physics, Hersonissos, Crete (Greece), June 9–13, 2008

F. MIRIZZI, A. CARDINALI, R. CESARIO, L. PANACCIONE, V. PERICOLI–RIDOLFINI, G.L. RAVERA, A.A. TUCCILLO: *Conceptual design of the lower hybrid additional heating system for FAST*
7th Intern. Workshop Strong Microwaves: Source and Applications (SMSA–2008) Nizhny Novgorod (Russia), July 27–August 2, 2008

A. AUGIERI, V. GALLUZZI, G. CELENTANO, A. ANGRISANI ARMENIO, A. MANCINI, A. RUFOLONI, A. VANNOZZI, E. SILVA, N. POMPEO, T, PETRISOR, L. CIONTEA, S. RUBANOV: *Miglioramento delle proprietà di trasporto mediante introduzione di nano-inclusioni di $BaZrO_3$ in film di YBCO cresciuti per PLD*
SATT14 - XIV Congresso Nazionale di Superconduttività, Parma (Italy), March 19–21, 2008

U. GAMBARDELLA, S. PACE, A. SAGGESE, A. ANGRISANI ARMENIO, A. AUGIERI, G. CELENTANO, V. GALLUZZI, A. MANCINI, A. RUFOLONI, G. POLLI, A. VANNOZZI: *Analisi della dinamica di propagazione della zona normale in nastri di YBCO–coated conductors commerciali*
SATT14 - XIV Congresso Nazionale di Superconduttività, Parma (Italy), March 19–21, 2008

A. ANGRISANI ARMENIO, A. AUGIERI, G. CELENTANO, L. CIONTEA, V. GALLUZZI, A. MANCINI, T. PETRISOR, A. RUFOLONI, A. VANNOZZI: *Film di $YBa_2Cu_3O_{7-x}$ con tecnica MOD TFA–modificata per la realizzazione di coated conductors*
SATT14 - XIV Congresso Nazionale di Superconduttività, Parma (Italy), March 19–21, 2008

I. COLANTONI, A. VANNOZZI, A. AUGIERI, G. CELENTANO, F. D'ACAPITO, I. DAVOLI, V. GALLUZZI, M. LUCCI, A. MANCINI, A. RUFOLONI: *Caratterizzazione spettroscopica di film di Pd su substrati di Ni–W per la realizzazione diYBCO–coated conductors*
SATT14 - XIV Congresso Nazionale di Superconduttività, Parma (Italy) March 19-21, 2008

E. GIOVANNOZZI, C. CASTALDO, G. APRUZZESE, G. MADDALUNO, S. RATYNSKAIA, A. RYDZY: *Dust in FTU with the Thomson scattering diagnostic*
5th Intern. Conference on the Physics of Dusty Plasmas (ICPDP5), Ponta Delgada (Azores), May 18–23, 2008

G.M. POLLI, L. RECCIA, A. CUCCHIARO, A. DELLA CORTE, A. DI ZENOBIO, L. MUZZI, A. PIZZUTO, G. RAMOGIDA, S. TURTU', R. VILLARI, M. NANNINI, C. PORTAFAIX, L. ZANI, P. BARABASCHI: *2D thermal analysis for heat transfer from casing to winding pack in JT–60SA TF coils*
25th Symposium on Fusion Technology (SOFT), Rostock (Germany), September 15–19, 2008

V. CORATO, L. MUZZI, A. DELLA CORTE, R. VIOLA: *The key role of twist pitch and mechanical pre–treatment in the transport properties of Mn_3Sn wires subject to bending strain*
25th Symposium on Fusion Technology (SOFT), Rostock (Germany), September 15–19, 2008

F. MIRIZZI, A. BRUSCHI, A. CARDINALI, R. CESARIO, G. GRANUCCI, R. MAGGIORA, L. PANACCIONE, V. PERICOLI–RIDOLFINI, G.L. RAVERA, A.A. TUCCILLO: *The three RF additional heating systems for FAST*
25th Symposium on Fusion Technology (SOFT), Rostock (Germany), September 15–19, 2008

G.L. RAVERA, A. CARDINALI, C. CASTALDO, R. CESARIO, R. MAGGIORA, F. MIRIZZI, A.A. TUCCILLO: *Preliminary analysis of the exteranal matching unit for the ICRH system for FAST*
25th Symposium on Fusion Technology (SOFT), Rostock (Germany), September 15–19, 2008

C. NARDI, S. PAPASTERGIOU: *ENEA study on vertical module segmentation for a DCLL blanket for DEMO*
25th Symposium on Fusion Technology (SOFT), Rostock (Germany), September 15–19, 2008

E. VISCA, F. ESCOURBIAC, S. LIBERA, A. MANCINI, G. MAZZONE, M. MEROLA, A. PIZZUTO: *Development and testing of high heat flux components for ITER divertor in ENEA*
25th Symposium on Fusion Technology (SOFT), Rostock (Germany), September 15–19, 2008

P. BATISTONI, M. ANGELONE, U. FISCHER, D. LEICHTLE, A. KLIX, I. KODELI, L. PETRIZZI, W. POHORECKI, A. TRKOV, R. VILLARI: *Design optimisation and measuring techniques for the neutronics experiment on a HCLL–TBM mock–up*
25th Symposium on Fusion Technology (SOFT), Rostock (Germany), September 15–19, 2008

C. NERI, A. COLETTI, M. FERRI DE COLLISBUS, G. FORNETTI, F. POLLASTRONE: *The upgraded laser in vessel viewing system (IVVS) for ITER*
25th Symposium on Fusion Technology (SOFT), Rostock (Germany), September 15–19, 2008

A. ASTOLFI, D. CARNEVALE, C. CENTIOLI, S. PODDA, L. ZACCARIAN: *A new extremum seeking schema for the maximization of the plasma RF heating on FTU*
25th Symposium on Fusion Technology (SOFT), Rostock (Germany), September 15–19, 2008

L. ZACCARIAN, L. BONCAGNI, D. CASCONE, C. CENTIOLI, S., CERINO, F. GRAVANTI, F. IANNONE, F. MECOCCI, L. PANGIONE, S. PODDA, V. VITALE, R. VITELLI: *Nonlinear instabilities induced by the F coil power amplifier at FTU: modeling and control*
25th Symposiun on Fusion Technology (SOFT), Rostock (Germany), September 15–19, 2008

L. BONCAGNI, C. CENTIOLI, L. LATTANZIO, M. PANELLA, C. TORELLI, L. ZACCARIAN: *A web services based system for the distribution of live information in fusion experiments*
25th Symposiun on Fusion Technology (SOFT), Rostock (Germany), September 15–19, 2008

P. ROSSI, A. PIZZUTO, L. SEMERARO, C. ANNINO, C. NARDI, L. BETTINALI, A. LO BUE, W. BAKER, G. MAZZONE, J. KNASTER: *Stress relaxation testing of pre–compression ring mock–up for the ITER magnet system*
25th Symposiun on Fusion Technology (SOFT), Rostock (Germany), September 15–19, 2008

F. BORGOGNONI, A. MORIANI, S. SANDRI, S. TOSTI: *Evaluation of tritium diffusion through the neutral beam injector calorimeter panel*
25th Symposiun on Fusion Technology (SOFT), Rostock (Germany), September 15–19, 2008

A. CAPRICCIOLI, P. FROSI: *Multipurpose ANSYS FE procedure for welding processes simulation*
25th Symposiun on Fusion Technology (SOFT), Rostock (Germany), September 15–19, 2008

T. PINNA, A. NATALIZIO: *Safety analysis of ITER failures and consequences during maintenance*
25th Symposiun on Fusion Technology (SOFT), Rostock (Germany), September 15–19, 2008

S. ROCCELLA, E. CACCIOTTI, F. ESCOURBIAC, A. PIZZUTO, B. RICCARDI, A. TATI', P. VARONE, E. VISCA: *Development of an ultrasonic test method for the non–destructive examination of ITER divertor components*
25th Symposiun on Fusion Technology (SOFT), Rostock (Germany), September 15–19, 2008

S. ROCCELLA, A. MARIN, F. LUCCA, A. PIZZUTO, G. RAMOGIDA: *Residual magnetic stray field in ITER building and field perturbation on the plasma due to ferromagnetic iron components outside the vessel*
25th Symposiun on Fusion Technology (SOFT), Rostock (Germany), September 15–19, 2008

G. RAMOGIDA, G. CALABRO', V. COCILOVO, F. CRISANTI, A. CUCCHIARO, A. PIZZUTO, C. RITA, R. ALBANESE, G. ARTASERSE, F. MAVIGLIA, M. MATTEI: *Plasma scenarios, equilibrium configurations and control in the design of FAST*
25th Symposiun on Fusion Technology (SOFT), Rostock (Germany), September 15–19, 2008

R. VILLARI, P. BARABSCHI, A. CUCCHIARO, A. DELLA CORTE, A. DI ZENOBIO, N. DOLGETTA, B. LACROIX, F. MORO, L. MUZZI, S. NICOLLET, L. PETRIZZI, A. PIZZUTO, G.M. POLLI, C. PORTAFAIX, G. RAMOGIDA, L. RECCIA, S. ROCCELLA, A. SUKEGAWA, S. TURTU, K. YOSHIDA, L. ZANI: *Neutronic analysis of the JT–60SA toroidal magnets*
25th Symposiun on Fusion Technology (SOFT), Rostock (Germany), September 15–19, 2008

D. LATTANZI, M. ANGELONE, M. PILLON, S. ALMAVIVA, M. MARINELLI, E. MILANI, G, PRESTOPINO, A. TUCCIARONE, C. VERONA, G. VERONA–RINATI, S. POPOVICHEV, R.M. MONTEREALI, M.A. VINCENTI, A. MURARI, and JET–EFDA CONTRIBUTORS: *Single crystal CVD diamonds as neutron detectors at JET*
25th Symposiun on Fusion Technology (SOFT), Rostock (Germany), September 15–19, 2008

M. UTILI, A. TINCANI et al.: *The European Breeding Blanket Test Facility: an integrated device to test European helium cooled TBMs in view of ITER*
25th Symposiun on Fusion Technology (SOFT), Rostock (Germany), September 15–19, 2008

A. TINCANI, P.A. DI MAIO, R. GIAMMUSSO, I. RICAPITO, G. VELLA: *Thermo–mechanical experiment and analysis on an HCPB–TBM mock–up*
25th Symposiun on Fusion Technology (SOFT), Rostock (Germany), September 15–19, 2008

A. AIELLO, M. UTILI, S. SCALIA, G. COCCOLUTO: *Experimental study of efficiency of natural oxide layers for reduction of tritium permeation through Eurofer 97*
25th Symposiun on Fusion Technology (SOFT), Rostock (Germany), September 15–19, 2008

G. MICCICHÈ, P. AGOSTINI, A. IBARRA, A. GARCIA, V. QUERAL: *IFMIF target assembly: Enhancement of the remote handling strategy for the replacable backplate bayonet concept*
25th Symposiun on Fusion Technology (SOFT), Rostock (Germany), September 15–19, 2008

G. MICCICHÈ, P. AGOSTINI et al.: *Proposal of an improved design of IFMIF test cell components for enhanced handling and reliability*
25th Symposiun on Fusion Technology (SOFT), Rostock (Germany), September 15–19, 2008

P. AGOSTINI, G. MICCICHÈ et al.: *Preliminary mapping of the expected radiation damage of the bayonet IFMIF back-plate*
25th Symposiun on Fusion Technology (SOFT), Rostock (Germany), September 15–19, 2008

D. GIUSTI, P. AGOSTINI, F.S. NITTI: *Lithium target design analysis and criteria for IFMIF design*
25th Symposiun on Fusion Technology (SOFT), Rostock (Germany), September 15–19, 2008

A. GESSI, P. AGOSTINI, M. AGOSTINI: *Explorative experiment of steel erosion/corrosion in high speed flowing lithium*

25th Symposiun on Fusion Technology (SOFT), Rostock (Germany), September 15–19, 2008

P. AGOSTINI, G. MICCICHÈ, P. TURRONI: *Approach to the lifetime assessment of the bayonet back plate for IFMIF target*
25th Symposiun on Fusion Technology (SOFT), Rostock (Germany), September 15–19, 2008

P. AGOSTINI, E. RAPEZZI, M. CIOTTI: *Cavitation sensor for the IFMIF/EVEDA experiment*
25th Symposiun on Fusion Technology (SOFT), Rostock (Germany), September 15–19, 2008

L. DI PACE, T. PINNA, A. NATALIZIO: *ITER post-accident recovery: a worker dose perspective*
18th TOFE, San Francisco (USA), September 28–October 2, 2008

L. BONCAGNI, C. CENTIOLI, L. FIASCA, F. IANNONE, M. PANELLA, V. VITALE, L. ZACCARIAN: *Introducing a virtualization technology for the FTU plasma control system*
18th TOFE, San Francisco (USA), September 28–October 2, 2008

F. ZONCA, L. CHEN: *Nonlinear dynamics and complex behaviors in magnetized plasmas of fusion interest*
Intern. Workshop on the Frontiers of Modern Plasma Physics (ICTP), Trieste (Italy), July 14–25, 2008

C. CASTALDO, A. CARDINALI: *Tritium minority heating with mode conversion of fast waves*
Theory of Fusion Plasmas, Joint Varenna – Lausanne International Workshop, Villa Monastero, Varenna (Italy), August 25–29, 2008

Reports

RT/2008/24/FPN	G. VLAD, S. BRIGUGLIO, G. FOGACCIA, C. DI TROIA *HMGC user guide*
RT/2008/43/FPN	A. PIZZUTO, G. CALABRO', F. CRISANTI, G. RAMOGIDA, R. ALBANESE, A. CARDINALI, A. CUCCHIARO, G. GRANUCCI, G. MADDALUNO, S. NOVAK, V. PERICOLI RIDOLFINI, A.A. TUCCILLO, F. ZONCA, S. BRIGUGLIO, C. DI TROIA, G. FOGACCIA, M. MARINUCCI, G. VLAD, R. ZAGÒRSKI, M.L. APICELLA, G. RAMOGIDA, G. AMBROSINO, G. BROLATTI, V. COCILOVO, A. COLETTI, R. COLETTI, P. COSTA, P. FROSI, F. CRESCENZI, C. RITA *CONTRIBUTIONS TO THE 22nd IAEA Fusion Energy Conference "Celebrating fifty years of fusion.....entering into the burning plasma era" (13–18 October 2008 Geneva, Switzerland)*
RT/2008/44/FPN	A. PIZZUTO, F. CRISANTI, F. ZONCA, A.A. TUCCILLO, M.L. APICELLA, G. CALABRO', A. CARDINALI, R. CESARIO, V. COCILOVO, A. COLETTI, R. COLETTI, P. COSTA, S. BRIGUGLIO, P. FROSI, F. CRESCENZI, A. CUCCHIARO, C. DI TROIA, B. ESPOSITO, G. FOGACCIA, G. MADDALUNO, M. MARINUCCI, D. MAROCCO, G. MAZZITELLI, F. MIRIZZI, L. PANACCIONE, G.L. RAVERA, F. ORSITTO, V. PERICOLI RIDOLFINI, G. RAMOGIDA, C. RITA, R. VILLARI, G. VLAD, F. GNESOTTO, P. MARTIN, M. VALISA, A. BRUSCHI, M. LONTANO, G. GRANUCCI, S. NOVAK, R. ALBANESE, G. AMBROSINO, V. COCCORESE, R. MAGGIORA, R. ZAGORSKI *FAST – the Fusion Advanced Studies Torus "A proposal for a facility in support of the development of fusion energy"*

Internal reports

RTI TT-G-R-002 (2008) A. CIAMPICHETTI, I. RICAPITO
Coolant purification system for HCPB–TBM

RTI TT-G-R-003 (2008) I. RICAPITO, A. CIAMPICHETTI
TBM-ITER tritium plant interfaces

RTI HB-G-R-008 (2008) A. TINCANI, G. BERTACCI, A. CANNETA, A. MALAVASI, A. NERI, E. RAPEZZI, L. RAPEZZI, I. RICAPITO, S. VITALI
Hexcaliber final report

RTI HB-G-R-009 (2008) A. TINCANI, G. COCCOLUTO, G. LAMMA, S. NUCCI, G. POLAZZI, L. RAPEZZI, I. SACCHETTI
Upgrading of the He-Fus 3 helium loop for testing TBMS - Final report

RTI SB-G-R-012 (2008) A. TINCANI, A. MALAVASI, A. BARBI, G. FOGACCI, E. GUZZINI, E. PANICHI, L. RAPEZZI, I. RICAPITO
Thermal fatigue testing of beryllium coated first wall mock–ups – Final Report (TW5-TVB-FWMUTF2)

RTI LH-A-R 004 (2008) A. AIELLO
Experimental study of efficiency of oxide layers in Helium Coolant System (HCS) for reduction of H permeation through Eurofer and heat exchanger material (Incoloy, Inconel)

7.2 Workshops and Seminars

Workshops

07/10/2008 Joint Meeting of the 4th IAEA Technical Meeting on Spherical Tori and The 14th International Workshop on Spherical Torus

27/10/2008 European Parliament – Committee on Industry, Research and Energy – ITRE Delegation to Frascati Research Area

13/11/2008 Delegazione giapponese del Jepic

21/11/2008 ITER: un'opportunità per le imprese – Seminario per le Camere di Commercio Italiane

Seminars

18/02/2008 F. ORSITTO – ENEA – Frascati (Italy)
Breve report dell'attività italiana al JET 2006-2007 e prospettive del programma 2008

18/02/2008 F. CRISANTI – ENEA – Frascati (Italy)
Breve report dell'attività italiana al JET 2006-2007 e prospettive del programma 2008

18/02/2008 R. CESARIO – ENEA – Frascati (Italy)
Breve report dell'attività italiana al JET 2006-2007 e prospettive del programma 2008

18/02/2008 P. BURATTI – ENEA – Frascati (Italy)
Breve report dell'attività italiana al JET 2006-2007 e prospettive del programma 2008

22/02/2008 M. BRAMBILLA - IPP – Garching (Germany)
Quasilinear description of radiofrequency-induced radial diffusion

27/02/2008 A. BIANCALANI - Univ. Pisa – Pisa (Italy)
Continuum spectrum of shear Alfvén waves in the presence of a magnetic island

19/05/2008 D. FANELLI – CISDC – Florence (Italy)
Out of equilibrium dynamics in mean field systems and the Vlasov equation

19/05/2008 S. RUFFO – CISDC – Florence (Italy)
Out of equilibrium dynamics in mean field systems and the Vlasov equation

19/05/2008 M. PETTINI – CISDC – Florence (Italy)
Control techniques in dissipative systems

19/05/2008 R. LIVI – CISDC – Florence (Italy)
Characterizing dynamics with covariant Lyapunov vectors

24/06/2008 F. D'ACAPITO – CNR–INFM–OGG – Grenoble (France)
Materials science studies at the Italian GILDA beamline at the European Synchrotron Radiation Facility

26/09/2008 K. BAYSTRUKOV – Kazakistan Republic
Present and future fusion in Russia and KTM tokamak status

29/09/2008 D. PAVARIN – Univ. Padova – Padova (Italy)
Il progetto "Helicon plasma hydrazine. Combined Micro" nell'ambito del 7° programma quadro "Space" - Coinvolgimento dell'ENEA di Frascati

Organisation Chart

The activities of the ENEA Research Group are performed in the Fusion Department.
The number of professionals and non-professionals working on Fusion in 2008 are the following:

Professional:	Physics activity 113	–	Technology Activity 13	=	Total 126
Non professional:	Physics activity 90	–	Technology Activity 3	=	Total 93

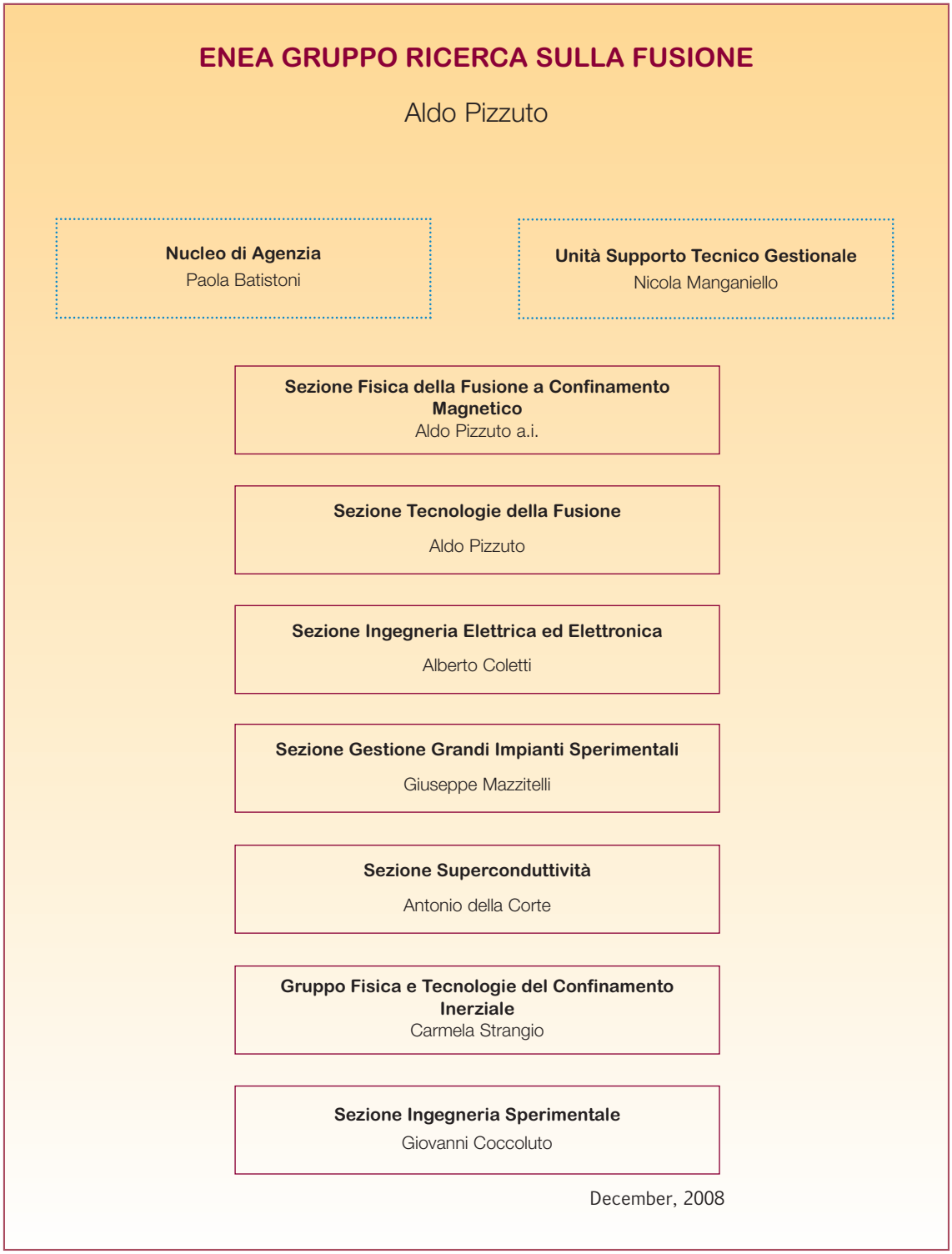

Abbreviations and Acronyms

A

ac	alternating current
ACP	activation corrosion product
ADC	analog–to digital converters
AGHS	active gas handling system
ALMA	Atacama Large Millimeter/submillimeter Array
APS	artificial pinning sites
AT	advanced tokamak
AT	advanced torus
ASDEX	Axisymmetric Divertor Experiment – Garching – Germany
ASDEX-U	Axisymmetric Divertor Experiment Upgrade – Garching – Germany

B

BAE	beta–induced Alfvén eigenmode

C

CAP	continuum accumulation point
CB	cassette body
CC	coated conductor
C/E	calculation/experiment
CEA	Commissariat à l'Energie Atomique – France
CERN	European Organisation for Nuclear Research – Geneva – Switzerland
CFC	carbon fibre composite
CFL-RAL	Central Laser Facility – Rutherford Appleton Laboratory – UK
CICC	cable–in–conduit conductor
CIEMAT	Centro de Investgaciones Energéticas, Medioambientales y Tecnológicas – Madrid – Spain
CNR	Consiglio Nazionale delle Ricerche (National Research Council) – Italy
CNS	compact neutron spectrometer
CPS	capillary porous system
CPS	coolant purification system
CRP	Coordinated Research Project
CRPP	Centre de Recherches en Physique des Plasmas – Villigen – Switzerland
CS	central solenoid
CSD	chemical solution deposition
CSU	Close Support Unit
CTS	collective Thomson scattering
CVCS	chemical volume control system
CVD	chemical vapour deposition
CVI	chemical vapour infiltration
CW	continuous wave
CXRS	exchange recombination spectroscopy

D

DBTT	ductile–to–brittle transition temperature
dc	direct current

DCR	design change request
DEMO	demonstration/prototype reactor
DPA	displacements per atom
DPSD	digital pulse shape discrimination
DRP	divertor refurbishment platform
DIII–D	Doublet III – D–shape. Tokamak at General Atomics – San Diego – USA
DTA	differential thermal analyser
DWT	drift-wave turbulence

E

EAF	European Activation File
EAS	European Advanced Superconductor
EASY	European Activation System
EBBTF	European Breeding Blanket Test Facility
EC	electron cyclotron
ECE	electron cyclotron emission
ECLIM	European Conference on Laser Interaction with Matter
ECRH	electron cyclotron resonance heating
ECWGB	electron cyclotron wave Gaussian beam
EDA	Engineering Design Activities
EDIPO	EFDA Dipole
EELT	European Extremely Large Telescope
EFBT	European Breeding Blanket Test Facility
EFDA	European Fusion Development Agreement
EFET	European Fusion and Technology
EFIT	equilibrium fitting code
ELM	edge localised mode
em	electromagnetic
EP	Enhanced Programme (JET)
EPM	energetic particle mode
EVEDA	Engineering Validation and Engineering Design Activities

F

FAST	Fusion Advanced Studies Torus
FCA	fast charge amplifier
FEB	fast electron bremsstrahlung
FEC	Fusion energy conference
FEM	finite-elements model
F4E	Fusion For Energy
FIGEX	Fast Ion Generation Experiment
FNG	Frascati neutron generator - ENEA
FP	fast particle
FPGA	field programmable gate array
FS	Faraday shield
FTU	Frascati Tokamak Upgrade - ENEA
FUS	fibreglass unidirectional S-glass
FW	first wall
FWHM	full width at half maximum
FZJ	Forschungzeuntrum – Julich – Germany
FZK	Forschungszeuntrum – Karlsruhe – Germany

G

GAM	geodesic acoustic mode
GEM	gas electron multiplier
GLC	gas liquid contactors
GM	Geiger – Müller
GSEP	Gyrokinetic simulation of energetic particle turbulence and transport
GSSR	Generic–Site Specific Safety Report

H

HCLL	helium–cooled lithium-lead
HCPB	helium–cooled pebble bed
HF	high–field
HFPI	high–frequency pellet injector
HiPER	High–Power Laser Energy Research Roadmap
HMGC	hybrid magnetohydrodynamic gyrokinetic code
HPC	high–performance computing
HRP	hot radial pressing
HTS	high–temperature superconductor
HV	high voltage

I

IAEA	International Atomic Energy Agency – Vienna – Austria
IBW	ion Bernstein waves
ICRH	ion cyclotron resonance heating
IEA	International Energy Agency
IFE	inertial fusion energy
IFMIF	International Fusion Materials Irradiation Facility
IFP	Institute of Plasma Physics – CNR Milan
ILA	ITER-like antenna
ILO	Industrial Liaison Officer
INFN	National Institute of Nuclear Physics – Italy
IPP	Institut für Plasma Physik - Garching
IPPE	Institute of Physics and Power Engineering – Russia
ISIP	Infrastructure and Software Integration Project
ITB	internal transport barrier
ITER	International Thermonuclear Experimental Reactor
ITG	ion turbulent gradient
ITM	Integrated tokamak modelling
ITPA	International Tokamak Physical Activity
IVVS	in–vessel viewing and ranging system

J

JAEA	Japan Atomic Energy Agency – Japan
JAERI	Japan Atomic Energy Research Institute
JET	Joint European Torus - Abingdon – UK
JT–60U	JAERI Tokamak 60 Upgrade, Naka, Japan
JT–60SA	JAERI Tokamak 60 Super Advanced

K

KTH	Royal Institute of Technology – Stockholm
KTI	kinetic thermal ion

L

LANL	Los Alamos National Laboratory – USA
LF	low–field
LH	lower hybrid
LHC	Large Hadran Collider (CERN)
LHCD	lower hybrid current drive
LLL	liquid lithium limiter
LOM	light optical microscopy
LOS	line of sight
LT	long time
LTS	low–temperature superconducting

M

MAST	Mega Ampère Spherical Tokamak – Culham – UK
MF	mechanical filters
MFG	motor flywheel generator
MHD	magnetohydrodynamic
MiAE	magnetic–isalnd–induced Alfvén eigenmode
MMS	multi–module–segment
MOD	metal organic deposition
MOPA	master oscillator power amplifier
MPI	Message Passing Interface
MSE	motional Stark effect
MSST	Measurement Simulation Software Tool

N

NBI	neutral beam injection
NDT	non–destructive testing
NICD	non–inductive current driven
NHFML	National High–Field Magnet Laboratory – Talahassee – USA

O

OpenMP	Open Multi–Processing
ORNL	Oak Ridge National Laboratory – Tennessee – USA
OST	Oxford Instruments Superconducting Technologies

P

PAM	passive active multijunction
PCU	Plasma Control Upgrade
PED	Pressure Equipment Directive
PF	poloidal field
PFC	plasma–facing component
PFCI	poloidal field coil insert
PHS	pulse height spectra

PHTS	primary heat transfer system
PIE	postulated initiating event
PIE	post–irradiation examination
PLD	pulsed laser deposition
POLITO	Turin Polytechnic
PS	power supply
PSD	pulse shape discrimination
PTB	Physikalisch-Technische Bundesanstalt -Braunschweig - Germany
PWI	plasma–wall interaction

Q

QA	Quality assurance
QDS	quick disconnecting system
QSPA	Quasi Stationary Plasma Accelerator Facility (TRINITY Russian Federation)

R

rf	radiofrequency
RFX	Reversed Field Pinch Experiment – Padua – Italy (Association Euratom–ENEA)
RH	remote handling
RNC	radial neutron camera
RO	responsible officer
RRR	residual resistivity ratio

S

SAW	shear Alfvén wave
SC	shape controller
SC	superconducting
SCD	single crystal diamond
SEM	scanning electron microscopy
SBD	surface barrier diode
SOC	saturated ohmic confinement
SOL	scrape–off layer
SP	screw pinch
SSEPN	steady–state electrical power network
SSQLFP	steady–state quasi–linear Fokker–Planck
ST	short time
ST	spherical torus
SXR	soft–x–ray

T

TBM	test blanket module
TBM-CA	TBM-Consortium of Euratom
TB	transport barrier
TES	tritium extraction system
TEXTOR	Torus Experiment for Technology Oriented Research. Tokamak at Jülich – Germany (Association EURATOM-FZJ)
TF	task force
TF	toroidal field
TFA	trifluoroacetate
TFC	toroidal field coil

TFR	toroidal field ripple
TIG	tungsten inert gas
TLD	thermoluminescent detector
TOF	time–of–flight
TOFD	time–of–flight diffraction
Tore–Supra	Large tokamak at Cadarache – France (Association Euratom–CEA)
TP	twist pitch
TPR	tritium production rate
PRF	permeation reduction factor
TRIEX	tritium extraction
TS	Thomson scattering
TS	tensile strain
TSA	temperature swing adsorption

U

UCI	University of California at Irvine – Usa
UHP	ultra–high purity
UKAEA	United Kingdom Atomic Energy Agency
UTS	ultimate tensile strength

V

VD	void fraction
VDE	vertical displacement event
VS	vertical stabilisation
VUV	vacuum ultraviolet
VV	vacuum vessel

W

WP	winding pack
WKB	Wenzel, Kramer, Brillouin code

X

XSC	extreme shape controller
XPS	x–ray photoemission spectroscopy

Z

ZF	zonal flow